

# Design and development of injectable polymeric formulations for the treatment of osteoarthritis

by

Gloria María Pontes Quero

A dissertation submitted by in partial fulfillment of the requirements for the degree of Doctor of Philosophy in

Program of Material Science and Engineering

Universidad Carlos III de Madrid

Advisors:

Maria Rosa Aguilar de Armas  
Blanca Vázquez Lasa

Tutor:

Diego Velasco Bayón

April

This thesis is distributed under license “Creative Commons **Attribution – Non Commercial – Non Derivatives**”.



# ACKNOWLEDGEMENTS

Después de tres años muy intensos al fin puedo decir que se acabó este periodo de tesis. No ha sido fácil debido a las limitaciones de tiempo, a temas burocráticos y al coronavirus pero, por fin llegó el momento. Esto ha sido posible gracias al trabajo a contrarreloj que hemos realizado mis tutoras de tesis y yo, por lo que lo primero que quiero hacer es darles las gracias a ellas.

Curra, aparte de ser mi tutora eres un modelo a seguir de mujer trabajadora, madre y jefa. Gracias a tus ideas, a tu tiempo, a tu energía y a tu optimismo esto ha sido posible. Aunque ha habido momentos en los que no teníamos tiempo ni de hablar y meses de angustia en los que el coronavirus no nos dejaba avanzar en el proyecto, hemos podido compartir otros momentos y conversaciones que sí recordaré con cariño. Aunque no te gusten los gatos, te aprecio mucho. Blanca, eres un pilar fundamental en esta tesis, tus ideas, comentarios, revisiones y aportaciones científicas son únicas, además de proporcionarme calma y calidez cada vez que hablo contigo. Me alegro de poder haber contado contigo como tutora y como guía y modelo científico. Finalmente, Julio, que voy a decir de Julio que no se haya dicho ya. Gracias a ti pude formar parte de este grupo y hacer mi tesis doctoral en un ambiente que no cambiaría por nada. Recordaré los *October Fest* en tu casa, la paella de rabo de toro, los momentos de charla sobre viajes y comida, la *Summer School* en Trento o el Congreso de Tenerife. Tu fuerza y alegría han hecho que en los momentos duros pudiera seguir adelante. A los tres de nuevo, muchas gracias por la oportunidad, por vuestro tiempo y dedicación en esta tesis. Por otro lado, este trabajo no se podría haber realizado sin Juan Pérez y ALODIA Farmacéutica. Gracias a él pude acceder a la beca que he disfrutado estos tres años, además, de otros proyectos extra que me permitirán estar en contacto con la industria, lo que me servirá en mi futuro laboral, no me cabe la menor duda. Por lo que, muchas gracias Juan y a seguir trabajando juntos.

Tengo que agradecer a todo el grupo de Biomateriales el ambiente de trabajo, ayuda y compañerismo que he podido disfrutar durante la tesis. Sin ellos todo se habría hecho mucho más cuesta arriba. En especial a mis compañeros de

desayuno. ¡Qué triste hubiera sido sin nuestras conversaciones! A Raquelita, mi pilar principal durante la tesis, sin su ayuda y sin su alegría no hubiera podido con esto. A Marisi, por la ayuda en el laboratorio y por las conversaciones, que me han hecho pensar, reír y despejarme. A Rosana, por la ayuda en el laboratorio de células, pero también por los cafés las conversaciones, por lo bien que nos lo pasamos en el Congreso de Tenerife y por ser como una mami para mí estos tres años. A Luis Rojo por ser un referente en la constancia y en las buenas formas. A Luisgar por toda la ayuda tecnológica e informática, por la ayuda en el vídeo del concurso, por la ayuda con los dibujos, esta tesis sería menos vistosa sin toda esa ayuda. A mi gallega favorita Virginia por las conversaciones de gatos y por tu alegría. A mis amigos mejicanos, Héctor, Marina y Marce, gracias por haber iluminado el laboratorio con paz, tranquilidad y buen rollo. Sois de lo mejor que he conocido. A Eva por su ayuda cuando la he necesitado y por estar mano a mano en el doctorado conmigo. A Miguel, por sus consejos alimenticios, deportivos y de materiales. A mi compañero de doctorado industrial Yeral, gracias por las charlas, por las cervezas y los cafés (aunque me hayas estado quitando la leche y la pasta de dientes, que no me olvido) y por la ayuda en la parte química, eres un cerebritito. A mi sufridor y superviviente de la selección natural Dani, mi proveedor de memes, de risas, de videos de Taylor Swift y de Mariah Carey. Nuestra simbiosis es eterna y te doy las gracias por todo este tiempo juntos, eres el mejor. Seguiré recordándole a la gente que el verdadero peligro de la humanidad son las superbacterias. A Alberto y Fátima, que, aunque en el laboratorio solo estuviéramos en la primera parte de la tesis os habéis convertido en gente imprescindible en mi vida. A Fátima por ser mi alma gemela, por todos los vídeos de gatos, por los momentos de fiesta y por estar siempre ahí. A Alberto, que, aunque no sea fan de los gatos le quiero y le agradezco de todo corazón toda la ayuda al principio de la tesis, igual que Raquel, has sido mi pilar en este trabajo. A todos vosotros, ¡muchas gracias! No solo he podido realizar esta tesis sino conocer personas a las que quiero un montón y con las que seguiré compartiendo momentos. También me acuerdo de Pepe, Rick y Antonio por haberme permitido hacer una estancia en la Universidad de Málaga. Por supuesto a Cristina, por implicarte conmigo en el trabajo, por sacarme de casa y por las risas que me pude echar.



Mi agradecimiento más especial es para mis padres. Ellos no solo me han apoyado en este periodo de tiempo, sino que han permitido que pudiera estudiar lo que quería apoyándome en todo momento. Sé que están muy orgullosos de mi, igual que yo de ellos. Todo lo que soy os lo debo a vosotros. Y quería agradecer por último a la persona más importante durante esta etapa, a mi persona favorita, a mi apoyo continuo, al único que puede aguantarme las 24 horas del día, a David. Tú has sido el que más ha sufrido conmigo, el que sabe lo que me ha costado y el que siempre ha estado ahí. Por todas las visitas inesperadas al trabajo, por todas las veces que madrugabas para llevarme al trabajo en coche, por intentar ayudarme en todo lo que podías y por escucharme hablar sobre temas que ni sabías que existían, gracias de todo corazón. Aunque a ti te queda todavía mucho que aguantar, te agradezco que sigas a mi lado, sé que no es fácil. Te quiero con locura y no puedo agradecerle más a la vida que te pusiera en mi camino.

A todos, mil gracias.



# PREFACE

**The following papers have been published during the accomplishment of this doctoral thesis and are included as a part of it:**

- Pontes-Quero GM, García-Fernández L, Aguilar MR, San Román J, Pérez-Cano J, Vázquez-Lasa B. **Active viscosupplements for osteoarthritis treatment**. Seminars in Arthritis and Rheumatism. 2019; 49:171-183. doi: 10.1016/j.semarthrit.2019.02.008. Review article partially included in Chapter I.
- Pontes-Quero GM, Benito-Garzón L, Pérez-Cano J, Aguilar MR, Vázquez-Lasa B. **Amphiphilic polymeric nanoparticles encapsulating curcumin: antioxidant, anti-inflammatory and biocompatibility studies**. Materials Science and Engineering C. 2021; 121, 111793. doi:10.1016/j.msec.2020.111793. Research article fully included in Chapter III.
- Pontes-Quero GM, Benito-Garzón L, Pérez-Cano J, Aguilar MR, Vázquez-Lasa B. **Modulation of inflammatory mediators by polymeric nanoparticles loaded with anti-inflammatory drugs**. Pharmaceutics. 2021; 13:290, doi:10.3390/pharmaceutics13020290. Research article fully included in Chapter IV.

## Other research merits include:

- **The publication of a book chapter:**

Pontes-Quero GM\*, Espinosa-Cano E, Fernández-Villa D, Huerta-Madroñal M, Aguilar MR, and Vázquez-Lasa B. **Characterization Techniques for Emulsion-Based Antioxidant Carriers with Biomedical Applications**. M. A. Aboudzadeh (ed.), *Emulsion-based Encapsulation of Antioxidants, Food Bioactive Ingredients*, 2021. [https://doi.org/10.1007/978-3-030-62052-3\\_12](https://doi.org/10.1007/978-3-030-62052-3_12). Book chapter included in Annex I.

- **A research article in collaboration with the Medicinal Chemistry Institute (IQM-CSIC).**

Pérez de Vega MJ, Moreno-Fernández S, Pontes-Quero GM, González-Amor M, Vázquez-Lasa B, Sabater-Muñoz B, Briones AM, Aguilar MR, Miguel M, González-Muñiz R. **Characterization of Novel Synthetic Polyphenols: Validation of Antioxidant and Vasculoprotective Activities**. *Antioxidants*. 2020; 9(9):787. doi:10.3390/antiox9090787. Research article included in Annex II.

- **Participation in national and international conferences:**

Pontes Quero GM, Aguilar MR, San Román J, Vázquez-Lasa B. *Encapsulation of hydrophobic agents into vitamin E-based polymeric nanoparticles*. Oral communication. XIII International Symposium on Frontiers in Biomedical Polymers. Tenerife (Spain). May, 2019.

Pontes Quero GM, García-Fernández L, Aguilar MR, San Román J, Pérez-Cano J, Vázquez-Lasa B. *Latest advances in viscosupplements for osteoarthritis treatment*. Oral communication. XVII Jornadas sobre Biomateriales y el Entorno Celular. Ávila (Spain). February, 2019.

Pontes Quero GM, Nakal A, Palao-Suay R, Aguilar MR, San Román J, Vázquez-Lasa B. *Polymeric nanoparticles with dual antioxidant and anti-inflammatory activity*. Oral communication. SEIIPOL2018. III Young Polymer Scientist Seminar. Madrid (Spain). October, 2018.

Pontes Quero GM, Nakal A, Palao-Suay R, Aguilar MR, San Román J, Vázquez-Lasa B. *Design and characterization of polymeric nanoparticles with dual antioxidant activity*. Oral communication. XLI Congreso de la Sociedad Ibérica de Biomecánica y Biomateriales. Madrid (Spain). October, 2018.

Pontes Quero GM, Nakal A, Palao-Suay R, Martín-Saldaña S, Aguilar MR, Vázquez-Lasa B, San Román J. *Polymeric Nanoparticles for the treatment of inflammatory processes*. Oral communication. Summer School on Tissue Engineering. University of Trento (Italia). June, 2018.

### **A short research stay was carried out during the execution of this doctoral thesis:**

**Project:** Development of new formulations for osteoarthritis treatment based on mesenchymal stem cells derived secretomes

**Research centre:** Universidad de Málaga, Málaga, Spain

**Supervisors:** Prof. José Becerra and Dr. Rick Visser

**Date:** from 14/09/2020 to 13/12/2020 (3 months)

**Financial support:** Industrial PhD project IND2017/IND7614, supported by the Comunidad de Madrid (Spain) and Alodia Farmacéutica SL

### **The content of this doctoral thesis has been included in several outreach events and contests:**

- **I Concurso Yo Investigo Yo Soy CSIC.** Organized by Departamento de Posgrado y Especialización del CSIC.  
<https://www.youtube.com/watch?v=FWzUUdp6418&t=93s>.
- **Que Siga La Ciencia.** Organized by Centro de Investigación Biomédica en Red, CIBER. <https://www.youtube.com/watch?v=k2iDgbQOqBU>.
- **IV Nanofestival** celebrated in the ICTP-CSIC the 10<sup>th</sup> of April, 2019. Oral communication. Title: ***Polymeric nanoparticles in medicine***.
- **Laboratory practice** about ***Polymers*** celebrated in the Nuestra Señora del Recuerdo High School, Madrid, the 11<sup>th</sup> of June, 2019.
- **Oral communication** about ***Women in Science*** in the Chambéry Maristas School, 13<sup>th</sup> of February, 2020 due to the International Day of Women in Science.

- **V Nanofestival** celebrated in the Rayuela High School, Móstoles, Madrid, the 29<sup>th</sup> of January, 2020. Title: ***Nanoscience and nanotechnology***.
- Participation in the CIBER initiative ***Inspiring Women*** to make women in science visible, the 11<sup>th</sup> of February, 2021.  
<https://www.ciberisciii.es/comunicacion/cultura-cientifica/cientificas-que-inspiran>.

**From this doctoral thesis have arisen the following projects and financial supports:**

- **Ayuda a proyectos de inicio a la investigación en cirugía ortopédica y traumatología. 2020. Funding: 6,000€**

**Title:** Eficacia de nuevos viscosuplementos activos en el comportamiento de un modelo experimental de osteoartritis

**Main researcher:** Roque Emilio Pérez Expósito

**Associated researchers:** Basilio José de la Torre Escuredo, Miguel Ángel Ortega Núñez and Julia Buján Varela

**Research center:** Traumatology Service of the Ramón y Cajal University Hospital - Alcalá University

**Financing entity:** Sociedad Española de Cirugía Ortopédica y Traumatología (Fundación SECOT)

- **Development of a gastroesophageal reflux protector for ALODIA Farmacéutica. ALODIA Farmacéutica S.L. – CSIC contract**

- **Technology CIBER-BBN Transfer Program. Funding: 30,000€**

**Title:** Polymeric Nanoparticles for the treatment of inflammatory respiratory diseases (POLYNARED)

**Main researchers:** Luis García Fernández and Maria Rosa Aguilar

**Industrial Partner:** Juan Pérez, ALODIA Farmacéutica

**Research center:** ICTP-CSIC

**Financing entity:** CIBER-BBN and ALODIA Farmacéutica SL

# ABSTRACT

Osteoarthritis, the most common form of arthritis, is a chronic, painful and disabling condition with an important impact on those affected, healthcare services and economy. Overall, the worldwide prevalence of osteoarthritis was around 303 million in 2017 and due to population ageing and the sedentary lifestyle, the number of osteoarthritis patients is expected to continuously increase. Because of its chronic nature, its current management is based on the reduction of patient symptomatology going from oral anti-inflammatories to intra-articular injections or surgical procedures. The oral administration of anti-inflammatory drugs is one of the most used strategy to reduce pain and inflammation. However, most of these drugs present low water solubility, limiting its bioavailability and making necessary the use of high systemic doses that lead to undesirable side effects. Their local intra-articular administration could solve some of these problems although their direct contact with cartilage can promote its degradation. The encapsulation of these drugs into drug delivery systems such as polymeric nanoparticles could reduce drug toxicity, provide a controlled release of the drug and extend their residence time.

Viscosupplementation, which is the intra-articular injection of hyaluronic acid-based products, is also a widely used treatment for mild to moderate cases. Its main objective is the restoration of the synovial fluid viscoelasticity impaired in osteoarthritic patients, providing joint lubrication and, as a consequence, pain relief. However, its efficacy is controversial, due to its rapid elimination from the synovial joint.

In this context, the aim of this thesis was the **development of injectable polymeric formulations for the treatment of osteoarthritis**. First, a polymeric nanocarrier based on a novel amphiphilic terpolymer was developed for the encapsulation of different hydrophobic anti-inflammatory drugs used in the treatment of osteoarthritis. Nanoparticles were prepared by the nanoprecipitation method. Curcumin, a natural polyphenol; celecoxib, a selective COX-2 inhibitor; tenoxicam, a traditional nonsteroidal anti-inflammatory drug; and dexamethasone, a glucocorticoid; were successfully

loaded into the polymeric nanocarrier. The nanovehicle proved to have an intrinsic antioxidant potential due to the presence of  $\alpha$ -tocopheryl methacrylate moieties. Loaded nanoparticles were extensively characterized in terms of size, morphology, stability, encapsulation efficiency, drug release and antioxidant activity, achieving suitable properties for their use in biological applications. *In vitro* cellular assays were performed on articular chondrocytes and macrophages to assess cytotoxicity, cellular uptake, and antioxidant and anti-inflammatory activities, evidencing remarkable antioxidant and anti-inflammatory properties through the reduction of oxidative and inflammatory mediators. Finally, the *in vivo* biocompatibility of the systems was demonstrated by subcutaneously injecting the NPs in Wistar rats.

On the other hand, advanced viscosupplements based on hyaluronic acid hydrogels loaded with anti-inflammatory drug delivery systems were prepared. Furthermore, studies on mesenchymal stem cells derived secretomes were carried out as an alternative therapy for osteoarthritis. This information is described in confidential Chapters V and VI.



# RESUMEN

La osteoartritis, la forma más común de artritis, es una condición crónica, dolorosa e inhabilitante con un importante impacto en aquellos que la padecen, los servicios de salud y la economía. La prevalencia de la osteoartritis a nivel mundial era en torno a los 303 millones en 2017 y debido al envejecimiento de la población y al estilo de vida sedentario, se espera que aumente de forma continuada. Debido a su naturaleza crónica, el tratamiento actual se basa en la reducción de la sintomatología del paciente, usando desde anti-inflamatorios orales, a las inyecciones intra-articulares o la cirugía. La administración oral de fármacos anti-inflamatorios es una de las estrategias más utilizadas para reducir el dolor y la inflamación. Sin embargo, la mayoría de estos fármacos presentan una baja solubilidad en agua, limitando su biodisponibilidad y haciendo necesario el uso de altas dosis que dan lugar a diversos efectos secundarios. Su administración intra-articular podría resolver alguno de estos problemas, aunque su contacto directo con el cartílago puede favorecer su degradación. La encapsulación de estos fármacos en sistemas de liberación como las nanopartículas poliméricas podría reducir la toxicidad del fármaco, aportar una liberación controlada del mismo y extender su tiempo de residencia.

La viscosuplementación, consistente en la inyección intra-articular de productos basados en el ácido hialurónico, es un método ampliamente utilizado para el tratamiento de los casos moderados de osteoartritis. Su principal objetivo es la restauración de las propiedades viscoelásticas del líquido sinovial que se encuentra dañado en los pacientes con osteoartritis, aportando lubricación a la articulación y, como consecuencia, alivio del dolor. Sin embargo, su eficacia es controvertida, debido a su rápida eliminación de la articulación sinovial.

En este contexto, el objetivo de esta tesis fue el **desarrollo de formulaciones poliméricas inyectables para el tratamiento de la osteoartritis**. En primer lugar, se desarrolló un nanovehículo polimérico basado en un terpolímero anfífilico para la encapsulación de fármacos anti-inflamatorios

hidrofóbicos usados para el tratamiento de la osteoartritis. Las nanopartículas se prepararon por el método de nanoprecipitación. La curcumina, un polifenol natural; el celecoxib, un inhibidor selectivo de COX-2; el tenoxicam, un anti-inflamatorio no esteroideo tradicional; y la dexametasona, un glucocorticoide, fueron encapsulados con éxito en el nanovehículo polimérico. El nanovehículo demostró un potencial antioxidante intrínseco debido a la presencia de dominios basados en el metacrilato de  $\alpha$ -tocoferilo. Las nanopartículas cargadas se caracterizaron detalladamente en términos de tamaño, morfología, estabilidad, eficiencia de encapsulación, liberación del fármaco y actividad antioxidante, logrando unas características apropiadas para su uso en aplicaciones biológicas. Los ensayos celulares *in vitro* se realizaron en condrocitos articulares y en macrófagos para estudiar la citotoxicidad, la captación celular y la actividad antioxidante y anti-inflamatoria y demostraron una alta capacidad antioxidante y anti-inflamatoria mediante la reducción de mediadores inflamatorios. Finalmente, la biocompatibilidad *in vivo* de los sistemas se demostró mediante su inyección subcutánea en ratas Wistar.

Por otro lado, se prepararon viscosuplementos avanzados basados en geles de ácido hialurónico cargados con sistemas de liberación de fármacos anti-inflamatorios. Además, se han realizado estudios para el uso de secretomas derivados de células madre mesenquimales como terapia alternativa para el tratamiento de la osteoartritis. Esta información se describe en los Capítulos confidenciales V y VI.

# INDEX OF CONTENTS

---

<b>Chapter I. Introduction</b>	<b>3</b>
<b>1. Osteoarthritis (OA)</b>	<b>3</b>
<b>1.1. Synovial joint and physiopathology in OA</b>	<b>3</b>
<b>1.2. Inflammation in OA</b>	<b>6</b>
1.2.1. Non-immune cells	8
1.2.2. Immune cells	9
1.2.3. Signaling pathways	11
1.2.4. Inflammatory mediators	12
<b>1.3. Management of OA</b>	<b>16</b>
1.3.1. Traditional treatments	16
1.3.2. Emerging pharmacological therapies	19
1.3.3. Surgical and emerging biological therapies	20
<b>2. Anti-inflammatory drugs for OA treatment</b>	<b>24</b>
<b>2.1. Natural anti-inflammatory compounds: curcumin</b>	<b>24</b>
<b>2.2. NSAIDs</b>	<b>26</b>
<b>2.3. Glucocorticoids</b>	<b>29</b>
<b>2.4. Nanoparticulate drug delivery systems of anti-inflammatory drugs</b>	<b>31</b>
2.4.1. Curcumin	34
2.4.2. Tenoxicam	35
2.4.3. Celecoxib	35
2.4.4. Dexamethasone	36
<b>3. Viscosupplementation</b>	<b>38</b>
<b>3.1. Combined viscosupplements</b>	<b>40</b>
3.1.1. Combination with free anti-inflammatory drugs	41
3.1.2. Combination with DDS	43
3.1.3. Combination with biological therapies	44
<b>Bibliography</b>	<b>46</b>
 <b>Chapter II. Objectives</b>	 <b>73</b>

<b>Chapter III. Amphiphilic polymeric nanoparticles encapsulating curcumin: antioxidant, anti-inflammatory and biocompatibility studies</b>	<b>77</b>
1. Introduction	78
2. Experimental section	81
3. Results and discussion	91
4. Conclusions	111
Bibliography	112
Supplementary material	119

<b>Chapter IV. Modulation of inflammatory mediators by polymeric nanoparticles loaded with anti-inflammatory drugs.</b>	<b>125</b>
1. Introduction	126
2. Experimental section	129
3. Results and discussion	135
4. Conclusions	154
Bibliography	155
Supplementary material	161

<b>Chapter V. Advanced viscosupplements based on hyaluronic acid hydrogels loaded with anti-inflammatory drug delivery systems. <i>CONFIDENCIAL</i></b>	<b>169</b>
---	------------

<b>Chapter VI. Studies on mesenchymal stem cells derived secretomes for the treatment of OA. <i>CONFIDENCIAL</i></b>	<b>199</b>
--	------------

<b>Chapter VII. Conclusions and future perspectives</b>	<b>219</b>
---	------------

## **Annexes**

**Annex I.** Characterization Techniques for Emulsion-Based Antioxidant Carriers with Biomedical Applications

**Annex II.** Characterization of Novel Synthetic Polyphenols: Validation of Antioxidant and Vasculoprotective Activities

## **Abbreviations**

# Chapter I. Introduction



# Chapter I. Introduction

---

## 1. Osteoarthritis

Osteoarthritis (OA), the most common form of arthritis, is a chronic, highly prevalent disease and a major contributor to functional disability in older adults. OA can affect any synovial joint, but it occurs most often in knees, hips and hands. According to the World Health Organization, in 2016, OA became the 12<sup>th</sup> leading cause of years lived with disability increasing from the 14<sup>th</sup> to the 12<sup>th</sup> within 10 years [1]. The incidence of OA increases with advancing age, affecting 9.6% of men and 18% of women aged over 60 years worldwide [2]. Men are affected more frequently than women among those aged below 45 years, whereas women are more often affected among those aged over 55 years, as a consequence of hormonal changes, primarily estrogen deficiency [3]. Overweight is also a well-recognized risk factor for knee [4] and, to a lesser degree, hand [5] and hip OA [6] due to the combination of increased mechanical loads and metabolic factors such as adipokines. There is also evidence that genetic factors play a major role in OA. Genetic polymorphism of genes encoding cartilage matrix proteins or proteins involved in the immune cascade can participate on the initiation and development of OA [7,8]. Other risk factors include previous joint injury or mechanical predisposition [9,10]. Moreover, population ageing and sedentary lifestyle suggest that the number of people affected by hip or knee OA will increase over the next decades [11].

### 1.1. Synovial joint and physiopathology in OA

Synovial joints are formed by two articulating bones surrounded by an articular capsule that defines a synovial cavity filled with the synovial fluid, as seen in figure 1 [12–14]. The synovial cavity is not an isolated system but, a highly efficient lymphatic and vascular system that allows the exchange of molecules between the synovial fluid and the exterior, leading to the rapid elimination of administered drugs [15]. The articulating surfaces of the bones are covered by a thin layer of articular cartilage and, externally, bones are

stabilized and held together by muscles and ligaments [14]. Lining the inner surface of the joint cavity is the synovial membrane or synovium that contains synoviocytes. There are two different types of synoviocytes: fibroblast-like synoviocytes (FLS) and macrophage-like synoviocytes (MLS). MLS absorb and degrade undesirable substances from the synovial fluid and clear the joint of particles, while FLS produce substances like collagen, fibronectin and hyaluronic acid (HA), essential for the preservation of the high viscosity and low coefficient of friction between the surfaces of articular cartilage [16]. Articular cartilage covering the bones of synovial joints is a 2 to 4 mm thick hyaline cartilage formed by extracellular matrix (ECM) with embedded chondrocytes [13]. The principal components of the cartilage ECM consist of collagen II and aggrecan, a proteoglycan in which chondroitin sulfate and keratan sulfate glycosaminoglycans (GAG) are attached to a HA chain [12,13].

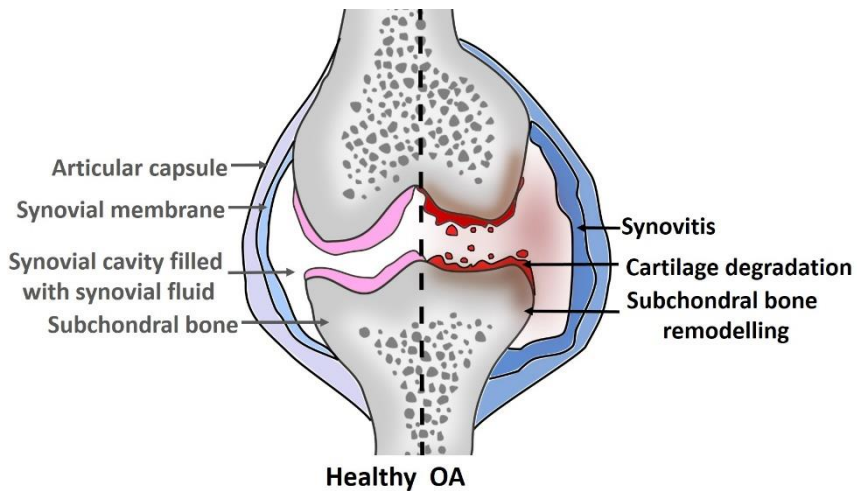


**Figure 1. Comparison of healthy and osteoarthritic synovial joints. Synovial joints are formed by an articular capsule defining the synovial cavity. Osteoarthritic synovial joints are characterized by a progressive cartilage loss, inflammation of synovial membrane and subchondral bone remodeling.**

Synovial fluid is an ultra-filtrate of blood plasma composed of proteins, HA, lubricin and interstitial fluid [17]. It is responsible of providing nutrients and oxygen to the articular cartilage [14]. Normal synovial fluid contains HA, the main contributor to the viscoelastic properties of synovial



fluid, in a concentration that ranges between 3 and 4 mg mL<sup>-1</sup> [18]. Viscoelasticity implies that HA acts like a viscous liquid at low shear rates and as an elastic material at high shear rates. This property allows synovial fluid to act as a shock absorber when it is subjected to high loads and as a lubricant during low loads, reducing friction between the articular cartilages [19].

In osteoarthritic joints, there is a progressive cartilage loss, subchondral bone remodeling and inflammation of synovium (figure 1). Cartilage degradation appears because ECM breakdown exceeds its synthesis. Different cytokines, chemokines, growth factors and proteases are responsible of this imbalance [20]. OA patients have an increased activity of matrix metalloproteinases (MMP) and A disintegrin and metalloproteinase with thrombospondin motifs (ADAMTS). MMP have the ability to cleave ECM components like collagen; while ADAMTS are involved in aggrecan cleavage, promoting cartilage destruction [10,21].

Inflammatory cytokines and chemokines, secreted by activated synoviocytes, chondrocytes and mononuclear cells, have a key role in the metabolic homeostasis loss in the articular capsule. Inflammatory cytokines such as interleukin-1 $\beta$  (IL-1 $\beta$ ) and tumor necrosis factor  $\alpha$  (TNF- $\alpha$ ) have a central role stimulating the production of reactive oxygen species (ROS), nitric oxide (NO), cyclooxygenase-2 (COX-2), prostaglandin E<sub>2</sub> (PGE<sub>2</sub>) and other inflammatory factors (*e.g.* IL-6, IL-15, IL-17, IL-18, leukemia inhibitory factor (LIF)) that in turn contribute to further OA progression [22,23]. On the other hand, the expression of cartilage anabolic factors, such as insulin-like growth factor-1 (IGF-1), transforming growth factor  $\beta$  (TGF- $\beta$ ) and bone morphogenetic proteins, are reduced in OA patients [22].

Bone remodeling is continuously maintained through an equilibrium between osteoblast activity, responsible for bone formation, and osteoclast activity, in charge of degrading the bone microenvironment. In OA, subchondral bone changes, such as a decrease in bone remodeling due to the activation of osteoclasts or the formation of osteophytes, have also a role in the initiation and progression of the disease [24,25]. Inflammation of the synovial membrane, or synovitis, also contributes to the progression of

cartilage loss by an increased vascularity, infiltration of mononuclear cells in the synovium and the synthesis of inflammatory mediators [26,27]. Additionally, patients with OA have a 50% reduction in concentration and molecular weight ( $M_w$ ) of HA in the synovial fluid [28,29]. As a consequence, synovial fluid becomes less viscoelastic and its properties as a lubricating, shock-absorbing and filtering agent are diminished.

### **1.2. Inflammation in OA**

The role of inflammation in the development and progression of OA, although less pronounced than for rheumatoid arthritis (RA), has been demonstrated in the last decades, proposing synovitis as a key factor in the disease [30]. Inflammation related to OA involves mainly an innate immune response prior to a low degree of adaptive immunity. In contrast to the adaptive immune system, innate immunity plays an essential role in modulation of tissue homeostasis by recognizing pathogen-associated molecular patterns (PAMPs) and damage-associated molecular patterns (DAMPs) by pattern recognition receptors (PRR), such as toll-like receptors (TLR) and nucleotide oligomerization domain (NOD)-like receptors (NLR) [31]. During tissue damage, DAMPs induce a protective response by cells to repair the damage tissue. Nevertheless, a prolong signaling of DAMPs leads to an exaggerated production of inflammatory factors that, in turn, causes negative effects on the tissue [32,33]. Inflammatory components are, therefore, overproduced by chondrocytes, synoviocytes and immune cells in the joints of OA patients, altering cell signaling pathways and gene expression, leading to enhanced activation of the inflammatory pathways and the release of more inflammatory mediators. Thus, the interplay of immune and non-immune cells, signaling pathways and inflammatory mediators is crucial for the progression of OA (see table 1).

**Table 1. Key players, types and action in the inflammatory pathogenesis of OA.**

Key player		Types	Activity in OA
Cells	Non-immune cells	Chondrocytes, fibroblast-like synoviocytes, osteoblasts, osteocytes, osteoclasts	Secretion of inflammatory factors, attraction of other immune cells
	Immune cells	Macrophages, mast cells, natural killers, T cells	
Signaling pathways		NF- $\kappa$ B, MAPK, JAK/STAT	Upon activation, regulation of gene expression of inflammatory factors
Inflammatory factors	Proteolytic enzymes	MMP-1, -3, -13, ADAMTS-4, -5, TIMP-1, -2, -3, -4	Destruction of collagen and aggrecan of cartilage ECM
	Cytokines	Pro-inflammatory: IL-1 $\beta$ , TNF- $\alpha$ , IL-6, IL-2, IL-7, IL-15, IL-17, IL-18	Activation of MMPs, ADAMTS and other pro-inflammatory cytokines and chemokines; recruitment of immune cells
		Anti-inflammatory: IL-4, IL-10, TGF- $\beta$	Anti-inflammatory and chondroprotective effects
	Chemokines	IL-8, MCP-1, RANTES, MIP-1 $\alpha$ , MIP-1 $\beta$ , IP-10	Attraction of immune cells, induction of MMPs
	Lipid mediators	PLA <sub>2</sub> , COX-2, PGE <sub>2</sub>	Activation of inflammatory pathways, cartilage destruction, osteoclastic bone resorption
	Reactive oxygen and nitrogen species	ROS	Damage to lipids, proteins and DNA
		RNS/NO	Induction of inflammatory factors release, cartilage destruction

NF- $\kappa$ B, nuclear factor kappa B; MAPK, mitogen-activated protein kinase; JAK/STAT; Janus kinase/signal transducer and activator of transcription proteins MMP, matrix metalloproteinase; ADAMTS, A disintegrin and metalloproteinase with thrombospondin motifs; TIMP, tissue inhibitors of metalloproteinase; IL, interleukin; TNF- $\alpha$ , tumor necrosis factor  $\alpha$ ; TGF- $\beta$ , transforming growth factor  $\beta$ ; MCP-1, monocyte chemoattractant protein-1; RANTES, Regulated upon Activation, Normal T Cell (T lymphocytes of the adaptive immunity) Expressed and Presumably Secreted; MIP-1 $\alpha$  and MIP-1 $\beta$ ,

macrophage inflammatory protein 1 $\alpha$ /1 $\beta$ ; IP-10, interferon gamma-induced protein; PLA<sub>2</sub>, phospholipase A<sub>2</sub>; COX-2, cyclooxygenase-2; PGE<sub>2</sub>, prostaglandin E<sub>2</sub>; ROS, reactive oxygen species; RNS, reactive nitrogen species; NO, nitric oxide.

### 1.2.1. Non-immune cells

**Chondrocytes.** Articular cartilage ECM is the main target of OA cartilage degradation. Cartilage cells (chondrocytes) are crucial during OA, as they are the cells responsible of the maintenance of the anabolic-catabolic balance in cartilage, through the synthesis and turnover of collagen, glycoproteins, proteoglycans and HA [34]. During OA, chondrocytes display abnormalities, such as inappropriate activation of anabolic and catabolic activities and alterations in cell number, through processes like proliferation and cell death [35]. The metabolic activities of osteoarthritic chondrocytes are altered due to the presence of additional stimuli such as non-physiologic loading conditions and by-products of cartilage ECM destruction, as well as abnormal levels of cytokines and growth factors [36]. Osteoarthritic chondrocytes then respond to these signals shifting toward a degradative and hypertrophy-like state, involving abnormal matrix production and increased aggrecanase and collagenase activities [37]. In this context, they are no longer able to maintain cartilage integrity (see figure 2).

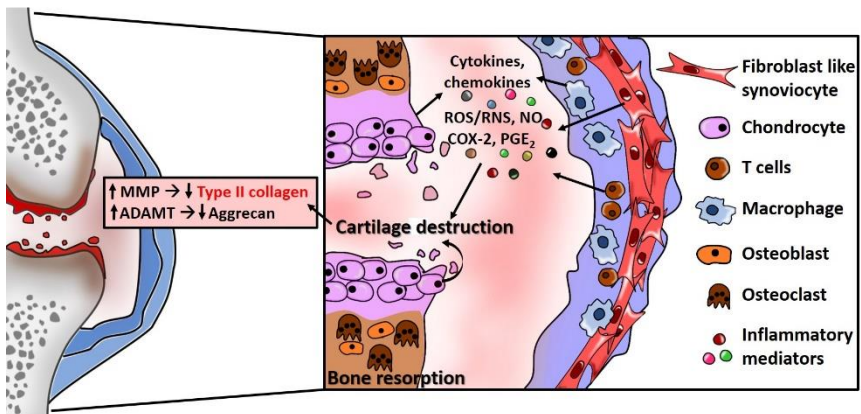


**Figure 2.** Main non-immune and immune cells participating in OA through the release of pro-inflammatory factors (cytokines, chemokines, NO, ROS, PGE<sub>2</sub>, COX-2) and proteolytic enzymes (MMP, ADAMT).

**Synoviocytes.** Synovitis and synoviocytes have demonstrated to be key effectors in chronic inflammatory diseases like RA [38]; however, its participation and role in OA is now widely accepted. In the inflamed synovium, resident FLS react to external inflammatory stimuli by releasing pro-inflammatory factors that induce a phenotypic shift in chondrocytes, further stimulate synoviocytes and attract immune cells [26]. A vicious cycle follows, as chondrocytes produce additional cytokines and proteolytic enzymes that eventually increase cartilage degradation and induce further synovial inflammation [39].

**Osteoblasts, osteocytes and osteoclasts.** Osteoblasts, osteocytes and osteoclasts are responsible of bone production and destruction by producing bone ECM proteins and inducing osteoclastogenesis [40]. Subchondral bone remodeling during OA has also a relationship with inflammation and degradation of the overlying articular cartilage. These bone cells are exposed to various pro-inflammatory cytokines produced by osteoarthritic chondrocytes and immune cells stimulating further bone remodeling; while inflammatory factors secreted by bone cells can induce chondrocyte changes stimulating cartilage degradation and demonstrating the crosstalk between cartilage and bone cells [41,42].

### 1.2.2. Immune cells

Most frequent types of immune cells found in OA are macrophages, mast cells, natural killers (innate immunity) and T cells (adaptive immunity) [43].

**Macrophages.** Macrophages ( $M_0$ ) are one of the most abundant cells present in the synovial infiltrates of OA patients [44]. They are phagocytic cells that can be found in almost every tissue with the function of maintaining tissue homeostasis and protecting the host from infections. Despite they are critical components of innate immunity, macrophages are capable of participating in the adaptive immune system by secreting inflammatory mediators [45]. In response to an inflammatory stimulus (*e.g.* interferon- $\gamma$  (IFN- $\gamma$ ), bacterial lipopolysaccharides (LPS) or TNF- $\alpha$ ),  $M_0$  are “classically activated” to their  $M_1$

pro-inflammatory phenotype usually through TLR, acquiring antimicrobial and pro-inflammatory functions such as the secretion of pro-inflammatory factors like PGE<sub>2</sub>, IL-1 $\beta$ , TNF- $\alpha$ , IL-6, ROS and NO [46,47]. M<sub>0</sub> can also be “alternatively” activated into M<sub>2</sub> macrophages in the presence of molecules such as IL-4 and IL-13, acquiring anti-inflammatory and pro-resolving effects like the secretion of anti-inflammatory molecules (*e.g.* IL-4, IL-10 and TGF- $\beta$ ) [48,49]. The imbalance between pro- and anti-inflammatory macrophages may lead to chronic low-grade inflammation and has been suggested to be critical in the development of several musculoskeletal diseases, including OA [48].

**Mast cells.** Mast cells are considered regulators of vascular permeability and also to have a role in OA joint inflammation by facilitating leukocyte infiltration [50]. Mast cells are capable of attracting other immune cells through the release of cytokines and chemokines, activating the inflammatory response and leading to cartilage and bone destruction [51]. In addition, they could also contribute to pain in OA, as they have been implicated in pain perception in several disorders [52].

**Natural killers (NK).** Although NK cells are classically known for their role in killing virally infected cells or tumor cells, they also infiltrate in the synovial tissue during OA. Upon activation, NK cells perform their cytotoxic activity by secreting proteases called granzyme A and B [53]. While granzyme B leads to cell death upon perforin-mediated internalization inside of target cells; granzyme A acts as a pro-inflammatory molecule regulating the production of pro-inflammatory cytokines like IL-1 $\beta$ , TNF- $\alpha$ , IL-6 and IL-8 [54–56].

**T cells.** Although the innate immunity appears to be predominantly in OA, T cells also appear to have a role in its pathogenesis [57]. T cells can be broadly classified into helper T cells (Th cells) and cytotoxic T cells (Tc cells). The Th cells (CD4+) secrete cytokines to stimulate proliferation and differentiation of cells involved in the immunologic response, while Tc cells (CD8+) are effector cells that eliminate targeted cells. Th cells appear in osteoarthritic patients infiltrates [58], where are able to stimulate monocytes to express several cytokines that contribute to the development of OA through

direct cell-cell contact or through soluble mediators such as IFN- $\gamma$  and IL-17 [59,60]; and also control osteoblasts and osteoclast leading to bone resorption [61].

### 1.2.3. Signaling pathways

Both mechanical stress and inflammatory mediators may induce an array of downstream signaling pathways in cells found in articular joints that regulate the expression of inflammatory and catabolic factors. The nuclear factor-kappa B (NF- $\kappa$ B) pathway is one of the main regulators of the inflammatory cytokine-induced catabolic actions in chondrocytes, synoviocytes and macrophages [62]. The NF- $\kappa$ B signaling pathway begins with the activation of I $\kappa$ B kinase, which phosphorylates the inhibitory protein I $\kappa$ B, normally bound to the NF- $\kappa$ B transcription factor. The previously cytoplasmic located NF- $\kappa$ B transcription factor is free to translocate to the nucleus [63,64]. These events activate the expression of several genes implicated in cartilage destruction, synovitis and increased subchondral bone resorption like the ones coding for MMP, ADAMTS, NO, COX-2, cytokines and chemokines [65].

Besides the NF- $\kappa$ B signaling pathway, the binding of inflammatory mediators to their respective receptors on the cell membrane can activate the stress-induced and mitogen-induced protein kinase (MAPK) pathways through extracellular signal-regulated kinase (ERK), c-Jun N-terminal kinase (JNK), and p38 kinase cascades [66]. The activation of these cascades coordinates the induction and activation of transcription factors, including members of the activator protein 1 (AP-1), ETS, and C/EBP families [30]. These transcription factors regulate the expression of genes relevant to OA including genes involved in the inflammatory response, regulation of cell proliferation, and production of matrix degrading enzymes [65]. JNK may be particularly important because of its unique ability to activate c-Jun, a key AP-1 component. In addition to promoting MMP expression, AP-1 can regulate the expression of pro-inflammatory cytokines such as TNF- $\alpha$  and IL-1 $\beta$ , cytokines that then act in an autocrine or paracrine manner to maintain JNK activation and activate JNK in additional cells, further increasing cytokine and MMP production [67,68].

The Janus kinase/Signal Transducers and Activators of Transcription (JAK/STAT) pathways also have a role in OA. Phosphorylation of STAT proteins *via* JAK activation facilitates STAT proteins to act as transcription factors in inflammation [64,69]. Depending on the inflammatory stimuli different signaling pathways can be activated. For example, LPS activates the NF- $\kappa$ B pathway [63], IL-1 $\beta$  is noted to predominantly activate the MAPK pathway [70] and IL-6 predominantly activates the JAK/STAT [71].

### 1.2.4. Inflammatory mediators

Cartilage destruction and synovial membrane inflammation are currently attributed to a complex network of biochemical factors, including proteolytic enzymes, inflammatory cytokines and chemokines, ROS, NO and PGE<sub>2</sub> secreted by activated chondrocytes, synoviocytes and immune cells [72].

**Proteolytic enzymes.** The effects of OA abnormal mechanical loading and synovial inflammation likely contribute to dysregulation of chondrocyte function, favoring the imbalance between the catabolic and anabolic activities of chondrocytes in remodeling cartilage ECM [73]. Collagen and aggrecan are the primary structural components of the cartilage ECM, and their degradation correlates with the progression of OA. MMP and ADAMTS are the main effectors in cartilage destruction due to the degradation of both collagen and aggrecan. The most common MMP found in OA are the collagenases MMP-1, -3, -8 and -13 [74] while the major aggrecan-degrading enzymes, ADAMTS, are ADAMTS-4 and -5 [75,76]. These proteolytic enzymes are activated by multiple cytokines like IL-1 $\beta$ , TNF- $\alpha$ , IL-6 and several chemokines [65]. A tight regulation of these proteolytic enzymes activity is critical for maintaining the balance between cartilage anabolism and catabolism. The tissue inhibitors of metalloproteinases (TIMP) are endogenous inhibitors of MMP and ADAMTS. MMP are strongly inhibited by TIMP-1, -2, -3 and -4 while ADAMTS-4 and -5 are effectively inhibited only by TIMP-3. In OA, the imbalance between TIMP and proteases favors cartilage catabolism [77].

**Cytokines and chemokines.** TNF- $\alpha$ , IL-1 $\beta$  and IL-6 along with other cytokines (*e.g.* IL-2, IL-7, IL-15, IL-17, IL-18) are among the most common



inflammatory factors noticed in the synovial fluid of OA patients [78]. TNF- $\alpha$  and IL-1 $\beta$  are considered the major mediators in the physiopathology of OA and are secreted not only by immune cells but also by chondrocytes and synoviocytes [79]. Cytokine signaling is organized as a cascade in which a primary cytokine acting upon a receptor leads to the expression of one or more secondary cytokines and so on. TNF- $\alpha$  and IL-1 $\beta$  are two of the cytokines often observed near the top of such signaling cascades [80].

Chondrocytes are the major cellular targets for IL-1 $\beta$ , activated through the binding of its specific receptor type I (IL-1RI) [81]. Destructive effects of IL-1 $\beta$  in OA include both elevation of cartilage catabolism and suppression of cartilage anabolism. Regarding the promotion of cartilage destruction, IL-1 $\beta$  upregulates MMP-1, -3 and -13 and ADAMTS-4 and -5 [65], and also pro-inflammatory mediators like other cytokines, chemokines and angiogenic factors. Apart from the increased degradation of cartilage ECM, IL-1 $\beta$  can decrease ECM synthesis by downregulating collagen type II and aggrecan synthesis, or inducing chondrocyte apoptosis [82].

IL-1 $\beta$  stimulates also the expression of TNF- $\alpha$  and surface expression of TNF receptor (TNFR) in chondrocytes. Binding of TNF- $\alpha$  to TNFR causes signal transduction and activates TNF receptor-associated factor 2 (TRAF2) that, in turn, activates important transcription pathways in the course of OA such as NF- $\kappa$ B, JNK, ERK and MAPK [65,78]. The effect of TNF- $\alpha$  in most cases coincides with the action of IL-1 $\beta$  in terms of cartilage destruction, and normally both act in a synergistic way. Besides, both, IL-1 $\beta$  and TNF- $\alpha$  increase the synthesis of PGE<sub>2</sub> by stimulating the gene expression or activities of COX-2, microsomal PGE synthase-1 (mPGES-1), and phospholipase A<sub>2</sub> (PLA<sub>2</sub>), and they upregulate the production of NO *via* inducible nitric oxide synthase (iNOS) [30]. IL-1 $\beta$  and TNF- $\alpha$  can also induce other pro-inflammatory cytokines, such as IL-6, IL-17, IL-18, LIF and chemokines, including IL-8; that synergize with one another in promoting chondrocyte catabolic responses [80,83].

IL-6 is also one of the keystone cytokines in OA. Its signaling pathways involve the activation of membrane bound IL-6 receptors (IL6R) or soluble IL6R (sIL6R) followed by the activation of several transduction pathways, recruiting

mononuclear cells like monocytes to the inflamed joint area [71,78]. Its production can be simulated by several cytokines including IL-1 $\beta$  and PGE<sub>2</sub>. Its effect on articular cartilage is not different from other cytokines and, in synergy with them, causes a decrease in the production of type II collagen and increases the production of MMP [83].

Some anti-inflammatory cytokines including IL-4, IL-10, IL-13 and TGF- $\beta$  usually limit the inflammatory response and are overproduced during OA [83]. They are associated with chondroprotective effects by reducing MMP and, therefore, the degradation of cartilage [79].

Chemokines are a subfamily of cytokines with low  $M_w$  which are classified into four families (CXC, CC, C, and CX3C), depending on the position of the cysteine (C) residues [84]. They act as chemoattractants, directing the migration of immune cells to damaged sites. Apart from their role as recruiters of immune cells, most of these chemokines, such as IL-8/CXCL-8, MCP-1/CCL-2, RANTES/CCL-5, MIP-1 $\alpha$ /CCL-3, MIP-1 $\beta$ /CCL-4 or IP-10/CXCL-10; have a key role in the pathogenesis of OA, inducing the production of MMP upon binding to their ligands [80,85].

In order to evaluate the immunomodulatory activity of the NPs, the cellular production of multiple cytokines (IL-1 $\beta$ , TNF- $\alpha$ , IL-6, IL-10) and chemokines (RANTES, MCP, MIP, IL-8) by both, a murine macrophage cell line (RAW264.7) and human articular chondrocytes (HC-a), has been *in vitro* tested in Chapters III and IV.

**Reactive oxygen and nitrogen species (ROS/RNS).** ROS/RNS are free radicals containing oxygen and nitrogen molecules including OH $^\cdot$ , H<sub>2</sub>O<sub>2</sub>, O<sub>2</sub> $^\cdot$  or NO $^\cdot$ . The presence of unpaired electrons in the valence shell causes ROS/RNS to be short-lived, unstable and highly reactive in order to achieve stability [86]. Oxidative stress, referred to elevated intracellular levels of ROS/RNS that cause damage to lipids, proteins and DNA; has a pivotal role in OA by the activation of several inflammatory pathways like JNK and NF- $\kappa$ B and downstream inflammatory gene induction, antioxidant gene transcription, and cytokine secretion [83,87]. NO is one of the main contributors to OA pathogenesis,

which is synthesized by a family of enzymes termed the NO synthases (NOS). The synthesis of NO is catalyzed by the inducible NO synthase (iNOS), which is not typically present in cells but expressed in response to different stimuli such as pro-inflammatory cytokines [83,88]. An excess of NO by chondrocytes or immune cells like macrophages lead to the release of inflammatory cytokines, the inhibition of both proteoglycan and collagen synthesis, the activation of MMP and chondrocyte apoptosis [89]. In this thesis, the NP effect on ROS and NO levels was assessed to study the radical scavenging and the anti-inflammatory properties of the NPs.

**Lipid mediators.** Pro-inflammatory cytokines like IL-1 $\beta$  or TNF- $\alpha$  lead to the activation of the enzyme PLA<sub>2</sub> which converts phospholipids of the cell membrane into arachidonic acid (AA), which is the substrate of two major enzymes COX or lipoxygenase [90]. The COX enzyme has two main isoforms, COX-1 and COX-2. While COX-1 exists constantly in our body and is primarily responsible for the production of thromboxanes and prostaglandins (PGs) that regulate normal body functions, COX-2 is expressed during an inflammatory response and induces PGs related to inflammation, pain and fever. PGE<sub>2</sub> is the most abundant PG in the human body and an excessive production has been reported in the synovial fluid of OA patients [91]. Besides its pro-inflammatory effects, PGE<sub>2</sub> inhibits chondrocyte proliferation and promotes MMP production, osteoclastic bone resorption and angiogenesis [92]. The anti-inflammatory effect of the NPs was also evaluated in terms of reduction of PGE<sub>2</sub> release by RAW264.7.

In this thesis, human chondrocytes have been used as non-immune cells to assess the cytotoxicity in the long term, the cellular uptake and the immunomodulatory activity of the developed systems, *i.e.* the loaded nanoparticles (NPs) described in Chapters III and IV. On the other hand, RAW264.7 macrophages were used to assess the cytotoxicity, cellular uptake, radical scavenging capacity and the immunomodulatory effect of the NPs. The immunomodulatory activity was evaluated in terms of reduction of inflammatory mediators using different enzyme-linked immunoabsorbent assays (ELISA) and the Griess test to quantify the NO production.

### 1.3. Management of OA

#### 1.3.1. Traditional treatments

Since OA is a chronic and non-reversible condition, the current management is primarily based on symptomatic treatments, directed to reducing pain and slowing disease progression. This requires a combination of non-pharmacological and pharmacological treatments that will depend on the symptomatology of the patient, as presented in figure 3. Treatment guidelines for the management of OA have been developed by the European League Against Rheumatism (EULAR), Osteoarthritis Research Society International (OARSI) and the American College of Rheumatology (ACR), based on research evidence.

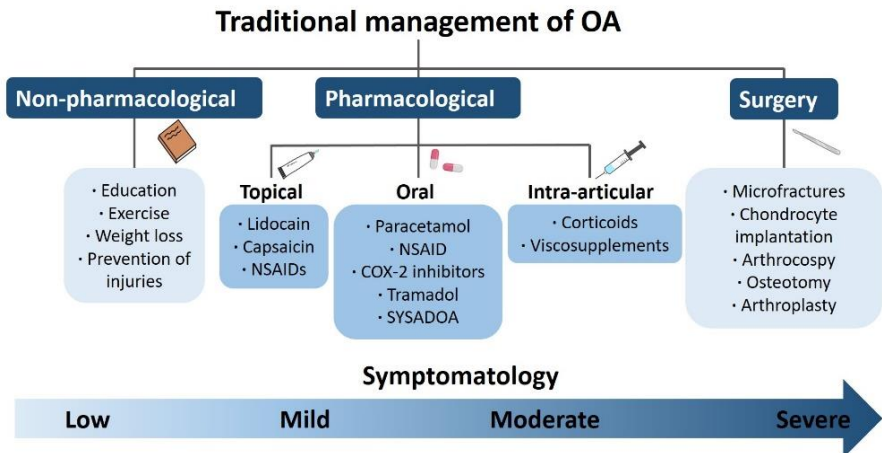


**Figure 3. Scheme of the traditional management of OA. The treatment approach depends on the severity of the symptoms and includes non-pharmacological therapies, pharmacological therapies and surgery.**

Non-pharmacological therapies are recommended for all patients and include education, self-management, weight loss, aerobic exercise and periarticular muscle strengthening [93c95]. Pharmacological therapies are the most common option for managing OA. Depending on the severity of the disease, physicians can recommend from simple analgesics to surgery. Usually, the treatment at the earliest stages of OA is based on the use of chondroprotective substances or slow-acting drugs for OA (SYSADOA) including

glucosamine, chondroitin sulfate and HA (cartilaginous matrix precursors) and diacerin (a cytokine modulator) [96]. SYSADOA provide symptomatic relief by targeting the underlying pathology of OA, but their efficacy in pain reduction is controversial and established as uncertain by the OARSI and ACR [97]. However, they are used due to their negligible minor side effects.

Patients with low to mild pain use short-term analgesics, *i.e.* paracetamol or tramadol, although their use is associated with adverse hepatic effects, multi-organ failure in the case of paracetamol [98], or constipation, nausea and dizziness in the case of tramadol [99]. When pain reaches mild to moderate levels and analgesics are not enough to relieve pain, traditional nonsteroidal anti-inflammatory drugs (NSAIDs) such as ibuprofen or diclofenac are used [100]. The main problem of NSAIDs for their long-term use is the secondary effects related to gastrointestinal, cardiovascular and hepatic problems [101].

Other option is the use of selective COX-2 inhibitors or coxibs, a subclass of NSAIDs that directly targets COX-2. This selectivity reduces gastrointestinal side effects, but some studies indicate that COX-2 inhibitors are related to increased cardiovascular problems [102,103]. Topical agents can be used as complements or alternatives to oral analgesics, especially for elderly people, due to their safer profile compared to oral NSAIDs [104]. ACR, OARSI and EULAR guidelines recommend the use of capsaicin as a topical analgesic for pain control [93–95]. In addition, lidocaine patches can be used as topical analgesics although there is small evidence of their efficacy [105].

Intra-articular therapies are commonly used in OA management when patient symptoms are severe, especially for knee OA. Corticoids injections are widely used to treat synovitis and pain in OA patients. Corticoids are anti-inflammatory drugs with several mechanisms of action. The most commonly used for OA treatment are crystalline triamcinolone and non-crystalline prednisolone and methylprednisolone. There is evidence that corticoids provide short-term pain relief but lack long-term effects due to their rapid elimination from the synovial cavity [106,107]. Moreover, the formation of crystals due to the crystalline nature of steroids may cause transient

inflammation of synovium, and repeated injections can damage articular cartilage [108].

Another conservative treatment for OA is the intra-articular injection of exogenous HA, also known as viscosupplementation. Viscosupplements were approved by the US Food and Drug Administration (FDA) in 2001, although there are not clear recommendations about its use. The rationale behind intra-articular HA injections is the restoration of the viscoelastic properties of synovial fluid [109].

Finally, most severe OA cases may require surgical treatments as the last procedure when pharmacological therapies have failed. These interventions are costly and highly invasive and include microfractures, osteotomy, arthroscopy, total joint arthroplasty or transplantation of articular cartilage and autologous chondrocytes in younger patients [110].

### **1.3.2. Emerging pharmacological therapies**

The traditional management of OA fails to modify the progression of the disease and to prevent long-term disability. Therefore, novel strategies including those targeting matrix-degrading proteases or inflammatory cytokines and chemokines, promoting cartilage repair or limiting bone remodeling are emerging as disease modifying OA drugs (DMOADs) [111]. Preclinical data have underlined multiple novel therapeutic targets in OA, some showing promising results in phase II-III clinical trials.

As cartilage deterioration is one of the major characteristics of osteoarthritic joints, different strategies trying to balance the synthesis and breakdown of cartilage ECM have reached clinical investigations. On the one hand, great efforts are being made to inhibit proteases such as ADAMTS-5 or MMP-13 using active site drug inhibitors or blocking antibodies [112,113]. Senolytic drugs have also raised as a potential disease modifying therapy, eliminating senescent cells, which secrete pro-inflammatory factors and matrix degrading enzymes [114]. On the other hand, the impairment of some growth factors in osteoarthritic joints have led to the intra-articular injection of some

of them such as the TGF- $\beta$  or the recombinant human fibroblast growth factor 18 (FGF18), also known as sprifermin, in order to induce cartilage regeneration [115]. In particular, sprifermin has demonstrated to prevent cartilage loss and protect subchondral bone in the short-term in OA patients, although long-term follow up is needed to determine if this effect is maintained over time [116,117].

The suppression of subchondral bone resorption is also an emerging target for managing OA. Bisphosphonates, which are commonly used drugs for the treatment of diseases involving excessive resorption of bone, such as osteoporosis, are the most used anti-resorptive substances for OA treatment and have shown to reduce pain, stiffness and accelerating functional recovery of patients in different clinical trials [118,119]. Cysteine cathepsin K is a key proteolytic enzyme in osteoclastic bone resorption able to cleave type II collagen and is up-regulated in OA patients [120]. Some cathepsin K inhibitors have shown to reduce bone and cartilage damage in phase II clinical trials while the investigations of others had to be stopped due to serious patient complications [121].

The inflammatory component of OA triggered by multiple inflammatory mediators such as IL-1 $\beta$  or TNF- $\alpha$  makes the inhibition of these cytokines an appealing approach to treat OA. However, no positive effects on OA symptoms have been confirmed yet in clinical trials. For example, anakinra, an IL-1 receptor antagonist (IL-1Ra) [122] and AMG108 antibody specific for IL-1 receptor type 1 that inhibits both IL-1 $\alpha$  and IL-1 $\beta$  [123] did not show symptomatology improvement in OA patients. In the same line, anti-TNF- $\alpha$  antibody adalimumab could not reduce OA patients in the short-term [124,125] but in the long-term it decreased joint erosion [126], similar to what happened with the long-term use of etanercept [127]. A promising strategy for the reduction of inflammation is the oral use of methotrexate. This chemotherapeutic drug, normally used to treat RA, has demonstrated in different studies to alleviate pain and clinical synovitis when was orally administrated to OA patients [128].

Pain is a basic symptom in OA patients. Its mechanism in OA is complex and not directly derived from tissue damage, as demonstrated by the disagreement between pain and structural damage in affected joints [129]. Although cartilaginous tissue is aneural and avascular, the synovium, ligaments, tendons meniscus and the subchondral bone present sensory nerves. Therefore, strategies targeting pain have their part in the emerging treatment therapies of OA. The nerve growth factor (NGF) is a neurotrophin involved in peripheral sensitization and an important regulator of OA pain. Some NGF inhibitors like anti- NGF neutralizing antibodies such as tanezumab have demonstrated greater effects in terms of patient pain reduction [130].

### **1.3.3. Surgical and emerging biological therapies**

The use of biologics to treat articular conditions is coming to the forefront of mainstream medicine, due to their potential to modify the disease and regenerate cartilage instead of just palliate the symptomatology, but there is a lack of consensus about their use and efficacy [131]. Some biological therapies are currently used in clinical practice. For example, the surgical technique based on performing microfractures in the subchondral bone takes advantage of the blood clot formed after the microfractures that contains precursor cell populations from the subchondral bone marrow. However, this technique usually leads to a fibrocartilaginous repair tissue [132]. Other example is the autologous chondrocyte implantation (ACI), in which a mass of cartilage from the patient is collected, the cartilage ECM is enzymatically eliminated and chondrocytes are isolated and cultured for their reimplantation. The ACI technique was followed by the matrix-assisted ACI (MACI), where chondrocytes are embedded in a matrix scaffold for their reimplantation. Although no severe clinical safety issues have been associated with the ACI technique, there are still some limitations such as reduced number of available cells, requirement of multiple surgical procedures, *in vitro* chondrocyte dedifferentiation or donor-site morbidity caused by cartilage harvest [133]. Figure 4 summarizes the main surgical therapies being employed in clinical practice along with the emerging biological therapies that are being used and investigated to treat OA.



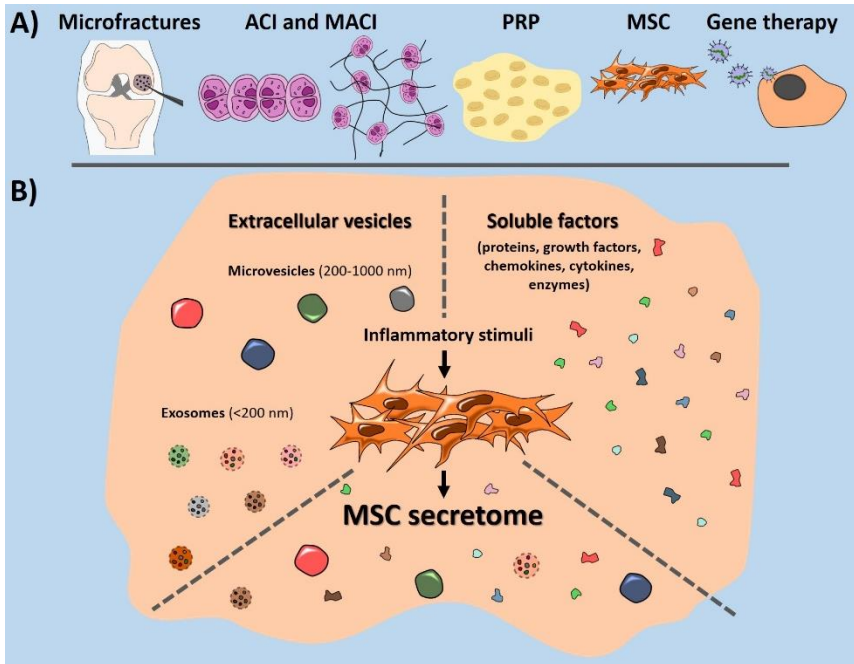


**Figure 4. A) Biological therapies for the treatment of OA: microfractures, autologous chondrocyte implantation (ACI) and matrix-assisted ACI (MACI), platelet-rich plasma (PRP), mesenchymal stem cells (MSC) and gene therapy. B) MSC derive secretome components: extracellular vesicles (microvesicles and exosomes) and soluble factors.**

Nowadays, the most investigated biological-based treatments are the intra-articular injection of platelet rich plasma (PRP), bone marrow aspirate concentrate (BMAC) and stem cells-based products [134]. Despite more research is needed to determine the long-term benefit of these therapies in the progression of OA, recent studies support that patients who receive those injections experience symptomatic relief and functional improvement [135].

Intra-articular PRP injections have gained attention due to its anti-inflammatory and anabolic properties [136]. In fact, PRP administration is currently applied in clinical practice since it is not considered a ‘drug’, as it comes from the blood of the patients, and is not subjected to FDA approval before they can be used in clinics. PRP is a concentrate of platelet-rich plasma

derived from autologous blood samples and obtained by a two-step centrifugation in which platelets are concentrated from fourfold to eightfold as compared to untreated blood [137,138]. The activation of PRP *via* the addition of calcium chloride or thrombin, among other, induces the degranulation of platelets and the release of different growth factors entrapped in the platelet granules including platelet-derived growth factor, epidermal growth factor (EGF), insulin like growth factor 1 (IGF-1) and vascular endothelial growth factor (VEGF) [139]. These growth factors have the ability to modulate tissue healing and matrix synthesis and, therefore, cartilage repair. Numerous clinical trials are being carried out in order to demonstrate the efficacy in the long-term of PRP treatments, especially in comparison to HA viscosupplementation therapy. The majority conclude better clinical outcomes in terms of pain relief and joint function in patients treated with PRP, although most of them claim that further investigations are needed [140–145].

As a paradigm of tissue engineering and regenerative medicine, stem cells (SC) are being extensively studied for the treatment of OA. In particular, mesenchymal stem cells (MSC) are of great interest due to their ability to differentiate into different cell types and their implication in multiple biological processes such as tissue repair, angiogenesis or immunomodulation [146]. Overall, the preliminary results demonstrated that MSC-based therapy is encouraging in reducing pain and improving joint function [147–149]. However, the efficacy of this cell approach may be impaired by cell manipulation, and its wide application is strongly limited by regulatory issues [150]. Besides, great heterogeneity in methodologies is found and more clinical trials with a larger number of patients and long-term follow-up are required before full-scale clinical translation.

Since MSC disappear from the target tissue quickly after administration but are still able to perform chondroprotective and immunomodulatory effects, their therapeutic efficacy seems to be independent of their engraftment and related to paracrine mediated effects [151]. MSC release multiple molecules, especially when stimulated with pro-inflammatory factors, like soluble factors, proteins, enzymes, growth factors, cytokines and chemokines apart from greater vesicles such as microvesicles or

exosomes (see figure 4) [152]. This heterogeneous collection of factors, called MSC derived secretome or conditioned medium could be used as an acellular regenerative therapy solving some of the limitations presented in the direct use of MSC [153]. Therefore, it is being investigated for its therapeutic use against OA with positive effects *in vitro* and *in vivo* in terms of anti-inflammatory and chondroprotective activity [151,154].

Bone marrow is one source of MSC as well as growth factors and cytokines that may aid anti-inflammation and regeneration of cartilage and bone. However, MSC in bone marrow usually occupy only a small fraction of nucleated cells [155]. In this context, the use of the so called bone marrow aspirate concentrate (BMAC), currently approved by the FDA, has gained attention in last years since, apart from MSC, it contains a plethora of bioactive molecules, growth factors, cytokines immune cells and platelets [156,157]. Recent clinical studies have reported relatively favorable effects of BMAC injection but, as in the case of the rest of biological therapies, there is a need for well-designed, randomized, controlled trials with large sample sizes to further evaluate the therapeutic action of BMAC [158–160].

Gene-based treatment approaches are an alternative strategy that enable the spatiotemporal control and persistent synthesis of gene products at target sites [135]. By delivering genes encoding growth factors, cytokines or anti-cytokines, or proteinase inhibitors to target cells through viral or non-viral vectors, modified cells can be directed to overproduce the desired protein into the synovial cavity continuously in large concentrations [161]. One promising example of gene therapy is TissueGene-C, a biological strategy consisting of intra-articularly injecting allogenic chondrocytes transduced with a retroviral vector to express TGF- $\beta$ 1, which has demonstrated to palliate patient symptoms in phase II and III clinical trials [162,163].

In this thesis, MSC derived secretomes for the intra-articular treatment of OA has been explored; initial results are shown in confidential Chapter VI.

## 2. Anti-inflammatory drugs for OA treatment

Non-pharmacological therapy based on education, exercise, weight loss and the prevention of injuries can have a significant impact on reducing pain and disability and the guidelines recommend them in the first instance. Besides, dietary supplements like glucosamine and chondroitin sulfate and natural herbal supplements like curcumin (CUR) or fish oil can help to palliate the symptomatology in low stages of OA. Nonetheless, when pain is not sufficiently alleviated, pharmacological treatment based on analgesics and anti-inflammatory drugs are recommended. Among the anti-inflammatory drugs used to treat OA, oral or topical NSAIDs and coxibs and intra-articularly injected corticoids are the most used. These drugs exert their anti-inflammatory effect by different routes but basically inhibiting the production of cytokines and lipid mediators.

In this work, two NSAIDs, tenoxicam and celecoxib, in addition to dexamethasone or the natural polyphenol curcumin, were encapsulated into a polymeric nanovehicle to reduce their cytotoxicity and improve their stability in aqueous media (Chapters III and IV). The immunomodulatory effect of the drug-loaded nanoparticulated systems was evaluated in terms of inflammatory mediators release by HC-a and RAW264.7.

### 2.1. Natural anti-inflammatory compounds: curcumin

Although NSAIDs and corticoids are the most widely used anti-inflammatory agents for the treatment of chronic inflammatory pathologies like OA, the side effect profiles of both lead to an increasing interest in natural compounds, such as dietary supplements and herbal remedies, which have been used for centuries to reduce pain and inflammation. Many of these natural compounds also work by inhibiting inflammatory pathways in a similar manner as NSAIDs or corticoids [164]. Some examples of this natural anti-inflammatory agents are fish oil, green tee, resveratrol or CUR.

CUR is one of the most investigated natural agents due to its multiple pharmacological activities such as antioxidant, anti-inflammatory, anti-bacterial, anti-viral, anti-cancer and neuroprotective properties [165]. It is a natural hydrophobic polyphenol extracted from the rhizome of turmeric with a long history of use in traditional medicines of China and India. [166]. It presents a characteristic yellow-orange color and have very low water solubility ( $3.12 \text{ mg mL}^{-1}$ ) [167]. While it seems to have countless therapeutic properties, most of them are due to its antioxidant and anti-inflammatory effects. CUR has demonstrated to be a highly pleiotropic molecule capable of interacting with numerous molecular targets involved in inflammation (*e.g.* transcription factors, protein kinases, enzymes, growth factors, inflammatory mediators, anti-apoptotic proteins) [168]. It inhibits the activity of NF- $\kappa$ B, MAPK and JAK/STAT pathways and activates the peroxisome proliferator-activated receptor-gamma (PPAR- $\gamma$ ), as observed in figure 5. It also acts as an antagonist of iNOS and has radical scavenging properties, reducing both NO and ROS [169–171].

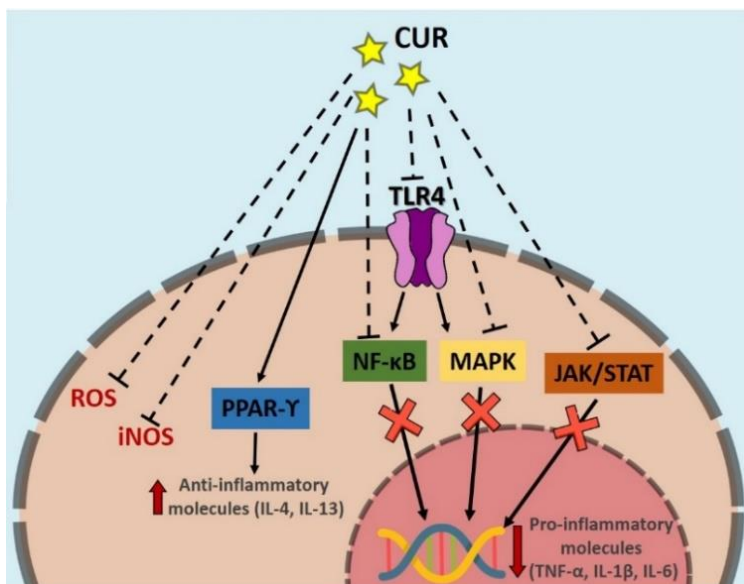


**Figure 5. Anti-inflammatory mechanisms of CUR through the inhibition of NF- $\kappa$ B, MAPK and JAK/STAT pathways, ROS and iNOS and the activation of the PPAR- $\gamma$  pathway.**

## 2.2. NSAIDs

NSAIDs are the most prescribed drugs worldwide due to their potent analgesic, anti-inflammatory, and antipyretic effects. Their mechanism of action is primarily based on the inhibition of the COX enzymes which take part in the biosynthesis of PGs and thromboxanes from AA (see figure 6) as explained in the subsubsection *Inflammatory mediators* of subsection 1.2.4. [172].

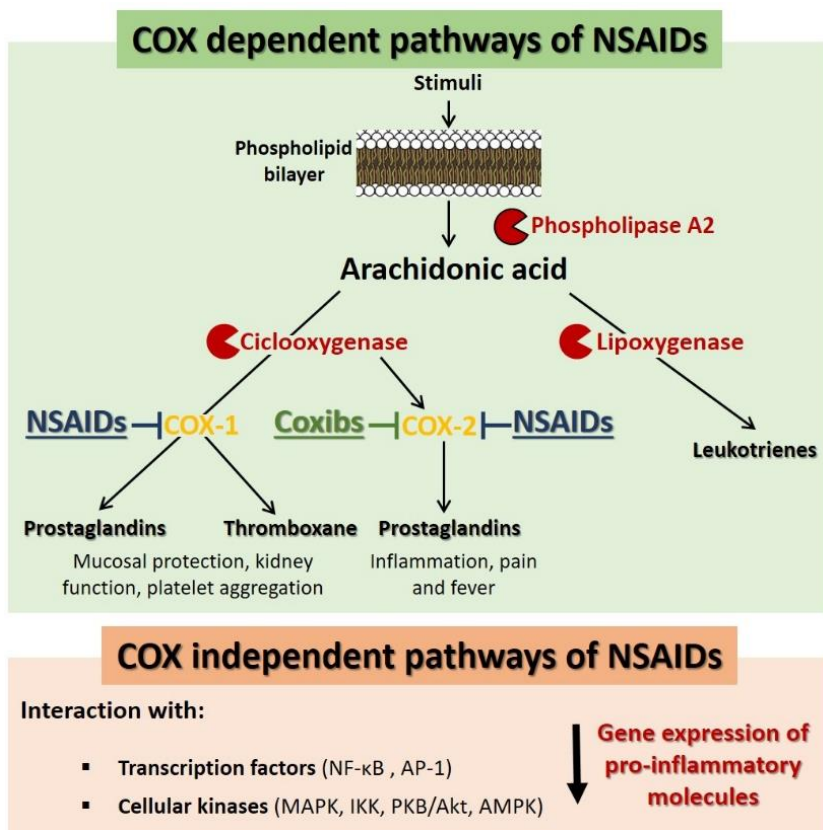


**Figure 6. Scheme of the anti-inflammatory effect of traditional NSAIDs through COX dependent and independent pathways.**

NSAIDs can be classified according to their COX selectivity. Traditional non-selective NSAIDs (such as aspirin, ibuprofen, naproxen and the oxicam

family), inhibit both COX-1 and COX-2 while coxibs or selective COX-2 inhibitors only target COX-2 and, as a consequence, have different side effect profiles. In fact, coxibs were developed with the prime object of minimizing gastrointestinal adverse effects of NSAIDs due to their inhibition of the mucosal protection effect of COX-1. However, coxibs present other side effects like increased cardiovascular risk [102,173] or adverse renal effects [174]. Table 2 summarizes the selectivity of some relevant NSAIDs used to treat OA referred as an  $IC_{50}$  value (the concentration at which NSAIDs produce 50% inhibition of COX-1 and/or COX-2). A selectivity index is then calculated from the ratio  $COX-1\ IC_{50}/COX-2\ IC_{50}$ .

**Table 2.  $IC_{50}$  values for the inhibition of COX-1 and COX-2 of relevant NSAIDs using human whole blood assays, selectivity index (ratio  $COX-1\ IC_{50}/COX-2\ IC_{50}$ ) and clinical doses to treat OA. Data adapted from [175].**

NSAID	$IC_{50}$ ( $\mu$ M)		Selectivity index	Clinical dose (mg)
	COX-1	COX-2		
Aspirin	1.7	>100	0.017	-
Diclofenac	0.075	0.038	1.97	100-150
Ibuprofen	7.6	7.2	1.05	1200-3200
Meloxicam	5.7	2.1	2.7	7.5-15
Paracetamol	>100	49	>2.04	2600-4000
Celecoxib	6.7	0.87	7.7	50-400
Etoricoxib	116	1.1	105.4	60

Since aspirin was reported to inhibit NF- $\kappa$ B activation [176], there is increasing evidence that some NSAIDs have various biological effects that are independent of the COX activity and may account for their anti-inflammatory effects. These COX-independent pathways occur largely at drug concentrations above the  $IC_{50}$  for COX-inhibition and, consequently, happen at high concentrations [177]. NF- $\kappa$ B and AP-1 transcription factors are two of the targets of some NSAIDs such as aspirin or ibuprofen, in the case of NF- $\kappa$ B; and aspirin, piroxicam or CLX, in the case of AP-1. Both regulate the expression of various pro-inflammatory genes, like those encoding cytokines and chemokines, and regulate the survival, activation and differentiation of innate immune cells and inflammatory T cells [63,178]. Thus, their suppression by some NSAIDs can lead to a reduction of several pro-inflammatory mediators.

The interaction of NSAIDs with different cellular kinases like MAPK, inhibitor  $\kappa$ B kinase complex (IKK), protein kinase B (PKB/Akt) or AMP-Activated kinase (AMPK) are other COX-independent anti-inflammatory mechanisms of some NSAIDs as CLX, leading to the reduction of multiple pro-inflammatory mediators [177,179].

TNX is a thienothiazine derivative of the oxicam class of NSAIDs that was patented in 1974 by Roche and approved for medical use in 1987. It is used as an analgesic and anti-inflammatory agent because of its prolonged half-life for the symptomatic treatment of OA, rheumatoid arthritis, ankylosing spondylitis and various rheumatic conditions [180]. Its solubility in water is relatively low ( $14.1 \text{ mg mL}^{-1}$ ) but it can be completely absorbed when taken orally [181,182]. For OA, it is mainly administered intra-articularly to provide postoperative analgesia. There is scarce and recent research on the use of TNX in OA. Nevertheless, latest investigations have been focused on its encapsulation into microparticles (MPs) to reduce its toxicity [183], its incorporation into hydrogels for its topical application [184,185] or the evaluation of its efficacy when injected intra-articularly alone [186,187] or in combination with other agents [188,189].

CLX was the first COX-2 inhibitor approved by the FDA, in 1998, for the treatment of OA and RA, due to its good selectivity for the COX-2 enzyme and for its gastrointestinal tolerability. It presents quite low water solubility  $4.3 \text{ mg mL}^{-1}$ , compromising its bioavailability [190], although it is mainly administered orally (doses from 100 to 400 mg) to relieve pain associated to OA. In the case of CLX, abundant recent investigations can be found about its use in OA. For example, its clinical efficacy compared to other treatments is being extensively tested [191–194]. Moreover, its encapsulation into multiple drug delivery systems (DDS) like MPs [195,196] to treat arthritic conditions is also under study. Furthermore, the widely demonstrated relationship between cancer and inflammation has made the use of several anti-inflammatory molecules like CLX to prevent or treat cancer to be in the spotlight in last years, due to the COX-2 overexpression in cancerous tissues [197–199].



### 2.3. Glucocorticoids

Corticoids are steroid hormones produced in the adrenal cortex of vertebrates related to many physiological functions. Corticoids can be classified into two general categories depending on their function: glucocorticoids related to intermediary metabolism, inflammation, immunity, wound healing, myocardial, and muscle integrity; and mineralocorticoid related to mineral metabolism [200]. Synthetic glucocorticoids like DEX, prednisolone, methylprednisolone or triamcinolone are among the most widely used drugs in the world and are effective in many diseases of the respiratory system, skin, blood or musculoskeletal system [201].

Glucocorticoids predominantly exert their anti-inflammatory effect by switching off multiple inflammatory genes encoding inflammatory mediators, such as cytokines, chemokines, adhesion molecules, inflammatory enzymes, receptors and proteins, that have been activated during a chronic inflammatory process [202]. The effect of glucocorticoids is largely mediated by the glucocorticoid receptor (GR) (see figure 6). Unbound glucocorticoids diffuse through the cell membrane and bind to GR residing in the cytoplasm as part of a large multiprotein complex. The activated GR translocates to the nucleus and can bind directly to specific sites on the DNA or to different transcription factors [203–205].

Direct DNA-binding can cause transcriptional repression (transrepression) of pro-inflammatory genes, repressing cytokine expression (IL-1 $\alpha$ , IL-1 $\beta$ , IL-6, IL-8 and IL-12) or suppressing chemokine release (MCP-1, MIP-1 $\alpha$ , MIP-1 $\beta$ ) [206]. DNA binding can also cause the transcriptional activation (transactivation) of anti-inflammatory genes inducing, for example, the MAPK phosphatase1 (MKP1) that interferes with the p38MAPK pathway; the GC-induced zipper (GILZ), that inhibits NF- $\kappa$ B; or the activation of kruppel like transcription factors (Klf), important for M<sub>1</sub> macrophage polarization [206,207]. The indirect interaction of GR with DNA occurs *via* direct or indirect interactions with other transcription factors, such as members of the AP-1 and NF- $\kappa$ B families [208]. The presence of GR at AP-1 or NF- $\kappa$ B binding sites is thought to inhibit transcriptional activation by impairing recruitment of

transcriptional co-activators or by promoting recruitment of co-repressors [206].

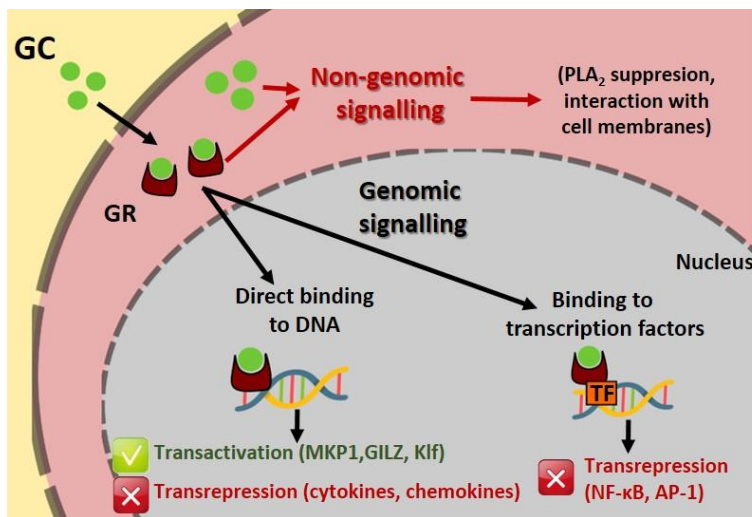


**Figure 7. Genomic and non-genomic effects of glucocorticoids. GC, glucocorticoid; GR, glucocorticoid receptor; TF, transcription factor.**

Non-genomic effects of glucocorticoids have been also described and can be GR dependent or GR independent (see figure 7). Some of the most described ones are the suppression of the enzyme PLA<sub>2</sub>; or the interaction of glucocorticoids with cellular membranes leading to immune cell suppression by different means [204,209].

DEX, approved by FDA in 1958, is a potent, long lasting glucocorticoid with approximately 30 times the binding activity for GR of endogenous cortisol [210]. However, it presents relatively low water solubility, 89 mg mL<sup>-1</sup>, limiting its bioavailability in biological fluids [211]. In OA, DEX can be orally administered or intra-articularly injected. Although it is currently used in the clinic, DEX is being extensively investigated for OA treatment. For example, macromolecular DEX prodrugs [212] or numerous DDS are being developed to improve its solubility, achieve a sustained release and reduce its toxicity. Some examples are photoresponsive nanosheets of chitosan modified molybdenum disulfide (MoS<sub>2</sub>) loading DEX [213], combinations with proteins like avidin

[214], HA or chitosan hydrogels [215,216], liposomes [217,218], NPs [219,220] or carbon nanotubes [221].

## **2.4. Nanoparticulate drug delivery systems of anti-inflammatory drugs**

The localized nature of OA makes the intra-articular administration one of the preferred routes of drug administration. However, it is limited by the rapid clearance of the intra-articularly injected drug in the synovial joint. In this context, the use of DDS that could provide a controlled drug delivery is a promising approach to satisfy this unmet medical need [222,223]. In last decades, the use of NPs to encapsulate drugs of very different nature is emerging to protect the nanoencapsulated compound from the environment, reduce its toxicity, increase its bioavailability or control its delivery [224,225]. In particular, polymeric NPs have received great interest due to their versatility in composition, structure and properties.

Some of the drawbacks of injecting free anti-inflammatory drugs into the joint cavity is the hydrophobicity that present most anti-inflammatory drugs that limit their bioavailability and their dispersion in the synovial joint; the toxicity of the direct contact with cartilage; and their rapid clearance and, therefore, short-term effect [226]. Their nanoencapsulation into polymeric NPs could solve these problems while allowing to prepare tailored systems in terms of size, surface properties and chemical structure. Although numerous investigations are being carried out to prepare DDS for the treatment of OA, till date, only one DDS encapsulating a corticoid, has been approved for its used in OA. In October 2017, the FDA approved the product Zilretta for the treatment of OA knee pain. It is an injectable suspension combining a poly(lactic-co-glycolic acid) (PLGA) matrix and the corticoid triamcinolone acetonide that have demonstrated to provide extended pain relief over 12 weeks [227].

As CLX, TNX, DEX and CUR have been the object of the present work, the most recent drug delivery systems used for their encapsulation are reviewed in this subsection, emphasizing the OA application. In the case of TNX, scarce literature has been found about its nanoencapsulation for OA

treatment. In table 3, last research on polymeric nanoparticles encapsulating CUR, CLX and DEX is summarized.

**Table 3. Latest research on polymeric NPs encapsulating CLX, DEX and CUR for OA/RA treatment.**

Drug	Polymeric vehicle	Size, surface charge	EE (%)	Model	Ref.
<b>CUR</b>	poly( $\beta$ -amino ester)	170 nm and positive charge	28	LPS-stimulated RAW264.7 and MIA induced rats	[228]
	poly( $\epsilon$ -caprolactone)	214-234 nm	100	AIA in rats	[229]
	HA	164 nm	N/A	CFA-induced RA rats	[230]
	carboxymethyl cellulose acetate butyrate	167 nm	73	CFA-induced RA rats	[231]
	silk fibroin	71 nm	49	IL-1 $\beta$ -stimulated human articular chondrocytes	[232]
<b>CLX</b>	silk fibroin	88 nm	5	IL-1 $\beta$ -stimulated human articular chondrocytes	[232]
	HA	255 nm	98	MIA-induced rats	[233]
	Soluplus®	59-61 nm	66-84	CFA-induced rats	[234]
<b>DEX</b>	Polythioketal urethane	~ 450 nm	N/A	LPS-stimulated macrophages and MIA induced rats	[235]
	4-(hydroxymethyl) phenylboronic acid pinacol ester-modified $\alpha$ -cyclodextrin	135-147 nm, -17, -18 mV	N/A	LPS-stimulated RAW264.7 and CIA mice	[220]
	Polyketal, HA	117 nm, +16 mV	41	LPS-stimulated RAW264.7 and CFA-induced RA rat model	[236]
	Polyethylenimine	150 nm, -3 mV	55	LPS-stimulated RAW264.7 and AIA rat model.	[237]
	PLGA	218 nm, -26 mV	35	H9C2 (rat cardiomyoblast) and C2C12 (mouse myoblast).	[238]
	Chitosan	330 nm, +19.5 mV	10	RAW264.7, HEK (human embryonic kidney cells) and CFA-induced arthritis in rats	[238]

EE, encapsulation efficiency; LPS, lipopolysaccharide; MIA, monoidioacetic; AIA, adjuvant-induced arthritic; CFA, complete Freund's adjuvant; PLGA, poly(lactic-co-glycolic) acid

### 2.4.1. Curcumin

CUR is a natural polyphenol widely investigated for the treatment of OA due its anti-inflammatory and antioxidant properties. However, its quite low water solubility limits its bioavailability in physiological fluids, being DDS an attractive option to improve its stability [239].

It has been encapsulated or incorporated into different polymeric nanocarriers for OA management. Recently, Kang *et al.* prepared acid-activable polymeric CUR NPs as OA therapeutic agents [228]. The system is a prodrug based on poly( $\beta$ -amino ester) in which CUR is incorporated. It takes advantage of the acidic environment present in OA joints to trigger the hydrophobic/hydrophilic transition of tertiary amine groups achieving a controlled release of CUR under acidic conditions. These micelles showed to decrease TNF- $\alpha$ , IL-1 $\beta$  and ROS levels in LPS-stimulated RAW264.7. Moreover, in a monoidioacetic (MIA)-induced OA model in rats the structural integrity of articular cartilage was preserved upon the treatment with the micelles. Other example are the silk fibroin NPs encapsulating either CLX or CUR developed by Crivelli *et al.* [232]. The effect of these NPs was evaluated in IL-1 $\beta$ -stimulated chondrocytes showing similar reduction of the inflammatory mediators NO, IL-6 and RANTES in both types of NPs while an additive antioxidant effect was observed in CUR-loaded silk fibroin NPs of both, the vehicle and the encapsulated CUR.

Different nanocarriers incorporating CUR have been also developed to treat RA. For example, CUR has been co-encapsulated with vitamin D3 into lipid-core NPs based on poly( $\epsilon$ -caprolactone) showing a reversion in purine metabolism changes in an arthritis rat model [229]. Fan *et al.* prepared biocompatible self-assembled HA-CUR micelles that reduced friction between articular cartilages in RA rats and diminished the expression of cytokines and VEGF [230]. Moreover, Dewangan *et al.* used carboxymethyl cellulose acetate butyrate to synthesize CUR-loaded NPs revealing that the loaded nanocarriers act as better anti-inflammatory agents and could give faster relief of pain than free CUR in arthritic rats [231]. Other DDS like CUR-loaded MPs embedded into

gels for topical administration [240], CUR-loaded liposomes [241] and hyalurosomes [242] are also being studied for arthritic conditions.

### 2.4.2. Tenoxicam

In the case of TNX, as far as our knowledge is concerned, no nanocarriers have been found encapsulating it for arthritic diseases. Nevertheless, other delivery systems recently developed are, for instance, microemulsion-based hydrogels of Carbopol® 940 with TNX for topical delivery at the affected site that have shown an anti-inflammatory efficacy equivalent to oral formulations in different *in vivo* models [184]. *In situ* forming MPs of Purasorb® Poly(DL-lactide) PDL 02 and sesame oil were loaded with TNX by Khattab *et al.* [183]. The efficacy of the encapsulated TNX was compared to the conventional oral administration revealing a sustained release for TNX-loaded MPs in a subcutaneous injection in rats, and a synergistic anti-inflammatory and antioxidant effect of TNX and sesame oil in a Complete Freund's adjuvant (CFA)-induced RA model in rats. Proniosomes, which are carrier vesicles coated with surfactants, have been also used to encapsulate TNX for its transdermal administration against arthritis [243]. Optimization of proniosomes lead to a non-irritant formulation, with significantly higher anti-inflammatory and analgesic effects compared to that of the oral market TNX tablets. In addition, Negi *et al.* prepared TNX loading ultradeformable vesicles of different surfactants and soya lecithin that were introduced in a Carbopol® 934 gel as a topical formulation [185]. The formulation evidenced almost twice the transdermal flux as compared to the gel with free TNX and the *in vivo* performance was also found to be significantly better than oral TNX in rats.

### 2.4.3. Celecoxib

CLX is one of the most investigated coxibs for the treatment of OA since, besides it is the first coxib approved to be used by the FDA in arthritic conditions, it possesses anti-inflammatory and analgesic activity and chondroprotective effects [244,245]. Nonetheless, its hydrophobic nature

compromises its solubility in water, leading to the need of its encapsulation to improve this stability.

Recently, CLX-loaded hyaluronan NPs were prepared using the nanoprecipitation method by El-Gogary *et al.* [233]. NPs were optimized in terms of size and encapsulation efficiency and showed superior performance in a MIA-induced OA rat model regarding histological, swelling and immunohistochemical parameters of OA. Since OA and RA share an inflammatory component, CLX-loaded nanocarriers for the treatment of RA have also been described. For instance, polymeric micelles encapsulating CLX were prepared using the commercially available Soluplus®, a poly(VC)-polyvinyl acetate-polyethylene glycol (PEG) graft copolymer and Kolliphor HS-15®, a non-ionic solubilizer and emulsifying agent [234]. NPs were tested in a CFA-induced RA rat model obtaining an improved anti-inflammatory effect and a reduction in edema in the nanoencapsulated system compared to Celebrex® (trade name of CLX).

CLX has been also loaded in other delivery systems for OA/RA treatment including polyesteramide microspheres [246], poly(lactic acid) MPs [195]; or CLX-loaded liposomes embedded in the commercial Carbopol® 934 gel, a cross-linked poly(acrylic acid) [247].

### 2.4.4. Dexamethasone

Among the four anti-inflammatory drugs used in this doctoral thesis, DEX is the most encapsulated one for its intra-articular administration in OA. Multiple nanocarriers have been recently developed to reduce its toxicity and to obtain a controlled release. Due to the implication of different inflammatory and oxidative factors in the development of OA, several systems are being developed to act as stimuli-responsive systems and release DEX upon contact with these OA factors. For instance, DEX-loaded ROS-responsive polythioketal urethane NPs were synthesized and capable of scavenging several kinds of ROS, accompanying with the degradation of polymers. Furthermore, in a MIA-induced rat model, NPs reduced ROS levels in the articular cavity, alleviated oxidative stress and resulted in a lower ratio of inflammatory M<sub>1</sub> macrophages



and a higher level of anti-inflammatory M<sub>2</sub> macrophages [235]. Other ROS-responsive NPs were developed by Ni *et al.* using 4-(hydroxymethyl) phenylboronic acid pinacol ester-modified  $\alpha$ -cyclodextrin [220]. NPs were efficiently uptaken by macrophages and accumulated in inflamed areas in mice with collagen-induced arthritis (CIA).

The same stimuli-responsive strategy was followed by He *et al.* but in this case using MMP as targets and PEGylated lipid NPs as DEX carriers [236]. Li and coworkers, for their part, prepared HA-coated pH-responsive NPs loaded with DEX and MCL-1 (myeloid cell leukemia-1, an anti-apoptotic factor with a crucial role in the apoptosis of activated macrophages) small interfering RNA (siRNA) [219]. Other example of HA coated pH-sensitive polymeric NPs are the ones prepared by Yu *et al.* composed of egg phosphatidylcholine, polyethylenimine, and poly(cyclohexane-1,4-diyl acetone dimethylene ketal) [237]. These optimized NPs proved to be able to target activated macrophages and to reduce inflammatory cell infiltration, bone damage and cartilage damage in adjuvant-induced arthritic (AIA) rats. PLGA [238] and chitosan [248] have been also used to prepare DEX-loaded NPs with promising *in vitro* and *in vivo* results.

Other systems including cyclodextrin-based NPs [249], PEG-cholesterol coated exosomes [250], liposomes [218,251], prodrugs based on pH-sensitive acetone-based ketal linked [252] and PEGylated palmitic acid systems [253] have been developed for the encapsulation or incorporation of DEX to treat arthritic diseases.

As mentioned above, in this work, four hydrophobic drugs (CUR, TNX, CLX, and DEX) have been encapsulated into NPs formed by an amphiphilic terpolymer system based on  $\alpha$ -tocopheryl methacrylate (MVE), 1-vinyl-2-pyrrolidone (VP) and *N*-vinylcaprolactam (VC) units (poly(MVE-*co*-VP-*co*-VC)) (see Chapters III and IV). As a preview, table 4 shows the characteristics of these loaded NPs for comparative purposes.

**Table 4. Main characteristics of the loaded NPs developed in this thesis.**

Drug	Polymeric vehicle	Size, surface charge	Encapsulation efficiency (%)	Model	Ref.
CUR		114-135 nm -3.3, -3.8 mV	72-79	LPS-stimulated RAW264.7, IL-1 $\beta$ - stimulated HC-a	[254]
CLX	Terpolymer poly(MVE-co-	110-121 nm -1.8, -4.7	39-72		
TNX	VP-co-VC)	111-128 nm -2.5, -4.6	20-24	LPS-stimulated RAW264.7	[255]
DEX		115-118 nm -2.4, -3.7 mV	14-26		

### 3. Viscosupplementation

HA is a GAG composed of alternating D-glucuronic acid and N-acetyl D-glucosamine connected by  $\beta$ -1,3 and  $\beta$ -1,4 glycosidic bonds (see figure 8). Viscosupplementation, or the intra-articular injection of exogenous HA, has the purpose of restoring the viscoelastic properties of synovial fluid [256]. Although the acceptance of intra-articular HA therapies is controversial, several systemic reviews have demonstrated the efficacy of viscosupplementation in alleviating pain [257,258]. In addition, several clinical trials have demonstrated that viscosupplement pain relief is longer than the one derived from oral NSAIDs and corticoid injections, lasting up to 6 months [107,259].

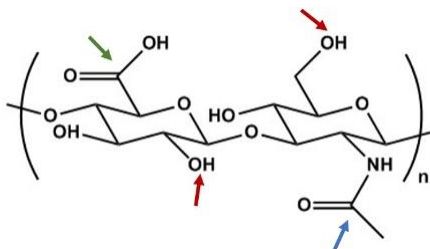


**Figure 8. Molecular structure of HA repeating disaccharide unit. Suitable groups for cross-linking: red corresponds to -OH groups, green corresponds to the -COOH group and blue corresponds to the -NHCOCH<sub>3</sub> group.**

*In vitro* and *in vivo* studies have shown various physiological effects of exogenous HA that may counteract the mechanisms involved in OA pathogenesis [260,261]. Chondroprotection and suppression of aggrecan degradation are the most reported effects [262]. HA injections can also reduce the production of pro-inflammatory mediators and MMP, and reduce nerve impulses and nerve sensitivity associated with OA pain [263]. HA binding to CD44 cell receptors inhibits IL-1 $\beta$  expression and, consequently, the production of MMP, ADAMTS and NO, responsible of cartilage destruction [264,265]. Proteoglycan and GAG synthesis, anti-inflammatory, analgesic and subchondral bone actions are also reported [263,266].

There are different commercial HA formulations for intra-articular administration that differ in  $M_w$ , reticulation grade and origin, among other properties [267]. Since viscosity is the key parameter of viscosupplements, several formulations are based on the chemical cross-linking of HA through the -OH, -COOH or -NHCOCH<sub>3</sub> groups to improve its rheological properties [256]. Some widely used cross-linkers are divinyl sulfone (DVS) and glutaraldehyde. Clinically, cross-linked and high  $M_w$  HA viscosupplements seem to exhibit superior capabilities than linear and low  $M_w$  HA, which may be due to the greatest difficulty to degrade cross-linked and high  $M_w$  products [268].

Table 5 summarizes the main commercial viscosupplements and their characteristics. Low, moderate and high  $M_w$  HA formulations include Hyalgan® (0.5-0.7 MDa), Euflexxa® (2.4-3.6 MDa) and Synvisc® (6.0 MDa), respectively. Avian-derived products include viscosupplements such as Hyalgan® or Synvisc® while bacterial products include, for example, Adant® and Monovisc®. Non-cross-linked viscosupplements include Adant® or Hyalone® while cross-linked ones include Monovisc® and Synvisc®. However, there is no product clearly recommended over others.

**Table 5. Main commercial viscosupplements and their characteristics. Conct: concentration**

Trade name	$M_w$ (MDa)	HA	Source	Cross-linking	Number of injections	Volume (mL) injected
		Conct. (mg mL <sup>-1</sup> )				
<b>Hyalgan®</b>	0.5-0.7	10	Avian	Not cross-linked	3-5	2
<b>Adant®</b>	0.6-1.2	10	Bacterial	Not cross-linked	5	2.5
<b>Hyalone®</b>	1.5-2.0	15	Bacterial	Not cross-linked	1	4
<b>Euflexxa®</b>	2.4-3.6	10	Bacterial	Not cross-linked	3	2
<b>Monovisc®</b>	1.0-2.9	22	Bacterial	Proprietary cross-linking agent	1	4
<b>Synvisc®</b>	6.0	8	Avian	Cross-linked with formaldehyde and DVS	3	2

In this thesis, advanced viscosupplements based on hyaluronic acid hydrogels were prepared and are discussed in confidential Chapter V.

### 3.1. Combined viscosupplements

One of the major problems of the intra-articular administration is the fast clearance and short residence time of drugs in the joint, due to the lymphatic system. As previously mentioned, DDS could increase drug residence time and control the release of therapeutic agents. Viscosupplements can be used as drug delivery vehicles for the progressive release of bioactive molecules and, at the same time, restore the viscoelasticity of synovial fluid. Nowadays, several commercial viscosupplements combine HA with other bioactive molecules, the most common being antioxidant molecules such as mannitol and sorbitol and cartilage extracellular components like the GAG chondroitin sulfate, acting as a chondroprotective agent (table 6). Moreover, free or encapsulated drugs and cell-based therapies are also being combined with viscosupplementation to obtain a double therapeutic effect. Since intra-articular injections of both corticoids and HA are common therapies for OA

treatment, their combination is under extensive investigation [215,269–273]. The introduction of DDS like loaded MPs into HA hydrogels is also under research [274–277]. Moreover, the combination of viscosupplementation and cell-based therapies could favor cartilage and synovial fluid regeneration [278–283].

**Table 6. Characteristics of commercial combined viscosupplements. Conct: concentration.**

Trade name	HA		Bioactive principle		Number of injections	Volume (mL) injected
	M <sub>w</sub> (MDa)	Conct. (mg mL <sup>-1</sup> )	Type	Conct. (mg mL <sup>-1</sup> )		
<b>Cingal®</b>	1.9	22	Triamcinolone acetonide (Corticoid)	4.5	1	4
<b>Arthrum HCS®</b>	2.8	20	Chondroitin sulfate (GAG)	20	1-3	2
<b>Synovium surgical®</b>	2.8	20	Chondroitin sulfate	20	1	3
<b>Ostenil plus®</b>	1.5	20	Mannitol (Antioxidant)	5	1	2
<b>Happyvisc®</b>	1.5	15.5	Mannitol	35	3	2
<b>Happycross®</b>	1.5	16	Mannitol	35	1	2.2
<b>Synolis V-A®</b>	2.0	20	Sorbitol (Antioxidant)	40	1-3	2

### 3.1.1. Combination with free anti-inflammatory drugs

The need for improving the clinical outcome of viscosupplements has led to the association of HA with free drugs. The introduction of drugs into HA networks can avoid some problems present in their direct intra-articular drug administration, such as drug crystallization and toxicity [109]. Moreover, these combined systems may couple the beneficial effects of both components, maintaining the viscosupplement properties. Anti-inflammatory drugs, specially corticoids, are the most investigated drugs to be loaded into HA

hydrogels due to their currently use in the treatment of OA (see section 2. *Anti-inflammatory drugs for OA treatment*).

Several *in vitro* and *in vivo* studies have demonstrated the synergistic effect of viscosupplements with NSAIDs [284]. For instance, carprofen has been combined with HA by Euppaya *et al.* Despite the introduction of carprofen into the HA hydrogel could not reduce its *in vitro* cytotoxicity, the combined system showed less cartilage loss compared to the control in explant cultures [285]. In other study, Ozkan *et al.* showed that the intra-articular injection of TNX in combination with the commercial viscosupplement Adant® and vitamin E improved the recovery of OA in a rat model [189]. Clinical studies of viscosupplements combined with NSAIDs have also been recently carried out. For instance, Palmieri *et al.* studied the clinical efficacy of diclofenac and sodium clodronate, a bisphosphonate, in combination with a viscosupplement [286]. HA alone or in combination with diclofenac was seen to alleviate pain, although to a lesser degree than the pain relief obtained with the combination of HA with sodium clodronate.

Concerning corticoids, *in vitro* and *in vivo* investigations and clinical trials have demonstrated the synergistic effect of both HA and corticoids [287]. As far as we are concerned, currently there is one commercial formulation called Cingal® combining a HA hydrogel (Monovisc®) and the corticoid triamcinolone hexacetonide (see characteristics in table 6). Triamcinolone is one of the most studied corticoids for its incorporation into HA hydrogels, that may be because of its highest potency compared to other corticoids [288]. In recent studies, the combination of HA, chitlac (a chitosan derivative based on chitosan backbones to which lactitol moieties have been chemically inserted *via* a reductive N-alkylation reaction with lactose) and triamcinolone has demonstrated to reduce triamcinolone toxicity while maintaining its anti-inflammatory effect in chondrocytes [272] and to improve knee articular cartilage degeneration, synovium inflammation and pain in a MIA-induced OA model [289]. The combined effect of triamcinolone with low  $M_w$  hyaluronan was studied *in vitro* and in cartilage explants by Euppaya *et al.* [269], and the performance of Hydros-TA, a hyaluronan-based hydrogel suspended in a

hyaluronan solution containing triamcinolone was studied in patients with knee OA, showing an increased pain relief with this system [290].

Other corticoids like prednisolone or DEX have been also studied. Siengdee *et al.* used porcine explants to test the effects of DEX and prednisolone with and without HA, observing a reduction of prednisolone but not DEX cytotoxicity when incorporated into the hydrogel [270]. Other study that obtained promising results for the use of HA with DEX was the one carried out by Zhang *et al.*, whose injectable cross-linked HA-DEX hydrogels provide a reduction of DEX toxicity and a reduction of cartilage damage in an anterior cruciate ligament transection (ACLT) OA rat model [215]. Prednisolone has been also introduced in a PEG diglycidyl ether cross-linked HA hydrogel, although no positive effect was observed with the loading of the corticoid into the hydrogel [291].

### 3.1.2. Combination with DDS

In order to increase drug bioavailability and reduce systemic effects, different DDS are under study for their local intra-articular delivery into the affected joint [225,292], as explained in subsection 2.4. *Nanoparticulate drug delivery systems of anti-inflammatory drugs*. DDS allow a controlled release of therapeutic agents, extend drug residence time and avoid crystal-induced arthritis of crystalline compounds such as corticoids, due to their encapsulation and the use of minimal doses [222,293]. The progressive nature of OA makes critical the maintenance of an effective drug action in the joint and, therefore, the use of DDS is a promising solution to extend their action. The addition of particulate vehicles to viscosupplements provides an additional control over the drug release. Drug release from the drug-loaded delivery system would occur by diffusion through the system into the HA hydrogel and then, diffusion from the hydrogel matrix to the joint cavity. Consequently, a dual controlled diffusion mechanism can be achieved.

Storozhylova *et al.* prepared an in situ forming fibrin-HA hydrogel loaded with nanocapsules (NCs) that consisted of an olive oil core surrounded by a HA shell in which two drugs DEX and a galectin-3 inhibitor (Gal-3) were

nanoencapsulated separately [274]. Besides the suitable rheological properties of the systems in terms of syringeability and mechanical properties, the results obtained in a preliminary *in vivo* acute knee synovitis rat model showed a remarkable suppression of inflammation by Gal-3 inhibitor containing hydrogel.

Other particulate carriers like MPs are being introduced into HA hydrogels [294]. For instance, cordycepin-loaded chitosan MPs were loaded in a photo-cross-linked hydrogel of HA methacrylate (HAMA) as a therapeutic for OA [277]. The authors found that cordycepin, an adenosine derivative, mitigated cartilage destruction by inducing autophagy, an adaptative response that could protect cells during OA progression, using *ex vivo* and *in vivo* models. Following the strategy mentioned above, Xie *et al.* encapsulated the anti-angiogenic drug crizotinib in the aforementioned chitosan MPs and introduced them in a photo-cross-linked hydrogel of gelatin methacrylate (GelMA) and HAMA (GelHA) [275]. *In vitro* and *ex vivo* cultures showed that crizotinib downregulated protein levels of VEGF and showed in the *in vivo* studies that the lowest cartilage structural changes were observed in mice treated with the hydrogels and the encapsulated drug. Other example are the hydrogels containing covalently bonded PEG-kartogenin (PEG-KGN) micelles developed by Kang *et al.* Kartogenin was used as an activator of MSC differentiation into chondrocytes, in order to favor cartilage repair. Covalent integration of the micelles into HA hydrogels (HA/PEG/KGN) reduced drug release rates and enzymatic degradation, while enhancing aggrecan and type II collagen expressions.

### 3.1.3. Combination with biological therapies

Tissue-engineering and regenerative strategies based on biomaterials, cells and other bioactive molecules have emerged as a possibility to repair osteoarthritic cartilage and reduce OA progression, as explained in the subsubsection 1.3.3. *Surgical and emerging biological therapies* of subsection 1.3. This regenerative approach tries to stimulate the regeneration of articular cartilage improving joint function and reducing pain. The combination of HA injections and tissue engineering therapies can consequently couple synovial



fluid viscoelasticity restoration and cartilage repair and is one of the most promising strategies in cartilage repair as reported recently in bibliography [295].

Since PRP is one of the most currently used biological therapies for OA treatment, it is also the most popular biological therapy to be combined with viscosupplementation. There are several clinical studies comparing the effects of intra-articular PRP injections alone or in combination with viscosupplements. Some of them conclude better results with the combined system [278,279,296] while others did not observed differences between the treatments alone or in combination [280,297]. *In vitro* and *in vivo* studies of PRP combined with HA are also being conducted. Chen *et al.* studied the combination of viscosupplements and PRP using a 3-dimensional neo-cartilage model and a mice model, demonstrating that the system recovered the expression of chondrogenic genes while decreased chemokine and cytokine expression [281], and enhanced cartilage recovery in mice. On the contrary, the group of Duan *et al.* saw no improvements when injecting the viscosupplement HYADD® 4-G with PRP in a mice model, in which joint injury was induced by axial tibial loading [282]. In order to study the influence of PRP introduction in the viscoelastic and biological properties of commercial viscosupplements, Russo *et al.* prepared mixtures containing both components [283]. Results showed a decrease in viscosity of about one order of magnitude after PRP addition, but chondrocyte proliferation and GAG production was higher in the mixtures compared to HA alone, showing improved biological behavior compared to viscosupplements alone.

MSC have also been introduced into HA hydrogels using them as vehicles for its intra-articular injection. One major challenge when applying cellular therapies is to deliver cells in the desired targeting site. To solve this problem Desando *et al.* studied the possible effect of HA in the modulation of cell migration in a rabbit OA model [298]. The authors prepared solutions of MSC and bone marrow concentrate aspirate (BMCA) in PBS or HA solutions and observed that, while MSC preferentially migrated to synovium, BMCA preferred to migrate toward cartilage, promoting cartilage and joint recovery.

In other study, researchers used magnetic resonance imaging and micro-computed tomography to test the efficacy of allogenic adipose-derived MSC (AD-MSC) combined with HA to block OA progression in sheep [299]. Results showed a cartilage layer almost identical to healthy cartilage in animals treated with AD-MSC+HA and suggested that a possible mechanism of action of cells for cartilage repair could be the secretion of chondrogenic factors. Similar results were obtained by Chiang *et al.* who evidenced that the combination of BM-MSC with HA provided better results in a rabbit OA model regarding recovery of cartilage, less surface abrasion and better histological scores compared to animals treated only with HA. The same happened in the canine model of Li *et al.* using BM-MSC with HA [300].

Due to the emerging potential applications of MSC derived secretomes it is also being introduced into HA hydrogels. For example, Shoma Suresh *et al.* prepared a nanocomposite material formed by poly-L-lactide NPs embedded in gelatin-HA hydrogel as a delivery vehicle for BM-MSC secretome [301]. Results evidenced that the sustained release of secretomes provided by the hydrogel prevented their dose-dependent cytotoxicity and that the nanocomposite material achieved an enhancement of fibroblast metabolic activity.

Here, MSC derived secretomes were obtained for the intra-articular treatment of OA (see confidential Chapter VI).

## Bibliography

- [1] Global, regional, and national incidence, prevalence, and years lived with disability for 354 diseases and injuries for 195 countries and territories, 1990-2017: a systematic analysis for the Global Burden of Disease Study 2017., *Lancet* (London, England). 392 (2018) 1789–1858.  
[https://doi.org/10.1016/S0140-6736\(18\)32279-7](https://doi.org/10.1016/S0140-6736(18)32279-7).
- [2] A.D. Woolf, B. Pfleger, Burden of major musculoskeletal conditions, *Bull. World Health Organ.* 81 (2003) 646–656.  
<https://pubmed.ncbi.nlm.nih.gov/14710506>.
- [3] M. Martín-Millán, S. Castañeda, Estrogens, osteoarthritis and inflammation., *Jt. Bone Spine.* 80 (2013) 368–373.  
<https://doi.org/10.1016/j.jbspin.2012.11.008>
- [4] L. Jiang, W. Tian, Y. Wang, J. Rong, C. Bao, Y. Liu, Y. Zhao, C. Wang, Body mass index and susceptibility to knee osteoarthritis: a systematic review and meta-analysis., *Jt. Bone Spine.* 79 (2012) 291–297.  
<https://doi.org/10.1016/j.jbspin.2011.05.015>

- [5] E. Yusuf, R.G. Nelissen, A. Ioan-Facsinay, V. Stojanovic-Susulic, J. DeGroot, G. van Osch, S. Middeldorp, T.W.J. Huizinga, M. Kloppenburg, Association between weight or body mass index and hand osteoarthritis: a systematic review., *Ann. Rheum. Dis.* 69 (2010) 761–765. <https://doi.org/10.1136/ard.2008.106930>.
- [6] C.D. McClung, C.A. Zahari, J.K. Higa, H.C. Amstutz, T.P. Schmalzried, Relationship between body mass index and activity in hip or knee arthroplasty patients., *J. Orthop. Res. Off. Publ. Orthop. Res. Soc.* 18 (2000) 35–39. <https://doi.org/10.1002/jor.1100180106>.
- [7] L.J. Sandell, Etiology of osteoarthritis: genetics and synovial joint development., *Nat. Rev. Rheumatol.* 8 (2012) 77–89. <https://doi.org/10.1038/nrrheum.2011.199>.
- [8] N.E. Lane, K. Shidara, B.L. Wise, Osteoarthritis year in review 2016: clinical., *Osteoarthr. Cartil.* 25 (2017) 209–215. <https://doi.org/10.1016/j.joca.2016.09.025>
- [9] F. Guilak, Biomechanical factors in osteoarthritis., *Best Pract. Res. Clin. Rheumatol.* 25 (2011) 815–823. <https://doi.org/10.1016/j.jberh.2011.11.013>.
- [10] M.B. Goldring, S.R. Goldring, Osteoarthritis., *J. Cell. Physiol.* 213 (2007) 626–634. <https://doi.org/10.1002/jcp.21258>.
- [11] J.H. Salmon, A.C. Rat, J. Sellam, M. Michel, J.P. Eschard, F. Guillemin, D. Jolly, B. Fautrel, Economic impact of lower-limb osteoarthritis worldwide: a systematic review of cost-of-illness studies., *Osteoarthr. Cartil.* 24 (2016) 1500–1508. <https://doi.org/10.1016/j.joca.2016.03.012>
- [12] J. Dudhia, Aggrecan, aging and assembly in articular cartilage., *Cell. Mol. Life Sci.* 62 (2005) 2241–2256. <https://doi.org/10.1007/s00018-005-5217-x>.
- [13] A.R. Poole, T. Kojima, T. Yasuda, F. Mwale, M. Kobayashi, S. Lavery, Composition and structure of articular cartilage: a template for tissue repair., *Clin. Orthop. Relat. Res.* (2001) S26–33. <https://doi.org/10.1097/00003086-200110001-00004>.
- [14] T.M. Tamer, Hyaluronan and synovial joint: function, distribution and healing, *Interdiscip. Toxicol.* 6 (2013) 111–125. <https://doi.org/10.2478/intox-2013-0019>.
- [15] N. Gerwin, C. Hops, A. Lucke, Intraarticular drug delivery in osteoarthritis., *Adv. Drug Deliv. Rev.* 58 (2006) 226–242. <https://doi.org/10.1016/j.addr.2006.01.018>.
- [16] T. Iwanaga, M. Shikichi, H. Kitamura, H. Yanase, K. Nozawa-Inoue, Morphology and functional roles of synoviocytes in the joint., *Arch. Histol. Cytol.* 63 (2000) 17–31. <https://doi.org/10.10679/aohc.63.17>.
- [17] M.E. Blewis, G.E. Nugent-Derfus, T.A. Schmidt, B.L. Schumacher, R.L. Sah, A model of synovial fluid lubricant composition in normal and injured joints., *Eur. Cell. Mater.* 13 (2007) 26–39. <https://doi.org/10.22203/ecm.v013a03>.
- [18] M.M. Temple-Wong, S. Ren, P. Quach, B.C. Hansen, A.C. Chen, A. Hasegawa, D.D. D'Lima, J. Koziol, K. Masuda, M.K. Lotz, R.L. Sah, Hyaluronan concentration and size distribution in human knee synovial fluid: variations with age and cartilage degeneration, *Arthritis Res. Ther.* 18 (2016) 18. <https://doi.org/10.1186/s13075-016-0922-4>.
- [19] R. Barbucci, S. Lamponi, A. Borzacchiello, L. Ambrosio, M. Fini, P. Torricelli, R. Giardino, Hyaluronic acid hydrogel in the treatment of osteoarthritis, *Biomaterials.* 23 (2002) 4503–4513. [https://doi.org/https://doi.org/10.1016/S0142-9612\(02\)00194-1](https://doi.org/https://doi.org/10.1016/S0142-9612(02)00194-1).

- [20] T.E. Cawston, A.J. Wilson, Understanding the role of tissue degrading enzymes and their inhibitors in development and disease., *Best Pract. Res. Clin. Rheumatol.* 20 (2006) 983–1002.  
<https://doi.org/10.1016/j.berh.2006.06.007>.
- [21] P. Wojdasiewicz, Ł.A. Poniatowski, D. Szukiewicz, The Role of Inflammatory and Anti-Inflammatory Cytokines in the Pathogenesis of Osteoarthritis, *Mediators Inflamm.* 2014 (2014) 561459.  
<https://doi.org/10.1155/2014/561459>.
- [22] L.J. Sandell, T. Aigner, Articular cartilage and changes in arthritis. An introduction: cell biology of osteoarthritis., *Arthritis Res.* 3 (2001) 107–113.  
<https://doi.org/10.1186/ar148>.
- [23] S.R. Goldring, M.B. Goldring, The role of cytokines in cartilage matrix degeneration in osteoarthritis., *Clin. Orthop. Relat. Res.* (2004) S27–36.  
<https://doi.org/10.1097/01.blo.0000144854.66565.8f>.
- [24] D.B. Burr, M.A. Gallant, Bone remodelling in osteoarthritis., *Nat. Rev. Rheumatol.* 8 (2012) 665–673.  
<https://doi.org/10.1038/nrrheum.2012.130>.
- [25] T. Hayami, M. Pickarski, G.A. Wesolowski, J. McLane, A. Bone, J. Destefano, G.A. Rodan, L.T. Duong, The role of subchondral bone remodeling in osteoarthritis: reduction of cartilage degeneration and prevention of osteophyte formation by alendronate in the rat anterior cruciate ligament transection model., *Arthritis Rheum.* 50 (2004) 1193–1206.  
<https://doi.org/10.1002/art.20124>.
- [26] A. Mathiessen, P.G. Conaghan, Synovitis in osteoarthritis: current understanding with therapeutic implications, *Arthritis Res. Ther.* 19 (2017) 18.  
<https://doi.org/10.1186/s13075-017-1229-9>.
- [27] C.R. Scanzello, S.R. Goldring, The role of synovitis in osteoarthritis pathogenesis., *Bone.* 51 (2012) 249–257.  
<https://doi.org/10.1016/j.bone.2012.02.012>.
- [28] Hyaluronan molecular weight distribution, (n.d.).
- [29] A. Fakhari, C. Berklund, Applications and emerging trends of hyaluronic acid in tissue engineering, as a dermal filler and in osteoarthritis treatment., *Acta Biomater.* 9 (2013) 7081–7092.  
<https://doi.org/10.1016/j.actbio.2013.03.005>.
- [30] M.B. Goldring, M. Otero, Inflammation in osteoarthritis, *Curr. Opin. Rheumatol.* 23 (2011) 471–478.  
<https://doi.org/10.1097/BOR.0b013e328349c2b1>.
- [31] G. Barreto, M. Manninen, K. K Eklund, Osteoarthritis and Toll-Like Receptors: When Innate Immunity Meets Chondrocyte Apoptosis, *Biology (Basel).* 9 (2020) 65.  
<https://doi.org/10.3390/biology9040065>.
- [32] D. Foell, H. Wittkowski, J. Roth, Mechanisms of disease: a “DAMP” view of inflammatory arthritis., *Nat. Clin. Pract. Rheumatol.* 3 (2007) 382–390.  
<https://doi.org/10.1038/ncprheum0531>.
- [33] J.H. Rosenberg, V. Rai, M.F. Dilisio, D.K. Agrawal, Damage-associated molecular patterns in the pathogenesis of osteoarthritis: potentially novel therapeutic targets., *Mol. Cell. Biochem.* 434 (2017) 171–179.  
<https://doi.org/10.1007/s11010-017-3047-4>.
- [34] A.H. Reddi, K. Iwasa, Chapter 25 - Morphogenesis, Bone Morphogenetic Proteins, and Regeneration of Bone and Articular Cartilage, in: A. Atala, R. Lanza, A.G. Mikos, R.B.T.-P. of R.M. (Third E. Nerem (Eds.), Academic Press, Boston, 2019: pp. 405–416.

<https://doi.org/https://doi.org/10.1016/B978-0-12-809880-6.00025-4>.

**[35]** T. Aigner, S. Söder, P.M. Gebhard, A. McAlinden, J. Haag, Mechanisms of Disease: role of chondrocytes in the pathogenesis of osteoarthritis—structure, chaos and senescence, *Nat. Clin. Pract. Rheumatol.* 3 (2007) 391–399. <https://doi.org/10.1038/ncprheum0534>.

**[36]** H. Akkiraju, A. Nohe, Role of Chondrocytes in Cartilage Formation, Progression of Osteoarthritis and Cartilage Regeneration, *J. Dev. Biol.* 3 (2015) 177–192. <https://doi.org/10.3390/jdb3040177>.

**[37]** P. Singh, K.B. Marcu, M.B. Goldring, M. Otero, Phenotypic instability of chondrocytes in osteoarthritis: on a path to hypertrophy., *Ann. N. Y. Acad. Sci.* 1442 (2019) 17–34. <https://doi.org/10.1111/nyas.13930>.

**[38]** B. Bartok, G.S. Firestein, Fibroblast-like synoviocytes: key effector cells in rheumatoid arthritis, *Immunol. Rev.* 233 (2010) 233–255. <https://doi.org/10.1111/j.0105-2896.2009.00859.x>.

**[39]** C.-H. Chou, V. Jain, J. Gibson, D.E. Attarian, C.A. Haraden, C.B. Yohn, R.-M. Laberge, S. Gregory, V.B. Kraus, Synovial cell cross-talk with cartilage plays a major role in the pathogenesis of osteoarthritis, *Sci. Rep.* 10 (2020) 10868. <https://doi.org/10.1038/s41598-020-67730-y>.

**[40]** N. Maruotti, A. Corrado, F.P. Cantatore, Osteoblast role in osteoarthritis pathogenesis, *J. Cell. Physiol.* 232 (2017) 2957–2963. <https://doi.org/10.1002/jcp.25969>.

**[41]** W. Hu, Y. Chen, C. Dou, S. Dong, Microenvironment in subchondral bone: predominant regulator for the treatment of osteoarthritis, *Ann. Rheum. Dis.* (2020) annrheumdis-2020-218089.

<https://doi.org/10.1136/annrheumdis-2020-218089>.

**[42]** T. Funck-Brentano, M. Cohen-Solal, Crosstalk between cartilage and bone: When bone cytokines matter, *Cytokine Growth Factor Rev.* 22 (2011) 91–97. <https://doi.org/https://doi.org/10.1016/j.cytogfr.2011.04.003>.

**[43]** B.J.E. de Lange-Brokaar, A. Ioan-Facsinay, G.J.V.M. van Osch, A.-M. Zuurmond, J. Schoones, R.E.M. Toes, T.W.J. Huizinga, M. Kloppenburg, Synovial inflammation, immune cells and their cytokines in osteoarthritis: a review., *Osteoarthr. Cartil.* 20 (2012) 1484–1499. <https://doi.org/10.1016/j.joca.2012.08.027>.

**[44]** A. Haseeb, T.M. Haqqi, Immunopathogenesis of osteoarthritis, *Clin. Immunol.* 146 (2013) 185–196. <https://doi.org/10.1016/j.clim.2012.12.011>

**[45]** J.L. Stow, P.C. Low, C. Offenhäuser, D. Sangermani, Cytokine secretion in macrophages and other cells: pathways and mediators., *Immunobiology.* 214 (2009) 601–612. <https://doi.org/10.1016/j.imbio.2008.11.005>

**[46]** Y. Wang, W. Smith, D. Hao, B. He, L. Kong, M1 and M2 macrophage polarization and potentially therapeutic naturally occurring compounds, *Int. Immunopharmacol.* 70 (2019) 459–466. <https://doi.org/https://doi.org/10.1016/j.intimp.2019.02.050>.

**[47]** Y.-C. Liu, X.-B. Zou, Y.-F. Chai, Y.-M. Yao, Macrophage polarization in inflammatory diseases., *Int. J. Biol. Sci.* 10 (2014) 520–529. <https://doi.org/10.7150/ijbs.8879>.

**[48]** Y. Sun, Z. Zuo, Y. Kuang, An Emerging Target in the Battle against Osteoarthritis: Macrophage Polarization, *Int. J. Mol. Sci.* 21 (2020) 8513. <https://doi.org/10.3390/ijms21228513>.

- [49] J. Van den Bossche, A.E. Neele, M.A. Hoeksema, M.P.J. de Winther, Macrophage polarization, *Curr. Opin. Lipidol.* 25 (2014) 367–373.  
<https://doi.org/10.1097/mol.0000000000000109>.
- [50] P.A. Nigrovic, D.M. Lee, Mast cells in inflammatory arthritis, *Arthritis Res. Ther.* 7 (2005) 1–11.  
<https://doi.org/10.1186/ar1446>.
- [51] P.A. Nigrovic, D.M. Lee, Synovial mast cells: role in acute and chronic arthritis., *Immunol. Rev.* 217 (2007) 19–37.  
<https://doi.org/10.1111/j.1600-065X.2007.00506.x>.
- [52] D. Chatterjea, T. Martinov, Mast cells: versatile gatekeepers of pain., *Mol. Immunol.* 63 (2015) 38–44.  
<https://doi.org/10.1016/j.molimm.2014.03.001>.
- [53] S.P. Cullen, S.J. Martin, Mechanisms of granule-dependent killing, *Cell Death Differ.* 15 (2008) 251–262.  
<https://doi.org/10.1038/sj.cdd.4402244>.
- [54] S.S. Metkar, C. Menaa, J. Pardo, B. Wang, R. Wallich, M. Freudenberg, S. Kim, S.M. Raja, L. Shi, M.M. Simon, C.J. Froelich, Human and mouse granzyme A induce a proinflammatory cytokine response., *Immunity.* 29 (2008) 720–733.  
<https://doi.org/10.1016/j.immuni.2008.08.014>.
- [55] J. Pardo, M.M. Simon, C.J. Froelich, Granzyme A is a proinflammatory protease., *Blood.* 114 (2009) 3968; author reply 3969–70. <https://doi.org/10.1182/blood-2009-07-231027>.
- [56] H. Ida, P.J. Utz, P. Anderson, K. Eguchi, Granzyme B and natural killer (NK) cell death, *Mod. Rheumatol.* 15 (2005) 315–322.  
<https://doi.org/10.3109/s10165-005-0426-6>.
- [57] L.I. Sakkas, C.D. Platsoucas, The role of T cells in the pathogenesis of osteoarthritis., *Arthritis Rheum.* 56 (2007) 409–424.  
<https://doi.org/10.1002/art.22369>.
- [58] Y.-S. Li, W. Luo, S.-A. Zhu, G.-H. Lei, T Cells in Osteoarthritis: Alterations and Beyond, *Front. Immunol.* 8 (2017) 356.  
<https://doi.org/10.3389/fimmu.2017.00356>.
- [59] T.A. Nees, N. Rosshirt, J.A. Zhang, H. Platzer, R. Sorbi, E. Tripel, T. Reiner, T. Walker, M. Schiltewolf, H.-M. Lorenz, T. Tretter, B. Moradi, S. Hagmann, T Helper Cell Infiltration in Osteoarthritis-Related Knee Pain and Disability, *J. Clin. Med.* 9 (2020) 2423.  
<https://doi.org/10.3390/jcm9082423>.
- [60] S. Sarkar, L.A. Cooney, D.A. Fox, The role of T helper type 17 cells in inflammatory arthritis, *Clin. Exp. Immunol.* 159 (2010) 225–237. <https://doi.org/10.1111/j.1365-2249.2009.04016.x>.
- [61] T. Nakashima, H. Takayanagi, Osteoimmunology: crosstalk between the immune and bone systems., *J. Clin. Immunol.* 29 (2009) 555–567.  
<https://doi.org/10.1007/s10875-009-9316-6>.
- [62] S. Rigoglou, A.G. Papavassiliou, The NF- $\kappa$ B signalling pathway in osteoarthritis, *Int. J. Biochem. Cell Biol.* 45 (2013) 2580–2584.  
<https://doi.org/https://doi.org/10.1016/j.bio cel.2013.08.018>.
- [63] T. Liu, L. Zhang, D. Joo, S.-C. Sun, NF- $\kappa$ B signaling in inflammation, *Signal Transduct. Target. Ther.* 2 (2017) 17023.  
<https://doi.org/10.1038/sigtrans.2017.23>.
- [64] L. Chen, H. Deng, H. Cui, J. Fang, Z. Zuo, J. Deng, Y. Li, X. Wang, L. Zhao, Inflammatory responses and inflammation-associated diseases in organs, *Oncotarget.* 9 (2017) 7204–7218.  
<https://doi.org/10.18632/oncotarget.23208>.

- [65] Y.Y. Chow, K.-Y. Chin, The Role of Inflammation in the Pathogenesis of Osteoarthritis, *Mediators Inflamm.* 2020 (2020) 8293921. <https://doi.org/10.1155/2020/8293921>.
- [66] R.F. Loeser, E.A. Erickson, D.L. Long, Mitogen-activated protein kinases as therapeutic targets in osteoarthritis, *Curr. Opin. Rheumatol.* 20 (2008) 581–586. <https://doi.org/10.1097/BOR.0b013e3283090463>.
- [67] T. Thalhamer, M.A. McGrath, M.M. Harnett, MAPKs and their relevance to arthritis and inflammation, *Rheumatology.* 47 (2008) 409–414. <https://doi.org/10.1093/rheumatology/kem297>.
- [68] M. Imajo, Y. Tsuchiya, E. Nishida, Regulatory mechanisms and functions of MAP kinase signaling pathways., *IUBMB Life.* 58 (2006) 312–317. <https://doi.org/10.1080/15216540600746393>.
- [69] D.A. Harrison, The Jak/STAT pathway, *Cold Spring Harb. Perspect. Biol.* 4 (2012) a011205. <https://doi.org/10.1101/cshperspect.a011205>.
- [70] M. Otori, ERK inhibitors as a potential new therapy for rheumatoid arthritis., *Drug News Perspect.* 21 (2008) 245–250. <https://doi.org/10.1358/DNP.2008.21.5.1219006>.
- [71] G. Akeson, C.J. Maleski, A Role for Soluble IL-6 Receptor in Osteoarthritis, *J. Funct. Morphol. Kinesiol.* 2 (2017) 27. <https://doi.org/10.3390/jfkmk2030027>.
- [72] J.E. Woodell-May, S.D. Sommerfeld, Role of Inflammation and the Immune System in the Progression of Osteoarthritis., *J. Orthop. Res. Off. Publ. Orthop. Res. Soc.* 38 (2020) 253–257. <https://doi.org/10.1002/jor.24457>.
- [73] J.A. Buckwalter, J.A. Martin, Osteoarthritis., *Adv. Drug Deliv. Rev.* 58 (2006) 150–167. <https://doi.org/10.1016/j.addr.2006.01.006>.
- [74] P.S. Burrage, K.S. Mix, C.E. Brinckerhoff, Matrix metalloproteinases: role in arthritis., *Front. Biosci.* 11 (2006) 529–543. <https://doi.org/10.2741/1817>.
- [75] J. Bondeson, S. Wainwright, C. Hughes, B. Caterson, The regulation of the ADAMTS4 and ADAMTS5 aggrecanases in osteoarthritis: a review., *Clin. Exp. Rheumatol.* 26 (2008) 139–145.
- [76] P. Verma, K. Dalal, ADAMTS-4 and ADAMTS-5: key enzymes in osteoarthritis., *J. Cell. Biochem.* 112 (2011) 3507–3514. <https://doi.org/10.1002/jcb.23298>.
- [77] L. Troeberg, H. Nagase, Proteases involved in cartilage matrix degradation in osteoarthritis, *Biochim. Biophys. Acta.* 1824 (2012) 133–145. <https://doi.org/10.1016/j.bbapap.2011.06.020>.
- [78] J.C. Fernandes, J. Martel-Pelletier, J.-P. Pelletier, The role of cytokines in osteoarthritis pathophysiology., *Biorheology.* 39 (2002) 237–246.
- [79] M.B. Goldring, Osteoarthritis and cartilage: The role of cytokines, *Curr. Rheumatol. Rep.* 2 (2000) 459–465. <https://doi.org/10.1007/s11926-000-0021-y>.
- [80] R.E. Miller, R.J. Miller, A.-M. Malfait, Osteoarthritis joint pain: the cytokine connection, *Cytokine.* 70 (2014) 185–193. <https://doi.org/10.1016/j.cyto.2014.06.019>.
- [81] M. Daheshia, J.Q. Yao, The interleukin 1beta pathway in the pathogenesis of osteoarthritis., *J. Rheumatol.* 35 (2008) 2306–2312. <https://doi.org/10.3899/jrheum.080346>.

- [82] M. Kapoor, J. Martel-Pelletier, D. Lajeunesse, J.-P. Pelletier, H. Fahmi, Role of inflammatory cytokines in the pathophysiology of osteoarthritis, *Nat. Rev. Rheumatol.* 7 (2011) 33–42. <https://doi.org/10.1038/nrrheum.2010.196>.
- [83] P. Wojdasiewicz, Ł.A. Poniowski, D. Szukiewicz, The role of inflammatory and anti-inflammatory cytokines in the pathogenesis of osteoarthritis., *Mediators Inflamm.* 2014 (2014) 561459. <https://doi.org/10.1155/2014/561459>.
- [84] M.C. Miller, K.H. Mayo, Chemokines from a Structural Perspective, *Int. J. Mol. Sci.* 18 (2017) 2088. <https://doi.org/10.3390/ijms18102088>.
- [85] C.R. Scanzello, Chemokines and inflammation in osteoarthritis: Insights from patients and animal models, *J. Orthop. Res.* 35 (2017) 735–739. <https://doi.org/10.1002/jor.23471>.
- [86] O.-M. Zahan, O. Serban, C. Gherman, D. Fodor, The evaluation of oxidative stress in osteoarthritis, *Med. Pharm. Reports.* 93 (2020) 12–22. <https://doi.org/10.15386/MPR-1422>.
- [87] P. Lepetsos, A.G. Papavassiliou, ROS/oxidative stress signaling in osteoarthritis, *Biochim. Biophys. Acta - Mol. Basis Dis.* 1862 (2016) 576–591. <https://doi.org/10.1016/j.bbadis.2016.01.003>.
- [88] A. Leonidou, P. Lepetsos, M. Mintzas, E. Kenanidis, G. Macheras, M. Tzetzis, M. Potoupnis, E. Tsidiris, Inducible nitric oxide synthase as a target for osteoarthritis treatment., *Expert Opin. Ther. Targets.* 22 (2018) 299–318. <https://doi.org/10.1080/14728222.2018.1448062>.
- [89] S.B. Abramson, Osteoarthritis and nitric oxide, *Osteoarthr. Cartil.* 16 (2008) S15–S20. [https://doi.org/https://doi.org/10.1016/S1063-4584\(08\)60008-4](https://doi.org/https://doi.org/10.1016/S1063-4584(08)60008-4).
- [90] D. Bar-Or, L.T. Rael, G.W. Thomas, E.N. Brody, Inflammatory Pathways in Knee Osteoarthritis: Potential Targets for Treatment, *Curr. Rheumatol. Rev.* 11 (2015) 50–58. <https://doi.org/10.2174/1573397111666150522094131>.
- [91] J. Martel-Pelletier, J.-P. Pelletier, H. Fahmi, Cyclooxygenase-2 and prostaglandins in articular tissues., *Semin. Arthritis Rheum.* 33 (2003) 155–167. [https://doi.org/10.1016/S0049-0172\(03\)00134-3](https://doi.org/10.1016/S0049-0172(03)00134-3).
- [92] H. Fahmi, mPGES-1 as a novel target for arthritis., *Curr. Opin. Rheumatol.* 16 (2004) 623–627. <https://doi.org/10.1097/01.bor.0000129664.81052.8e>.
- [93] L. Fernandes, K.B. Hagen, J.W.J. Bijlsma, O. Andreassen, P. Christensen, P.G. Conaghan, M. Doherty, R. Geenen, A. Hammond, I. Kjekens, L.S. Lohmander, H. Lund, C.D. Mallen, T. Nava, S. Oliver, K. Pavelka, I. Pitsillidou, J.A. da Silva, J. de la Torre, G. Zanolini, T.P.M. Vliet Vlieland, EULAR recommendations for the non-pharmacological core management of hip and knee osteoarthritis., *Ann. Rheum. Dis.* 72 (2013) 1125–1135. <https://doi.org/10.1136/annrheumdis-2012-202745>.
- [94] R.R. Bannuru, M.C. Osani, E.E. Vaysbrot, N.K. Arden, K. Bennell, S.M.A. Bierma-Zeinstra, V.B. Kraus, L.S. Lohmander, J.H. Abbott, M. Bhandari, F.J. Blanco, R. Espinosa, I.K. Haugen, J. Lin, L.A. Mandl, E. Moilanen, N. Nakamura, L. Snyder-Mackler, T. Trojian, M. Underwood, T.E. McAlindon, OARSI guidelines for the non-surgical management of knee, hip, and polyarticular osteoarthritis., *Osteoarthr. Cartil.* 27 (2019) 1578–1589. <https://doi.org/10.1016/j.joca.2019.06.011>.



- [95] M.C. Hochberg, R.D. Altman, K.T. April, M. Benkhalti, G. Guyatt, J. McGowan, T. Towheed, V. Welch, G. Wells, P. Tugwell, American College of Rheumatology 2012 recommendations for the use of nonpharmacologic and pharmacologic therapies in osteoarthritis of the hand, hip, and knee., *Arthritis Care Res. (Hoboken)*. 64 (2012) 465–474.  
<https://doi.org/10.1002/acr.21596>.
- [96] M. Permuy, D. Guede, M. López-Peña, F. Muñoz, J.-R. Caeiro, A. González-Cantalapiedra, Comparison of various SYSADOA for the osteoarthritis treatment: an experimental study in rabbits, *BMC Musculoskelet. Disord.* 16 (2015) 120.  
<https://doi.org/10.1186/s12891-015-0572-8>.
- [97] J.A. Roman-Blas, S. Castañeda, O. Sánchez-Pernaute, R. Largo, G. Herrero-Beaumont, Combined Treatment With Chondroitin Sulfate and Glucosamine Sulfate Shows No Superiority Over Placebo for Reduction of Joint Pain and Functional Impairment in Patients With Knee Osteoarthritis: A Six-Month Multicenter, Randomized, Double-Blind, Placebo-C, *Arthritis Rheumatol. (Hoboken, N.J.)*. 69 (2017) 77–85.  
<https://doi.org/10.1002/art.39819>.
- [98] D.G.N. Craig, C.M. Bates, J.S. Davidson, K.G. Martin, P.C. Hayes, K.J. Simpson, Staggered overdose pattern and delay to hospital presentation are associated with adverse outcomes following paracetamol-induced hepatotoxicity, *Br. J. Clin. Pharmacol.* 73 (2012) 285–294.  
<https://doi.org/10.1111/j.1365-2125.2011.04067.x>.
- [99] M.S. Cepeda, F. Camargo, C. Zea, L. Valencia, Tramadol for osteoarthritis: a systematic review and metaanalysis., *J. Rheumatol.* 34 (2007) 543–555.
- [100] W. Badri, K. Miladi, Q.A. Nazari, H. Greige-Gerges, H. Fessi, A. Elaissari, Encapsulation of NSAIDs for inflammation management: Overview, progress, challenges and prospects., *Int. J. Pharm.* 515 (2016) 757–773.  
<https://doi.org/10.1016/j.ijpharm.2016.11.002>.
- [101] J.-P. Pelletier, J. Martel-Pelletier, F. Rannou, C. Cooper, Efficacy and safety of oral NSAIDs and analgesics in the management of osteoarthritis: Evidence from real-life setting trials and surveys., *Semin. Arthritis Rheum.* 45 (2016) S22–7.  
<https://doi.org/10.1016/j.semarthrit.2015.11.009>.
- [102] L. Laine, W.B. White, A. Rostom, M. Hochberg, COX-2 selective inhibitors in the treatment of osteoarthritis., *Semin. Arthritis Rheum.* 38 (2008) 165–187.  
<https://doi.org/10.1016/j.semarthrit.2007.10.004>.
- [103] L.-C. Chen, D.M. Ashcroft, Risk of myocardial infarction associated with selective COX-2 inhibitors: meta-analysis of randomised controlled trials., *Pharmacoepidemiol. Drug Saf.* 16 (2007) 762–772. <https://doi.org/10.1002/pds.1409>.
- [104] F. Rannou, J.-P. Pelletier, J. Martel-Pelletier, Efficacy and safety of topical NSAIDs in the management of osteoarthritis: Evidence from real-life setting trials and surveys., *Semin. Arthritis Rheum.* 45 (2016) S18–21.  
<https://doi.org/10.1016/j.semarthrit.2015.11.007>.
- [105] A.R. Gammaitoni, B.S. Galer, R. Onawola, M.P. Jensen, C.E. Argoff, Lidocaine patch 5% and its positive impact on pain qualities in osteoarthritis: results of a pilot 2-week, open-label study using the Neuropathic Pain Scale, *Curr. Med. Res. Opin.* 20 (2004) S13–S19.  
<https://doi.org/10.1185/030079904X12951>.

- [106] P. Jüni, R. Hari, A.W.S. Rutjes, R. Fischer, M.G. Sillelta, S. Reichenbach, B.R. da Costa, Intra-articular corticosteroid for knee osteoarthritis., *Cochrane Database Syst. Rev.* (2015) CD005328. <https://doi.org/10.1002/14651858.CD005328.pub3>.
- [107] W. He, M. Kuang, J. Zhao, L. Sun, B. Lu, Y. Wang, J. Ma, X. Ma, Efficacy and safety of intraarticular hyaluronic acid and corticosteroid for knee osteoarthritis: A meta-analysis, *Int. J. Surg.* 39 (2017) 95–103. <https://doi.org/https://doi.org/10.1016/j.ijisu.2017.01.087>.
- [108] N. Butoescu, O. Jordan, E. Doelker, Intra-articular drug delivery systems for the treatment of rheumatic diseases: a review of the factors influencing their performance., *Eur. J. Pharm. Biopharm. Off. J. Arbeitsgemeinschaft Fur Pharm. Verfahrenstechnik e.V.* 73 (2009) 205–218. <https://doi.org/10.1016/j.ejpb.2009.06.009>.
- [109] Z. He, B. Wang, C. Hu, J. Zhao, An overview of hydrogel-based intra-articular drug delivery for the treatment of osteoarthritis., *Colloids Surf. B. Biointerfaces.* 154 (2017) 33–39. <https://doi.org/10.1016/j.colsurfb.2017.03.003>.
- [110] K. Rönn, N. Reischl, E. Gautier, M. Jacobi, Current surgical treatment of knee osteoarthritis, *Arthritis.* 2011 (2011) 454873. <https://doi.org/10.1155/2011/454873>.
- [111] A. Latourte, M. Kloppenburg, P. Richette, Emerging pharmaceutical therapies for osteoarthritis, *Nat. Rev. Rheumatol.* 16 (2020) 673–688. <https://doi.org/10.1038/s41584-020-00518-6>.
- [112] K. Yamamoto, D. Wilkinson, G. Bou-Gharios, Targeting Dysregulation of Metalloproteinase Activity in Osteoarthritis, *Calcif. Tissue Int.* (2020).
- <https://doi.org/10.1007/s00223-020-00739-7>.
- [113] S.S. Apte, Anti-ADAMTS5 monoclonal antibodies: implications for aggrecanase inhibition in osteoarthritis, *Biochem. J.* 473 (2016) e1–e4. <https://doi.org/10.1042/BJ20151072>.
- [114] J.A. Collins, B.O. Diekman, R.F. Loeser, Targeting aging for disease modification in osteoarthritis, *Curr. Opin. Rheumatol.* 30 (2018) 101–107. <https://doi.org/10.1097/BOR.0000000000000456>.
- [115] S.S. Shah, K. Mithoefer, Current Applications of Growth Factors for Knee Cartilage Repair and Osteoarthritis Treatment, *Curr. Rev. Musculoskelet. Med.* 13 (2020) 641–650. <https://doi.org/10.1007/s12178-020-09664-6>.
- [116] F.W. Roemer, A. Aydemir, S. Lohmander, M.D. Crema, M.D. Marra, N. Muurahainen, D.T. Felson, F. Eckstein, A. Guermazi, Structural effects of sprifermin in knee osteoarthritis: a post-hoc analysis on cartilage and non-cartilaginous tissue alterations in a randomized controlled trial, *BMC Musculoskelet. Disord.* 17 (2016) 267. <https://doi.org/10.1186/s12891-016-1128-2>.
- [117] A.C. Bay-Jensen, A. Manginelli, F. Moreau, Y. He, Y. Luo, J.R. Andersen, A.R. Bihlet, M. Karsdal, H. Gühring, C. Ladel, OP0189 Assessment of cartilage degradation and protective markers in synovial fluid from osteoarthritis patients before and after cycles of intra-articular injections with sprifermin, *Ann. Rheum. Dis.* 79 (2020) 117 LP – 118. <https://doi.org/10.1136/annrheumdis-2020-eular.3855>.
- [118] E.F. Eriksen, M. Shabestari, A. Ghouri, P.G. Conaghan, Bisphosphonates as a treatment modality in osteoarthritis, *Bone.* 143 (2021) 115352.

<https://doi.org/https://doi.org/10.1016/j.bo.2020.115352>.

**[119]** R.L. Xing, L.R. Zhao, P.M. Wang, Bisphosphonates therapy for osteoarthritis: a meta-analysis of randomized controlled trials, Springerplus. 5 (2016) 1704. <https://doi.org/10.1186/s40064-016-3359-y>.

**[120]** H.J. Salminen-Mankonen, J. Morko, E. Vuorio, Role of cathepsin K in normal joints and in the development of arthritis., Curr. Drug Targets. 8 (2007) 315–323. <https://doi.org/10.2174/138945007779940188>.

**[121]** M.R. McClung, M.L. O'Donoghue, S.E. Papapoulos, H. Bone, B. Langdahl, K.G. Saag, I.R. Reid, D.P. Kiel, I. Cavallari, M.P. Bonaca, S.D. Wiviott, T. de Villiers, X. Ling, K. Lippuner, T. Nakamura, J.-Y. Reginster, J.A. Rodriguez-Portales, C. Roux, J. Zanchetta, C.A.F. Zerbin, J.-G. Park, K. Im, A. Cange, L.T. Grip, N. Heyden, C. DaSilva, D. Cohn, R. Massaad, B.B. Scott, N. Verbruggen, D. Gurner, D.L. Miller, M.L. Blair, A.B. Polis, S.A. Stoch, A. Santora, A. Lombardi, A.T. Leung, K.D. Kaufman, M.S. Sabatine, Odanacatib for the treatment of postmenopausal osteoporosis: results of the LOFT multicentre, randomised, double-blind, placebo-controlled trial and LOFT Extension study., Lancet. Diabetes Endocrinol. 7 (2019) 899–911. [https://doi.org/10.1016/S2213-8587\(19\)30346-8](https://doi.org/10.1016/S2213-8587(19)30346-8).

**[122]** X. Chevalier, P. Goupille, A.D. Beaulieu, F.X. Burch, W.G. Bensen, T. Conrozier, D. Loeuille, A.J. Kivitz, D. Silver, B.E. Appleton, Intraarticular injection of anakinra in osteoarthritis of the knee: a multicenter, randomized, double-blind, placebo-controlled study., Arthritis Rheum. 61 (2009) 344–352. <https://doi.org/10.1002/art.24096>.

**[123]** S.B. Cohen, S. Proudman, A.J. Kivitz, F.X. Burch, J.P. Donohue, D. Burstein, Y.-N. Sun, C. Banfield, M.S. Vincent, L. Ni, D.J. Zack, A randomized, double-blind study of AMG 108 (a fully human monoclonal antibody to IL-

1R1) in patients with osteoarthritis of the knee., Arthritis Res. Ther. 13 (2011) R125. <https://doi.org/10.1186/ar3430>.

**[124]** X. Chevalier, P. Ravaud, E. Maheu, G. Baron, A. Rialland, P. Vergnaud, C. Roux, Y. Maugars, D. Mulleman, C. Lukas, D. Wendling, P. Lafforgue, D. Loeuille, V. Foltz, P. Richette, Adalimumab in patients with hand osteoarthritis refractory to analgesics and NSAIDs: a randomised, multicentre, double-blind, placebo-controlled trial., Ann. Rheum. Dis. 74 (2015) 1697–1705. <https://doi.org/10.1136/annrheumdis-2014-205348>.

**[125]** D. Aitken, L.L. Laslett, F. Pan, I.K. Haugen, P. Otahal, N. Bellamy, P. Bird, G. Jones, A randomised double-blind placebo-controlled crossover trial of HUMira (adalimumab) for erosive hand Osteoarthritis - the HUMOR trial., Osteoarthritis. 26 (2018) 880–887. <https://doi.org/10.1016/j.joca.2018.02.899>.

**[126]** G. Verbruggen, R. Wittoek, B. Vander Cruyssen, D. Elewaut, Tumour necrosis factor blockade for the treatment of erosive osteoarthritis of the interphalangeal finger joints: a double blind, randomised trial on structure modification, Ann. Rheum. Dis. 71 (2012) 891 LP – 898. <https://doi.org/10.1136/ard.2011.149849>.

**[127]** M. Kloppenburg, R. Ramonda, K. Bobacz, W.-Y. Kwok, D. Elewaut, T.W.J. Huizinga, F.P.B. Kroon, L. Punzi, J.S. Smolen, B. Vander Cruyssen, R. Wolterbeek, G. Verbruggen, R. Wittoek, Etanercept in patients with inflammatory hand osteoarthritis (EHOA): a multicentre, randomised, double-blind, placebo-controlled trial, Ann. Rheum. Dis. 77 (2018) 1757 LP – 1764. <https://doi.org/10.1136/annrheumdis-2018-213202>.

**[128]** A. Enteshari-Moghaddam, K. Isazadehfard, A. Habibzadeh, M. Hemmati,

Efficacy of methotrexate on pain severity reduction and improvement of quality of life in patients with moderate to severe knee osteoarthritis, *Anesthesiol. Pain Med.* 9 (2019).  
<https://doi.org/10.5812/aapm.89990>.

**[129]** D.J. Hunter, J.J. McDougall, F.J. Keefe, The symptoms of osteoarthritis and the genesis of pain, *Rheum. Dis. Clin. North Am.* 34 (2008) 623–643.  
<https://doi.org/10.1016/j.rdc.2008.05.004>.

**[130]** T.J. Schnitzer, J.A. Marks, A systematic review of the efficacy and general safety of antibodies to NGF in the treatment of OA of the hip or knee, *Osteoarthr. Cartil.* 23 (2015) S8–S17.  
<https://doi.org/https://doi.org/10.1016/j.joc.a.2014.10.003>.

**[131]** E.J. Cotter, R.M. Frank, B. Mandelbaum, Management of osteoarthritis - biological approaches: current concepts, *J. ISAKOS Jt. Disord. & Orthop. Sport. Med.* 5 (2020) 27 LP – 31.  
<https://doi.org/10.1136/jisakos-2019-000377>.

**[132]** J.R. Steadman, W.G. Rodkey, J.J. Rodrigo, Microfracture: surgical technique and rehabilitation to treat chondral defects., *Clin. Orthop. Relat. Res.* (2001) S362-9.  
<https://doi.org/10.1097/00003086-200110001-00033>.

**[133]** R.L. Davies, N.J. Kuiper, Regenerative Medicine: A Review of the Evolution of Autologous Chondrocyte Implantation (ACI) Therapy, *Bioeng. (Basel, Switzerland)*. 6 (2019) 22.  
<https://doi.org/10.3390/bioengineering6010022>.

**[134]** R.E. Delanois, J.I. Etcheson, N. Sodhi, R.F. 3rd Henn, C.U. Gwam, N.E. George, M.A. Mont, Biologic Therapies for the Treatment of Knee Osteoarthritis., *J. Arthroplasty.* 34

(2019) 801–813.  
<https://doi.org/10.1016/j.arth.2018.12.001>.

**[135]** W. Zhang, H. Ouyang, C.R. Dass, J. Xu, Current research on pharmacologic and regenerative therapies for osteoarthritis., *Bone Res.* 4 (2016) 15040.  
<https://doi.org/10.1038/boneres.2015.40>.

**[136]** I. Andia, N. Maffulli, Platelet-rich plasma for managing pain and inflammation in osteoarthritis., *Nat. Rev. Rheumatol.* 9 (2013) 721–730.  
<https://doi.org/10.1038/nrrheum.2013.141>.

**[137]** B. O'Connell, N.M. Wragg, S.L. Wilson, The use of PRP injections in the management of knee osteoarthritis, *Cell Tissue Res.* 376 (2019) 143–152.  
<https://doi.org/10.1007/s00441-019-02996-x>.

**[138]** G. Intini, The use of platelet-rich plasma in bone reconstruction therapy., *Biomaterials.* 30 (2009) 4956–4966.  
<https://doi.org/10.1016/j.biomaterials.2009.05.055>.

**[139]** V. Pavlovic, M. Ciric, V. Jovanovic, P. Stojanovic, Platelet Rich Plasma: a short overview of certain bioactive components, *Open Med. (Warsaw, Poland)*. 11 (2016) 242–247.  
<https://doi.org/10.1515/med-2016-0048>.

**[140]** J.W. Belk, M.J. Kraeutler, D.A. Houck, J.A. Goodrich, J.L. Dragoo, E.C. McCarty, Platelet-Rich Plasma Versus Hyaluronic Acid for Knee Osteoarthritis: A Systematic Review and Meta-analysis of Randomized Controlled Trials., *Am. J. Sports Med.* (2020) 363546520909397.  
<https://doi.org/10.1177/0363546520909397>

**[141]** E. Hohmann, K. Tetsworth, V. Glatt, Is platelet-rich plasma effective for the treatment of knee osteoarthritis? A systematic review and meta-analysis of level 1 and 2 randomized controlled trials, *Eur. J.*

Orthop. Surg. Traumatol. 30 (2020) 955–967.  
<https://doi.org/10.1007/s00590-020-02623-4>.

**[142]** G. Filardo, D. Previtali, F. Napoli, C. Candrian, S. Zaffagnini, A. Grassi, PRP Injections for the Treatment of Knee Osteoarthritis: A Meta-Analysis of Randomized Controlled Trials, *Cartilage*. (2020).

<https://doi.org/10.1177/1947603520931170>

**[143]** S.A. Raeissadat, S.M. Rayegani, H. Hassanabadi, M. Fathi, E. Ghorbani, M. Babaee, K. Azma, Knee osteoarthritis injection choices: Platelet-rich plasma (PRP) versus hyaluronic acid (A one-year randomized clinical trial), *Clin. Med. Insights Arthritis Musculoskelet. Disord.* 8 (2015).  
<https://doi.org/10.4137/CMAMD.S17894>.

**[144]** G. Görmeli, C.A. Görmeli, B. Ataoglu, C. Çolak, O. Aslantürk, K. Ertem, Multiple PRP injections are more effective than single injections and hyaluronic acid in knees with early osteoarthritis: a randomized, double-blind, placebo-controlled trial, *Knee Surgery, Sport. Traumatol. Arthrosc.* 25 (2017) 958–965. <https://doi.org/10.1007/s00167-015-3705-6>.

**[145]** Y.U. Yaradilmis, I. Demirkale, A. Safa Tagral, M. Caner Okkaoglu, A. Ates, M. Altay, Comparison of two platelet rich plasma formulations with viscosupplementation in treatment of moderate grade gonarthrosis: A prospective randomized controlled study., *J. Orthop.* 20 (2020) 240–246.  
<https://doi.org/10.1016/j.jor.2020.01.041>.

**[146]** A.-T. Wang, Y. Feng, H.-H. Jia, M. Zhao, H. Yu, Application of mesenchymal stem cell therapy for the treatment of osteoarthritis of the knee: A concise review, *World J. Stem Cells.* 11 (2019) 222–235.  
<https://doi.org/10.4252/wjsc.v11.i4.222>.

**[147]** B. Maheshwer, E.M. Polce, K. Paul, B.T. Williams, T.S. Wolfson, A. Yanke, N.N. Verma,

B.J. Cole, J. Chahla, Regenerative Potential of Mesenchymal Stem Cells for the Treatment of Knee Osteoarthritis and Chondral Defects: A Systematic Review and Meta-analysis, *Arthrosc. - J. Arthrosc. Relat. Surg.* 37 (2021) 362–378.

<https://doi.org/10.1016/j.arthro.2020.05.037>.

**[148]** W. Ma, C. Liu, S. Wang, H. Xu, H. Sun, X. Fan, Efficacy and safety of intra-articular injection of mesenchymal stem cells in the treatment of knee osteoarthritis: A systematic review and meta-analysis, *Medicine (Baltimore)*. 99 (2020) e23343–e23343.

<https://doi.org/10.1097/MD.00000000000023343>.

**[149]** E.C. Doyle, N.M. Wragg, S.L. Wilson, Intraarticular injection of bone marrow-derived mesenchymal stem cells enhances regeneration in knee osteoarthritis., *Knee Surg. Sports Traumatol. Arthrosc.* 28 (2020) 3827–3842. <https://doi.org/10.1007/s00167-020-05859-z>.

**[150]** B.O. Diekman, F. Guilak, Stem cell-based therapies for osteoarthritis: challenges and opportunities, *Curr. Opin. Rheumatol.* 25 (2013) 119–126.  
<https://doi.org/10.1097/BOR.0b013e32835aa28d>.

**[151]** P. Mancuso, S. Raman, A. Glynn, F. Barry, J.M. Murphy, Mesenchymal Stem Cell Therapy for Osteoarthritis: The Critical Role of the Cell Secretome., *Front. Bioeng. Biotechnol.* 7 (2019) 9.  
<https://doi.org/10.3389/fbioe.2019.00009>.

**[152]** S. Eleuteri, A. Fierabracci, Insights into the Secretome of Mesenchymal Stem Cells and Its Potential Applications, *Int. J. Mol. Sci.* 20 (2019) 4597.  
<https://doi.org/10.3390/ijms20184597>.

**[153]** C.R. Harrell, N. Jovicic, V. Djonov, N. Arsenijevic, V. Volarevic, Mesenchymal Stem

Cell-Derived Exosomes and Other Extracellular Vesicles as New Remedies in the Therapy of Inflammatory Diseases, *Cells*. 8 (2019) 1605. <https://doi.org/10.3390/cells8121605>.

[154] M. Bousnaki, A. Bakopoulou, A. Kritis, P. Koidis, The Efficacy of Stem Cells Secretome Application in Osteoarthritis: A Systematic Review of In Vivo Studies., *Stem Cell Rev. Reports*. 16 (2020) 1222–1241. <https://doi.org/10.1007/s12015-020-09980-x>.

[155] S. Mohamed-Ahmed, I. Fristad, S.A. Lie, S. Suliman, K. Mustafa, H. Vindenes, S.B. Idris, Adipose-derived and bone marrow mesenchymal stem cells: a donor-matched comparison, *Stem Cell Res. Ther.* 9 (2018) 168. <https://doi.org/10.1186/s13287-018-0914-1>.

[156] G.B. Kim, M.-S. Seo, W.T. Park, G.W. Lee, Bone Marrow Aspirate Concentrate: Its Uses in Osteoarthritis., *Int. J. Mol. Sci.* 21 (2020). <https://doi.org/10.3390/ijms21093224>.

[157] J. Chahla, S. Mannava, M.E. Cinque, A.G. Geeslin, D. Codina, R.F. LaPrade, Bone Marrow Aspirate Concentrate Harvesting and Processing Technique, *Arthrosc. Tech.* 6 (2017) e441–e445. <https://doi.org/10.1016/j.eats.2016.10.024>.

[158] G.B. Kim, J.-D. Kim, Y. Choi, C.H. Choi, G.W. Lee, Intra-articular bone marrow aspirate concentrate injection in patients with knee osteoarthritis, *Appl. Sci.* 10 (2020). <https://doi.org/10.3390/app10175945>.

[159] A.W. Anz, R. Hubbard, N.K. Rendos, P.A. Everts, J.R. Andrews, J.G. Hackel, Bone Marrow Aspirate Concentrate Is Equivalent to Platelet-Rich Plasma for the Treatment of Knee Osteoarthritis at 1 Year: A Prospective, Randomized Trial, *Orthop. J. Sport. Med.* 8 (2020). <https://doi.org/10.1177/2325967119900958>

[160] F. Rodriguez-Fontan, N.S. Piuze, M.J. Kraeutler, C. Pascual-Garrido, Early Clinical Outcomes of Intra-Articular Injections of Bone Marrow Aspirate Concentrate for the Treatment of Early Osteoarthritis of the Hip and Knee: A Cohort Study, *PM R.* 10 (2018) 1353–1359. <https://doi.org/10.1016/j.pmrj.2018.05.016>.

[161] C.H. Evans, J.N. Gouze, E. Gouze, P.D. Robbins, S.C. Ghivizzani, Osteoarthritis gene therapy., *Gene Ther.* 11 (2004) 379–389. <https://doi.org/10.1038/sj.gt.3302196>.

[162] B. Lee, J. Parvizi, D. Bramlet, D.W. Romness, A. Guermazi, M. Noh, N. Sodhi, A. Khlopas, M.A. Mont, Results of a Phase II Study to Determine the Efficacy and Safety of Genetically Engineered Allogeneic Human Chondrocytes Expressing TGF-β1., *J. Knee Surg.* 33 (2020) 167–172. <https://doi.org/10.1055/s-0038-1676803>.

[163] M.-K. Kim, C.-W. Ha, Y. In, S.-D. Cho, E.-S. Choi, J.-K. Ha, J.-H. Lee, J.-D. Yoo, S.-I. Bin, C.-H. Choi, H.-S. Kyung, M.-C. Lee, A Multicenter, Double-Blind, Phase III Clinical Trial to Evaluate the Efficacy and Safety of a Cell and Gene Therapy in Knee Osteoarthritis Patients., *Hum. Gene Ther. Clin. Dev.* 29 (2018) 48–59. <https://doi.org/10.1089/humc.2017.249>.

[164] J.C. Maroon, J.W. Bost, A. Maroon, Natural anti-inflammatory agents for pain relief, *Surg. Neurol. Int.* 1 (2010) 80. <https://doi.org/10.4103/2152-7806.73804>.

[165] Z. Hussain, H.E. Thu, M.W. Amjad, F. Hussain, T.A. Ahmed, S. Khan, Exploring recent developments to improve antioxidant, anti-inflammatory and antimicrobial efficacy of curcumin: A review of new trends and future perspectives., *Mater. Sci. Eng. C. Mater. Biol. Appl.* 77 (2017) 1316–1326. <https://doi.org/10.1016/j.msec.2017.03.226>.

[166] H. Hatcher, R. Planalp, J. Cho, F.M. Torti, S. V Torti, Curcumin: from ancient medicine to

current clinical trials., *Cell. Mol. Life Sci.* 65 (2008) 1631–1652.  
<https://doi.org/10.1007/s00018-008-7452-4>.

**[167]** National Center for Biotechnology Information, PubChem Compound Summary for CID 969516, Curcumin, (n.d.).

**[168]** B.B. Aggarwal, B. Sung, Pharmacological basis for the role of curcumin in chronic diseases: an age-old spice with modern targets, *Trends Pharmacol. Sci.* 30 (2009) 85–94.  
<https://doi.org/https://doi.org/10.1016/j.tip.s.2008.11.002>.

**[169]** Y. He, Y. Yue, X. Zheng, K. Zhang, S. Chen, Z. Du, Curcumin, inflammation, and chronic diseases: how are they linked?, *Molecules.* 20 (2015) 9183–9213.  
<https://doi.org/10.3390/molecules20059183>

**[170]** K. Shimizu, M. Funamoto, Y. Sunagawa, S. Shimizu, Y. Katanasaka, Y. Miyazaki, H. Wada, K. Hasegawa, T. Morimoto, Anti-inflammatory Action of Curcumin and Its Use in the Treatment of Lifestyle-related Diseases, *Eur. Cardiol.* 14 (2019) 117–122.  
<https://doi.org/10.15420/ecr.2019.17.2>.

**[171]** M.S. Baliga, N. Joseph, M. V Venkataranganna, A. Saxena, V. Ponemone, R. Fayad, Curcumin, an active component of turmeric in the prevention and treatment of ulcerative colitis: preclinical and clinical observations, *Food Funct.* 3 (2012) 1109–1117. <https://doi.org/10.1039/C2FO30097D>.

**[172]** M. Tomić, A. Micov, U. Pecikoza, R. Stepanović-Petrović, Chapter 1 - Clinical Uses of Nonsteroidal Anti-Inflammatory Drugs (NSAIDs) and Potential Benefits of NSAIDs Modified-Release Preparations, in: B.B.T.-M. and N.C. for N.A.-I.D. Čalijs (Ed.), Academic Press, Boston, 2017: pp. 1–29.  
<https://doi.org/https://doi.org/10.1016/B978-0-0-12-804017-1.00001-7>.

**[173]** C.D. Funk, G.A. FitzGerald, COX-2 inhibitors and cardiovascular risk., *J. Cardiovasc. Pharmacol.* 50 (2007) 470–479.  
<https://doi.org/10.1097/FJC.0b013e318157f72d>.

**[174]** D.C. Brater, C. Harris, J.S. Redfern, B.J. Gertz, Renal effects of COX-2-selective inhibitors., *Am. J. Nephrol.* 21 (2001) 1–15.  
<https://doi.org/10.1159/000046212>.

**[175]** P. Rao, E.E. Knaus, Evolution of nonsteroidal anti-inflammatory drugs (NSAIDs): cyclooxygenase (COX) inhibition and beyond., *J. Pharm. Pharm. Sci. a Publ. Can. Soc. Pharm. Sci. Soc. Can. Des. Sci. Pharm.* 11 (2008) 81s–110s.  
<https://doi.org/10.18433/j3t886>.

**[176]** E. Kopp, S. Ghosh, Inhibition of NF-kappa B by sodium salicylate and aspirin., *Science.* 265 (1994) 956–959.  
<https://doi.org/10.1126/science.8052854>.

**[177]** E. Niederberger, I. Tegeder, NSAIDs, COX-Independent Actions, *Encycl. Pain.* (2006) 1470–1473.  
[https://doi.org/10.1007/978-3-540-29805-2\\_2850](https://doi.org/10.1007/978-3-540-29805-2_2850).

**[178]** R. Zenz, R. Eferl, C. Scheinecker, K. Redlich, J. Smolen, H.B. Schonthaler, L. Kenner, E. Tschachler, E.F. Wagner, Activator protein 1 (Fos/Jun) functions in inflammatory bone and skin disease, *Arthritis Res. Ther.* 10 (2008) 201. <https://doi.org/10.1186/ar2338>.

**[179]** E. Gurbinar, W. Grizzle, G. Piazza, COX-Independent Mechanisms of Cancer Chemoprevention by Anti-Inflammatory Drugs, *Front. Oncol.* 3 (2013) 181.  
<https://doi.org/10.3389/fonc.2013.00181>.

**[180]** P.A. Todd, S.P. Clissold, Tenoxicam. An update of its pharmacology and therapeutic efficacy in rheumatic diseases., *Drugs.* 41 (1991) 625–646.  
<https://doi.org/10.2165/00003495-199141040-00008>.

- [181] National Center for Biotechnology Information, PubChem Compound Summary for CID 54677971, Tenoxicam, (n.d.). <https://pubchem.ncbi.nlm.nih.gov/compound/Tenoxicam> (accessed December 4, 2020).
- [182] T.W. Guentert, R.C. Heintz, R. Joly, Overview on the pharmacokinetics of tenoxicam., *Eur. J. Rheumatol. Inflamm.* 9 (1987) 15–25.
- [183] A. Khattab, D.M.N. Abouhoussein, E. Mohammad F, Development of injectable tenoxicam in situ forming microparticles based on sesame oil and poly-DL-lactide: Characterization, efficacy and acute toxicity, *J. Drug Deliv. Sci. Technol.* 51 (2019) 682–694. <https://doi.org/https://doi.org/10.1016/j.jddst.2019.04.001>.
- [184] S. Goindi, M. Narula, A. Kalra, Microemulsion-Based Topical Hydrogels of Tenoxicam for Treatment of Arthritis, *AAPS PharmSciTech.* 17 (2016) 597–606. <https://doi.org/10.1208/s12249-015-0383-0>.
- [185] L.M. Negi, M. Chauhan, A.K. Garg, Nano-appended transdermal gel of Tenoxicam via ultradeformable drug carrier system, *J. Exp. Nanosci.* 8 (2013) 657–669. <https://doi.org/10.1080/17458080.2011.597441>.
- [186] M. Erbas, T. Simsek, H.A. Kiraz, H. Sahin, H. Toman, Comparison of the effectivity of oral and intra-articular administration of tenoxicam in patients with knee osteoarthritis, *Brazilian J. Anesthesiol.* 65 (2015) 333–337. <https://doi.org/10.1016/j.bjan.2013.12.003>.
- [187] R. Jawish, H. Najdi, C. Abi Safi, A. Chameseddine, The effect of intra-articular Tenoxicam on knee effusion after arthroscopy, *Int. Orthop.* 39 (2015) 1423–1426. <https://doi.org/10.1007/s00264-014-2640-3>.
- [188] E. Yilmaz, The evaluation of the effectiveness of intra-articular steroid, tenoxicam, and combined steroid–tenoxicam injections in the treatment of patients with knee osteoarthritis, *Clin. Rheumatol.* 38 (2019) 3243–3252. <https://doi.org/10.1007/s10067-019-04641-Y>.
- [189] F.U. Ozkan, G. Uzer, I. Türkmen, Y. Yıldız, S. Senol, K. Ozkan, F. Turkmensoy, S. Ramadan, I. Aktas, Intra-articular hyaluronate, tenoxicam and vitamin e in a rat model of osteoarthritis: Evaluation and comparison of chondroprotective efficacy, *Int. J. Clin. Exp. Med.* 8 (2015) 1018–1026. <https://www.scopus.com/inward/record.uri?eid=2-s2.0-84922960155&partnerID=40&md5=42bf7e26573fcc8d84ef809efb7e4ebb>.
- [190] National Center for Biotechnology Information, PubChem Compound Summary for CID 2662, Celecoxib, (n.d.). <https://pubchem.ncbi.nlm.nih.gov/compound/Celecoxib> (accessed December 4, 2020).
- [191] J.-P. Pelletier, J.-P. Raynauld, M. Dorais, L. Bessette, E. Dokoupilova, F. Morin, K. Pavelka, P. Paiement, J. Martel-Pelletier, D.T.I. Group, An international, multicentre, double-blind, randomized study (DISSCO): effect of diacerein vs celecoxib on symptoms in knee osteoarthritis, *Rheumatology (Oxford)*. 59 (2020) 3858–3868. <https://doi.org/10.1093/rheumatology/keaa072>.
- [192] R. Reyes-Sosa, A. Lugo-Radillo, M.R. Ruiz-Olivera, L. Cruz-Santiago, C.R. García-Cruz, O. Mendoza-Cano, Clinical comparison of platelet-rich plasma injection and daily celecoxib administration in the treatment of early knee osteoarthritis: A randomized clinical trial, *J. Appl. Biomed.* 18 (2020) 41–45. <https://doi.org/10.32725/jab.2020.012>.
- [193] M.S. Park, C.-N. Kang, W.-S. Lee, H.-J. Kim, S. Lee, J.H. Kim, S.-J. Shin, S.-H. Moon, A



comparative study of the efficacy of NAXOZOL compared to celecoxib in patients with osteoarthritis, *PLoS One*. 15 (2020). <https://doi.org/10.1371/journal.pone.0226184>.

[194] D. Gang, C. Xiaguang, Y. Kanghua, W. Aiping, Z. Guangxuan, Combined effect of celecoxib and glucosamine sulfate on inflammatory factors and oxidative stress indicators in patients with knee osteoarthritis, *Trop. J. Pharm. Res.* 18 (2019) 397–402. <https://doi.org/10.4314/tjpr.v18i2.25>.

[195] C. Salgado, L. Guénée, R. Černý, E. Allémann, O. Jordan, Nano wet milled celecoxib extended release microparticles for local management of chronic inflammation, *Int. J. Pharm.* 589 (2020). <https://doi.org/10.1016/j.ijpharm.2020.119783>.

[196] I.J. Villamagna, T.N. Gordon, M.B. Hurtig, F. Beier, E.R. Gillies, Poly(ester amide) particles for controlled delivery of celecoxib, *J. Biomed. Mater. Res. - Part A*. 107 (2019) 1235–1243. <https://doi.org/10.1002/jbm.a.36632>.

[197] S.I. Grivennikov, F.R. Greten, M. Karin, Immunity, inflammation, and cancer, *Cell*. 140 (2010) 883–899. <https://doi.org/10.1016/j.cell.2010.01.025>.

[198] N. Tołoczko-Iwaniuk, D. Dziemiańczyk-Pakieła, B.K. Nowaszewska, K. Celińska-Janowicz, W. Milyk, Celecoxib in cancer therapy and prevention - review, *Curr. Drug Targets*. 20 (2019) 302–315. <https://doi.org/10.2174/1389450119666180803121737>.

[199] P. Saxena, P.K. Sharma, P. Purohit, A journey of celecoxib from pain to cancer, *Prostaglandins Other Lipid Mediat.* 147 (2020). <https://doi.org/10.1016/j.prostaglandins.2019.106379>.

[200] M.D. Taves, C.E. Gomez-Sanchez, K.K. Soma, Extra-adrenal glucocorticoids and mineralocorticoids: evidence for local synthesis, regulation, and function, *Am. J. Physiol. Endocrinol. Metab.* 301 (2011) E11–E24. <https://doi.org/10.1152/ajpendo.00100.2011>.

[201] P.J. Barnes, Glucocorticosteroids: current and future directions, *Br. J. Pharmacol.* 163 (2011) 29–43. <https://doi.org/10.1111/j.1476-5381.2010.01199.x>.

[202] A. Grzanka, M. Misiótek, W. Golusiński, J. Jarząb, Molecular mechanisms of glucocorticoids action: implications for treatment of rhinosinusitis and nasal polyposis, *Eur. Arch. Otorhinolaryngol.* 268 (2011) 247–253. <https://doi.org/10.1007/s00405-010-1330-z>.

[203] B. Liu, T.N. Zhang, J.K. Knight, J.E. Goodwin, The Glucocorticoid Receptor in Cardiovascular Health and Disease, *Cells*. 8 (2019) 1–21. <https://doi.org/10.3390/cells8101227>.

[204] A.A. Alangari, Genomic and non-genomic actions of glucocorticoids in asthma, *Ann. Thorac. Med.* 5 (2010) 133–139. <https://doi.org/10.4103/1817-1737.65040>.

[205] P.J. Barnes, How corticosteroids control inflammation: Quintiles Prize Lecture 2005, *Br. J. Pharmacol.* 148 (2006) 245–254. <https://doi.org/10.1038/sj.bjp.0706736>.

[206] L. Escoter-Torres, G. Caratti, A. Mechtidou, J. Tuckermann, N.H. Uhlenhaut, S. Vettorazzi, Fighting the Fire: Mechanisms of Inflammatory Gene Regulation by the Glucocorticoid Receptor, *Front. Immunol.* 10 (2019) 1859. <https://doi.org/10.3389/fimmu.2019.01859>.

[207] E. Joanny, Q. Ding, L. Gong, P. Kong, J. Saklatvala, A.R. Clark, Anti-inflammatory

effects of selective glucocorticoid receptor modulators are partially dependent on up-regulation of dual specificity phosphatase 1, *Br. J. Pharmacol.* 165 (2012) 1124–1136. <https://doi.org/10.1111/j.1476-5381.2011.01574.x>.

**[208]** K. De Bosscher, I.M. Beck, L. Dejager, N. Bougarne, A. Gaigneaux, S. Chateauvieux, D. Ratman, M. Bracke, J. Tavernier, W. Vanden Bergh, C. Libert, M. Diederich, G. Haegeman, Selective modulation of the glucocorticoid receptor can distinguish between transrepression of NF- $\kappa$ B and AP-1., *Cell. Mol. Life Sci.* 71 (2014) 143–163. <https://doi.org/10.1007/s00018-013-1367-4>.

**[209]** E. Ayroldi, L. Cannarile, G. Migliorati, G. Nocentini, D. Delfino, C. Riccardi, Mechanisms of the anti-inflammatory effects of glucocorticoids: Genomic and nongenomic interference with MAPK signaling pathways, *FASEB J.* 26 (2012). <https://doi.org/10.1096/fj.12-216382>.

**[210]** E.S. Zabirowicz, T.J. Gan, 34 - Pharmacology of Postoperative Nausea and Vomiting, in: H.C. Hemmings, T.D.B.T.-P. and P. for A. (Second E. Egan (Eds.), Elsevier, Philadelphia, 2019: pp. 671–692. <https://doi.org/https://doi.org/10.1016/B978-0-323-48110-6.00034-X>.

**[211]** National Center for Biotechnology Information, PubChem Compound Summary for CID 5743, Dexamethasone, (n.d.). <https://pubchem.ncbi.nlm.nih.gov/compound/Dexamethasone> (accessed December 4, 2020).

**[212]** Z. Jia, G. Zhao, X. Wei, D. Kong, Y. Sun, Y. Zhou, S.M. Lele, E. V Fehring, K.L. Garvin, S.R. Goldring, D. Wang, Structural optimization of HPMA copolymer-based dexamethasone prodrug for improved treatment of inflammatory arthritis, *J. Control. Release.* 324 (2020) 560–573. <https://doi.org/https://doi.org/10.1016/j.jconrel.2020.05.028>.

**[213]** Y. Zhao, C. Wei, X. Chen, J. Liu, Q. Yu, Y. Liu, J. Liu, Drug Delivery System Based on Near-Infrared Light-Responsive Molybdenum Disulfide Nanosheets Controls the High-Efficiency Release of Dexamethasone To Inhibit Inflammation and Treat Osteoarthritis, *ACS Appl. Mater. Interfaces.* 11 (2019) 11587–11601. <https://doi.org/10.1021/acsami.8b20372>.

**[214]** A.G. Bajpayee, R.E. De la Vega, M. Scheu, N.H. Varady, I.A. Yannatos, L.A. Brown, Y. Krishnan, T.J. Fitzsimons, P. Bhattacharya, E.H. Frank, A.J. Grodzinsky, R.M. Porter, Sustained intra-cartilage delivery of low dose dexamethasone using a cationic carrier for treatment of post traumatic osteoarthritis., *Eur. Cell. Mater.* 34 (2017) 341–364. <https://doi.org/10.22203/eCM.v034a21>.

**[215]** Z. Zhang, X. Wei, J. Gao, Y. Zhao, Y. Zhao, L. Guo, C. Chen, Z. Duan, P. Li, L. Wei, Intra-Articular Injection of Cross-Linked Hyaluronic Acid-Dexamethasone Hydrogel Attenuates Osteoarthritis: An Experimental Study in a Rat Model of Osteoarthritis., *Int. J. Mol. Sci.* 17 (2016) 411. <https://doi.org/10.3390/ijms17040411>.

**[216]** Q.-S. Wang, B.-X. Xu, K.-J. Fan, Y.-W. Li, J. Wu, T.-Y. Wang, Dexamethasone-Loaded Thermosensitive Hydrogel Suppresses Inflammation and Pain in Collagen-Induced Arthritis Rats., *Drug Des. Devel. Ther.* 14 (2020) 4101–4113. <https://doi.org/10.2147/DDDT.S256850>.

**[217]** Q. Wang, L. He, D. Fan, W. Liang, J. Fang, Improving the anti-inflammatory efficacy of dexamethasone in the treatment of rheumatoid arthritis with polymerized stealth liposomes as a delivery vehicle., *J. Mater. Chem. B.* 8 (2020) 1841–1851. <https://doi.org/10.1039/c9tb02538c>.

**[218]** R.R. Meka, S.H. Venkatesha, B. Acharya, K.D. Moudgil, Peptide-targeted liposomal delivery of dexamethasone for arthritis therapy., *Nanomedicine (Lond).* 14 (2019)

1455–1469. <https://doi.org/10.2217/nmm-2018-0501>.

**[219]** X. Li, C. Yu, X. Meng, Y. Hou, Y. Cui, T. Zhu, Y. Li, L. Teng, F. Sun, Y. Li, Study of double-targeting nanoparticles loaded with MCL-1 siRNA and dexamethasone for adjuvant-induced arthritis therapy, *Eur. J. Pharm. Biopharm.* 154 (2020) 136–143. <https://doi.org/https://doi.org/10.1016/j.ejpb.2020.07.009>.

**[220]** R. Ni, G. Song, X. Fu, R. Song, L. Li, W. Pu, J. Gao, J. Hu, Q. Liu, F. He, D. Zhang, G. Huang, Reactive oxygen species-responsive dexamethasone-loaded nanoparticles for targeted treatment of rheumatoid arthritis via suppressing the iRhom2/TNF- $\alpha$ /BAFF signaling pathway., *Biomaterials.* 232 (2020) 119730. <https://doi.org/10.1016/j.biomaterials.2019.119730>.

**[221]** Y.K. Lee, S.-W. Kim, J.-Y. Park, W.C. Kang, Y.J. Kang, D. Khang, Suppression of human arthritis synovial fibroblasts inflammation using dexamethasone-carbon nanotubes via increasing caveolin-dependent endocytosis and recovering mitochondrial membrane potential., *Int. J. Nanomedicine.* 12 (2017) 5761–5779. <https://doi.org/10.2147/IJN.S142122>.

**[222]** X. Yang, H. Du, G. Zhai, Progress in intra-articular drug delivery systems for osteoarthritis., *Curr. Drug Targets.* 15 (2014) 888–900. <https://doi.org/10.2174/1389450115666140804155830>.

**[223]** P. Maudens, O. Jordan, E. Allémann, Recent advances in intra-articular drug delivery systems for osteoarthritis therapy, *Drug Discov. Today.* 23 (2018) 1761–1775. <https://doi.org/https://doi.org/10.1016/j.drudis.2018.05.023>.

**[224]** H.M. Burt, A. Tsallas, S. Gilchrist, L.S. Liang, Intra-articular drug delivery systems:

Overcoming the shortcomings of joint disease therapy., *Expert Opin. Drug Deliv.* 6 (2009) 17–26.

<https://doi.org/10.1517/17425240802647259>.

**[225]** M.L. Kang, G.-I. Im, Drug delivery systems for intra-articular treatment of osteoarthritis., *Expert Opin. Drug Deliv.* 11 (2014) 269–282. <https://doi.org/10.1517/17425247.2014.867325>.

**[226]** T.E. Kavanaugh, T.A. Werfel, H. Cho, K.A. Hasty, C.L. Duvall, Particle-based technologies for osteoarthritis detection and therapy, *Drug Deliv. Transl. Res.* 6 (2016) 132–147. <https://doi.org/10.1007/s13346-015-0234-2>.

**[227]** J. Paik, S.T. Duggan, S.J. Keam, Triamcinolone Acetonide Extended-Release: A Review in Osteoarthritis Pain of the Knee, *Drugs.* 79 (2019) 455–462. <https://doi.org/10.1007/s40265-019-01083-3>.

**[228]** C. Kang, E. Jung, H. Hyeon, S. Seon, D. Lee, Acid-activatable polymeric curcumin nanoparticles as therapeutic agents for osteoarthritis, *Nanomedicine Nanotechnology, Biol. Med.* 23 (2020). <https://doi.org/10.1016/j.nano.2019.102104>

**[229]** J.L.G. da Silva, D.F. Passos, V.M. Bernardes, F.L. Cabral, P.G. Schimites, A.G. Manzoni, E.G. de Oliveira, C. de Bona da Silva, R.C.R. Beck, M.H. Jantsch, R.M. Maciel, D.B.R. Leal, Co-Nanoencapsulation of Vitamin D3 and Curcumin Regulates Inflammation and Purine Metabolism in a Model of Arthritis, *Inflammation.* 42 (2019) 1595–1610. <https://doi.org/10.1007/s10753-019-01021-1>.

**[230]** Z. Fan, J. Li, J. Liu, H. Jiao, B. Liu, Anti-Inflammation and Joint Lubrication Dual Effects of a Novel Hyaluronic Acid/Curcumin Nanomicelle Improve the Efficacy of

Rheumatoid Arthritis Therapy, ACS Appl. Mater. Interfaces. 10 (2018) 23595–23604. <https://doi.org/10.1021/acsami.8b06236>.

**[231]** A.K. Dewangan, Y. Perumal, N. Pavurala, K. Chopra, S. Mazumder, Preparation, characterization and anti-inflammatory effects of curcumin loaded carboxymethyl cellulose acetate butyrate nanoparticles on adjuvant induced arthritis in rats, J. Drug Deliv. Sci. Technol. 41 (2017) 269–279. <https://doi.org/https://doi.org/10.1016/j.jddst.2017.07.022>.

**[232]** B. Crivelli, E. Bari, S. Perteghella, L. Catenacci, M. Sorrenti, M. Mocchi, S. Faragò, G. Tripodo, A. Prina-Mello, M.L. Torre, Silk fibroin nanoparticles for celecoxib and curcumin delivery: ROS-scavenging and anti-inflammatory activities in an in vitro model of osteoarthritis, Eur. J. Pharm. Biopharm. 137 (2019) 37–45. <https://doi.org/10.1016/j.ejpb.2019.02.008>.

**[233]** R.I. El-Gogary, M.A. Khattab, H. Abd-Allah, Intra-articular multifunctional celecoxib loaded hyaluronan nanocapsules for the suppression of inflammation in an osteoarthritic rat model, Int. J. Pharm. 583 (2020). <https://doi.org/10.1016/j.ijpharm.2020.119378>.

**[234]** J.-S. Choi, D.-H. Lee, J. Bin Ahn, S. Sim, K.-S. Heo, C.-S. Myung, J.-S. Park, Therapeutic effects of celecoxib polymeric systems in rat models of inflammation and adjuvant-induced rheumatoid arthritis, Mater. Sci. Eng. C. 114 (2020) 111042. <https://doi.org/https://doi.org/10.1016/j.msec.2020.111042>.

**[235]** H. Zhang, H. Xiong, W. Ahmed, Y. Yao, S. Wang, C. Fan, C. Gao, Reactive oxygen species-responsive and scavenging polyurethane nanoparticles for treatment of osteoarthritis in vivo, Chem. Eng. J. 409 (2021) 128147.

<https://doi.org/https://doi.org/10.1016/j.cej.2020.128147>.

**[236]** L. He, D. Fan, W. Liang, Q. Wang, J. Fang, Matrix Metalloproteinase-Responsive PEGylated Lipid Nanoparticles for Controlled Drug Delivery in the Treatment of Rheumatoid Arthritis, ACS Appl. Bio Mater. 3 (2020) 3276–3284. <https://doi.org/10.1021/acsabm.0c00242>.

**[237]** C. Yu, X. Li, Y. Hou, X. Meng, D. Wang, J. Liu, F. Sun, Y. Li, Hyaluronic Acid Coated Acid-Sensitive Nanoparticles for Targeted Therapy of Adjuvant-Induced Arthritis in Rats., Molecules. 24 (2019). <https://doi.org/10.3390/molecules24010146>

**[238]** V. Sutariya, J. Tur, S. Kelly, K. Halasz, K.C. Chapalamadugu, R. Nimbalkar, Y. V Pathak, R. Weigel, T. Daviau, T. Webb, J. Cacace, M. Brotto, S.M. Tipparaju, Nanodrug delivery platform for glucocorticoid use in skeletal muscle injury., Can. J. Physiol. Pharmacol. 96 (2018) 681–689. <https://doi.org/10.1139/cjpp-2017-0795>.

**[239]** Y. Chen, Y. Lu, R.J. Lee, G. Xiang, Nano Encapsulated Curcumin: And Its Potential for Biomedical Applications, Int. J. Nanomedicine. 15 (2020) 3099–3120. <https://doi.org/10.2147/IJN.S210320>.

**[240]** P. Singh, S. Dabre, Controlled release gel encompassing curcumin microspheres and diclofenac diethylamine for feat against arthritis inflammation, Curr. Rheumatol. Rev. 16 (2020) 119–128. <https://doi.org/10.2174/15733397115666191105142827>.

**[241]** Z. Sun, T. Wei, X. Zhou, Liposomes encapsulated dimethyl curcumin regulates dipeptidyl peptidase I activity, gelatinase release and cell cycle of spleen lymphocytes in-vivo to attenuate collagen induced arthritis in rats., Int. Immunopharmacol. 65 (2018) 511–521.

<https://doi.org/10.1016/j.intimp.2018.10.039>.

**[242]** M.L. Manca, D. Lattuada, D. Valenti, O. Marelli, C. Corradini, X. Fernández-Busquets, M. Zaru, A.M. Maccioni, A.M. Fadda, M. Manconi, Potential therapeutic effect of curcumin loaded hyalurosomes against inflammatory and oxidative processes involved in the pathogenesis of rheumatoid arthritis: The use of fibroblast-like synovial cells cultured in synovial fluid, *Eur. J. Pharm. Biopharm.* 136 (2019) 84–92. <https://doi.org/10.1016/j.ejpb.2019.01.012>.

**[243]** H.O. Ammar, M. Ghorab, S.A. El-Nahhas, I.M. Higazy, Proniosomes as a carrier system for transdermal delivery of tenoxicam., *Int. J. Pharm.* 405 (2011) 142–152. <https://doi.org/10.1016/j.ijpharm.2010.11.003>.

**[244]** L. Puljak, A. Marin, D. Vrdoljak, F. Markotic, A. Utrobicic, P. Tugwell, Celecoxib for osteoarthritis., *Cochrane Database Syst. Rev.* 5 (2017) CD009865. <https://doi.org/10.1002/14651858.CD009865.pub2>.

**[245]** U.T. Timur, M.M.J. Caron, R.M. Jeuken, Y.M. Bastiaansen-Jenniskens, T.J.M. Welting, L.W. van Rhijn, G.J.V.M. van Osch, P.J. Emans, Chondroprotective Actions of Selective COX-2 Inhibitors In Vivo: A Systematic Review., *Int. J. Mol. Sci.* 21 (2020). <https://doi.org/10.3390/ijms21186962>.

**[246]** A.R. Tellegen, I. Rudnik-Jansen, B. Pouran, H.M. de Visser, H.H. Weinans, R.E. Thomas, M.J.L. Kik, G.C.M. Grinwis, J.C. Thies, N. Woike, G. Mihov, P.J. Emans, B.P. Meij, L.B. Creemers, M.A. Tryfonidou, Controlled release of celecoxib inhibits inflammation, bone cysts and osteophyte formation in a preclinical model of osteoarthritis, *Drug Deliv.* 25 (2018) 1438–1447. <https://doi.org/10.1080/10717544.2018.1482971>.

**[247]** P. Nirbhavane, G. Sharma, B. Singh, G.K. Khuller, V.G. Goni, A.B. Patil, O.P. Katare, Preclinical Explorative Assessment of Celecoxib-Based Biocompatible Lipidic Nanocarriers for the Management of CFA-Induced Rheumatoid Arthritis in Wistar Rats., *AAPS PharmSciTech.* 19 (2018) 3187–3198. <https://doi.org/10.1208/s12249-018-1148-3>.

**[248]** V. Kumar, A. Leekha, A. Tyagi, A. Kaul, A.K. Mishra, A.K. Verma, Preparation and evaluation of biopolymeric nanoparticles as drug delivery system in effective treatment of rheumatoid arthritis., *Pharm. Res.* 34 (2017) 654–667. <https://doi.org/10.1007/s11095-016-2094-y>.

**[249]** D. Jadhav, P. Vavia, Dexamethasone Sodium Phosphate Loaded Modified Cyclodextrin Based Nanoparticles: An Efficient Treatment for Rheumatoid Arthritis, *J. Pharm. Sci.* (2020). <https://doi.org/https://doi.org/10.1016/j.xphs.2020.10.023>.

**[250]** F. Yan, Z. Zhong, Y. Wang, Y. Feng, Z. Mei, H. Li, X. Chen, L. Cai, C. Li, Exosome-based biomimetic nanoparticles targeted to inflamed joints for enhanced treatment of rheumatoid arthritis, *J. Nanobiotechnology.* 18 (2020) 115. <https://doi.org/10.1186/s12951-020-00675-6>.

**[251]** X. Wang, Y. Feng, J. Fu, C. Wu, B. He, H. Zhang, X. Wang, W. Dai, Y. Sun, Q. Zhang, A Lipid Micellar System Loaded with Dexamethasone Palmitate Alleviates Rheumatoid Arthritis, *AAPS PharmSciTech.* 20 (2019) 316. <https://doi.org/10.1208/s12249-019-1449-1>.

**[252]** Y. Xu, J. Mu, Z. Xu, H. Zhong, Z. Chen, Q. Ni, X.-J. Liang, S. Guo, Modular Acid-Activatable Acetone-Based Ketal-Linked Nanomedicine by Dexamethasone Prodrugs for Enhanced Anti-Rheumatoid Arthritis with Low Side Effects, *Nano Lett.* 20 (2020) 2558–2568.

<https://doi.org/10.1021/acs.nanolett.9b05340>.

**[253]** M. Lorscheider, N. Tsapis, M. Ur-Rehman, F. Gaudin, I. Stofa, S. Abreu, S. Mura, P. Chaminade, M. Espeli, E. Fattal, Dexamethasone palmitate nanoparticles: An efficient treatment for rheumatoid arthritis., *J. Control. Release.* 296 (2019) 179–189. <https://doi.org/10.1016/j.jconrel.2019.01.015>.

**[254]** G.M. Pontes-Quero, L. Benito-Garzón, J. Pérez Cano, M.R. Aguilar, B. Vázquez-Lasa, Amphiphilic polymeric nanoparticles encapsulating curcumin: Antioxidant, anti-inflammatory and biocompatibility studies, *Mater. Sci. Eng. C.* 121 (2021) 111793. <https://doi.org/https://doi.org/10.1016/j.msec.2020.111793>.

**[255]** G.M. Pontes-Quero, L. Benito-Garzón, J. Pérez Cano, M.R. Aguilar, B. Vázquez-Lasa, Modulation of Inflammatory Mediators by Polymeric Nanoparticles Loaded with Anti-Inflammatory Drugs, *Pharmaceutics.* 13 (2021). <https://doi.org/10.3390/pharmaceutics13020290>.

**[256]** S. Khunmanee, Y. Jeong, H. Park, Crosslinking method of hyaluronic-based hydrogel for biomedical applications, *J. Tissue Eng.* 8 (2017) 2041731417726464–2041731417726464. <https://doi.org/10.1177/2041731417726464>

**[257]** V. Strand, L.F. McIntyre, W.R. Beach, L.E. Miller, J.E. Block, Safety and efficacy of US-approved viscosupplements for knee osteoarthritis: A systematic review and meta-analysis of randomized, saline-controlled trials, *J. Pain Res.* 8 (2015) 217–228. <https://doi.org/10.2147/JPR.S83076>.

**[258]** S.-B. Han, I.-W. Seo, Y.-S. Shin, Intra-Articular Injections of Hyaluronic Acid or Steroids Associated With Better Outcomes Than Platelet-Rich Plasma, *Adipose*

*Mesenchymal Stromal Cells, or Placebo in Knee Osteoarthritis: A Network Meta-analysis, Arthrosc. - J. Arthrosc. Relat. Surg.* 37 (2021) 292–306. <https://doi.org/10.1016/j.arthro.2020.03.041>.

**[259]** A. Askari, T. Gholami, M.M. NaghiZadeh, M. Farjam, S.A. Kouhpayeh, Z. Shahabfard, Hyaluronic acid compared with corticosteroid injections for the treatment of osteoarthritis of the knee: a randomized control trail, *Springerplus.* 5 (2016) 442. <https://doi.org/10.1186/s40064-016-2020-0>.

**[260]** R.D. Altman, A. Manjoo, A. Fierlinger, F. Niazi, M. Nicholls, The mechanism of action for hyaluronic acid treatment in the osteoarthritic knee: a systematic review, *BMC Musculoskelet. Disord.* 16 (2015) 321. <https://doi.org/10.1186/s12891-015-0775-z>.

**[261]** L.W. Moreland, Intra-articular hyaluronan (hyaluronic acid) and hylans for the treatment of osteoarthritis: mechanisms of action, *Arthritis Res. Ther.* 5 (2003) 54–67. <https://doi.org/10.1186/ar623>.

**[262]** V. Legré-Boyer, Viscosupplementation: Techniques, indications, results, *Orthop. Traumatol. Surg. Res.* 101 (2015) S101–S108. <https://doi.org/https://doi.org/10.1016/j.otsr.2014.07.027>.

**[263]** R.C. Gupta, R. Lall, A. Srivastava, A. Sinha, Hyaluronic Acid: Molecular Mechanisms and Therapeutic Trajectory, *Front. Vet. Sci.* 6 (2019) 192. <https://doi.org/10.3389/fvets.2019.00192>.

**[264]** T. Yatabe, S. Mochizuki, M. Takizawa, M. Chijiwa, A. Okada, T. Kimura, Y. Fujita, H. Matsumoto, Y. Toyama, Y. Okada, Hyaluronan inhibits expression of ADAMTS4 (aggrecanase-1) in human osteoarthritic chondrocytes., *Ann. Rheum. Dis.* 68 (2009) 1051–1058. <https://doi.org/10.1136/ard.2007.086884>.

- [265] S.M. Julovi, H. Ito, K. Nishitani, C.J. Jackson, T. Nakamura, Hyaluronan inhibits matrix metalloproteinase-13 in human arthritic chondrocytes via CD44 and P38., *J. Orthop. Res. Off. Publ. Orthop. Res. Soc.* 29 (2011) 258–264. <https://doi.org/10.1002/jor.21216>.
- [266] R. Altman, A. Bedi, A. Manjoo, F. Niazi, P. Shaw, P. Mease, Anti-Inflammatory Effects of Intra-Articular Hyaluronic Acid: A Systematic Review, *Cartilage.* 10 (2019) 43–52. <https://doi.org/10.1177/1947603517749919>
- [267] M.A. Goldwire, L.A. Shea, Intra-articular hyaluronic acids for osteoarthritis of the knee, *Drugs Ther. Perspect.* 36 (2020) 440–450. <https://doi.org/10.1007/s40267-020-00764-4>.
- [268] P. Snetkov, K. Zakharova, S. Morozkina, R. Olekhovich, M. Uspenskaya, Hyaluronic Acid: The Influence of Molecular Weight on Structural, Physical, Physico-Chemical, and Degradable Properties of Biopolymer, *Polymers (Basel).* 12 (2020) 1800. <https://doi.org/10.3390/polym12081800>.
- [269] T. Euppayo, P. Siengdee, K. Buddhachat, W. Pradit, S. Chomdej, S. Ongchai, K. Nganvongpanit, In vitro effects of triamcinolone acetonide and in combination with hyaluronan on canine normal and spontaneous osteoarthritis articular cartilage., *In Vitro Cell. Dev. Biol. Anim.* 52 (2016) 723–735. <https://doi.org/10.1007/s11626-016-0022-4>.
- [270] P. Siengdee, T. Radeerom, S. Kuanon, T. Euppayo, W. Pradit, S. Chomdej, S. Ongchai, K. Nganvongpanit, Effects of corticosteroids and their combinations with hyaluronan on the biochemical properties of porcine cartilage explants, *BMC Vet. Res.* 11 (2015) 298. <https://doi.org/10.1186/s12917-015-0611-6>.
- [271] T. Conrozier, J. Patarin, P. Mathieu, M. Rinaudo, Steroids, lidocain and ioxaglic acid modify the viscosity of hyaluronic acid: in vitro study and clinical implications., *Springerplus.* 5 (2016) 170. <https://doi.org/10.1186/s40064-016-1762-z>.
- [272] E. Tarricone, R. Elia, E. Mattiuzzo, A. Faggian, A. Pozzuoli, P. Ruggieri, P. Brun, The Viability and Anti-Inflammatory Effects of Hyaluronic Acid-Chitlac-Tracimolone Acetonide- $\beta$ -Cyclodextrin Complex on Human Chondrocytes, *Cartilage.* (2020). <https://doi.org/10.1177/1947603520908658>
- [273] F. Mohammadi, S.M. Samani, N. Tanideh, F. Ahmadi, Hybrid scaffolds of hyaluronic acid and collagen loaded with prednisolone: An interesting system for osteoarthritis, *Adv. Pharm. Bull.* 8 (2018) 11–19. <https://doi.org/10.15171/apb.2018.002>.
- [274] N. Storozhylova, J. Crecente-Campo, D. Cabaleiro, L. Lugo, C. Dussouy, S. Simões, M. Monteiro, C. Grandjean, M.J. Alonso, An In Situ Hyaluronic Acid-Fibrin Hydrogel Containing Drug-Loaded Nanocapsules for Intra-Articular Treatment of Inflammatory Joint Diseases, *Regen. Eng. Transl. Med.* 6 (2020) 201–216. <https://doi.org/10.1007/s40883-020-00154-2>.
- [275] P. Chen, S. Mei, C. Xia, R. Zhu, Y. Pang, J. Wang, J. Zhang, F. Shao, S. Fan, The amelioration of cartilage degeneration by photo-crosslinked GelHA hydrogel and crizotinib encapsulated chitosan microspheres., *Oncotarget.* 8 (2017) 30235–30251. <https://doi.org/10.18632/oncotarget.15750>.
- [276] M.-L. Kang, S.-Y. Jeong, G.-I. Im, Hyaluronic Acid Hydrogel Functionalized with Self-Assembled Micelles of Amphiphilic PEGylated Kartogenin for the Treatment of Osteoarthritis., *Tissue Eng. Part A.* 23 (2017) 630–639. <https://doi.org/10.1089/ten.tea.2016.0524>.

- [277] C. Xia, P. Chen, S. Mei, L. Ning, C. Lei, J. Wang, J. Zhang, J. Ma, S. Fan, Photocrosslinked HAMA hydrogel with cordycepin encapsulated chitosan microspheres for osteoarthritis treatment, *Oncotarget*. 8 (2017) 2835–2849. <https://doi.org/10.18632/oncotarget.13748>.
- [278] J.F.S.D. Lana, A. Weglein, S.E. Sampson, E.F. Vicente, S.C. Huber, C. V Souza, M.A. Ambach, H. Vincent, A. Urban-Paffaro, C.M.K. Onodera, J.M. Annichino-Bizzacchi, M.H.A. Santana, W.D. Belangero, Randomized controlled trial comparing hyaluronic acid, platelet-rich plasma and the combination of both in the treatment of mild and moderate osteoarthritis of the knee, *J. Stem Cells Regen. Med.* 12 (2016) 69–78. <https://doi.org/10.46582/jsrm.1202011>.
- [279] K. Kurapati, S. Tapadia, M. Rao, K. Anbarasu, V.K. Verma, S.S. Beevi, Efficacy of Intra-Articular Injection of Platelet Rich Plasma and Hyaluronic Acid in Early Knee Osteoarthritis – Case Series, *Eur. J. Mol. Clin. Med.* 5 (2018) 30–36. [https://ejmcm.com/article\\_1169.html](https://ejmcm.com/article_1169.html).
- [280] D. Dallari, C. Stagni, N. Rani, G. Sabbioni, P. Pelotti, P. Torricelli, M. Tschon, G. Giavaresi, Ultrasound-Guided Injection of Platelet-Rich Plasma and Hyaluronic Acid, Separately and in Combination, for Hip Osteoarthritis: A Randomized Controlled Study., *Am. J. Sports Med.* 44 (2016) 664–671. <https://doi.org/10.1177/0363546515620383>
- [281] W.-H. Chen, W.-C. Lo, W.-C. Hsu, H.-J. Wei, H.-Y. Liu, C.-H. Lee, S.-Y. Tina Chen, Y.-H. Shieh, D.F. Williams, W.-P. Deng, Synergistic anabolic actions of hyaluronic acid and platelet-rich plasma on cartilage regeneration in osteoarthritis therapy., *Biomaterials*. 35 (2014) 9599–9607. <https://doi.org/10.1016/j.biomaterials.2014.07.058>.
- [282] X. Duan, L.J. Sandell, N. Chinzei, N. Holguin, M.J. Silva, A. Schiavinato, M.F. Rai, Therapeutic efficacy of intra-articular hyaluronan derivative and platelet-rich plasma in mice following axial tibial loading., *PLoS One*. 12 (2017) e0175682. <https://doi.org/10.1371/journal.pone.0175682>.
- [283] F. Russo, M. D’Este, G. Vadalà, C. Cattani, R. Papalia, M. Alini, V. Denaro, Platelet Rich Plasma and Hyaluronic Acid Blend for the Treatment of Osteoarthritis: Rheological and Biological Evaluation., *PLoS One*. 11 (2016) e0157048. <https://doi.org/10.1371/journal.pone.0157048>.
- [284] T. Euppayo, V. Punyapornwithaya, S. Chomdej, S. Ongchai, K. Nganvongpanit, Effects of hyaluronic acid combined with anti-inflammatory drugs compared with hyaluronic acid alone, in clinical trials and experiments in osteoarthritis: a systematic review and meta-analysis, *BMC Musculoskelet. Disord.* 18 (2017) 387. <https://doi.org/10.1186/s12891-017-1743-6>.
- [285] T. Euppayo, P. Siengdee, K. Buddhachat, W. Pradit, N. Viriyakhasem, S. Chomdej, S. Ongchai, Y. Harada, K. Nganvongpanit, Effects of low molecular weight hyaluronan combined with carprofen on canine osteoarthritis articular chondrocytes and cartilage explants in vitro., *In Vitro Cell. Dev. Biol. Anim.* 51 (2015) 857–865. <https://doi.org/10.1007/s11626-015-9908-9>.
- [286] B. Palmieri, V. Rottigni, T. Iannitti, Preliminary study of highly cross-linked hyaluronic acid-based combination therapy for management of knee osteoarthritis-related pain., *Drug Des. Devel. Ther.* 7 (2013) 7–12. <https://doi.org/10.2147/DDDT.S37330>.
- [287] S.-Z. Wang, D.-Y. Wu, Q. Chang, Y.-D. Guo, C. Wang, W.-M. Fan, Intra-articular, single-shot co-injection of hyaluronic acid and corticosteroids in knee osteoarthritis: A randomized controlled trial, *Exp. Ther. Med.*



16 (2018) 1928–1934.  
<https://doi.org/10.3892/etm.2018.6371>.

**[288]** C. Wernecke, H.J. Braun, J.L. Dragoo, The Effect of Intra-articular Corticosteroids on Articular Cartilage: A Systematic Review., *Orthop. J. Sport. Med.* 3 (2015) 2325967115581163.  
<https://doi.org/10.1177/2325967115581163>

**[289]** M. Tschon, F. Salamanna, L. Martini, G. Giavaresi, L. Lorenzini, L. Calzà, M. Fini, Boosting the Intra-Articular Efficacy of Low Dose Corticosteroid through a Biopolymeric Matrix: An In Vivo Model of Osteoarthritis, *Cells.* 9 (2020) 1571.  
<https://doi.org/10.3390/cells9071571>.

**[290]** R.J. Petrella, P.J. Emans, J. Alleyne, F. Dellaert, D.P. Gill, M. Maroney, Safety and performance of Hydros and Hydros-TA for knee osteoarthritis: a prospective, multicenter, randomized, double-blind feasibility trial., *BMC Musculoskelet. Disord.* 16 (2015) 57.  
<https://doi.org/10.1186/s12891-015-0513-6>.

**[291]** F. Mohammadi, A. Vosough, N. Tanideh, S. Mohammadi Samani, F. Ahmadi, Hyaluronic Acid Scaffolds and Injectable Gels for Healing of Induced Arthritis in Rat Knee: Effect of Prednisolone Revisited, *Regen. Eng. Transl. Med.* (2020).  
<https://doi.org/10.1007/s40883-020-00158-y>.

**[292]** M.F. Rai, C.T. Pham, Intra-articular drug delivery systems for joint diseases, *Curr. Opin. Pharmacol.* 40 (2018) 67–73.  
<https://doi.org/10.1016/j.coph.2018.03.013>.

**[293]** Z. Zhang, G. Huang, Micro- and Nano-Carrier Mediated Intra-Articular Drug Delivery Systems for the Treatment of Osteoarthritis, *J. Nanotechnol.* 2012 (2012) 748909.  
<https://doi.org/10.1155/2012/748909>.

**[294]** J. Siepmann, F. Siepmann, Microparticles Used as Drug Delivery Systems BT - Smart Colloidal Materials, in: W. Richtering (Ed.), Springer Berlin Heidelberg, Berlin, Heidelberg, 2006: pp. 15–21.

**[295]** G.-I. Im, T.-K. Kim, Regenerative therapy for osteoarthritis: A perspective, *Int. J. Stem Cells.* 13 (2020) 177–181.  
<https://doi.org/10.15283/IJSC20069>.

**[296]** J. Zhao, H. Huang, G. Liang, L.-F. Zeng, W. Yang, J. Liu, Effects and safety of the combination of platelet-rich plasma (PRP) and hyaluronic acid (HA) in the treatment of knee osteoarthritis: A systematic review and meta-analysis, *BMC Musculoskelet. Disord.* 21 (2020). <https://doi.org/10.1186/s12891-020-03262-w>.

**[297]** M. Abate, S. Verna, C. Schiavone, P. Di Gregorio, V. Salini, Efficacy and safety profile of a compound composed of platelet-rich plasma and hyaluronic acid in the treatment for knee osteoarthritis (preliminary results)., *Eur. J. Orthop. Surg. Traumatol.* 25 (2015) 1321–1326. <https://doi.org/10.1007/s00590-015-1693-3>.

**[298]** G. Desando, I. Bartolotti, C. Cavallo, A. Schiavinato, C. Secchieri, E. Kon, G. Filardo, M. Paro, B. Grigolo, Short-Term Homing of Hyaluronan-Primed Cells: Therapeutic Implications for Osteoarthritis Treatment., *Tissue Eng. Part C. Methods.* 24 (2018) 121–133.  
<https://doi.org/10.1089/ten.TEC.2017.0336>.

**[299]** C. Feng, X. Luo, N. He, H. Xia, X. Lv, X. Zhang, D. Li, F. Wang, J. He, L. Zhang, X. Lin, L. Lin, H. Yin, J. He, J. Wang, W. Cao, R. Wang, G. Zhou, W. Wang, Efficacy and Persistence of Allogeneic Adipose-Derived Mesenchymal Stem Cells Combined with Hyaluronic Acid in Osteoarthritis After Intra-articular Injection in a Sheep Model., *Tissue Eng. Part A.* 24 (2018) 219–233.  
<https://doi.org/10.1089/ten.TEA.2017.0039>.

**[300]** L. Li, X. Duan, Z. Fan, L. Chen, F. Xing, Z. Xu, Q. Chen, Z. Xiang, Mesenchymal Stem Cells in Combination with Hyaluronic Acid for Articular Cartilage Defects, *Sci. Rep.* 8 (2018) 9900. <https://doi.org/10.1038/s41598-018-27737-y>.

**[301]** K. Shoma Suresh, S. Bhat, B.R. Guru, M.S. Muttigi, R.N. Seetharam, A nanocomposite hydrogel delivery system for mesenchymal stromal cell secretome, *Stem Cell Res. Ther.* 11 (2020) 205. <https://doi.org/10.1186/s13287-020-01712-9>.

# **Chapter II. Objectives**



## Chapter II. Objectives

---

The general aim of this doctoral thesis is **the development of bioactive anti-inflammatory-loaded NPs and advanced viscosupplements based on HA hydrogels**. In order to achieve this general aim, the following specific objectives are explored throughout this thesis and are grouped in different chapters:

In Chapter III entitled ***Amphiphilic polymeric nanoparticles encapsulating curcumin: antioxidant, anti-inflammatory and biocompatibility studies*** the following specific goals are attempted:

- Design and characterization of a novel amphiphilic antioxidant terpolymer based on  $\alpha$ -tocopheryl methacrylate (MVE), 1-vinyl-2-pyrrolidone (VP) and *N*-vinylcaprolactam (VC) to be used as a nanovehicle of hydrophobic drugs.
- Synthesis of NPs using the amphiphilic terpolymer (poly(MVE-co-VP-co-VC). Loading of the natural antioxidant and anti-inflammatory hydrophobic polyphenol curcumin into the amphiphilic NPs.
- Analysis of CUR-loaded NP physicochemical properties and *in vitro* behavior in terms of hydrodynamic diameter, polydispersity index, surface charge, morphology, stability, encapsulation efficiency and drug release.
- Evaluation of the NP biological performance in terms of cytotoxicity and antioxidant activity in two different cellular models, human articular chondrocytes (HC-a) and murine macrophages (RAW264.7). Assessment of the cellular uptake of the NPs using a fluorescent model.
- *In vivo* assessment of the biocompatibility of the nanocarrier and optimum CUR-loaded NPs by subcutaneously injecting the NPs in a Wistar rat model.

In **Chapter IV (*Modulation of inflammatory mediators by polymeric nanoparticles loaded with anti-inflammatory drugs*)** the introduction of three anti-inflammatory molecules (celecoxib, tenoxicam, and dexamethasone) into the terpolymer NPs is studied. These drugs are three widely used anti-inflammatory molecules in the treatment of OA sharing common characteristics, *i.e.* low water solubility and toxicity in its free form. Therefore, the specific aims of this chapter are:

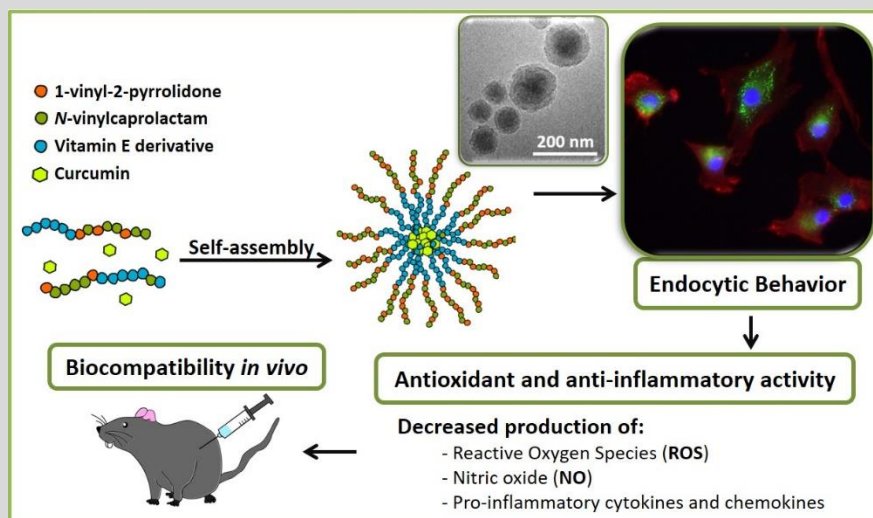
- Synthesis of CLX, TNX and DEX-loaded NPs and their physicochemical characterization analyzing the hydrodynamic diameter, polydispersity index, surface charge and morphology. Determination of encapsulation efficiency and *in vitro* stability.
- Assessment of the reduction of drug cytotoxicity provided by the nanoencapsulation process in both HC-a and RAW264.7. Study of the biological performance of the NPs in terms of cytotoxicity and inhibition of NO release by RAW264.7.
- For the optimum NPs,
  - Characterization of the anti-inflammatory activity of the loaded NPs regarding the release of different inflammatory factors.
  - *In vivo* biocompatibility evaluation of the systems by subcutaneously injecting the drug-loaded NPs in a rat model.

**Chapter V**, named ***Advanced viscosupplements based on hyaluronic acid hydrogels loaded with anti-inflammatory drug delivery systems***, aims to develop intra-articularly injected viscosupplements based on hyaluronic acid hydrogels and drug delivery systems. This information is confidential.

Finally, in **Chapter VI**, entitled ***Studies on mesenchymal stem cells derived secretomes for the treatment of OA***, an alternative biological intra-articular therapy for OA based on mesenchymal stem cell derived secretomes is explored. This information is confidential.

# Chapter III. Amphiphilic polymeric nanoparticles encapsulating curcumin: antioxidant, anti-inflammatory and biocompatibility studies

Gloria María Pontes-Quero, Lorena Benito-Garzón, Juan Pérez Cano, María Rosa Aguilar, Blanca Vázquez-Lasa







# Chapter III. Amphiphilic polymeric nanoparticles encapsulating curcumin: antioxidant, anti-inflammatory and biocompatibility studies

---

**Abstract:** Oxidative stress and inflammation are two related processes common to many diseases. Curcumin is a natural compound with both antioxidant and anti-inflammatory properties, among others, that is recently being used as a natural occurring product alternative to traditional drugs. However, it has a hydrophobic nature that compromises its solubility in physiological fluids and its circulation time and also presents cytotoxicity problems in its free form, limiting the range of concentrations to be used. In order to overcome these drawbacks and taking advantage of the benefits of nanotechnology, the aim of this work is the development of curcumin-loaded polymeric nanoparticles that can provide a controlled release of the drug and enlarge their application in the treatment of inflammatory and oxidative stress related diseases. Specifically, the vehicle is a bioactive terpolymer based on a  $\alpha$ -tocopheryl methacrylate, 1-vinyl-2-pyrrolidone and *N*-vinylcaprolactam. Nanoparticles were obtained by nanoprecipitation and characterized in terms of size, morphology, stability, encapsulation efficiency and drug release. *In vitro* cellular assays were performed in human articular chondrocyte and RAW264.7 cultures to assess cytotoxicity, cellular uptake, antioxidant and anti-inflammatory properties. The radical scavenging activity of the systems was confirmed by the DPPH test and the quantification of cellular reactive oxygen species. The anti-inflammatory potential of these systems was demonstrated by the reduction of different pro-inflammatory factors such as IL-8, MCP and MIP in chondrocytes; and nitric oxide, IL-6, TNF- $\alpha$  and MCP-1, among others, in RAW264.7. Finally, *in vivo* biocompatibility was confirmed in a rat model by the

subcutaneous injection of the nanoparticle suspensions. Therefore, the reduction of curcumin toxicity and the antioxidant, anti-inflammatory and biocompatibility properties open the door to deeper *in vitro* and *in vivo* research on these curcumin-loaded polymeric NPs to treat inflammation and oxidative stress based diseases.

**Keywords:** curcumin, polymeric, nanoparticles, drug delivery systems, antioxidant, anti-inflammatory

## 1. Introduction

Inflammation and oxidative stress are two interconnected processes with a key role in many different diseases such as cancer, cardiovascular, rheumatic or neurological diseases [1]. Oxidative stress is defined as an imbalance between the production of reactive oxygen and nitrogen species (ROS/RNS) and their elimination by the intrinsic antioxidant systems in our body. This imbalance can lead to irreversible cell damage and cell death because of the attack of free radicals to the cells. Oxidative stress can enhance chronic inflammation by the activation of different transcription factors related to inflammatory events, resulting in the production of inflammatory cytokines and chemokines and, at the same time, inflammation causes the overproduction of ROS/RNS, inducing further oxidation [2]. Current treatment for managing chronic inflammation is based on the systemic administration of nonsteroidal anti-inflammatory drugs and corticosteroids. Nevertheless, its long-term use can result in different side effects including gastrointestinal, cardiovascular, renal or hepatic problems, in the case of nonsteroidal anti-inflammatories [3,4]; or gastrointestinal bleeding, infections, cardiovascular problems and bone fragility, in the case of corticosteroids [5–7].

Curcumin (CUR) is a natural hydrophobic polyphenol extracted from the rhizome of turmeric. In recent years, it has become very popular in the biomedical field because of its wide range of pharmacological activities such as antioxidant, anti-inflammatory, anti-bacterial, anti-viral, anti-cancer and neuroprotective properties [8]. While it seems to have countless therapeutic properties, most of them are due to its antioxidant and anti-inflammatory

effects. Nonetheless, its use has been limited because of its low water solubility and bioavailability, poor intestinal absorption and rapid systemic elimination. In order to overcome these problems, different CUR delivery systems are being extensively studied to encapsulate or conjugate this natural compound. Liposomes [9–11], polymeric nanoparticles (NPs) [12–14] or hydrogels [15] are the most studied CUR delivery systems.

Polymeric NPs have received great interest to encapsulate both hydrophobic and hydrophilic molecules due to their versatility in composition, structure and properties [16]. CUR has been widely encapsulated in different types of polymeric NPs or micelles. Polymers such as chitosan [17–19], poly(lactide-co-glycolide) (PLGA) combined with polyethylene glycol (PEG) [20,21] or PNIPAAm-MAA [22] are some of the most used polymeric vehicles for CUR delivery. In particular, NPs synthesized from amphiphilic polymers in aqueous media have shown to be optimal systems for the encapsulation of hydrophobic drugs like CUR, creating spherical systems with an inner core loaded with the drug and a biocompatible hydrophilic shell that stabilizes the NP [23–25]. Regarding the application, cancer is one of the main targets for CUR NPs. For instance, polymeric nanocarriers of CUR using vinylpyrrolidone [26] or vinylcaprolactam in combination with chitosan [27] have been recently used for CUR delivery for cancer treatment. Moreover, other inflammatory and oxidative stress related diseases have been treated with CUR NPs such as arthritis [28,29] or neurological disorders [30].

Recent innovative approaches based on terpolymer nanocarriers have been attempted as CUR delivery systems. Terpolymer systems can enhance the intrinsic properties of the nanocarriers compared to those of copolymers. Composition of terpolymers can modulate different properties of the drug delivery system ranging from physicochemical to biological functions. For example, Petrov *et al.* have developed silver NPs and CUR-loaded poly(ethylene oxide)-*b*-poly(*n*-butyl acrylate)-*b*-poly(acrylic acid) (PEO-*b*-PnBA-*b*-PAA) triblock terpolymer micelles for acute myeloid leukemia [31]. These authors have developed CUR nanocarriers for mitochondrial targeted delivery using similar polymeric systems [32,33]. In other work, amphiphilic triblock terpolymers of poly(methyl acrylate)-*b*-[(7-(allyloxy)-2H-chromen-2-one)-co-(2-

hydroxyethyl methacrylate(*-b-N-vinylpyrrolidone*) P(MA-*b*-[AC-*co*- HEMA]-*b*-NVP) with three different lengths of the hydrophobic PMA block were synthesized by atom transfer radical polymerization and reversible addition-fragmentation chain-transfer/macromolecular design by interchange of xanthate polymerization [34]. These terpolymers self-assembled in aqueous media encapsulating CUR, and the authors studied the release profiles of CUR under different conditions. Triblock copolymers and terpolymers like poly( $\epsilon$ -caprolactone)-poly(ethylene glycol)-poly( $\epsilon$ -caprolactone) (PCL-PEG-PCL) [35], poly(dimethylaminoethyl methacrylate)-poly( $\epsilon$ -caprolactone)-poly(dimethylaminoethyl methacrylate) (PDMAEMA9-PCL70-PDMAEMA9) [36], methoxy poly(ethylene glycol)-*b*-poly(caprolactone)-*b*-poly(1, 4, 8-Trioxa [4.6] spiro-9-undecanone) (mPEG-*b*-PCL-*b*-PTOSUO) [37] or poly( $\beta$ -thioether ester)-*b*-poly(ethylene glycol)-*b*-poly( $\beta$ -thioether ester) (PTE-*b*-PEG-*b*-PTE) [38] have been also recently used to prepare CUR nanocarriers with promising *in vitro* and *in vivo* results in terms of biocompatibility, antioxidant effects or anti-tumor activity.

The goal of this work is the development of CUR-loaded polymeric NPs that can reduce the *in vitro* cytotoxic effects of free CUR and maintain or improve its antioxidant and anti-inflammatory properties to treat pathologies associated with inflammation and oxidative stress. The nanoencapsulation of CUR will also provide new alternatives for its administration and will maximize its effect, as it will be delivered in a controlled manner to the aqueous medium. NPs are fabricated by nanoprecipitation using a terpolymer bearing vitamin E moieties, a known fat-soluble antioxidant molecule [39]. Specifically, the terpolymer is based on  $\alpha$ -tocopheryl methacrylate (MVE), 1-vinyl-2-pyrrolidone (VP) and *N*-vinylcaprolactam (VC) (poly(MVE-*co*-VP-*co*-VC)). This terpolymer composition would allow its self-assembly in presence of CUR, giving NPs in which the  $\alpha$ -tocopheryl moieties in the core will allow the encapsulation of hydrophobic CUR, whereas the hydrophilic VP in the shell will provide stability to the nanocarrier. The amphiphilic VC will modulate the hydrophilic/hydrophobic balance of the system and is expected to provide good NP stability and CUR entrapment. Our group has a wide experience in the synthesis of vitamin E derived copolymers for different applications *e.g.* acrylic bone cements [40], anti-cancer treatment [41–44] or the treatment of

sensorineural hearing loss [45–47]. Antecedents of vitamin E based copolymer NPs have been reported by our group, *i.e.* poly(MVE-co-VP) [44]. They were successful in the entrapment of 6 $\alpha$ -methylprednisolone and effective in providing otoprotective activity against cisplatin [45]. In the present work, the novel CUR-loaded terpolymer NPs are deeply investigated. Physicochemical, structural, morphological and stability properties of the NPs are studied. CUR encapsulation efficiency and release are assessed in physiological conditions. Finally, cytotoxicity, cellular uptake, antioxidant and anti-inflammatory properties of the systems are assessed using different *in vitro* and cellular assays, in addition to an *in vivo* biocompatibility test using a subcutaneous injection in a rat model.

## 2. Experimental section

### 2.1. Materials

$\alpha$ -tocopherol (Sigma-Aldrich), methacryloyl chloride (Sigma-Aldrich) and triethylamine (Scharlau) were used for the synthesis of MVE as previously described [44]. Tetrabutylammonium iodide (Sigma-Aldrich), dichloromethane (Sigma-Aldrich), hexane (Sigma-Aldrich), hydrochloric acid (VWR), sodium hydroxide (Sigma-Aldrich), 1,4-dioxane (Panreac), anhydrous dioxane (Sigma-Aldrich), *N*-vinylcaprolactam (VC, Sigma-Aldrich), ethanol (VWR), sodium chloride (NaCl, PanReac), sodium phosphate dibasic (Na<sub>2</sub>HPO<sub>4</sub>, Sigma-Aldrich), deuterated chloroform (CDCl<sub>3</sub>, Sigma-Aldrich), curcumin (CUR, ChengDu Biopurify Phytochemicals Ltd.), 2,2-diphenyl-1-picrylhydrazyl free radical (DPPH, Alfa Aesar), esterase from porcine liver (Sigma-Aldrich), tween-80 (Sigma-Aldrich) and coumarin-6 (C6, Sigma-Aldrich) were used without further purification for the synthesis and characterization of the terpolymer and the NPs. 1-vinyl-2-pyrrolidone (VP, Sigma-Aldrich) was purified by distillation under reduced pressure and 2,2'-azobisisobutyronitrile (AIBN, Merck) was recrystallized from methanol for the preparation of the terpolymer poly(MVE-co-VP-co-VC).

## 2.2. Synthesis and characterization of the terpolymer

The terpolymer was prepared by free radical polymerization as previously described [44], using a MVE:VP:VC feed molar composition of 10:85:5. Briefly, poly(MVE-*co*-VP-*co*-VC) was synthesized in anhydrous dioxane using AIBN ( $1.5 \times 10^{-2}$  M) as radical initiator at 60 °C for 24 h, purified by dialysis ( $M_w$  cut off: 3.5 KDa) against milli-Q water for 96 h and isolated by freeze-drying to obtain a white amorphous powder. Homopolymers poly(1-vinyl-2-pyrrolidone) (PVP) and poly(*N*-vinylcaprolactam) (PVC) were prepared following the same protocol and used as controls for thermal characterization. The terpolymer composition was determined by  $^1\text{H}$  NMR in deuterated chloroform ( $\text{CDCl}_3$ ) using a Mercury 400BB apparatus operating at 400 MHz.  $^1\text{H}$  NMR spectra of MVE and poly(MVE-*co*-VP-*co*-VC) were analyzed using the MestreNova 9.0 software. The thermal stability of the terpolymer and homopolymers was analyzed by thermogravimetric analysis using a TGA Q500 (TA Instruments) under nitrogen atmosphere at  $10\text{ }^\circ\text{C min}^{-1}$  heating rate from 25 to 600 °C. Maximum weight loss rate was calculated using the TRIOS software. Thermal transitions were studied and analyzed using differential scanning calorimetry (DSC) with a TA Q-2000 instrument in nitrogen atmosphere ( $50\text{ mL min}^{-1}$ ) at  $20\text{ }^\circ\text{C min}^{-1}$ . Polymer molecular weight ( $M_w$  and  $M_n$ ) and polydispersity ( $\text{Đ}$ ) were obtained by size exclusion chromatography (SEC) using a Waters 515 HPLC pump 250 coupled to a Waters refraction index detector (24,214.3). Three Polymer Laboratories columns coupled in series were used: PLgel 100 Å (lineal range until  $4000\text{ g mol}^{-1}$ ), PLgel 500 Å (lineal range  $500\text{--}30,000\text{ g mol}^{-1}$ ) and MixedC (lineal range  $200\text{--}2,000,000\text{ g mol}^{-1}$ ). Tetrahydrofuran was used as mobile phase at  $1\text{ mL min}^{-1}$  flow rate.

## 2.3. Synthesis and characterization of CUR-loaded NPs

The amphiphilic nature of poly(MVE-*co*-VP-*co*-VC) allowed its self-assembly into NPs by the nanoprecipitation method and the entrapment of CUR in the inner core. CUR (2, 5 and 10% w/w respect to the polymer) and poly(MVE-*co*-VP-*co*-VC) ( $50\text{ mg mL}^{-1}$ ) were dissolved in dioxane and added drop by drop over a  $\text{Ca}^{+2}$  and  $\text{K}^{+1}$  free PBS (0.852% NaCl, 0.06%  $\text{Na}_2\text{HPO}_4$ , 2 M HCl to adjust pH to 7.4) that was in constant stirring. Final NP concentration was 2.00

mg mL<sup>-1</sup>. NP dispersions were dialyzed against PBS during 72 h to eliminate dioxane and the non-encapsulated CUR. Finally, NPs were sterilized by filtration through 0.22  $\mu$ m polyethersulfone membranes (Millex-GP PES Millipore Express®) and stored at 4 °C. Three CUR-loaded NPs, varying in CUR composition, were obtained and designated as CUR-2, CUR-5 and CUR-10, respectively, according to initial CUR content. Empty NPs (herein designated as Empty) were fabricated in absence of CUR following the same methodology for comparison purposes. Coumarin 6 (C6)-loaded NPs were also obtained by nanoprecipitation (1% w/w respect to the polymer) as a fluorescent model to test the NP uptake by cells.

### **2.3.1. NP morphology, size distribution, stability and encapsulation efficiency**

The particle size distribution and zeta potential were determined by Dynamic Light Scattering (DLS) and Laser Doppler Electrophoresis (LDE), respectively, using a Malvern Nanosizer Nano-ZS at 25 °C. The electrophoretic mobility values, measured by laser Doppler velocimetry, were converted to zeta potentials by the Smoluchowski equation. Measurements were performed at a NP concentration of 0.50 mg mL<sup>-1</sup>. Stability of the NP dispersions stored at 4 °C was studied by assessing the particle size distribution over 7 months. The statistical average and standard deviation (SD) of data were calculated from three measurements of 20 runs each one and results were expressed as mean value  $\pm$  SD.

Scanning electron microscopy (SEM) was used for the morphological visualization of Empty and CUR-5 NPs at a NP concentration of 0.04 mg mL<sup>-1</sup> using a Hitachi SU8000 TED, cold-emission field emission SEM microscope working with an accelerating voltage 1 kV-D. These NPs were prepared in ultrapure water instead of PBS using the same methodology described in Section 2.3. Cryogenic transmission electron microscopy (Cryo-TEM) was also used for the NP morphological analysis at 2.00 mg mL<sup>-1</sup>. Cryo-TEM images were taken in a JEOL 1230 electron microscope (Bergen, Norway) operating at 100 kV and equipped with a Gatan liquid nitrogen specimen holder (Warrendale, PA, United States) and a CMOS Tvips TemCam-F416 camera (Gauting,

Germany), at 40,000 nominal magnification under low dose conditions. NP samples were applied to holey carbon grids (Quantifoil, Großschadowitz, Germany) after glow-discharge and immediately blotted and vitrified using a FEI Vitrobot cryo-plunger (Thermo Scientific, Madrid, Spain).

In order to quantify the encapsulation efficiency (EE) of CUR, NPs were first freeze-dried obtaining an amorphous powder with a yield higher than 90%. Dried NPs were dissolved in ethanol, where both the terpolymer and CUR are soluble, and let stirred 24 h to dissolve the NPs and release the CUR content. Powders were then centrifuged at 10,000 rpm and the supernatant containing the encapsulated CUR was studied by fluorescence spectroscopy using an excitation/emission of 420/430 nm with a Nanodrop OneC Microvolume UV-Vis Spectrophotometer (Thermo Scientific™). Empty NPs were studied as a blank, whose absorbance value was subtracted to the one of CUR-loaded NPs. The experimental concentration of CUR was obtained using a CUR serial dilution curve and the EE (%) was calculated according to equation 1:

$$EE (\%) = \frac{[\text{loaded CUR}]_i}{[\text{loaded CUR}]_0} * 100 \quad (1)$$

where  $[\text{loaded drug}]_i$  and  $[\text{loaded drug}]_0$  are the experimentally detected and the initial drug concentration, respectively. Three replicates were used for each formulation and results were expressed as mean value  $\pm$  SD.

### 2.3.2. Esterase-mediated *in vitro* CUR release

The *in vitro* CUR release of CUR-5 NPs was studied by an esterase-mediated dialysis diffusion method. 5 mL of the NP dispersion ( $0.50 \text{ mg mL}^{-1}$ ), with  $15 \text{ u mL}^{-1}$  of esterases from porcine liver, replenish each 48 h, were dialyzed against PBS (with 0.5% of Tween-80 in order to enhance CUR water solubility) at  $37^\circ\text{C}$  using a Float-A-Lyzer G2 Dialysis Device ( $M_w$  cut off of 3.5-5 kDa, Spectrum Laboratories). Drug release was monitored at different time periods taking 1 mL of PBS and replenishing it with fresh one. CUR concentration was obtained by fluorescence spectroscopy



(excitation/emission of 420/430 nm) using a CUR serial dilution curve. Three replicates were studied and results were expressed as mean value  $\pm$  SD.

### 2.3.3. Radical scavenging activity of NPs by DPPH test

The radical scavenging activity (RSA) was tested using a DPPH (1,1-diphenyl-2-picryl-hydrazyl) assay at different times (10, 20, 30, 60 and 120 min). NPs were freeze-dried and dissolved in ethanol at different concentrations (1.00, 0.50, 0.25, 0.12 and 0.06 mg mL<sup>-1</sup>). Vitamin E (Vit. E, 120 mg mL<sup>-1</sup>) was used as antioxidant control reference to obtain the maximum RSA value to be achieved. Free CUR at the corresponding encapsulated concentration of each NP system was also tested for the most concentrated samples (1.00 mg mL<sup>-1</sup>). DPPH was also dissolved in ethanol (0.127 mM). 100  $\mu$ L of the DPPH solution were added to 100  $\mu$ L of the ethanol extracts under dark conditions. The absorbance was determined at 515 nm using a Multi-Detection Microplate Reader Synergy HT (BioTek Instruments; Vermont, USA). RSA (%) was calculated using equation 2:

$$\text{RSA (\%)} = \frac{(A_{\text{DPPH}} - A_{\text{EXTRACT}})}{A_{\text{DPPH}}} \cdot 100 \quad (2)$$

where  $A_{\text{EXTRACT}}$  and  $A_{\text{DPPH}}$  correspond to the absorbance values of DPPH with and without the extracts, respectively. ANOVA was performed at  $p < 0.05$ ,  $p < 0.005$  and  $p < 0.001$  significance levels. Eight replicates were used for each formulation and results were expressed as mean value  $\pm$  SD.

## 2.4. *In vitro* biological studies

### 2.4.1. Cells and materials

Cells used in the biological experiments were RAW264.7 (murine macrophage cell line, Sigma-Aldrich, 91062702) and HC-a (human articular chondrocytes, Innoprot, P10970). Dulbecco's Modified Eagles Medium-high glucose (DMEM, Sigma-Aldrich, D6546), supplemented with 10% Fetal Bovine Serum (FBS), 2% L-glutamine and 1% penicillin/ streptomycin, was used as the RAW264.7 culture medium and a chondrocyte medium kit (Innoprot, P60137)

as the chondrocyte culture medium. Additionally, DMEM-high glucose, HEPES, no phenol red (Gibco, 2106329) was used to prepare the AlamarBlue® solution. Trypsin-EDTA solution (Sigma-Aldrich), Trypan Blue solution (Sigma-Aldrich), AlamarBlue® (Bio-Rad), Dulbecco's Phosphate Buffered Saline (PBS, Sigma-Aldrich), 2',7'-dichlorofluorescein diacetate (DCFH-DA, Sigma-Aldrich), Hoechst (Invitrogen), phalloidin-tetramethylrhodamine B isothiocyanate (Sigma-Aldrich), Griess reagent (Sigma-Aldrich), formaldehyde (Alfa Aesar), lipopolysaccharides from *Escherichia coli* (LPS, Sigma-Aldrich) and hydrogen peroxide 30% (H<sub>2</sub>O<sub>2</sub>, PanReac) were used as received. For the cellular assays, NP dispersions in PBS were prepared at different concentrations (0.06, 0.12, 0.25, 0.50 and 1.00 mg mL<sup>-1</sup>).

#### 2.4.2. NP cytotoxicity

NP cytotoxic effects on HC-a were assessed in time (after 24 and 48 h and 7 and 14 days of treatment) using an AlamarBlue® assay. Cells were seeded in 24-well plates at  $2 \times 10^4$  cells/well. After 24 h of incubation at 37 °C and 5% CO<sub>2</sub>, cells were exposed to the NP dispersions. After treatment with the NPs for 24 h, NPs were removed in all cases. For the 24 h analysis, cells were washed with PBS and an AlamarBlue® solution (10% AlamarBlue® in phenol red free DMEM) was added to each well and incubated for 3 h. Fluorescence was measured with the Multi- Detection Microplate Reader (excitation/emission of 530/590 nm). For the rest of the times, NPs were replaced with fresh chondrocyte culture medium each two days and performed the same AlamarBlue® assay after 48 h, 7 and 14 days of NP exposure. For each studied time, cells exposed to PBS without NPs were used as the 100% viability control (CNT). NP results were normalized and analyzed for statistical significance using ANOVA ( $p < 0.05$ ). Eight replicates were used for each formulation and results were expressed as mean value  $\pm$  SD.

Evaluation of NP toxicity on RAW264.7 was also investigated using an AlamarBlue® assay after 24 h. In this case, cells were seeded at  $2 \times 10^4$  cells/well in 96-well plates and incubated for 24 h. The medium was replaced with the NP dispersions in fresh medium (1:1) and incubated for 24 h. Then, NPs were removed and cells were treated with the 10% AlamarBlue® solution to measure

the fluorescence. Cells exposed to PBS without NPs were used as the 100% viability control (CNT). NP results were normalized and analyzed for statistical significance using ANOVA ( $p < 0.05$ ). Eight replicates were used for each formulation and results were expressed as mean value  $\pm$  SD.

Cytotoxicity of free CUR on RAW264.7 was investigated after 24 h and compared to encapsulated CUR in the different NP systems (CUR-2, CUR-5 and CUR-10) at the different NP concentrations. Due to the low solubility of CUR in aqueous media, a mother solution of CUR in DMSO was prepared. Serial dilutions of CUR were prepared using this mother solution and the RAW264.7 culture medium, maintaining the final DMSO concentration lower than 1% v/v in the cell culture experiments. Cells were seeded at  $2 \times 10^4$  cells/well in a 96-well plate and incubated for 24 h. The medium was replaced by the serial CUR solutions and incubated for additional 24 h. Then, the medium was removed, cells were washed with PBS and treated with a 10% AlamarBlue® solution. After 3 h of incubation, fluorescence was monitored. Cells treated with the RAW264.7 culture medium were used as the 100% viability control. Eight replicates were used for each CUR solution. Cell viability half maximal inhibitory concentration ( $IC_{50}$ ) values of free CUR and encapsulated CUR in CUR-10 NPs were obtained by a non-linear fit using the software GraphPad Prism 7.

#### **2.4.3. Antioxidant activity assessment by cellular ROS quantification**

ROS production was estimated using the fluorescence probe DCFH-DA. RAW264.7 were seeded into 96-well plates at  $2.5 \times 10^4$  cells/well and incubated for 24 h. The medium was replaced with fresh one and the NP dispersions (1:1) and incubated for 24 h. Non-endocytosed NPs were removed by gently washing with PBS. Cells were incubated with the probe 2,7'-dichlorodihydrofluorescein diacetate (DCFH-DA) in PBS at a concentration of 40  $\mu$ M for 45 min under dark conditions. Plates were washed twice with PBS and exposed to 100  $\mu$ L of  $H_2O_2$  (100 mM) to stimulate the production of ROS. After 15 min of stimulation, fluorescence was measured with the Multi-Detection Microplate Reader with an excitation/emission of 485/528 nm.

Results of CUR-loaded NPs were normalized to the  $\text{H}_2\text{O}_2$  stimulated cells treated with PBS group (CNT  $\text{H}_2\text{O}_2$ + group) in which the ROS production was taken as 100%. Unstimulated cells, treated with PBS (CNT  $\text{H}_2\text{O}_2$ -) were studied to test the cellular basal level of ROS, which was 15% (data not shown). Eight replicates for each NP formulation were used and results were expressed as mean value  $\pm$  SD. ANOVA of the results was performed at significance levels of  $p < 0.05$ ,  $p < 0.005$  and  $p < 0.001$ .

#### **2.4.4. Anti-inflammatory effect assessment by NO quantification**

The anti-inflammatory effect of the NPs was analyzed by the quantification of RAW264.7 nitric oxide (NO) production. RAW264.7 were seeded into 96-well plates at  $2 \times 10^4$  cells/well and incubated 24 h. Pro-inflammatory RAW264.7 cells were induced by the treatment of LPS ( $1 \mu\text{g mL}^{-1}$ ) in culture medium and treated with the NP dispersions (1:1). The production of NO was estimated by the Griess test. After 24 h of NP exposure, 100  $\mu\text{L}$  of the supernatants of each well were mixed with 100  $\mu\text{L}$  of Griess reagent and let react during 15 min under dark conditions. Absorbance was measured with the Multi-Detection Microplate Reader at 540 nm. NO production was calculated using a sodium nitrite serial dilution curve. After removing the supernatant for the Griess test, cells were washed with PBS and exposed to an AlamarBlue® solution. After 3 h of incubation, fluorescence was read. Results were normalized to the PBS treated and LPS stimulated cells group (CNT LPS+) in which the NO production was taken as 100%. PBS treated and unstimulated cells (CNT LPS-) were studied to test cellular basal level of NO, which was 5% (data not shown). Eight replicates for each formulation were used and results were expressed as mean value  $\pm$  SD. ANOVA of the results was performed at  $p < 0.05$ ,  $p < 0.005$  and  $p < 0.001$ .

#### **2.4.5. Human and mouse inflammation antibody arrays**

The effect of CUR-5 NPs in the production of different inflammatory mediators was analyzed using a Human Inflammation Antibody Array kit (ab134003, abcam) for HC-a and a Mouse Inflammation Antibody Array kit

(ab133999, abcam) for RAW264.7, following the manufacturer instructions. 40 targets were studied in each membrane (see table S1). Three membranes were used in each study: a control membrane treated with culture media without FBS (CNT), an inflammatory membrane where cells were stimulated with IL-1 $\beta$  (in the case of HC-a) or LPS (in the case of RAW264.7) (INF); and a NP treated membrane where cells were stimulated and exposed to CUR-5 NPs (INF + CUR-5). HC-a were seeded at  $2.5 \times 10^5$  cells/well into 6-well plates and incubated for 24 h. The medium was replaced with 1 mL of CUR-5 NPs ( $0.50 \text{ mg mL}^{-1}$ ) and 1 mL of culture medium or with 2 mL of culture medium in the case of cells used in the inflammatory control membrane (INF). After an overnight incubation, the medium was replaced with culture medium without FBS containing IL-1 $\beta$  ( $400 \text{ ng mL}^{-1}$ ), in order to stimulate inflammation on HC-a. Supernatants were collected and well plates and incubated for 24 h. The medium was replaced with 1 mL of CUR-5 NPs ( $0.50 \text{ mg mL}^{-1}$ ) and 1 mL of DMEM without FBS containing LPS ( $400 \text{ ng mL}^{-1}$ ) in order to stimulate inflammation. Finally, membrane chemiluminescence was detected and quantified using a ChemoDoc™ XRS (BioRad). An AlamarBlue® assay was performed to the cells, as previously explained, for data normalization. Each membrane had two replicates for each inflammatory mediator. Inflammatory factors whose levels were increased with the inflammatory stimuli (IL-1 $\beta$  or LPS) and reduced with the CUR-5 NP treatment are represented. Mean  $\pm$  SD values are relative to the positive control (Positive) on each membrane, which is given an arbitrary value of 1. ANOVA of the results was performed at  $p < 0.05$ ,  $p < 0.005$  and  $p < 0.001$  significance levels.

#### 2.4.6. C6-loaded NP cellular uptake

Fluorescent C6-loaded NPs were used as model to study the cellular internalization of the NPs. HC-a and RAW264.7 were seeded at  $2 \times 10^5$  cells/well into 6-well plates. 3 wells were used to measure the cellular uptake and the other 3 were used for cell counting and data normalization. After 24 h, the medium was replaced by 1 mL of NPs ( $1.00 \text{ mg mL}^{-1}$ ) and 1 mL of DMEM and incubated at different times (2, 4, 8 and 24 h). After the required time, NPs were removed and cells were washed twice with PBS. Then, cells were detached with trypsin in the case of HC-a and by scraping the surface in the

case of RAW264.7. Cell suspensions were centrifuged at 1,000 rpm during 5 min. Pellets were resuspended in ethanol to break cells and release C6 and centrifuged again to deposit cell rests. Supernatants were collected for fluorescence measurements using the Multi-Detection Microplate Reader at excitation/emission of 458/540 nm. Cellular uptake measurements were normalized to the total number of cells obtained by Trypan-Blue treated cells counting with a Countess II Automated Cell Counter. Results are pictured as mass of C6 (pg) over the number of live cells at each time. The mass of C6 was obtained using a C6 serial dilution curve. Three replicates were used for each time and results were expressed as mean value  $\pm$  SD.

C6 fluorescence inside the cells was visualized by fluorescence microscopy in glass disks (12 mm). Microscopic visualization was only done with HC-a because its form and size allowed a better visualization of C6 fluorescence in comparison to RAW264.7. HC-a were seeded at 20,000 cells/well into 24-well plates containing the glass disks and exposed to the NP dispersion in the same way that in the 6-well plates. After the treatment, wells were washed twice and fixed with 3.7% formaldehyde for 20 min at room temperature. After washing with PBS twice, cells were permeabilized with Triton 0.05% in PBS for 20 min and washed again twice with PBS. Cell nuclei were dyed using a Hoescht stain and cellular actin filaments were dyed with phalloidin-tetramethylrhodamine B isothiocyanate during 20 min and washed with distilled water three times. Disks were observed using a Nikon TE2000-S Eclipse Microscope.

## **2.5. *In vivo* biocompatibility assay**

All animals were housed in plastic cages with water and food available *ad libitum*, and maintained on 12 h light/dark cycle. Experiments involving animals were carried out in accordance with the ethics Committee on Animal Experimentation of University of Salamanca (register number: 035), the National Spanish law (RD53/2013) and the European Directive (2010/63/EU).

### 2.5.1. *In vivo* subcutaneous model

For the *in vivo* biocompatibility tests, the NPs were sterilized by filtration through 0.22  $\mu\text{m}$  polyethersulfone membranes. A total of six Wistar rats per formulation were used to perform the *in vivo* tests. Each rat was anesthetized by inhalation of 1.5% isoflurane (Vetflurane®). After shaving the animal with an electric shaver and sterilizing the site of injection with an antiseptic solution (povidone-iodine, Betadine®), 1 mL of NP solution (0.50 mg mL<sup>-1</sup>) was administered by a dorsal subcutaneous injection using a syringe equipped with a 21G needle. Three groups were tested: a Control group (PBS), Empty and CUR-5 NPs. These NP compositions and concentrations were chosen because these conditions presented the best physicochemical and cellular properties. A total of four injections were done in each rat and tested samples were randomly divided. Animals were subjected to euthanasia by anesthetic overdose after one and two weeks of injection. Tissues around the injection sites were collected for histological evaluation.

### 2.5.2. Histological study

Subcutaneous tissues extracted from the rats were processed for histological analysis. Tissues were fixed in 10% neutral buffered formalin overnight, dehydrated with ethyl alcohol series and embedded in paraffin. Five-micron sections were cut and stained with hematoxylin and eosin (H-E) for histological analysis. Stained sections were evaluated and photographed by a bright field microscope (Nikon Eclipse 90i) equipped with a Nikon Digital Sight DS-smc camera (Nikon Corporation, Japan).

## 3. Results and discussion

### 3.1. Terpolymer characterization

A terpolymer with a pseudogradient block microstructure based on MVE-rich hydrophobic segments and VP- and VC-rich hydrophilic segments was obtained by free radical polymerization. Kinetics of free radical polymerization of monomers with large reactivity ratio differences lead to polymers whose

composition sensitively depends on the conversion degree. In this system, the reactivity ratio of MVE is much higher than those of VP and VC [44] and, as a consequence, propagating species preferably will add monomeric units of the acrylic monomer at low conversions, leading to monomeric sequences rich in the acrylic monomer, whereas, as conversion increases, pseudoblock sequences rich in the vinyl monomers will be formed. This microstructure confers to the pseudoblock terpolymer an amphiphilic nature. Poly(MVE-co-VP-co-VC) was successfully synthesized with a yield of 85%. PVP and PVC were also synthesized with yields of 85 and 87%, respectively, to be used as controls in thermal experiments. Chemical structure of poly(MVE-co-VP-co-VC) represented in figure 1 was confirmed by  $^1\text{H}$  NMR by the disappearance of the signal due to MVE methacrylic groups (figure S1), and the appearance of the signals due to methylene protons of both VP (3.5-4.0 ppm) and VC (4.2-4.8 ppm) groups. Moreover, poly(MVE-co-VP-co-VC) spectrum showed the general signal broadening attributed to the macromolecular character of the terpolymer. The average terpolymer molar fractions were determined from the  $^1\text{H}$  NMR spectrum by comparing the signal between 0.8 and 1.0 ppm corresponding to 12 protons of MVE ( $\text{CH}_3$ -16-19) and the signals between 3.5 and 4.0 ppm assigned to 1 proton of VP ( $\text{CH}_3$ -a) and signals between 4.2 and 4.8 ppm assigned to 1 proton of VC ( $\text{CH}_3$ -b). A terpolymer MVE:VP:VC molar ratio of 19:73:8 was obtained in contrast to the 10:85:5 feed molar ratio. These differences between terpolymer and feed molar ratios were attributed to the higher reactivity of methacrylates compared to vinyl monomers that facilitates the incorporation of MVE in the terpolymer chain before the vinyl groups at low conversions. Terpolymer molecular weight distribution was analyzed by SEC. The chromatogram showed an unimodal distribution indicating the formation of poly(MVE-co-VP-co-VC) macromolecular chains and the absence of homopolymer species.  $M_w$  and  $M_n$  values were 20 and 17 kDa respectively, while a low  $\bar{D}$ , 1.18, was obtained, indicating that vitamin E exerted certain control in the radical polymerization process. Poly(MVE-co-VP-co-VC) thermal stability was studied by TGA (see table 1). The onset of the major decay and maximum thermal degradation rate temperatures ( $T_{\text{onset}}$  and  $T_{\text{max}}$ ) of the terpolymer approached those of the vinyl homopolymers, due to the higher content of these units in the terpolymer structure. However, they showed a small reduction that may be due to the presence of MVE units in the



terpolymer macromolecules at sight of the lower thermal stability of PMVE. Finally, thermal transitions of poly(MVE-co-VP-co-VC) were assessed using DSC and compared to those of homopolymers. Poly(MVE-co-VP-co-VC) showed two glass transition temperatures ( $T_g$ ), 162 °C ( $T_{g1}$ ) and 178 °C ( $T_{g2}$ ), as seen in table 1.  $T_g$  of PVP and PVC were 172 and 195 °C while  $T_g$  of the homopolymer of MVE (PMVE), calculated by the authors and reported in previous studies, was 159 °C [48]. Therefore, the first transition of the terpolymer ( $T_{g1}$ ) should correspond to polymer segments rich in MVE while  $T_{g2}$  should correspond to macromolecular segments rich in vinyl units, since  $T_{g2}$  of terpolymer was approximately the average of  $T_g$  of PVP and PVC homopolymers.

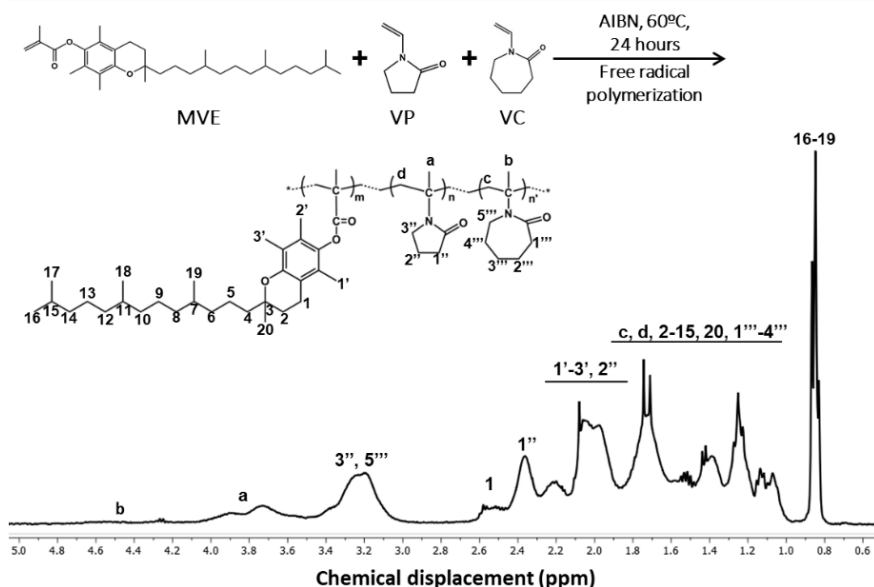


**Figure 1.** Scheme of the terpolymer poly(MVE-co-VP-co-VC) synthesis *via* free radical polymerization, its chemical structure and its  $^1\text{H}$ -NMR spectrum (400 MHz) in  $\text{CDCl}_3$ .

**Table 1. Thermal properties of poly(MVE-co-VP-co-VC) and homopolymers analyzed by TGA and DSC.**

Sample	TGA		DSC	
	T <sub>onset</sub> (°C)	T <sub>max</sub> (°C)	T <sub>g1</sub> (°C)	T <sub>g2</sub> (°C)
<b>Terpolymer</b>	386	418	162	178
<b>PMVE</b>	272	295 and 380 (main)	159 [48]	-
<b>PVP</b>	404	432	-	172
<b>PVC</b>	394	428	-	195

## 3.2. NP characterization

### 3.2.1. Physicochemical properties, stability and encapsulation efficiency

The amphiphilic nature of the terpolymer based on MVE-rich hydrophobic segments and VP- and VC-rich hydrophilic segments allows its self-assembly into NPs by the nanoprecipitation method. The resulting NP dispersions obtained are displayed in figure 2A. Empty NPs were whitish while those NPs entrapping CUR had its characteristic orange color that increased in intensity with drug content. Features in terms of hydrodynamic diameter ( $D_h$ ), polydispersity index (PDI), zeta potential ( $\xi$ ) and encapsulation efficiency (EE) are summarized in table 2.  $D_h$  of CUR NPs ranged between 114 and 135 nm, showing in all cases unimodal size distributions with PDI below 0.20 (see figure 2B). The small values of PDI indicated the size homogeneity of the NPs. A slight decrease of  $D_h$  with increasing CUR content was observed, which could be attributed to the increasing drug hydrophobic interactions and hydrogen bonding mainly through MVE moieties constraining the core, but also with the amphiphilic VC unit. Interestingly, sizes of CUR NPs were lower than those of homologous NPs obtained with the poly(MVE-co-VP) system fabricated following the same methodology described in Subsection 2.3. Results of  $D_h$  of CUR-loaded copolymer NPs are described in table S2. The lower values of CUR-loaded terpolymer NPs can be favorable for the hydrophobic CUR stabilization in the core and for their further endocytosis by cells [49,50]. Zeta potentials ( $\xi$ ) of CUR-loaded terpolymer NPs were slightly negative, with values between  $-3$  and  $-4$  mV, near to neutral charge. Similar values have been previously described for nude and  $6\alpha$ -methylprednisolone-loaded poly(MVE-co-VP) NPs [45] that indicated that the NP cover was based on hydrophilic VP-rich

domains. These poly(MVE-co-VP) NPs were shown to be successfully endocytosed by House Ear Institute-Organ of Corti 1 (HEI-OC1), despite it is generally admitted that positively charged NPs are more prone to be uptaken by cells than neutral and negatively charged ones because of favorable interactions with the negatively charged cell membrane [51-53]. In this work,  $\xi$  values for CUR NPs were relatively less negative than those of homologous copolymer NPs (see table S2) which can favor their endocytosis by cells.

On the other hand, CUR encapsulation efficiency in the terpolymer NPs resulted over 70% in all cases with no significant differences ( $p < 0.05$ ) comparing the samples to each other, and they were slightly higher than values obtained for the copolymer NPs (see table S2). In addition, encapsulation efficiency values were consistent with those reported recently for other CUR-loaded polymeric NPs also prepared by precipitation methods [54]. These high encapsulation efficiencies are due to the hydrophobic nature of CUR that favors the hydrophobic interactions with MVE-rich segments and hydrophobic residues of VC, forming the inner core of NPs, as well as hydrogen bonding between the vehicle and the drug. NP stability was assessed by analyzing the  $D_h$  and the NP size distribution while storing the NPs at 4 °C under static conditions over 7 months. After this period, an increase of 10 nm was observed for CUR-2 and CUR-5 NPs and 20 nm for Empty and CUR-10 NPs but no NP agglomeration occurred after the studied period (figure S2A) while size distributions continued to be unimodal (figure S2B). SEM and cryo-TEM micrographs of Empty and CUR-5 NPs (figure 2C and D) showed spherical morphologies and NP diameters were confirmed to be lower than 200 nm, although size heterogeneity was noticed, especially for CUR-5 NPs.

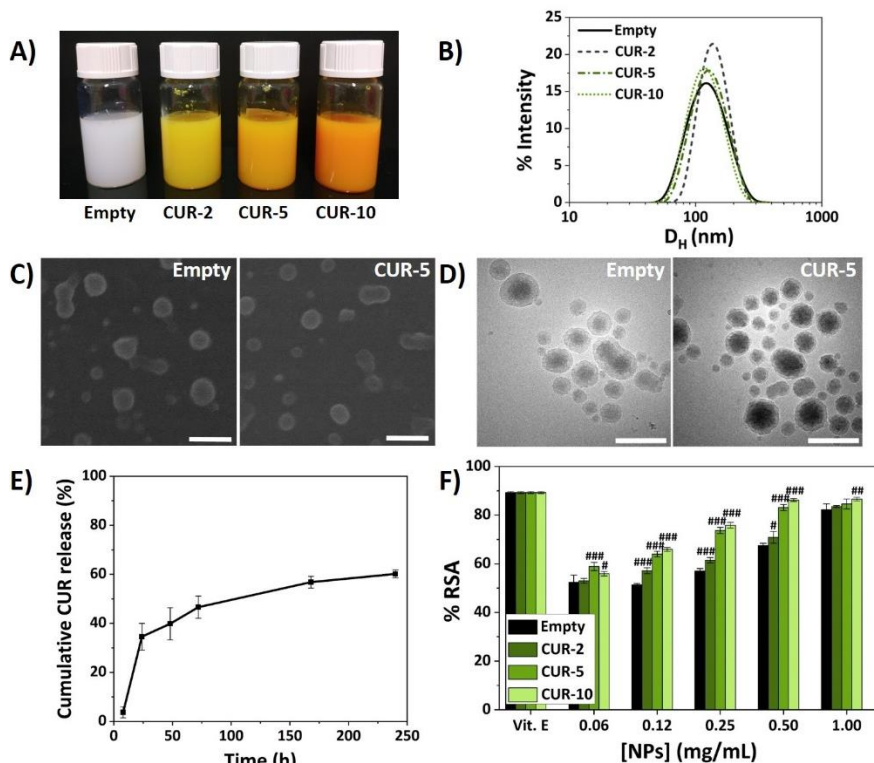


**Figure 2.** Physicochemical characterization of CUR NPs. **A)** NP dispersions obtained by the nanoprecipitation method. From left to right, Empty and NPs initially loaded with 2, 5 and 10% of CUR. **B)** NP size distributions by intensity. **C)** SEM and **D)** cryo-TEM micrographs of Empty and CUR-5 NPs. Scale bars: 200 nm. **E)** Esterase-mediated *in vitro* CUR release profile at 37 °C of CUR-5 NPs. **F)** RSA (%) of Empty, CUR-2, CUR-5 and CUR-10 NPs after 10 minutes of reaction compared to the vitamin E control reference. ANOVA was performed between CUR-loaded NPs and their corresponding Empty NPs at each NP concentration (\* $p < 0.05$ , \*\* $p < 0.005$ , \*\*\* $p < 0.001$ ). Values represent mean  $\pm$  SD.

**Table 2. Values of hydrodynamic diameter ( $D_h$ ), polydispersity index (PDI), zeta potential ( $\xi$ ), encapsulation efficiency (EE) and encapsulated drug concentrations of Empty, CUR and C6-loaded NPs. Values represent mean  $\pm$  SD.**

NPs	% Drug (w/w)	[Drug] mg mL <sup>-1</sup>	$D_h$ (nm)	PDI	$\xi$ (mV)	EE (%)	[Encapsulated drug] mg mL <sup>-1</sup>
Empty	-	-	117.1 $\pm$ 0.2	0.09 $\pm$ 0.01	-3.9 $\pm$ 0.4	-	-
CUR-2	2	0.04	135.1 $\pm$ 0.8	0.02 $\pm$ 0.02	-3.3 $\pm$ 0.3	73 $\pm$ 6	0.0293 $\pm$ 0.0024
CUR-5	5	0.10	123.0 $\pm$ 0.4	0.07 $\pm$ 0.01	-3.6 $\pm$ 1.2	79 $\pm$ 4	0.0789 $\pm$ 0.0039
CUR-10	10	0.20	114.1 $\pm$ 0.6	0.07 $\pm$ 0.02	-3.8 $\pm$ 0.3	72 $\pm$ 4	0.1443 $\pm$ 0.0076
C6	1	0.02	130.0 $\pm$ 0.6	0.18 $\pm$ 0.01	-3.1 $\pm$ 0.4	32 $\pm$ 5	0.0064 $\pm$ 0.0001

### 3.2.2. *In vitro* CUR release

Drug delivery systems such as NPs are carriers that deliver a therapeutic agent or drug in a controlled rate, time or place in the body. Therefore, the slow release of the drug over an extended period of time is an ideal characteristic of these delivery systems. Here, CUR release from CUR-5 NPs was studied at 37 °C at physiological pH using a diffusion method. In order to simulate the cytoplasmic environment that would face NPs once they are internalized by the cells, the medium was supplemented with esterases. Esterases are a type of hydrolase enzymes widely present in the cytoplasm of human cells that split esters into an acid and an alcohol during hydrolysis. The *in vitro* release profile of CUR-5 NPs (figure 2E) showed a moderate burst release in the first 24 h, commonly observed in this type of polymeric nanovehicles [55,56]. Following the burst release, a prolonged and sustained CUR release was observed for 10 days, due to the esterase-induced cleavage of esters in the terpolymer matrix that triggers polymer erosion and drug release by diffusion. After 10 days, 40% of CUR remained in the NPs, which can be attributed to the protective effect of the nanocarrier on CUR, its slow release and its retention by their interaction with the amphiphilic VC.

### 3.2.3. Antioxidant activity of NPs by DPPH scavenging

Free radicals are known to have a key role on the regulation of physiological cellular functions *via* redox signaling, but also detrimental if produced in excess [57]. A DPPH test based on the reduction of the stable radical DPPH in the presence of a hydrogen-donating antioxidant molecule was performed in order to assess the antioxidant activity of Empty and CUR-loaded NPs. In the first place, the test was performed at different NPs - DPPH reaction times (10, 20, 30, 60 and 120 min) to determine the equilibrium time. It was observed that the maximum RSA value was reached after 10 min, and from then on, a plateau was maintained in time for all the formulations. In figure 2F, results of the 10 min test are illustrated. In this assay, vitamin E (vit. E) was used as a radical scavenger control, to obtain the maximum RSA possible to be achieved in the assay. Free CUR at the CUR encapsulation concentrations achieved for CUR-2, CUR-5 and CUR-10 at the most concentrated systems ( $1.00 \text{ mg mL}^{-1}$ ) were also investigated and compared to their corresponding NP systems (figure S3A). Empty NPs had an intrinsic scavenging activity due to the presence of vitamin E moieties, mainly located in the polymeric core of NPs. When CUR was introduced in the core, RSA values increased in a CUR concentration dependent manner. RSA also increased with NP concentration. All concentrations of CUR NPs showed significant differences with their corresponding Empty NPs except for CUR-2 at  $0.06 \text{ mg mL}^{-1}$  and CUR-2 and CUR-5 at  $1.00 \text{ mg mL}^{-1}$ , in these last cases, RSA values were close to the maximum value obtained for the control (*i.e.* free vit. E) (89%). When comparing free and encapsulated CUR, as observed in figure S3A, significant differences are observed. In the case of CUR-2 an improvement of the RSA for the encapsulated system was reached while for CUR-5 and CUR-10 a 5% reduction of RSA occurred. Nevertheless, RSA values were very close to the ones obtained for vit. E with values over 83% in the three cases. RSA was also represented against the encapsulated CUR concentration as shown in figure S3B. When comparing similar encapsulated CUR concentration for the three systems at different NP concentrations, the higher RSA values were obtained for the most concentrated NP dispersions. This can confirm that not only CUR provides the antioxidant effect to the system but the vehicle does, making clear the advantage of using more NP concentrated systems with less CUR-loaded

instead of less NP concentrated systems with more CUR-loaded, from an antioxidant point of view.

### **3.3. *In vitro* biological behavior**

#### **3.3.1. NP cytotoxicity**

Cytotoxicity of NP dispersions was evaluated in HC-a and analyzed by an AlamarBlue® assay after 24 and 48 h, 7 and 14 days of treatment. NP results were normalized and analyzed for statistical significance using ANOVA ( $p < 0.05$ ) with respect to CNT groups. Results are shown in figure 3. Non-loaded NPs did not exert cytotoxic effects as cell viabilities were over 90% at all concentrations and times. However, for CUR NPs, there were CUR and NP concentration dependent cytotoxic effects. As the percentage of encapsulated CUR increased, cell viability decreased, reaching values below 70% for some CUR-5 and CUR-10 NP dispersions. Besides, the higher the NP concentration, the lower the HC-a viability, especially for CUR-10 NPs. Likewise, there was a time dependent effect on cell viability, specially marked for CUR-10 NPs. Cell viability was maximum at 24 h and decreased at 48 h and 7 days. For CUR-2 and CUR-5 NPs, cell viability was recovered after 14 days of treatment but it was not the case for CUR-10 NPs. From these results, it can be stated that CUR is the responsible of the cytotoxic effect observed in this assay, since Empty NPs did not exert any detrimental effect on cell viability. Free CUR is quickly degraded at physiological pH [58]. However, the highest cytotoxicity was observed after 7 days, which could be due to the protective effect of the self-assembled polymeric NPs that have to be disassembled in order to release CUR entrapped in the core. This result, although it was obtained in different experimental conditions, matches with the one obtained in the *in vitro* release study performed with CUR-5 NPs (figure 2E), where the highest CUR release (around 55%) was achieved after 7 days.

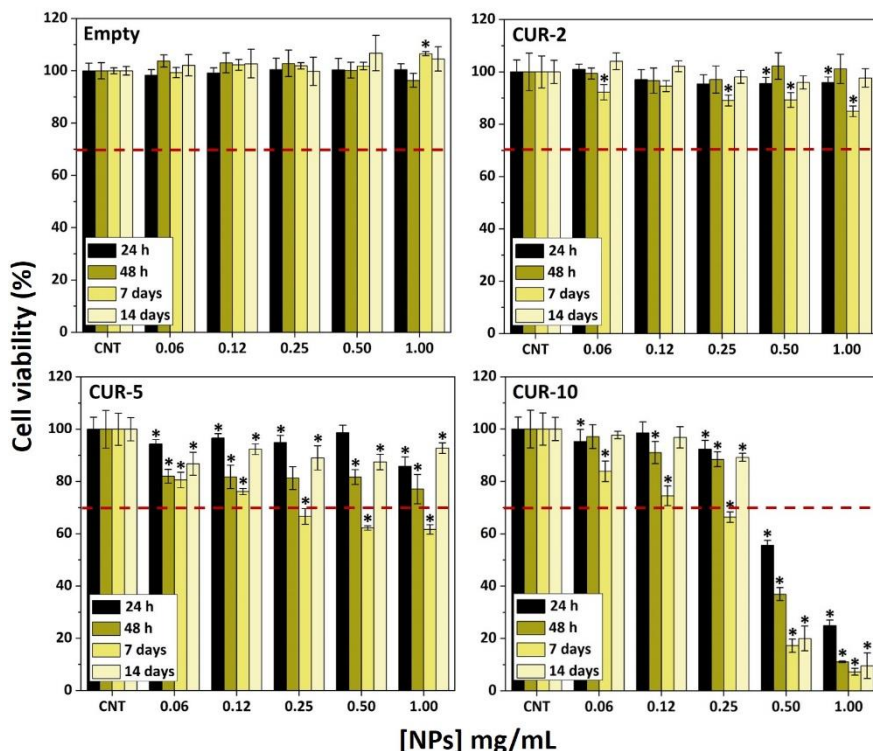


**Figure 3.** HC-a viability (% with respect to their corresponding CNT group, for each time) after 24 h, 48 h, 7 and 14 days of treatment with Empty, CUR-2, CUR-5 and CUR-10 NPs. Values represent mean  $\pm$  SD. ANOVA between formulations and their CNT groups was performed (\* $p < 0.05$ ).

RAW264.7 viability when in contact with the NPs was also investigated using an AlamarBlue® test after 24 h of NP exposure, obtaining toxic effects for CUR-10 (0.25 - 1.00 mg mL<sup>-1</sup>) and CUR-5 (1.00 mg mL<sup>-1</sup>) NPs, as represented in figure 4A. Consequently, these concentrations were not used for the following biological antioxidant and anti-inflammatory assays. In figure 4B, RAW264.7 viability when in contact with free or encapsulated CUR against CUR concentration is pictured. For the same CUR concentration, free CUR leads to lower cell viability in contrast to encapsulated one. Cell viability IC<sub>50</sub> values for free (0.0099 mg mL<sup>-1</sup>) and encapsulated CUR in CUR-10 NPs (0.0244 mg mL<sup>-1</sup>) demonstrate a 2.5-fold reduction of CUR toxicity in CUR-10 NPs compared to



its free form. CUR-2 and CUR-5 cell viability  $IC_{50}$  values could not be calculated as not enough toxic effects were observed in the studied conditions to obtain this value. In spite of that, taking into account the cell viability tendency of both formulations, higher  $IC_{50}$  values are expected. Therefore, it can be concluded that this terpolymer nanocarrier can significantly reduce *in vitro* CUR toxicity.

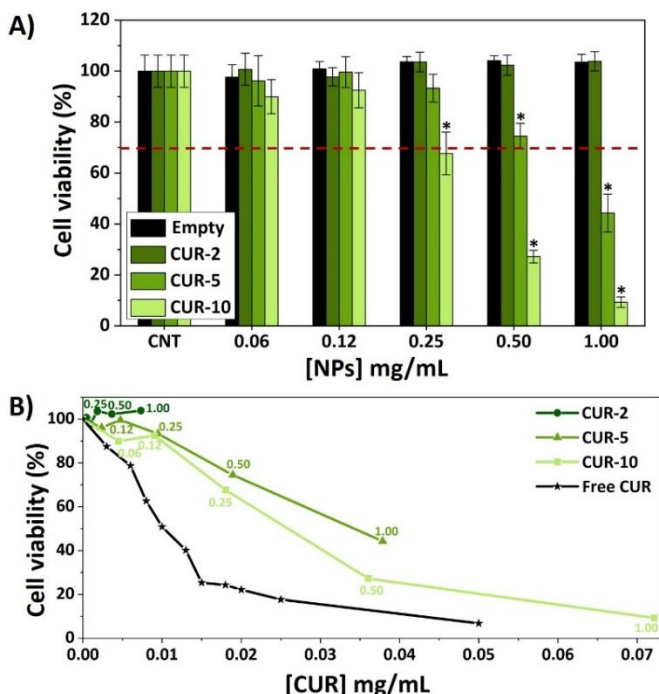
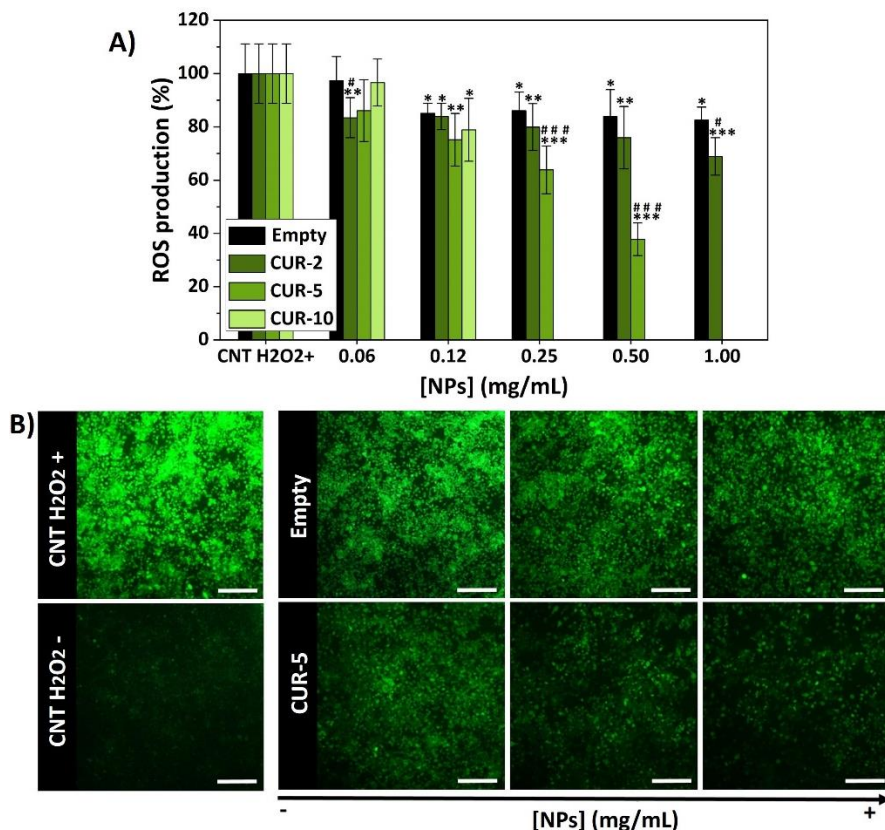


Figure 4. A) RAW264.7 viability (% with respect to CNT group) of each NP formulation after 24 h. ANOVA between formulations and CNT group was performed (\* $p < 0.05$ ). Values represent mean  $\pm$  SD. B) RAW264.7 viability represented against the encapsulated CUR concentration for each NP concentration and compared to free CUR. Numbers on each point represent the NP concentration ( $mg\ mL^{-1}$ ) of the system.

### 3.3.2. Antioxidant activity of NPs by the inhibition of cellular ROS

During the innate immune response, macrophages are responsible for ROS secretion upon early exposure to an inflammatory stimulus. However, when this production exceeds normal levels, it can lead to the production of inflammatory mediators and further tissue inflammation. Therefore, the reduction of excessive ROS can be a strategy to treat inflammation. Cellular ROS production by RAW264.7 was assessed using the DCFH-DA probe. This cell-permeable non-fluorescent probe is intracellularly deacetylated by esterases to form 2,7'-dichlorodihydrofluorescein (DCFH), which is rapidly oxidized to the fluorescent compound dichlorofluorescein (DCF) in the presence of ROS. The higher the fluorescence intensity the higher the quantity of ROS. Results of cellular ROS production for the non-toxic formulations are represented in figure 5A.  $H_2O_2$  stimulated cells without NP treatment (CNT  $H_2O_2$ +) were taken as 100% of ROS production. The same antioxidant tendency was observed as for the DPPH test (figure 2F). Empty NPs had antioxidant capacity by themselves which was enhanced by the load of CUR in a CUR concentration and NP concentration dependent manner, noticed for 0.25 - 1.00 mg mL<sup>-1</sup> NP concentrations. The representation of ROS production against the encapsulated CUR concentration is shown in figure S4A. As in the case of DPPH, for similar encapsulated CUR concentrations most concentrated NP samples achieved higher antioxidant activities (*i.e.* lower ROS production), demonstrating again the higher activity of most concentrated samples with less CUR-loaded. ROS assay samples were finally observed by fluorescence microscopy. The images corresponding to Empty (0.06, 0.25 and 1.00 mg mL<sup>-1</sup>) and CUR-5 NPs (0.06, 0.25 and 0.50 mg mL<sup>-1</sup>) are displayed in figure 5B. As can be seen, NP treatment decreased fluorescence intensity, *i.e.* ROS, in both Empty and CUR-loaded NPs, although in a greater extent for the loaded NPs, in agreement with quantitative tests.



**Figure 5.** A) Quantification of ROS production by RAW264.7 (% with respect to CNT H<sub>2</sub>O<sub>2</sub>+). ANOVA between formulations and CNT H<sub>2</sub>O<sub>2</sub>+ (\**p* < 0.05, \*\**p* < 0.005, \*\*\**p* < 0.001) and between Empty and CUR-loaded NPs for each NP concentration (#*p* < 0.05, ##*p* < 0.005, ###*p* < 0.001) were performed. Values represent mean ± SD. B) Fluorescence microscopy images, where higher intensity of fluorescence means higher ROS content. CNT H<sub>2</sub>O<sub>2</sub>+ refers to PBS treated and H<sub>2</sub>O<sub>2</sub> stimulated cells and CNT H<sub>2</sub>O<sub>2</sub>- to PBS treated and unstimulated cells. From left to right, Empty NPs are at 0.06, 0.25 and 1.00 mg mL<sup>-1</sup> and CUR-5 NPs are at 0.06, 0.25 and 0.50 mg mL<sup>-1</sup>. Scale bars: 500 μm.

Several CUR-loaded polymeric NPs have shown to have antioxidant potential [59]. Vitamin E and CUR are two well-known radical scavengers. Vitamin E exerts its activity by scavenging lipid peroxyl radicals during lipid peroxidation [60] while CUR has a conjugated structure containing two

methoxylated phenols and an enol form of  $\beta$ -diketone showing radical trapping activity [61]. In the systems developed in this work, both CUR and vitamin E residues are found in the inner core of the NPs and, thereby, the antioxidant effect will be related with this inner part of the system. In both DPPH and cellular ROS assays, Empty NPs had antioxidant power by themselves, which was significantly enhanced for CUR-5 NPs at 0.25 and 0.50 mg mL<sup>-1</sup> and for CUR-2 NPs at 1.00 mg mL<sup>-1</sup>. According to these findings, the NP vehicle based on this terpolymer has an intrinsic antioxidant activity because of the presence of the vitamin E based monomeric units, and the antiradical effect is further improved when CUR is loaded inside, providing a combined effect of both antioxidants.

### 3.3.3. Anti-inflammatory activity of CUR-loaded NPs

NO has demonstrated to be a versatile molecule in the regulation of inflammation. It is released by activated macrophages in response to different stimuli, like pathogens, and regulates the activity of different inflammatory cells in terms of function, growth and death. Consequently, it has been widely used as an *in vitro* inflammation marker. To ascertain the anti-inflammatory effect of the NPs, the NO production in LPS-stimulated RAW264.7 was investigated using a Griess test (figure 6). Empty NPs did not exert any significant effect on NO production with respect to the control (CNT LPS+). Nonetheless, when CUR was loaded, NPs substantially inhibited NO production in a NP and CUR concentration dependent manner. CUR-loaded NPs were capable of significantly reduce NO with respect to CNT LPS+ and with respect to their corresponding Empty formulations for all samples and concentrations except for 0.06 mg mL<sup>-1</sup> of CUR-2 and CUR-5 NPs. Moreover, CUR-5 NPs at 0.50 mg mL<sup>-1</sup> reached NO levels very close to basal levels of unstimulated cells or LPS- (5%). CUR reduction of NO production by RAW264.7 has been widely reported over the past years [62–64]. In this sense, although this polymeric vehicle was not capable of reducing NO levels itself, when loading an anti-inflammatory molecule, in this case CUR, inside the NPs, the system was able to maintain its anti-inflammatory effect. Figure S4B shows the NO production against the encapsulated CUR concentration, showing a similar effect as for the DPPH and ROS assays but in a less pronounced manner. In this case, the vehicle

does not have anti-inflammatory potential in terms of NO reduction. Hence, differences between formulations with similar CUR load but different NP concentration are less pronounced than for DPPH and ROS assays. This demonstrates that this effect was mainly due to the antioxidant potential of the nanocarrier.

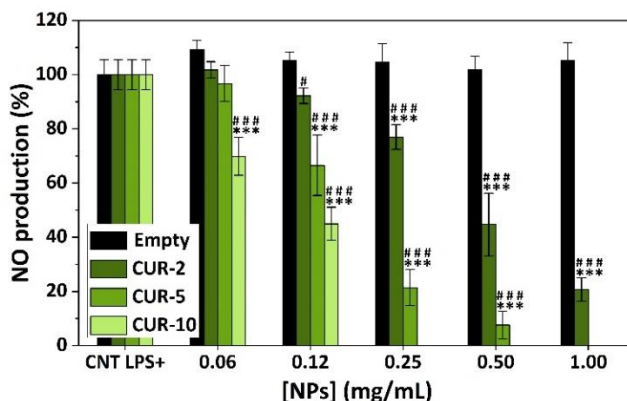


**Figure 6.** Quantification of NO production by RAW264.7 (% with respect to CNT LPS+). Values represent mean  $\pm$  SD. ANOVA between formulations and CNT LPS+ (\* $p$  < 0.05, \*\* $p$  < 0.005, \*\*\* $p$  < 0.001) and between Empty and CUR-loaded NPs for each NP concentration (# $p$  < 0.05, ## $p$  < 0.005, ### $p$  < 0.001) were performed.

In order to further investigate the anti-inflammatory effect of CUR NPs in the cellular production of inflammatory mediators, human and mouse inflammation antibody arrays were performed for HC-a and RAW264.7 in two different experiments. In the case of HC-a (figure 7), culture medium levels of five inflammatory mediators were reduced by exposing HC-a to CUR-5 NPs and then stimulating with IL-1 $\beta$ : interleukin-8 (IL-8), monocyte chemoattractant proteins 1 and 2 (MCP-1/CCL2, MCP-2/CCL8) and macrophage inflammatory proteins 1 $\alpha$  and 1 $\beta$  (MIP-1 $\alpha$ /CCL3, MIP-1 $\beta$ /CCL4).

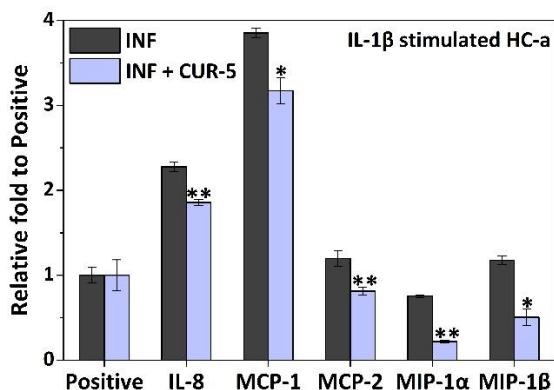


**Figure 7.** Inflammatory factor levels in culture media that were increased in IL-1 $\beta$  stimulated HC-a and decreased upon exposure to CUR-5 NPs. Mean  $\pm$  SD values are relative to the positive control (Positive) of the respective membrane, which is given an arbitrary value of 1. ANOVA of results of INF + CUR-5 membrane with respect to those of INF for each factor was performed at significance levels of \* $p < 0.05$  and \*\* $p < 0.005$ .

Regarding LPS stimulated RAW264.7, five inflammatory factor levels were increased with LPS stimulation and then reduced upon CUR-5 NP treatment: IL-6, tumor necrosis factor  $\alpha$  (TNF- $\alpha$ ), soluble tumor necrosis factor receptors I and II (sTNF-R I and II), RANTES (CCL5) and the previous mentioned MCP-1 (see figure 8).

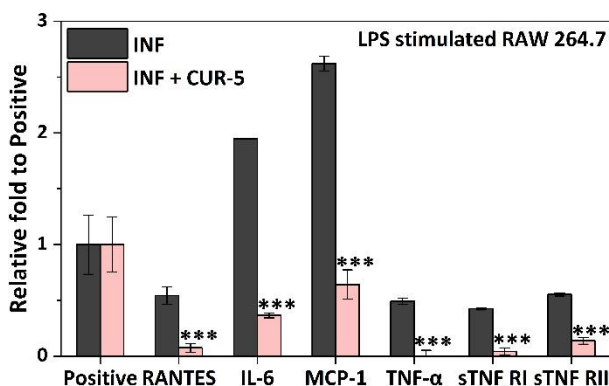


**Figure 8.** Inflammatory factor levels in culture media that were increased in LPS stimulated RAW264.7 and decreased upon exposure to CUR-5 NPs. Mean  $\pm$  SD

values are relative to the positive control (Positive) of the respective membrane, which is given an arbitrary value of 1. ANOVA of results of INF + CUR-5 membrane with respect to those of INF for each factor was performed at a significance level \*\*\* $p < 0.001$ .

CUR has shown to have anti-inflammatory properties by different mechanisms of actions. It has been reported that CUR is capable of down-regulating transcription factors such as NF- $\kappa$ B (Nuclear factor-kappa B), activator protein 1 (AP-1), early growth response 1 (EGR-1) or intracellular signaling pathways including mitogen-activated protein kinase (MAPK) and Janus kinase/signal transducers and activators of transcription (JAK/STAT) [65]. These factors and signaling pathways are responsible for regulating the gene expression of pro-inflammatory molecules like matrix metalloproteinases (MMP), cyclooxygenase-2 (COX-2), TNF- $\alpha$ , inducible nitric oxide synthase (iNOS), interleukins (IL-1 $\beta$ , IL-6, IL-8) and other pro-inflammatory cytokines and chemokines. Besides, CUR is also capable of reducing chemokines such as MIP and MCP, which are included in a group called CC chemokines [66,67]. Chemokines are known to be chemoattractants for leukocyte sequestration in inflammation sites, having a key role in chronic inflammation. In the present study, five pro-inflammatory chemokines IL-8, MIP-1 $\alpha$ , MIP-1 $\beta$ , MCP-1 and MCP-2 were significantly reduced in HC-a when pre-treated with CUR-5 NPs, which is in agreement with the anti-inflammatory effect of CUR reported in articular chondrocytes *via* the inflammatory pathways mentioned above [68]. As far as RAW267.4 results, levels of IL-6 and TNF- $\alpha$ , two of the main pro-inflammatory targets of CUR anti-inflammatory action, were significantly reduced ( $p < 0.001$ ), in accordance with recent bibliography about other CUR-loaded polymeric vehicles [28,69]. As in the case of HC-a, CUR-5 NPs treatment was also capable of reducing MCP-1 chemokine levels in RAW264.7 in a significant manner ( $p < 0.001$ ). The RANTES chemokine was also reduced, as it has been recently reported by other CUR drug delivery systems [70,71]. The levels of the two anti-inflammatory factors, sTNF-R I and II, which are TNF receptors able to bind and inactivate TNF- $\alpha$ ; were increased in LPS stimulated RAW264.7 and reduced when treated with the NPs. The presence of elevated levels of these receptors in LPS stimulated cells is a cellular mechanism to counteract the effect of TNF- $\alpha$  [72]. Since cells treated with CUR-5 NPs revealed negligible levels of TNF- $\alpha$  in the culture medium, levels of these receptors

needed to counteract the effect of  $\text{TNF-}\alpha$ , are thought to be decreased as well. Although deeper quantitative analysis of the inflammatory factors should be done to completely elucidate the anti-inflammatory effect of these CUR-5 NPs, it can be confirmed that the encapsulation of CUR into this polymeric vehicle does not diminish the described anti-inflammatory effect of CUR, in terms of reduction of pro-inflammatory factors such as NO and pro-inflammatory cytokines and chemokines.

### 3.3.4. Cellular C6 NP uptake

NP internalization was monitored by fluorescence spectroscopy. Multiple factors modulate this internalization, such as NP shape, surface charge and surface composition; or the cell type and its environment [73]. C6-loaded NPs were used as a model to assess NP cellular uptake by measuring C6 fluorescence inside HC-a and RAW264.7. Kinetics of NP internalization was different for each cell type, as seen in figure 9A. In the case of HC-a, the internalization seems to follow a first order kinetic model where a plateau is reached after 8 h, meaning that the internalization occurred mainly in the first 8 h of contact between cells and NPs. On the other hand, for RAW264.7, the internalization kinetics seems to better fit a zero order kinetic model, where a linear increase of C6 was observed in the whole studied period. HC-a are metabolically active cells found in articular cartilage and dedicated to the synthesis of cartilage extracellular matrix components, such as collagen and proteoglycans, while RAW264.7 are monocyte/macrophage-like cells responsible of the phagocytosis and pinocytosis of particles and microbes for its elimination. In our case, HC-a were able to internalized the NPs in a lesser degree in contrast to RAW264.7 because of the phagocytic nature of the latter. Fluorescence microscopy was further employed in C6-loaded NPs treated HC-a to localize C6 after NP treatment. In figure 9B, green fluorescence corresponds to C6 while blue represents cell nuclei and red cellular actin filaments. After 8 and 24 h, the fluorescence intensity of C6 was higher compared to 2 and 4 h after treatment, in agreement with the quantitative study. Moreover, C6 is present in the cell cytoplasm and mainly accumulated around the nucleus in the form of small spots.



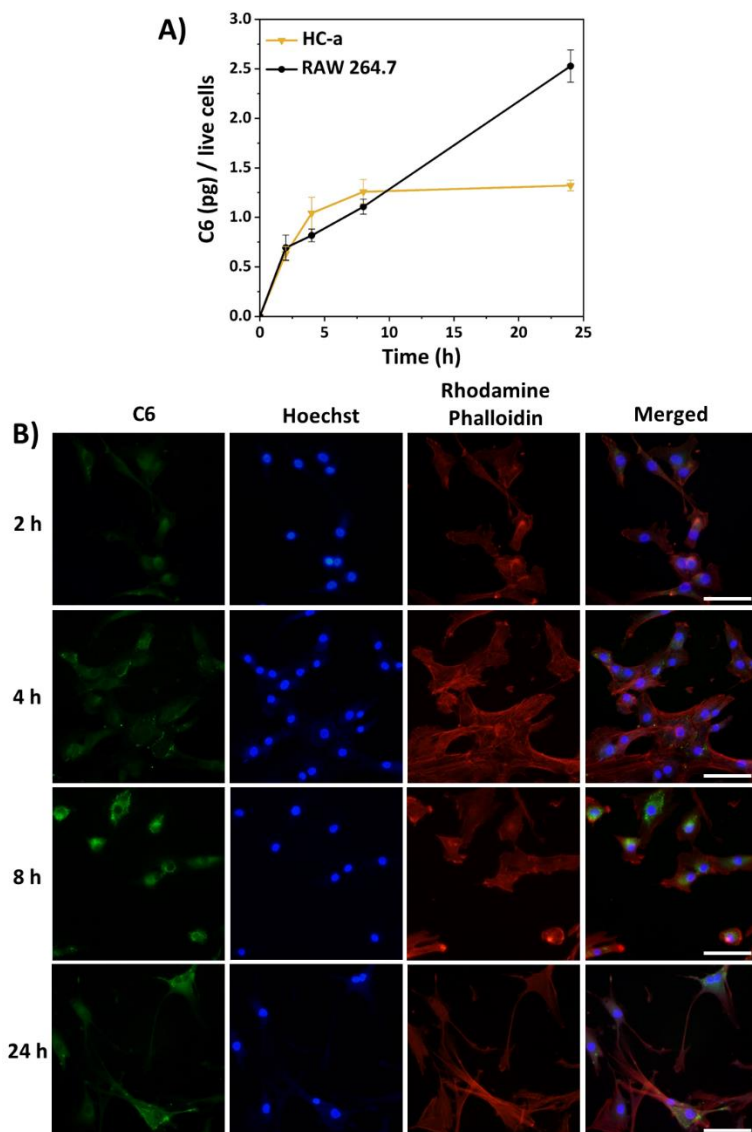


**Figure 9.** A) Quantitative HC-a and RAW264.7 uptake of C6-loaded NPs in time. Values represent mean  $\pm$  SD. B) Fluorescence microscope images showing qualitative uptake of C6-loaded NPs by HC-a after 2, 4, 8 and 24 h of treatment. Green fluorescent intensity corresponds to C6, blue corresponds to cell nuclei and red correspond to cellular actin filaments. Scale bars: 100  $\mu$ m.

### 3.4. *In vivo* biocompatibility

The *in vivo* response was evaluated by a subcutaneous injection of the NPs into the dorsal tissue of Wistar rats. Three groups: Control (PBS), Empty and CUR-5 NPs were evaluated after one and two weeks of injection. NP dispersions could be smoothly injected. After the injection, the animals returned to their normal activities and no complications or adverse reaction signs were observed. Once experimentation time was elapsed, animals were euthanized and macroscopic alteration attributed to NPs could not be noticed. Histological observation of skin sections showed no dermo-epidermal alterations, as presented in figure 10, in any experimentation time. The epidermis and dermis appeared intact at the injection surrounded tissue. Normal morphology of subcutaneous tissue in Control, Empty and CUR-5 groups was appreciated. In addition, as shown in figure 10, no inflammatory infiltrate, after NP injection, was observed, neither after one nor two weeks of injection, which confirms the *in vivo* biocompatibility of both, the polymeric vehicle and CUR-5 NPs. These biocompatibility results agree with those of other CUR delivery systems described in bibliography, where no toxicity was seen and even anti-inflammatory potential was demonstrated. For instance, CUR-loaded PLGA microparticles showed to diminish the inflammatory effect caused by Empty PLGA microparticles for cancer treatment in a mice model [74]. Other CUR delivery systems have demonstrated *in vivo* its biocompatible nature for the treatment of arthritis [75], anticancer activity [76] experimental periodontal disease [77] or wound healing [78]. In this work, the *in vivo* biocompatibility results of CUR-5 NPs agree with the *in vitro* cellular non-cytotoxic results for the formulation CUR-5 ( $0.50 \text{ mg mL}^{-1}$ ) using both HC-a and RAW264.7 cell lines. The biocompatibility property could be related to the degree of the hydrophilicity of the material surface [79]. In these NPs, the hydrophilic VP may account for a good biocompatibility and will ensure the stability of the nanocarrier. Besides, this formulation was the one reaching the best antioxidant and anti-inflammatory values for ROS (reduction of ROS to 35%) and NO quantification (reduction of NO to 10%). Therefore, these systems can assure the antioxidant and anti-inflammatory properties of CUR-5 without compromising the required *in vivo* biocompatibility.

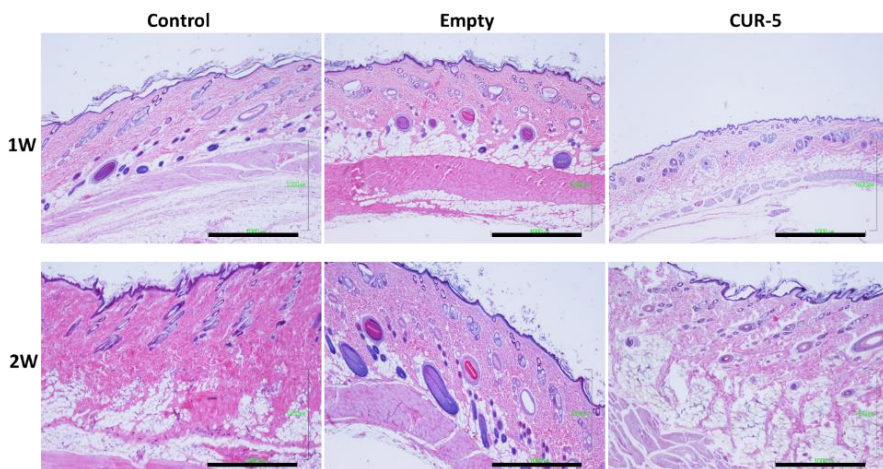


**Figure 10.** Histologic micrographs of skin longitudinal sections of subcutaneous injection site of Control, Empty, and CUR-5 NPs samples at different times (one and two weeks). H-E, 4x, scale bars: 1000  $\mu\text{m}$ .

## 4. Conclusions

In summary, CUR-loaded NPs based on a novel terpolymer system have been designed and characterized and have demonstrated to possess promising anti-inflammatory, antioxidant and biocompatible characteristics, while being stable in aqueous media, unlike free CUR. By the nanoprecipitation method, the amphiphilic nature of the terpolymer, allowed their self-assembly providing NPs with high CUR encapsulation efficiencies, good CUR release profile and adequate sizes and morphologies for their endocytosis by both, chondrocytes and macrophages. CUR-loaded NPs were non-cytotoxic in a wide range of CUR loads and concentrations. NP radical scavenging properties obtained by the DPPH test were high, obtaining RSA values nearly equal to the antioxidant control vitamin E for most concentrated NPs. These findings were supported by the cellular ROS quantification, in which both Empty and CUR NPs had antioxidant activity reaching a 50% reduction of ROS for CUR-5 NPs at 0.50  $\text{mg mL}^{-1}$ . The anti-inflammatory capacity of the CUR bearing system was demonstrated in terms of reduction of intracellular NO and pro-inflammatory cytokines and chemokines, being this reduction more significant in the case of

IL-8, MIP-1 $\alpha$  and MCP-2 in HC-a; and IL-6, MCP-1, TNF- $\alpha$  and RANTES in RAW264.7. Finally, NP biocompatibility was confirmed in an *in vivo* rat model where no histological differences were found between Control and Empty or CUR-5 NPs treated groups. These systems are proposed as promising drug delivery systems for applications in oxidative stress and inflammatory related diseases in order to reduce CUR cytotoxicity while maintaining its anti-inflammatory activity and improving its antioxidant capacity. Further *in vitro* and *in vivo* studies are being developed to deeply explore the anti-inflammatory potential and the possible applications of these NPs.

## Acknowledgement

The authors appreciatively acknowledge financial support from the project IND2017/IND7614, supported by the Comunidad de Madrid (Spain) and Alodia Farmacéutica SL. The authors are also grateful to the Histology Area of the Department of Human Anatomy and Histology of Faculty of Medicine (University of Salamanca) for assistance in the histological processing, Rosa Ana Ramirez for the help in the cell culture experiments and David Gómez (ICTP-CSIC) and Rafael Nuñez (Center of Biological Research, CIB-CSIC) for the SEM and Cryo-TEM studies, respectively.

## Bibliography

[1] S. Reuter, S.C. Gupta, M.M. Chaturvedi, B.B. Aggarwal, Oxidative stress, inflammation, and cancer: how are they linked? *Free Radic. Biol. Med.* 49 (2010) 1603-1616.

[2] L. Zuo, E.R. Prather, M. Stetskiv, D.E. Garrison, J.R. Meade, T.I. Peace, T. Zhou, Inflammaging and Oxidative Stress in Human Diseases: From Molecular Mechanisms to Novel Treatments, *International Journal of Molecular Sciences*, 20, 2019.

[3] G.H. Gislason, J.N. Rasmussen, S.Z. Abildstrom, T.K. Schramm, M.L. Hansen, E. L. Fosbol, R. Sorensen, F. Folke, P. Buch, N.

Gadssboll, S. Rasmussen, H.E. Poulsen, L. Kober, M. Madsen, C. Torp-Pedersen, Increased mortality and cardiovascular morbidity associated with use of nonsteroidal anti-inflammatory drugs in chronic heart failure, *Arch. Intern. Med.* 169 (2009) 141-149.

[4] N. Bhala, J. Emberson, A. Merhi, S. Abramson, N. Arber, J.A. Baron, C. Bombardier, C. Cannon, M.E. Farkouh, G.A. FitzGerald, P. Goss, H. Halls, E. Hawk, C. Hawkey, C. Hennekens, M. Hochberg, L.E. Holland, P.M. Kearney, L. Laine, A. Lanus, P. Lance, A. Laupacis, J. Oates, C. Patrono, T.J. Schnitzer, S. Solomon, P. Tugwell, K. Wilson, J. Wittes, C. Baigent, Vascular and upper gastrointestinal effects of non-steroidal anti-

inflammatory drugs: meta-analyses of individual participant data from randomised trials, *Lancet* (London, England) 382 (2013) 769-779.

[5] A.K. McDonough, J.R. Curtis, K.G. Saag, The epidemiology of glucocorticoid-associated adverse events, *Curr. Opin. Rheumatol.* 20 (2008) 131-137.

[6] J.B. Rice, A.G. White, L.M. Scarpato, G. Wan, W.W. Nelson, Long-term systemic corticosteroid exposure: a systematic literature review, *Clin. Ther.* 39 (2017) 2216-2229.

[7] S. Wongrakpanich, A. Wongrakpanich, K. Melhado, J. Rangaswami, A comprehensive review of non-steroidal anti-inflammatory drug use in the elderly, *Aging Dis.* 9 (2018) 143-150.

[8] Z. Hussain, H.E. Thu, M.W. Amjad, F. Hussain, T.A. Ahmed, S. Khan, Exploring recent developments to improve antioxidant, anti-inflammatory and antimicrobial efficacy of curcumin: a review of new trends and future perspectives, *Materials science & engineering, C, Materials for biological applications* 77 (2017) 1316-1326.

[9] M.A. Chaves, S.C. Pinho, Curcumin-loaded proliposomes produced by the coating of micronized sucrose: influence of the type of phospholipid on the physicochemical characteristics of powders and on the liposomes obtained by hydration, *Food Chem.* 291 (2019) 7-15.

[10] K. Tai, M. Rappolt, X. He, Y. Wei, S. Zhu, J. Zhang, L. Mao, Y. Gao, F. Yuan, Effect of beta-sitosterol on the curcumin-loaded liposomes: vesicle characteristics, physicochemical stability, in vitro release and bioavailability, *Food Chem.* 293 (2019) 92-102.

[11] A.S. Reddy, B.A. Lakshmi, S. Kim, J. Kim, Synthesis and characterization of acetyl curcumin-loaded core/shell liposome

nanoparticles via an electrospray process for drug delivery, and theranostic applications, *European journal of pharmaceuticals and biopharmaceutics: official journal of Arbeitsgemeinschaft fur Pharmazeutische Verfahrenstechnik e.V* 142 (2019) 518-530.

[12] C. Guo, J. Yin, D. Chen, Co-encapsulation of curcumin and resveratrol into novel nutraceutical hyalurosomes nano-food delivery system based on oligo-hyaluronic acid-curcumin polymer, *Carbohydr. Polym.* 181 (2018) 1033-1037.

[13] J.D. Yuan, D.L. ZhuGe, M.Q. Tong, M.T. Lin, X.F. Xu, X. Tang, Y.Z. Zhao, H.L. Xu, pH-sensitive polymeric nanoparticles of mPEG-PLGA-PGLu with hybrid core for simultaneous encapsulation of curcumin and doxorubicin to kill the heterogeneous tumour cells in breast cancer, *Artificial cells, nanomedicine, and biotechnology* 46 (2018) 302-313.

[14] Y.C. Kuo, H.C. Tsai, Rosmarinic acid- and curcumin-loaded polyacrylamide-cardiolipin-poly(lactide-co-glycolide) nanoparticles with conjugated 83-14 monoclonal antibody to protect beta-amyloid-insulted neurons, *Materials science & engineering, C, Materials for biological applications* 91 (2018) 445-457.

[15] L. Sun, Z. Liu, L. Wang, D. Cun, H.H.Y. Tong, R. Yan, X. Chen, R. Wang, Y. Zheng, Enhanced topical penetration, system exposure and anti-psoriasis activity of two particle-sized, curcumin-loaded PLGA nanoparticles in hydrogel, *Journal of controlled release: official journal of the Controlled Release Society* 254 (2017) 44-54.

[16] S. Brown, S. Kumar, B. Sharma, Intra-articular targeting of nanomaterials for the treatment of osteoarthritis, *Acta Biomater.* 93 (2019) 239-257.

[17] W. Song, X. Su, D.A. Gregory, W. Li, Z. Cai, X. Zhao, Magnetic Alginate/Chitosan Nanoparticles for Targeted Delivery of

Curcumin into Human Breast Cancer Cells, *Nanomaterials*, 8, 2018.

**[18]** M. Kamalabadi-Farahani, M. Vasei, N. Ahmadbeigi, S. Ebrahimi-Barough, M. Soleimani, R. Roozafzoon, Anti-tumour effects of TRAIL-expressing human placental derived mesenchymal stem cells with curcumin-loaded chitosan nanoparticles in a mice model of triple negative breast cancer, *Artificial cells, nanomedicine, and biotechnology* 46 (2018) S1011-S1021.

**[19]** G. Arya, M. Das, S.K. Sahoo, Evaluation of curcumin loaded chitosan/PEG blended PLGA nanoparticles for effective treatment of pancreatic cancer, *Biomedicine & pharmacotherapy = Biomedecine & pharmacotherapie* 102 (2018) 555-566.

**[20]** F.S. Tabatabaei Mirakabad, A. Akbarzadeh, M. Milani, N. Zarghami, M. Taheri- Anganeh, V. Zeighamian, F. Badrzadeh, M. Rahmati-Yamchi, A Comparison between the cytotoxic effects of pure curcumin and curcumin-loaded PLGA-PEG nanoparticles on the MCF-7 human breast cancer cell line, *Artificial cells, nanomedicine, and biotechnology* 44 (2016) 423-430.

**[21]** H. Jin, J. Pi, Y. Zhao, J. Jiang, T. Li, X. Zeng, P. Yang, C.E. Evans, J. Cai, EGFR-targeting PLGA-PEG nanoparticles as a curcumin delivery system for breast cancer therapy, *Nanoscale* 9 (2017) 16365-16374.

**[22]** V. Zeighamian, M. Darabi, A. Akbarzadeh, M. Rahmati-Yamchi, N. Zarghami, F. Badrzadeh, R. Salehi, F.S. Mirakabad, M. Taheri-Anganeh, PNIPAAm-MAA nanoparticles as delivery vehicles for curcumin against MCF-7 breast cancer cells, *Artificial cells, nanomedicine, and biotechnology* 44 (2016) 735-742.

**[23]** A.N. Kuskov, P.P. Kulikov, A.V. Goryachaya, M.N. Tzatzarakis, A.M. Tsatsakis, K. Velonia, M.I. Shtilman, Self-assembled

amphiphilic poly-N-vinylpyrrolidone nanoparticles as carriers for hydrophobic drugs: stability aspects, *J. Appl. Polym. Sci.* 135 (2018) 45637.

**[24]** A.N. Kuskov, P.P. Kulikov, A.V. Goryachaya, M.N. Tzatzarakis, A.O. Docea, K. Velonia, M.I. Shtilman, A.M. Tsatsakis, Amphiphilic poly-N-vinylpyrrolidone nanoparticles as carriers for non-steroidal, anti-inflammatory drugs: in vitro cytotoxicity and in vivo acute toxicity study, *Nanomedicine: nanotechnology, biology, and medicine* 13 (2017) 1021-1030.

**[25]** M.A. Raja, S. Zeenat, M. Arif, C. Liu, Self-assembled nanoparticles based on amphiphilic chitosan derivative and arginine for oral curcumin delivery, *Int. J. Nanomedicine* 11 (2016) 4397-4412.

**[26]** A.L. Luss, P.P. Kulikov, S.B. Romme, C.L. Andersen, C.P. Pennisi, A.O. Docea, A. N. Kuskov, K. Velonia, Y.O. Mezhev, M.I. Shtilman, A.M. Tsatsakis, L. Gurevich, Nanosized carriers based on amphiphilic poly-N-vinyl-2-pyrrolidone for intranuclear drug delivery, *Nanomedicine (London, England)* 13 (2018) 703-715.

**[27]** N. Sanoj Rejinold, M. Muthunarayanan, V.V. Divyarani, P.R. Sreerekha, K. P. Chennazhi, S.V. Nair, H. Tamura, R. Jayakumar, Curcumin-loaded biocompatible thermoresponsive polymeric nanoparticles for cancer drug delivery, *J. Colloid Interface Sci.* 360 (2011) 39-51.

**[28]** C. Kang, E. Jung, H. Hyeon, S. Seon, D. Lee, Acid-activatable polymeric curcumin nanoparticles as therapeutic agents for osteoarthritis, *Nanomedicine: nanotechnology, biology, and medicine* 23 (2020) 102104.

**[29]** A.K. Dewangan, Y. Perumal, N. Pavurala, K. Chopra, S. Mazumder, Preparation, characterization and anti-inflammatory effects of curcumin loaded carboxymethyl

cellulose acetate butyrate nanoparticles on adjuvant induced arthritis in rats, *Journal of Drug Delivery Science and Technology* 41 (2017) 269-279.

[30] H. Yavarpour-Bali, M. Ghasemi-Kasman, M. Pirzadeh, Curcumin-loaded nanoparticles: a novel therapeutic strategy in treatment of central nervous system disorders, *Int. J. Nanomedicine* 14 (2019) 4449-4460.

[31] P.D. Petrov, K. Yoncheva, V. Gancheva, S. Konstantinov, B. Trzebicka, Multifunctional block copolymer nanocarriers for co-delivery of silver nanoparticles and curcumin: synthesis and enhanced efficacy against tumor cells, *Eur. Polym. J.* 81 (2016) 24-33.

[32] D. Babikova, R. Kalinova, D. Momekova, I. Ugrinova, G. Momekov, I. Dimitrov, Multifunctional polymer Nanocarrier for efficient targeted cellular and subcellular anticancer drug delivery, *ACS Biomaterials Science & Engineering* 5 (2019) 2271-2283.

[33] D. Momekova, I. Ugrinova, M. Slavkova, G. Momekov, G. Grancharov, V. Gancheva, P.D. Petrov, Superior proapoptotic activity of curcumin-loaded mixed block copolymer micelles with mitochondrial targeting properties, *Biomaterials science* 6 (2018) 3309-3317.

[34] E. Rostami-Tapeh-Esmail, M. Golshan, M. Salami-Kalajahi, H. Roghani-Mamaqani, A. Kahaie-Khosrowshahi, Temperature-induced self-assembly of amphiphilic triblock terpolymers to low cytotoxic spherical and cubic structures as curcumin carriers, *J. Mol. Liq.* 313 (2020) 113504.

[35] F. Guo, D. Guo, W. Zhang, Q. Yan, Y. Yang, W. Hong, G. Yang, Preparation of curcumin-loaded PCL-PEG-PCL triblock copolymeric nanoparticles by a microchannel technology, *Eur. J. Pharm. Sci.* 99 (2017) 328-336.

[36] V. Tzankova, C. Gorinova, M. Kondeva-Burdina, R. Simeonova, S. Philipov, S.

Konstantinov, P. Petrov, D. Galabov, K. Yoncheva, Antioxidant response and biocompatibility of curcumin-loaded triblock copolymeric micelles, *Toxicol. Mech. Methods* 27 (2017) 72-80.

[37] Y. Shi, W. Ma, M. Gao, Y. Yang, Development of curcumin-loaded methoxy poly (ethylene glycol)-block-poly (caprolactone)-block-poly(1, 4, 8-Trioxa [4.6] spiro-9- undecanone) nanoparticles and studies on their in vitro anti-tumor activities, *Colloids and Surfaces B: Biointerfaces* 184 (2019) 110525.

[38] W.-X. Wu, X.-L. Yang, X. Wang, Y. Zhang, H.-M. Li, L. Lan, J. Deng, N. Wang, X.-Q. Yu, Lipase-catalyzed synthesis of pH-responsive poly( $\beta$ -thioether ester)-b-poly (ethylene glycol)-b-poly( $\beta$ -thioether ester) amphiphilic triblock copolymers for drug delivery, *Int. J. Polym. Mater. Polym. Biomater.* 68 (2019) 564-574.

[39] Q. Jiang, Natural forms of vitamin E: metabolism, antioxidant, and anti-inflammatory activities and their role in disease prevention and therapy, *Free Radic. Biol. Med.* 72 (2014) 76-90.

[40] J.A. Méndez, M.R. Aguilar, G.A. Abraham, B. Vázquez, M. Dalby, L. Di Silvio, J. San Román, New acrylic bone cements conjugated to vitamin E: curing parameters, properties, and biocompatibility, *J. Biomed. Mater. Res.* 62 (2002) 299-307.

[41] R. Palao-Suay, M.R. Aguilar, F.J. Parra-Ruiz, S. Maji, R. Hoogenboom, N.A. Rohner, S.N. Thomas, J. San Román,  $\alpha$ -TOS-based RAFT block copolymers and their NPs for the treatment of cancer, *Polym. Chem.* 7 (2016) 838-850.

[42] R. Palao-Suay, M.R. Aguilar, F.J. Parra-Ruiz, S. Martín-Saldaña, N.A. Rohner, S. N. Thomas, J. San Román, Multifunctional Decoration of Alpha-Tocopheryl Succinate-Based NP for Cancer Treatment: Effect of TPP

and LTVSPWY Peptide, *Journal of Materials Science: Materials in Medicine*, 28, 2017.

[43] R. Palao-Suay, F.M. Martín-Saavedra, M. Rosa Aguilar, C. Escudero-Duch, S. Martín-Saldaña, F.J. Parra-Ruiz, N.A. Rohner, S.N. Thomas, N. Vilaboa, J. San Román, Photothermal and photodynamic activity of polymeric nanoparticles based on  $\alpha$ -tocopheryl succinate-RAFT block copolymers conjugated to IR-780, *Acta Biomater.* 57 (2017) 70-84.

[44] R. Palao-Suay, M.R. Aguilar, F.J. Parra-Ruiz, M. Fernandez-Gutierrez, J. Parra, C. Sanchez-Rodriguez, R. Sanz-Fernandez, L. Rodriganez, J.S. Roman, Anticancer and antiangiogenic activity of surfactant-free nanoparticles based on self-assembled polymeric derivatives of vitamin E: structure-activity relationship, *Biomacromolecules* 16 (2015) 1566-1581.

[45] S. Martín-Saldana, R. Palao-Suay, A. Trinidad, M.R. Aguilar, R. Ramirez-Camacho, J. San Roman, Otoprotective properties of 6 $\alpha$ -methylprednisolone-loaded nanoparticles against cisplatin: in vitro and in vivo correlation, *Nanomedicine: nanotechnology, biology, and medicine* 12 (2016) 965-976.

[46] S. Martín-Saldaña, R. Palao-Suay, M.R. Aguilar, L. García-Fernández, H. Arévalo, A. Trinidad, R. Ramírez-Camacho, J. San Román, pH-sensitive polymeric nanoparticles with antioxidant and anti-inflammatory properties against cisplatin-induced hearing loss, *J. Control. Release* 270 (2018) 53-64.

[47] S. Martín-Saldaña, R. Palao-Suay, M.R. Aguilar, R. Ramírez-Camacho, J. San Román, Polymeric nanoparticles loaded with dexamethasone or  $\alpha$ -tocopheryl succinate to prevent cisplatin-induced ototoxicity, *Acta Biomater.* 53 (2017) 199-210.

[48] B. Vázquez, C. Ortiz, J.S. Roman, M.A. Plasencia, A. Lopez-Bravo, Hydrophilic

polymers derived from vitamin E, *J. Biomater. Appl.* 14 (2000) 367-388.

[49] P. Foroozandeh, A.A. Aziz, Insight into cellular uptake and intracellular trafficking of nanoparticles, *Nanoscale Res. Lett.* 13 (2018) 339.

[50] N.D. Donahue, H. Acar, S. Wilhelm, Concepts of nanoparticle cellular uptake, intracellular trafficking, and kinetics in nanomedicine, *Adv. Drug Deliv. Rev.* 143 (2019) 68-96.

[51] A. Panariti, G. Miserocchi, I. Rivolta, The effect of nanoparticle uptake on cellular behavior: disrupting or enabling functions? *Nanotechnol. Sci. Appl.* 5 (2012) 87-100.

[52] X.J. Du, J.L. Wang, S. Iqbal, H.J. Li, Z.T. Cao, Y.C. Wang, J.Z. Du, J. Wang, The effect of surface charge on oral absorption of polymeric nanoparticles, *Biomaterials science* 6 (2018) 642-650.

[53] S. Jeon, J. Clavadetscher, D.K. Lee, S.V. Chankeshwara, M. Bradley, W.S. Cho, Surface Charge-Dependent Cellular Uptake of Polystyrene Nanoparticles, *Nanomaterials*, 8, 2018.

[54] S. Yang, L. Dai, C. Sun, Y. Gao, Characterization of curcumin loaded gliadin-lecithin composite nanoparticles fabricated by antisolvent precipitation in different blending sequences, *Food Hydrocoll.* 85 (2018) 185-194.

[55] B. Lu, X. Lv, Y. Le, Chitosan-modified PLGA Nanoparticles for Control-released Drug Delivery, *Polymers*, 11, 2019.

[56] M.A. Vakilinezhad, A. Amini, T. Dara, S. Alipour, Methotrexate and Curcumin co-encapsulated PLGA nanoparticles as a potential breast cancer therapeutic system: In vitro and in vivo evaluation, *Colloids and surfaces. B, Biointerfaces* 184 (2019) 110515.



- [57] L. Milkovic, A. Cipak Gasparovic, M. Cindric, P.A. Mouthuy, N. Zarkovic, Short Overview of ROS as Cell Function Regulators and Their Implications in Therapy Concepts, *Cells*, 8, 2019.
- [58] C. Schneider, O.N. Gordon, R.L. Edwards, P.B. Luis, Degradation of Curcumin: from mechanism to biological implications, *J. Agric. Food Chem.* 63 (2015) 7606-7614.
- [59] M.S. Zafar, A. Quarta, M. Marradi, A. Ragusa, Recent Developments in the Reduction of Oxidative Stress through Antioxidant Polymeric Formulations, *Pharmaceutics*, 11, 2019.
- [60] E. Niki, Role of vitamin E as a lipid-soluble peroxyl radical scavenger: in vitro and in vivo evidence, *Free Radic. Biol. Med.* 66 (2014) 3-12.
- [61] T. Ak, I. Gulcin, Antioxidant and radical scavenging properties of curcumin, *Chem. Biol. Interact.* 174 (2008) 27-37.
- [62] P. Ben, J. Liu, C. Lu, Y. Xu, Y. Xin, J. Fu, H. Huang, Z. Zhang, Y. Gao, L. Luo, Z. Yin, Curcumin promotes degradation of inducible nitric oxide synthase and suppresses its enzyme activity in RAW264.7 cells, *Int. Immunopharmacol.* 11 (2011) 179-186.
- [63] E. Blanco-Garcia, F.J. Otero-Espinar, J. Blanco-Mendez, J.M. Leiro-Vidal, A. Luzardo-Alvarez, Development and characterization of anti-inflammatory activity of curcumin-loaded biodegradable microspheres with potential use in intestinal inflammatory disorders, *Int. J. Pharm.* 518 (2017) 86-104.
- [64] J. Wang, R. Zhu, D. Sun, X. Sun, Z. Geng, H. Liu, S.L. Wang, Intracellular uptake of curcumin-loaded solid lipid nanoparticles exhibit anti-inflammatory activities superior to those of curcumin through the NF-kappaB signaling pathway, *J. Biomed. Nanotechnol.* 11 (2015) 403-415.
- [65] H. Zhou, C.S. Beevers, S. Huang, The targets of curcumin, *Curr. Drug Targets* 12 (2011) 332-347.
- [66] S. Hasanzadeh, M.I. Read, A.R. Bland, M. Majeed, T. Jamialahmadi, A. Sahebkar, Curcumin: an inflammasome silencer, *Pharmacol. Res.* 159 (2020) 104921.
- [67] M.S. Karimian, M. Pirro, M. Majeed, A. Sahebkar, Curcumin as a natural regulator of monocyte chemoattractant protein-1, *Cytokine Growth Factor Rev.* 33 (2017) 55-63.
- [68] Y. Henrotin, A.L. Clutterbuck, D. Allaway, E.M. Lodwig, P. Harris, M. Mathy-Hartert, M. Shakibaei, A. Mobasheri, Biological actions of curcumin on articular chondrocytes, *Osteoarthr. Cartil.* 18 (2010) 141-149.
- [69] F.N. Sorasitthyanukarn, C. Muangnoi, W. Thaweeseest, P. Rojsitthisak, P. Rojsitthisak, Enhanced cytotoxic, antioxidant and anti-inflammatory activities of curcumin diethyl disuccinate using chitosan-tripolyphosphate nanoparticles, *Journal of Drug Delivery Science and Technology* 53 (2019) 101118.
- [70] B. Crivelli, E. Bari, S. Perteghella, L. Catenacci, M. Sorrenti, M. Mocchi, S. Farag`o, G. Tripodo, A. Prina-Mello, M.L. Torre, Silk fibroin nanoparticles for celecoxib and curcumin delivery: ROS-scavenging and anti-inflammatory activities in an in vitro model of osteoarthritis, *Eur. J. Pharm. Biopharm.* 137 (2019) 37-45.
- [71] P. Krupa, B. Svobodova, J. Dubisova, S. Kubinova, P. Jendelova, L. Machova Urdzikova, Nano-formulated curcumin (Lipodisq™) modulates the local inflammatory response, reduces glial scar and preserves the white matter after spinal cord injury in rats, *Neuropharmacology* 155 (2019) 54-64.
- [72] L. Jin, D.P. Raymond, T.D. Crabtree, S.J. Pelletier, C.W. Houlgrave, T.L. Pruett, R. G. Sawyer, Enhanced murine macrophage TNF

receptor shedding by cytosine-guanine sequences in oligodeoxynucleotides, *J. Immunol.* 165 (2000) 5153-5160.

**[73]** S. Behzadi, V. Serpooshan, W. Tao, M.A. Hamaly, M.Y. Alkawareek, E.C. Dreaden, D. Brown, A.M. Alkilany, O.C. Farokhzad, M. Mahmoudi, Cellular uptake of nanoparticles: journey inside the cell, *Chem. Soc. Rev.* 46 (2017) 4218-4244.

**[74]** K. Shahani, S.K. Swaminathan, D. Freeman, A. Blum, L. Ma, J. Panyam, Injectable sustained release microparticles of curcumin: a new concept for cancer chemoprevention, *Cancer Res.* 70 (2010) 4443-4452.

**[75]** Z. Zheng, Y. Sun, Z. Liu, M. Zhang, C. Li, H. Cai, The effect of curcumin and its nanoformulation on adjuvant-induced arthritis in rats, *Drug design, development and therapy* 9 (2015) 4931-4942.

**[76]** Z. Song, Y. Lu, X. Zhang, H. Wang, J. Han, C. Dong, Novel curcumin-loaded human serum albumin nanoparticles surface functionalized with folate: characterization

and in vitro/vivo evaluation, *Drug design, development and therapy* 10 (2016) 2643-2649.

**[77]** L.M.G. Zambrano, D.A. Brandao, F.R.G. Rocha, R.P. Marsiglio, I.B. Longo, F. L. Primo, A.C. Tedesco, M.R. Guimaraes-Stabili, C. Rossa Junior, Local administration of curcumin-loaded nanoparticles effectively inhibits inflammation and bone resorption associated with experimental periodontal disease, *Sci. Rep.* 8 (2018) 6652.

**[78]** M. Alibolandi, M. Mohammadi, S.M. Taghdisi, K. Abnous, M. Ramezani, Synthesis and preparation of biodegradable hybrid dextran hydrogel incorporated with biodegradable curcumin nanomicelles for full thickness wound healing, *Int. J. Pharm.* 532 (2017) 466-477.

**[79]** A. Hezi-Yamit, C. Sullivan, J. Wong, L. David, M. Chen, P. Cheng, D. Shumaker, J. N. Wilcox, K. Udiipi, Impact of polymer hydrophilicity on biocompatibility: implication for DES polymer design, *J. Biomed. Mater. Res. A* 90 (2009) 133-141.

# Supplementary material

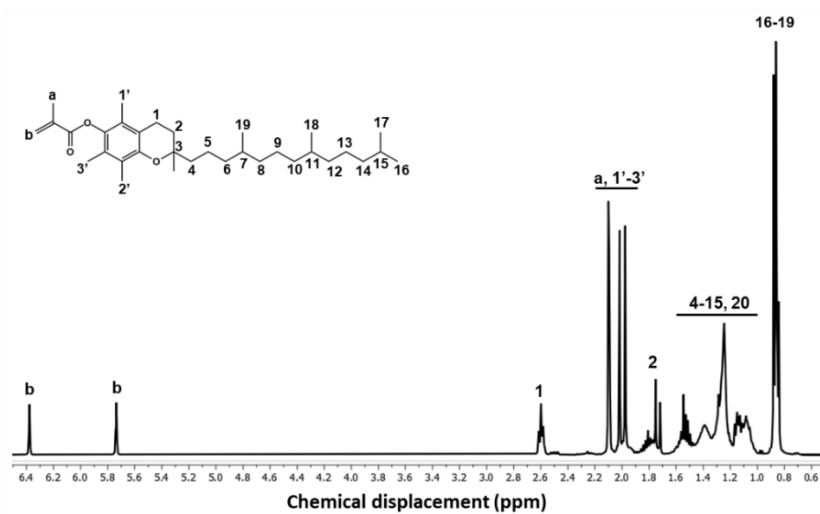


Figure S1.  $^1\text{H}$  NMR spectrum (400 MHz) of the monomer MVE in  $\text{CDCl}_3$ .

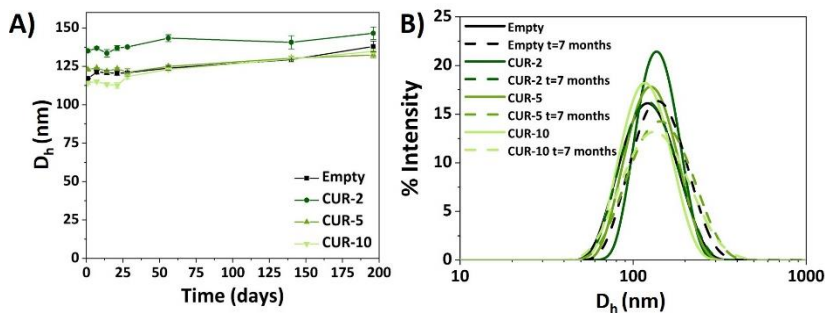


Figure S2. A) Hydrodynamic diameter changes with time of Empty, CUR-2, CUR-5 and CUR-10 NPs. B) NP size distributions immediately after synthesis and after being stored at 4 °C under static conditions during 7 months.

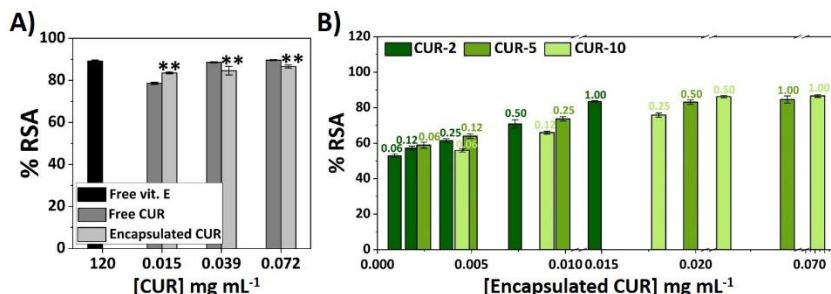


Figure S3. A) Comparison of RSA (%) values of free and encapsulated CUR in CUR-2, CUR-5 and CUR-10 NPs at 1.00 mg mL<sup>-1</sup> after 10 minutes of DPPH reaction. ANOVA was performed between free and encapsulated CUR in each system (\**p* < 0.05, \*\**p* < 0.005, \*\*\**p* < 0.001). B) RSA (%) of CUR-2, CUR-5 and CUR-10 NPs after 10 minutes of DPPH reaction against the encapsulated CUR concentration. Values represent mean ± SD. Numbers on the top of the columns represent the NP concentration (mg mL<sup>-1</sup>).

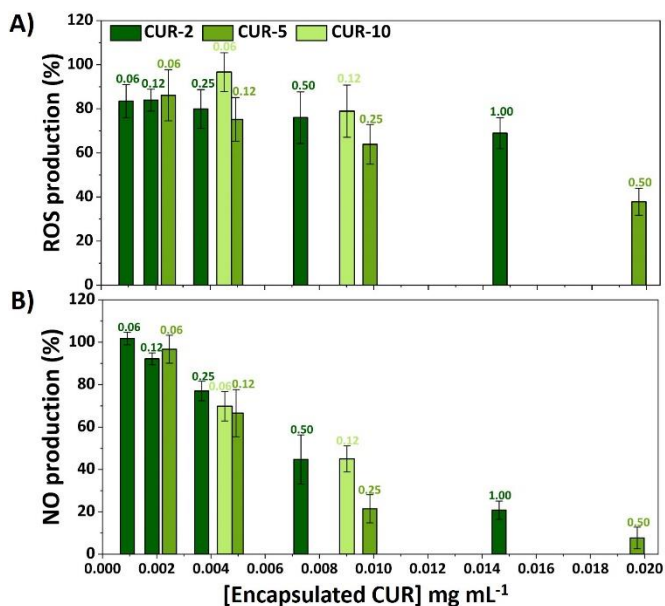


Figure S4. A) ROS and B) NO production by RAW264.7 (% with respect to CNT H<sub>2</sub>O<sub>2</sub> and LPS+, respectively) against the encapsulated CUR concentration. Numbers on the top of the columns represent the NP concentration (mg mL<sup>-1</sup>).

**Table S1. Inflammatory factors studied in the human and mouse inflammation antibody arrays**

<b>Human inflammation antibody array</b>	<b>Mouse inflammation antibody array</b>
Eotaxin, Eotaxin-2, GCSF, GM-CSF, ICAM-1, IFN-gamma, I-309, IL-1alpha, IL-1beta, IL-2, IL-3, IL-4, IL-6, IL-6sR, IL-7, IL-8, IL-10, IL-11, IL-12p40, IL-12p70, IL-13, IL-15, IL-16, IL-17, IP-10, MCP-1, MCP-2, M-CSF, MIG, MIP-1alpha, MIP-1beta, MIP-1delta, RANTES, TGF-beta1, TNF-alpha, TNF-beta, sTNF RI, sTNF-RII, PDGF-BB, TIMP-2	BLC, CD30L, Eotaxin, Eotaxin-2, Fas Ligand, Fractalkine, GCSF, GM-CSF, IFN-gamma, IL-1alpha, IL-1beta, IL-2, IL-3, IL-4, IL-6, IL-9, IL-10, IL-12 p40/p70, IL-12 p70, IL-13, IL-17, I-TAC, KC/CXCL1, Leptin/OB, LIX, Lymphotoctin, MCP-1, MCSF, MIG, MIP-1 alpha, MIP-1 gamma, RANTES, SDF-1, TCA-3, TECK, TIMP-1, TIMP-2, TNF-alpha, sTNF RI, sTNF-RII

**Table S2. Physicochemical characterization of CUR-loaded poly(MVE-co-VP) NPs.**

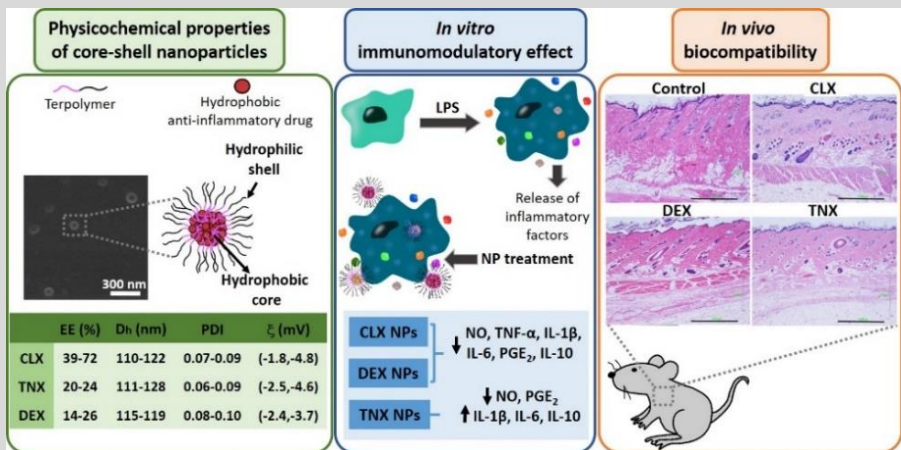
<b>NPs</b>	<b>% Drug (w/w)</b>	<b>D<sub>h</sub> (nm)</b>	<b>PDI</b>	<b>ξ (mV)</b>	<b>EE (%)</b>
<b>Empty</b>	<b>0</b>	173.3 ± 5.3	0.07 ± 0.02	-5.54 ± 0.66	0
<b>CUR-2 (COP)</b>	<b>2</b>	167.9 ± 3.4	0.08 ± 0.01	-4.51 ± 0.55	68 ± 2
<b>CUR-5 (COP)</b>	<b>5</b>	173.4 ± 2.5	0.05 ± 0.03	-5.32 ± 0.25	74 ± 2
<b>CUR-10 (COP)</b>	<b>10</b>	176.0 ± 7.6	0.06 ± 0.04	-5.37 ± 0.93	66 ± 6

D<sub>h</sub>, hydrodynamic diameter; PDI, polydispersity index; ξ, zeta potential; EE, encapsulation efficiency.



# Chapter IV. Modulation of inflammatory mediators by polymeric nanoparticles loaded with anti-inflammatory drugs

Gloria María Pontes-Quero, Lorena Benito-Garzón, Juan Pérez Cano, María Rosa Aguilar, Blanca Vázquez-Lasa



*Pharmaceutics 2021, 13, 290*





## Chapter IV. Modulation of inflammatory mediators by polymeric nanoparticles loaded with anti-inflammatory drugs

---

**Abstract:** The first-line treatment of osteoarthritis is based on anti-inflammatory drugs, the most currently used being nonsteroidal anti-inflammatory drugs, selective cyclooxygenase 2 (COX-2) inhibitors and corticoids. Most of them present cytotoxicity and low bioavailability in physiological conditions, making necessary the administration of high drug concentrations causing several side effects. The goal of this work was to encapsulate three hydrophobic anti-inflammatory drugs of different natures (celecoxib, tenoxicam and dexamethasone) into core-shell terpolymer nanoparticles with potential applications in osteoarthritis. Nanoparticles presented hydrodynamic diameters between 110 and 130 nm and almost neutral surface charges (between  $-1$  and  $-5$  mV). Encapsulation efficiencies were highly dependent on the loaded drug and its water solubility, having higher values for celecoxib (39-72%) followed by tenoxicam (20-24%) and dexamethasone (14-26%). Nanoencapsulation reduced celecoxib and dexamethasone cytotoxicity in human articular chondrocytes and murine RAW264.7 macrophages. Moreover, the three loaded systems did not show cytotoxic effects in a wide range of concentrations. Celecoxib and dexamethasone-loaded nanoparticles reduced the release of different inflammatory mediators (NO, TNF- $\alpha$ , IL-1 $\beta$ , IL-6, PGE $_2$  and IL-10) by lipopolysaccharide (LPS) stimulated RAW264.7. Tenoxicam-loaded nanoparticles reduced NO and PGE $_2$  production, although an overexpression of IL-1 $\beta$ , IL-6 and IL-10 was observed. Finally, all nanoparticles proved to be biocompatible in a subcutaneous injection model in rats. These findings suggest that these loaded nanoparticles could be suitable candidates for the treatment of inflammatory processes associated to osteoarthritis due to their

demonstrated *in vitro* activity as regulators of inflammatory mediator production.

**Keywords:** celecoxib, tenoxicam, dexamethasone, osteoarthritis, inflammatory mediators, nanoparticles

## 1. Introduction

Osteoarthritis (OA) is the most prevalent joint condition causing pain and physical disability in affected patients. It is characterized by the inflammation of the synovial joint, the progressive degradation of cartilage and alterations in the subchondral bone [1]. Cartilage degradation is the hallmark of OA, and the lack of intrinsic cartilage healing capacity makes the progression of OA an irreversible process. The inflammatory response is also crucial for the initiation and development of OA [2]. In response to a sustained inflammatory activation, chondrocytes and immune cells, such as macrophages, trigger the release of pro-inflammatory mediators like interleukin-1 $\beta$  (IL-1 $\beta$ ), IL-6, IL-8, tumor necrosis factor- $\alpha$  (TNF- $\alpha$ ), reactive oxygen species (ROS) and nitric oxide (NO) [3–6]. These inflammatory molecules increase the production of proteolytic enzymes (matrix metalloproteinases (MMP), A disintegrin and metalloproteinase with thrombospondin motifs, ADAMTS), leading to the degradation of collagen and aggrecan cartilage components [7]. In turn, degraded cartilage fragments further stimulate inflammation, generating a damaging cycle that promotes OA progression. These inflammatory mediators are, therefore, key targets for therapeutic strategies in the treatment of OA [8].

The initial treatment of OA patients with mild to moderate symptoms is based on oral, topical or intra-articularly administered anti-inflammatory drugs, including nonsteroidal anti-inflammatory drugs (NSAIDs), selective cyclooxygenase 2 (COX-2) inhibitors (coxibs) and glucocorticoids [9]. NSAIDs, which are the most prescribed drugs worldwide, owe their potent analgesic and anti-inflammatory effects to the unspecific inhibition of COX enzymes, which take part in the biosynthesis of both physiological and inflammatory prostaglandins [10]. On the other hand, coxibs specifically inhibit the COX-2 enzyme, which synthesizes prostaglandins related to inflammation, pain and

fever. Beside this COX-dependent anti-inflammatory pathway, NSAIDs may exert their effect through their interaction with transcription factors, such as nuclear factor kappa B (NF- $\kappa$ B) or the activator protein 1 (AP-1), both regulators of the expression of various pro-inflammatory genes [11]. In the case of glucocorticoids, they predominantly exert their anti-inflammatory effect by switching off multiple inflammatory genes encoding inflammatory mediators such as cytokines, chemokines, adhesion molecules, inflammatory enzymes, receptors and proteins, that have been activated during a chronic inflammatory process [12]. Celecoxib (CLX, a selective COX-2 inhibitor), tenoxicam (TNX, a traditional NSAID) and dexamethasone (DEX, a glucocorticoid) are some of the most frequently used anti-inflammatory drugs for the treatment of OA in the clinic.

CLX was the first COX-2 inhibitor approved by the FDA (U.S Food and Drug Administration) for the treatment of OA and rheumatoid arthritis, due to its good selectivity for the COX-2 enzyme and for its gastrointestinal tolerability [13]. TNX is used for postoperative analgesia because of its prolonged half-life and potent immediate effect [14]. Finally, DEX is a long-lasting glucocorticoid widely used for the treatment of multiple inflammatory-related diseases such as OA, since it is one of the most potent glucocorticoids available [15]. Although these drugs exert their anti-inflammatory activity at different levels of the inflammatory cascade, all of them share notable cytotoxicity and poor water solubility that limit their physiological bioavailability [16]. To overcome these limitations, the use of tailored nanocarriers for their encapsulation has gained great attention in recent years [17]. Particularly, polymer-based nanoparticles (NPs) are promising anti-inflammatory delivery systems to control drug release, prolong drug stability, reduce drug toxicity and increase drug bioavailability; and have been the object of numerous investigations [18].

In this sense, some advances on the encapsulation of anti-inflammatory drugs into polymeric nanovehicles have been made for OA therapy. In particular, considerable work trying to combine DEX with nanotechnology has been developed, since DEX possesses powerful anti-inflammatory activity, even at low doses [19]. It has been recently encapsulated alone [20–22], or in combination with other factors, such as

other anti-inflammatory molecules like ketoprofen [23] or small interfering RNA [24], and covalently conjugated, for example, with the avidin protein [25] with positive effects both *in vitro* and *in vivo*. In the case of CLX, CLX poly(1-vinyl-2-pyrrolidone) solid dispersion NPs [26], or CLX-loaded hyaluronan NPs [27], were prepared to improve this drug bioavailability. In other work, CLX-loaded silk fibroin NPs showed anti-inflammatory and antioxidant activities by the *in vitro* reduction of NO, IL-6 and RANTES [28]. On the other hand, to the best of our knowledge, scarce literature on TNX-loaded polymeric NPs can be found for the treatment of arthritic diseases. Injectable formulations like *in situ* forming microparticles, showed promising results as TNX delivery vehicles in terms of anti-inflammatory and antioxidant activity for rheumatoid arthritis [29]. Moreover, TNX has been encapsulated into delivery systems such as microemulsion-based formulations [30], proniosomes [31] and ultradeformable vesicles based on surfactant molecules [32], for transdermal and topical applications.

In this context, we hypothesized that the use of biocompatible amphiphilic core-shell NPs, which are able to entrap into their hydrophobic core anti-inflammatory drugs, could provide a nanocarrier platform to act *in situ* as immunomodulatory therapeutic systems of OA by regulating the cellular release of inflammatory factors. Antecedents of this type of nanocarrier by the authors have given promising results for their application in cancer, sensorineural hearing loss, inflammatory and oxidative stress related pathologies [33–39]. Thus, the aim of this work was the nanoencapsulation of three types of anti-inflammatory drugs (CLX, TNX and DEX) into core-shell terpolymer NPs consisting of vitamin E methacrylate, 1-vinyl-2-pyrrolidone and *N*-vinylcaprolactam (poly(MVE-*co*-VP-*co*-VC)), and the study of their physicochemical parameters and the cellular release of osteoarthritic inflammatory mediators. These nanoparticulated systems are proposed to be intra-articularly injected for the treatment of mild to moderate OA. Physicochemical characterization of the loaded NPs was performed in terms of morphological evaluation, size distribution, zeta potential and encapsulation efficiency. Stability of the NPs in the long term was followed up to seven months in static conditions. The *in vitro* cytotoxicity of the NPs was studied on human articular chondrocytes and murine RAW264.7 macrophages, while the

anti-inflammatory potential was characterized in terms of modulation of the release of osteoarthritic inflammatory mediators (NO, TNF- $\alpha$ , IL-1 $\beta$ , IL-6, PGE<sub>2</sub> and IL-10) by LPS-stimulated RAW264.7. Eventually, the *in vivo* biocompatibility was assessed by subcutaneously injecting the NPs in a rat model, followed by a histological evaluation.

## 2. Experimental section

### 2.1. Chemicals

$\alpha$ -tocopherol (Sigma-Aldrich), methacryloyl chloride (Sigma-Aldrich), triethylamine (Scharlau), tetrabutylammonium iodide (Sigma-Aldrich), dichloromethane (Sigma-Aldrich), hexane (Sigma-Aldrich), hydrochloric acid (VWR), sodium hydroxide (Sigma-Aldrich), 1,4-dioxane (Panreac), anhydrous dioxane (Sigma-Aldrich), *N*-vinylcaprolactam (VC, Sigma-Aldrich), 1-vinyl-2-pyrrolidone (VP, Sigma-Aldrich) and 2,2'-azobisisobutyronitrile (AIBN, Sigma-Aldrich) were used for the preparation of a terpolymer (poly(MVE-*co*-VP-*co*-VC)), as described in a previous work [40].

Celecoxib (CLX, Sigma-Aldrich), dexamethasone (DEX, Sigma-Aldrich), tenoxicam (TNX, Alfa Aesar) and ethanol (VWR) were used as received for the synthesis of the NPs. Sodium chloride (NaCl, Sigma-Aldrich) and sodium phosphate dibasic (Na<sub>2</sub>HPO<sub>4</sub>, Sigma-Aldrich) were used for the preparation of a phosphate buffered saline (PBS) solution in which NPs were synthesized and diluted.

### 2.2. Preparation and physicochemical characterization of NPs

NPs were prepared by the nanoprecipitation method [40]. Different initial drug concentrations (2-20% w/w with respect to the terpolymer) were used in order to optimize the NPs in terms of physicochemical and biological properties. Briefly, the terpolymer (50 mg mL<sup>-1</sup>) and the corresponding drug at different % w/w (5, 10, 20 for CLX; 2, 5, 10 for TNX; and 10, 15, 20 for DEX) were dissolved in dioxane and added dropwise over PBS under constant stirring.

Unloaded NPs were prepared using the same methodology as a blank for the encapsulation efficiency studies. NP suspensions were obtained at a final concentration of  $2 \text{ mg mL}^{-1}$  and were named according to the initial drug content (CLX-5, CLX-10, CLX-20, TNX-2, TNX-5, TNX-10, DEX-10, DEX-15, DEX-20). Suspensions were purified by dialysis against PBS for 72 h to eliminate the dioxane and the non-encapsulated drug, and finally stored at  $4^\circ\text{C}$ . Physicochemical and biological characterization of unloaded NPs was not studied because it was assessed in a previous work [40].

NP mean hydrodynamic diameter ( $D_h$ ), size distribution and polydispersity index (PDI) were determined by Dynamic Light Scattering (DLS) while zeta potential ( $\xi$ ) was measured by Laser Doppler Electrophoresis (LDE) using a Zetasizer Nano ZS (Malvern Instruments) at  $25^\circ\text{C}$ . Experiments were performed using a NP concentration of  $0.50 \text{ mg mL}^{-1}$ . NP stability was investigated by assessing the  $D_h$  and the size distribution of the NPs when stored under static conditions for seven months at  $4^\circ\text{C}$  at different time points. Experiments were performed in triplicate and results were expressed as mean value  $\pm$  SD. Drug encapsulation efficiency (EE) was studied by ultraviolet (UV) spectroscopy. First, NP suspensions were freeze-dried and dissolved in ethanol for 24 h. Samples were then centrifuged at 10,000 rpm and supernatants containing the drugs were analyzed at the UV absorption maxima of the corresponding drug (*i.e.*, 255, 355 and 238 nm for CLX, TNX and DEX, respectively) with a Nanodrop OneC Microvolume UVVis Spectrophotometer (Thermo Scientific<sup>TM</sup>). Unloaded NPs were used as a blank, whose absorbance value was subtracted to the one of loaded NPs. EE (%) was then calculated as (experimental drug/initial drug)  $\times$  100 being the experimentally detected and the initial drug concentrations, respectively. Experiments were performed in triplicate for each formulation and expressed as mean value  $\pm$  SD. Scanning electron microscopy (SEM) was used for the morphological characterization of the NPs at a NP concentration of  $0.04 \text{ mg mL}^{-1}$  using a Hitachi SU8000 TED, cold-emission field emission SEM microscope working at an accelerating voltage 30 kV.

## 2.3. Cell cultures and biological products

High glucose Dulbecco's Modified Eagle's Medium (DMEM, D6546, Sigma-Aldrich); high glucose, HEPES, no phenol red DMEM (Gibco, 2106329), AlamarBlue® (Invitrogen), Trypsin-EDTA solution (Sigma-Aldrich), Trypan Blue (Sigma-Aldrich), Dulbecco's Phosphate Buffered Saline (PBS), Griess reagent (Sigma-Aldrich) and lipopolysaccharide from *Escherichia coli* (LPS, Sigma-Aldrich) were used for the cellular assays.

NP toxicity was assessed using human articular chondrocytes (HC-a, Innoprot, P10970) and a murine macrophage cell line (RAW264.7, Sigma-Aldrich). RAW264.7 was also used for the NO quantification, the mouse inflammation antibody array and TNF- $\alpha$ , IL-1 $\beta$ , IL-6, PGE<sub>2</sub> and IL-10 ELISA kits. HC-a were grown and maintained using a chondrocyte medium kit (Innoprot) while RAW264.7 were grown and maintained in high glucose DMEM supplemented with 10% Fetal Bovine Serum (FBS, Gibco), 2% L-glutamine (Sigma-Aldrich) and 1% penicillin/streptomycin (Sigma-Aldrich), both at 37 °C in a humidified atmosphere of 5% CO<sub>2</sub>. When reaching 80% confluence, HC-a were detached with trypsin-EDTA and RAW264.7 by scraping. NP suspensions were sterilized by filtering through 0.22  $\mu$ m polyethersulfone membranes (Millex-GP PES Millipore Express, Sigma-Aldrich) and diluted with PBS to obtain different NP concentrations (0.06, 0.12, 0.25, 0.50, 1.00 mg mL<sup>-1</sup>).

## 2.4. NP cytotoxicity

NP toxicity was investigated on HC-a at different periods of time (24 and 48 h, 7 and 14 days).  $2 \times 10^4$  cells/well were seeded into 24-well culture plates and incubated for 24 h. The culture medium was then replaced with fresh one and with the NPs (1:1). After each time (24 and 48 h, 7 and 14 days) NPs were removed, cells were washed with PBS, treated with a 10% AlamarBlue® solution in phenol red-free DMEM and incubated for 3 h. After this time, fluorescence was quantified at an excitation/emission of 590/530 nm using a fluorescence microplate reader (Biotek Synergy HT spectrophotometer, BioTek Instruments, Winooski, VT, US). For 48 h, 7 and 14 day assays, NPs and culture medium were replaced each two days. For each time, cells treated with

PBS were used as control (CNT). Experiments were performed using eight replicates per formulation and results were expressed as mean  $\pm$  SD. ANOVA was performed at a significance level of  $p < 0.05$ . Cytotoxicity of free drugs on HC-a was also investigated after 24 h and compared to nanoencapsulated drugs in the different NP systems at the different NP concentrations. Due to the low solubility of these drugs in aqueous media, a mother solution of each drug was prepared in DMSO. Serial dilutions were prepared using HC-a culture medium, maintaining the final DMSO concentration lower than 1 %v/v in the cell culture experiments. Cells were seeded at  $2 \times 10^4$  cells/well into 24-well culture plates and incubated for 24 h. The medium was then replaced by the serial drug solutions and incubated for additional 24 h. Then, the medium was removed, cells were washed with PBS and treated with a 10% AlamarBlue® solution. After 3 h of incubation, fluorescence was monitored. Cells treated with the HC-a culture medium were used as the 100% viability control. Eight replicates were used for each sample.

The cytotoxicity of the NPs was also studied in RAW264.7 after 24 h. In this case, cells were seeded at  $2 \times 10^4$  cells/well into 96-well culture plates and incubated for 24 h. The medium was then replaced with a fresh one and with the NPs (1:1) for 24 h. Finally, the same AlamarBlue® protocol used for HC-a was followed. Cells treated with PBS were used as control (CNT). Experiments were performed using eight replicates per formulation and results were expressed as mean  $\pm$  SD. ANOVA was performed at a significance level of  $p < 0.05$ .

Cytotoxicity of free drugs on RAW264.7 was also investigated after 24 h. A mother solution of each drug was prepared in DMSO and serial dilutions were prepared with RAW264.7 culture medium. Cells were seeded at  $2 \times 10^4$  cells/well into 96-well culture plates and incubated for 24 h. The medium was replaced by the serial drug solutions and incubated for an additional 24 h. Then, the medium was removed, cells were washed with PBS and treated with a 10% AlamarBlue® solution. After 3 h of incubation, fluorescence was monitored. Cell viability of RAW264.7 treated with culture medium was taken as 100%. Eight replicates were used for each sample. ANOVA was performed at a significance level of  $p < 0.05$ .



## 2.5. Quantification of NO cellular release

NO quantification in LPS-stimulated RAW264.7 was used as an *in vitro* inflammation model. RAW264.7 were cultured in 96-well culture plates at  $2 \times 10^4$  cells/well and incubated for 24 h, then, the medium was replaced by fresh one containing LPS ( $1 \mu\text{g mL}^{-1}$ ) and the NP suspensions (1:1). After 24 h, supernatants were collected, and NO was quantified using the Griess method by reacting the extracts with the Griess solution (1:1). After 15 min of reaction, absorbance was detected using a microplate reader at 540 nm. The concentration of NO was obtained using a sodium nitrite serial dilution curve. After the collection of the extracts, an AlamarBlue® assay was performed to the cells following the protocol described in 2.4 for data normalization. LPS-stimulated cells treated with PBS were used as control (LPS+). NO basal levels of unstimulated cells were also studied (LPS-). Experiments were performed using eight replicates per formulation and results were expressed as mean  $\pm$  SD. ANOVA was performed at significance levels of  $p < 0.05$ ,  $p < 0.005$  and  $p < 0.001$ .

## 2.6. Semi-quantitative inflammation antibody array

A mouse inflammation antibody array (ab133999, abcam, Spain) with 40 inflammatory targets was used to semi-quantitatively study the anti-inflammatory effect of the NPs. RAW264.7 were stimulated with LPS ( $500 \text{ ng mL}^{-1}$ ) in culture medium without FBS to simulate inflammatory conditions. Five membranes were used for this experiment: a control membrane (CNT) was exposed to RAW264.7 culture medium without FBS; an inflammatory membrane (LPS) was exposed to supernatants of LPS-stimulated cells exposed to PBS and three membranes were exposed to the cellular supernatants of LPS-stimulated cells treated with the corresponding NPs at  $0.50 \text{ mg mL}^{-1}$  (CLX-10, TNX-5 or DEX-15). RAW264.7 were seeded at  $3 \times 10^5$  cells/well into 6-well plates. After 24 h of incubation, the culture medium was replaced with 1 mL of NPs and 1 mL of fresh culture medium without FBS containing LPS ( $500 \text{ ng mL}^{-1}$ ). For the LPS membrane, the medium was replaced with 1 mL of culture medium without FBS containing LPS ( $500 \text{ ng mL}^{-1}$ ) and 1 mL of PBS. Finally, supernatants were taken after 24 h of exposure to NPs and stored at  $-20^\circ\text{C}$ .

until use. Membrane chemiluminescence was detected and quantified using a ChemiDoc™ XRS. Two replicates for each inflammatory mediator were studied per membrane. Results are expressed as mean  $\pm$  SD and values are relative to the Positive control of each membrane, which is given an arbitrary value of 1. ANOVA was performed at significance levels of  $p < 0.05$ ,  $p < 0.005$  and  $p < 0.001$ .

## **2.7. Quantification of TNF- $\alpha$ , IL-1 $\beta$ , IL-6, PGE<sub>2</sub> and IL-10 cellular release**

NP effect on the release of five inflammatory mediators in LPS+ RAW264.7 was further quantified using mouse TNF- $\alpha$ , IL-1 $\beta$  and IL-10 ELISA kits purchased from Sigma-Aldrich (RAB0477, RAB0274 and RAB0245); and mouse IL-6 and PGE<sub>2</sub> ELISA kits purchased from abcam (ab222503 and ab133021). In brief, cells were seeded into 6-well culture plates at a density of  $3 \times 10^5$  cells/well and cultured for 24 h, then, cells were activated with LPS in RAW264.7 culture medium ( $1 \mu\text{g mL}^{-1}$  for IL-1 $\beta$  quantification and  $500 \text{ ng mL}^{-1}$  for TNF- $\alpha$ , IL-6, PGE<sub>2</sub> and IL-10) and exposed simultaneously to NPs (CLX-10, TNX-5 and DEX-15 at  $0.50 \text{ mg mL}^{-1}$ ). Following a 24 h incubation, supernatants were collected and stored at  $-20^\circ\text{C}$  until use. Levels of TNF- $\alpha$ , IL-1 $\beta$ , IL-6, PGE<sub>2</sub> and IL-10 in cell culture supernatants were determined by the corresponding ELISA kit according to the protocol recommended by the manufacturer. LPS-stimulated and unstimulated cells treated with PBS were used as controls (LPS+ and LPS-, respectively). Experiments were performed using five replicates per formulation and results were expressed as mean  $\pm$  SD. ANOVA was performed comparing tested NPs and LPS+ at significance levels of  $p < 0.05$ ,  $p < 0.005$  and  $p < 0.001$  and comparing NPs with each other at significance levels of  $p < 0.05$ ,  $p < 0.005$  and  $p < 0.001$ .

## **2.8. *In vivo* biocompatibility evaluation**

### **2.8.1. Animals**

Animal experiments were carried out according to the European Directive (2010/63/EU) and the National Spanish Law (RD 53/2013). The Ethical

Committee of University of Salamanca approved the surgical protocols (register number: 035).

### **2.8.2. *In vivo* subcutaneous injection of NPs**

Animals were acclimatized for at least two weeks prior to surgery. Ten Wistar rats were anesthetized with 1.5% isoflurane (Vetflurane®), shaved with an electric shaver and sterilized with an antiseptic solution (povidone-iodine, Betadine®). Four dorsal subcutaneous injections of PBS (control) or NPs (CLX-10, TNX-5 and DEX-15, 0.50 mg mL<sup>-1</sup>) using 21G needles and a volume of 1 mL, were performed in each rat. Animals were euthanized by anesthetic overdose at one and two weeks post injection. Rat backs were shaved over the injection site and tissues were harvested for histological evaluation.

### **2.8.3. Histological study**

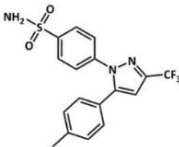
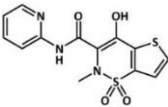
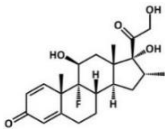
To evaluate the inflammatory reaction to NPs, tissue fragments around the injection site were fixed with 10% formalin solution and embedded in paraffin. Samples were sectioned (5 µm) along the longitudinal axis of the skin and stained with hematoxylin and eosin (H-E). The images were obtained with a light microscope (Nikon Eclipse 90i) coupled to a Nikon Digital Sight DS-smc camera (Nikon Corporation, Tokio, Japan).

## **3. Results and discussion**

NSAIDs (both traditional or specific COX-2 inhibitors) and glucocorticoids, are the keystone of the treatment of inflammation and pain related to OA. NSAIDs are normally prescribed for oral administration or as topical agents when patients present gastrointestinal problems, while glucocorticoids can be taken orally for mild stages of OA or intra-articularly administered for patients with more severe OA symptoms [9]. In the present study, tenoxicam as a traditional NSAID, celecoxib as a selective COX-2 inhibitor and dexamethasone as a glucocorticoid, were selected for studying their anti-inflammatory potential after their nanoencapsulation into polymeric NPs

based on an amphiphilic terpolymer, in order to reduce drug cytotoxicity and improve drug stability in aqueous media. Some relevant properties of the three drugs are summarized in table 1.

**Table 1. Summary of celecoxib, tenoxicam and dexamethasone properties related to the treatment of OA.**

	Celecoxib	Tenoxicam	Dexamethasone
<b>Type</b>	Coxib, selective COX-2 inhibitor	Oxicam, class of NSAID	Glucocorticoid, class of corticoid
<b>Chemical structure</b>			
<b>Main mechanism of action</b>	Selective inhibition of COX-2	Inhibition of both COX-1 and COX-2	Binding to cellular glucocorticoid receptors, inducing or repressing the transcription of multiple genes
<b>Solubility in water (mg L<sup>-1</sup>)</b>	4.3 [41]	14.1 [42]	89.0 [43]
<b>LogP (partition coefficient)</b>	3.53 [41]	1.9 [42]	1.83 [43]
<b>Most common administration route</b>	Oral	Intra-articular injection, oral	Intra-articular injection, oral
<b>Current used in OA</b>	Inflammation and pain relief in mild or moderate OA	Post-operative pain relief	Inflammation and pain relief in mild or moderate OA

### 3.1. Preparation and physicochemical characterization of NPs

Nanoprecipitation is a simple, cost-effective technique widely used for the encapsulation of poorly-water soluble drugs [44–46]. Here, CLX, TNX or DEX-loaded polymeric NPs were obtained by the nanoprecipitation method using the terpolymer poly(MVE-co-VP-co-VC) (figure 1A). A scheme of the synthesis of poly(MVE-co-VP-co-VC) showing its chemical structure, its <sup>1</sup>H-NMR

spectrum and its main physicochemical parameters is presented in figure S1. The appropriate hydrophilic-hydrophobic balance of the polymer allows its self-assembly during nanoprecipitation, giving rise to NPs entrapping the drug into the hydrophobic core [40]. In all cases, NPs showed narrow unimodal size distributions by light scattering, as shown in figure 1B, with polydispersity index (PDI) values below 0.1, demonstrating good size homogeneity in all systems independently of the encapsulated drug. Mean hydrodynamic diameter ( $D_h$ ), PDI and zeta potential ( $\xi$ ) of NPs are given in figure 1C. Hydrodynamic diameters ranged between 110 and 130 nm. Based on the literature, particle diameters below 200 nm are appropriate for particle cellular internalization, while NPs with diameters higher than 100 nm are capable of avoiding their elimination by the reticuloendothelial system [47], making this range of sizes (100–200 nm) particularly suitable for nanocarriers used in biological applications.

NP aggregation is one of the key problems of this type of drug delivery system. Consequently, stability of the NPs in terms of aggregation was evaluated when stored under static conditions at 4 °C during seven months. As indicated by Dynamic Light Scattering (DLS) (figure S2), after seven months all NPs maintained their size below 140 nm, PDI values below 0.2 and unimodal size distributions, suggesting the stability of the NPs and minimal aggregation.

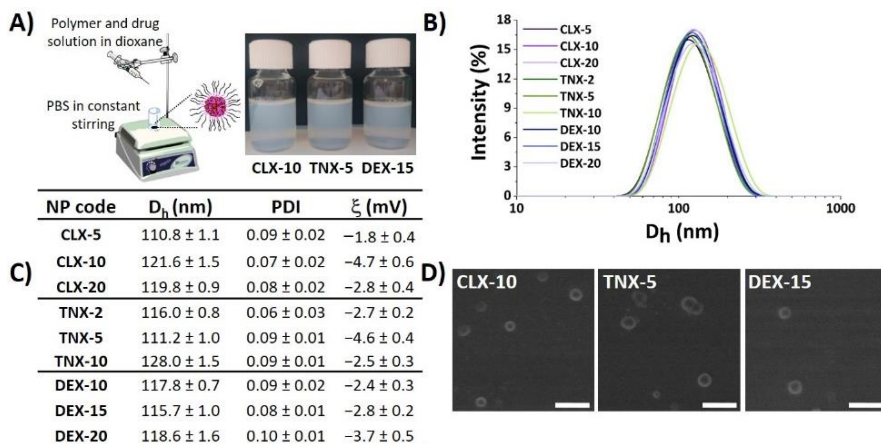


**Figure 1. Physicochemical properties of CLX, TNX and DEX-loaded NPs. (A) NP suspensions obtained by the nanoprecipitation method. Image created using ChemDraw. (B) NP size distribution immediately after synthesis. (C) Hydrodynamic diameter ( $D_h$ ), polydispersity index (PDI) and zeta potential ( $\xi$ ) values of NPs. (D) SEM micrographs of CLX-10, TNX-5 and DEX-15 NPs. Scale bar: 300 nm.**

Zeta potentials were slightly negative, ranging between  $-1$  and  $-5$  mV, as observed in figure 1C, due to the presence of 1-vinyl-2-pyrrolidone (VP) and *N*-vinylcaprolactam (VC)-rich domains in the shell of the NPs [37]. It is widely reported that cationic and neutrally charged NPs show the highest transport efficiency compared to negatively charged ones due to the charge attraction between positive NPs and negative cell membrane surfaces, thereby increasing the rate and extent of particle internalization [48]. SEM images, presented in figure 1D, showed spherical particles for the three types of loaded NPs, morphology that has demonstrated to facilitate NP internalization compared to other like cubic or rod morphologies [49,50]. In addition, the average diameter and size distribution homogeneity agreed with the hydrodynamic light scattering studies. NP physicochemical properties including size, surface charge, surface chemistry or morphology, among others, are important factors in order to be sequestered by cells, especially inflammatory cells like macrophages [51]. In general, spherical, positively charged or neutral charged NPs having sizes between 100–200 nm, are thought to be optimal systems to

be cell-sequestered. Thus, the hydrodynamic properties of the NPs prepared here are ideal for an efficient cellular uptake.

Polymer composition and an appropriate hydrophilic-hydrophobic balance of amphiphilic polymers are critical parameters in drug encapsulation efficiency. In this sense, Thayumanavan *et al.* discovered that varying the combination between random and block copolymers in polymeric co-assemblies leads to the possibility of modulating hydrophobic cargo loading capacity and cargo release behavior [52]. In the investigations of Therasima and coworkers, controlling the primary polymer structure in terms of composition and chain length could tune thermoresponsive nanomicelle size, aggregation number and cloud points [53]. Here, the amphiphilic structure of poly(MVE-co-VP-co-VC) (see figure S1) allowed the encapsulation of three hydrophobic drugs. Drug hydrophilicity was also critical for its encapsulation since the higher the water solubility, the lower the encapsulation efficiency achieved. As seen in table 1, DEX is the most water soluble drug, followed by TNX and CLX. Furthermore, drug logP, which is the partition coefficient of a molecule between aqueous and lipophilic phases, is higher for the most hydrophobic drug (CLX) followed by TNX and DEX (see table 1). In the case of the encapsulation efficiency, the highest values were obtained for CLX followed by TNX and DEX (table 2), in agreement with logP values and opposing water solubility values. This core shell nanovehicle is formed by a core of hydrophobic MVE rich moieties and a shell or corona of hydrophilic rich moieties, based mainly on VP [40]. MVE-based hydrophobic blocks forming the inner core entrapped the drug by hydrophobic interactions and hydrogen bonding. The higher the hydrophobicity of the drug, the greater the affinity between the core and the drug and, as a consequence, the greater the amount of entrapped drug. Besides, for CLX NPs the encapsulation efficiency was also dependent of the feed drug concentration, being higher (72%) for the lower initial drug amount (2% w/w). For TNX NPs, EE was similar for the three formulations, while for DEX NPs the highest value was reached for the lowest feed drug concentration assayed (10% w/w), as in the case of CLX NPs. Encapsulated drug concentrations are also shown in table 2. As can be ascertained, for CLX NPs and TNX NPs encapsulated drug concentrations increased with feed concentration, reaching the highest value for CLX-20 ( $0.156 \text{ mg mL}^{-1}$ ). In the

case of DEX NPs, very similar values, around  $0.050 \text{ mg mL}^{-1}$ , were achieved. These encapsulated drug concentrations determine the bioactivity of the NPs in terms of cytotoxicity and NO reduction, as will be explained in the following sections.

**Table 2. Concentrations of feed and encapsulated drugs in NP suspensions ( $2.00 \text{ mg mL}^{-1}$ ) in terms of % w/w with respect to the terpolymer and  $\text{mg mL}^{-1}$ .**

NP code	[Drug]		EE(%)	[Encapsulated drug]	
	%w/w	$\text{mg mL}^{-1}$		%w/w	$\text{mg mL}^{-1}$
CLX-5	5	0.10	$72 \pm 8$	$3.60 \pm 0.29$	$0.072 \pm 0.006$
CLX-10	10	0.20	$50 \pm 7$	$5.00 \pm 0.35$	$0.100 \pm 0.007$
CLX-20	20	0.40	$39 \pm 6$	$7.80 \pm 0.47$	$0.156 \pm 0.009$
TNX-2	2	0.04	$22 \pm 5$	$0.44 \pm 0.03$	$0.009 \pm 0.001$
TNX-5	5	0.10	$20 \pm 4$	$1.00 \pm 0.07$	$0.020 \pm 0.001$
TNX-10	10	0.20	$24 \pm 5$	$2.50 \pm 0.18$	$0.050 \pm 0.004$
DEX-10	10	0.20	$26 \pm 6$	$2.60 \pm 0.34$	$0.052 \pm 0.003$
DEX-15	15	0.30	$16 \pm 7$	$2.40 \pm 0.35$	$0.048 \pm 0.002$
DEX-20	20	0.40	$14 \pm 7$	$2.80 \pm 0.35$	$0.056 \pm 0.003$

Comparing the hydrodynamic properties and the EE acquired here to those of previously described CUR-loaded NPs, very similar results were achieved regarding diameters (114–135 nm for CUR NPs) and zeta potentials (around  $-4 \text{ mV}$  for CUR NPs) [40]. However, EE were higher in the case of CUR, with values between 72–79% due to the lower water solubility of this drug ( $3.12 \text{ mg mL}^{-1}$ ) [54] in comparison to CLX, TNX and DEX, which may allow more and stronger interactions of CUR with the particle core. Nanoprecipitation has been recently used for the encapsulation of these drugs into different polymeric nanovehicles, obtaining systems with different physicochemical properties. In the case of CLX, higher encapsulation efficiencies (around 90%) were obtained in the CLX-loaded hyaluronan nanocapsules of El-Gogary *et al.* [27] or in the propylene glycol alginate sodium sulfate based pH-sensitive nanotherapeutic systems of Zhang *et al.* [55]. However, highly negatively charged particles were obtained in both cases, below  $-26 \text{ mV}$ , with bigger particle sizes ( $>129 \text{ nm}$ ) and PDI values ( $>0.1$ ). The same happened with recently described DEX-loaded NPs, in which encapsulation efficiencies were around 50% for the DEX-loaded PLGA-PEG NPs of Albisa *et al.* [56], although sizes between 250–400 nm were obtained. In the case of Chiesa *et al.* [57]



smaller NPs (150 nm) entrapping DEX and using a dodecapeptide (GE11)-PLGA based conjugate were fabricated, although NPs presented highly negative surface charges ( $-25$  mV). DEX has also been nanoencapsulated, for instance, into a mixture of two pseudoblock polymer drugs, poly(VP-co-MVE) and poly(VI-co-HEI), VI being 1-vinylimidazole and HEI being a methacrylic derivative of ibuprofen, with NP sizes of 179–211 nm, surface charges of  $-2.6$  to  $-0.5$  mV and encapsulation efficiencies of 36–59% [38]. These results were closer to those reached here due to the presence of the copolymer system poly(VP-co-MVE) with a similar composition to the terpolymer poly(MVE-co-VP-co-VC) used in this work. In the case of TNX, no polymeric nanocarriers prepared by nanoprecipitation have been found. All in all, these CLX and DEX-loaded NPs have, in general, smaller hydrodynamic diameters than those reported in recent polymeric NPs prepared by nanoprecipitation, and surface charges nearer neutral, due to the presence of vinyl groups at the NP shell, making this nanoparticulated system appropriate for biological applications. Furthermore, with similar characteristics compared to these systems, previously described terpolymer NPs encapsulating CUR demonstrated to be successfully endocytosed by human articular chondrocytes (HC-a) and murine macrophages (RAW264.7) [40]. Moreover, encapsulation efficiencies were high enough to observe *in vitro* biological effects, as explained hereafter.

### 3.2. Effect on HC-a viability

One of the main drawbacks of intra-articularly injecting free anti-inflammatory drugs is their high toxicity when in contact with cartilage, and the formation of crystals and further cartilage damage due to the crystalline nature of some of them [9]. Therefore, in order to assess possible toxic effects of these drug-loaded NPs, an AlamarBlue® test was carried out on HC-a at different time periods (24 and 48 h, 7 and 14 days). Results of HC-a viability are represented in figure 2 for all tested NPs.

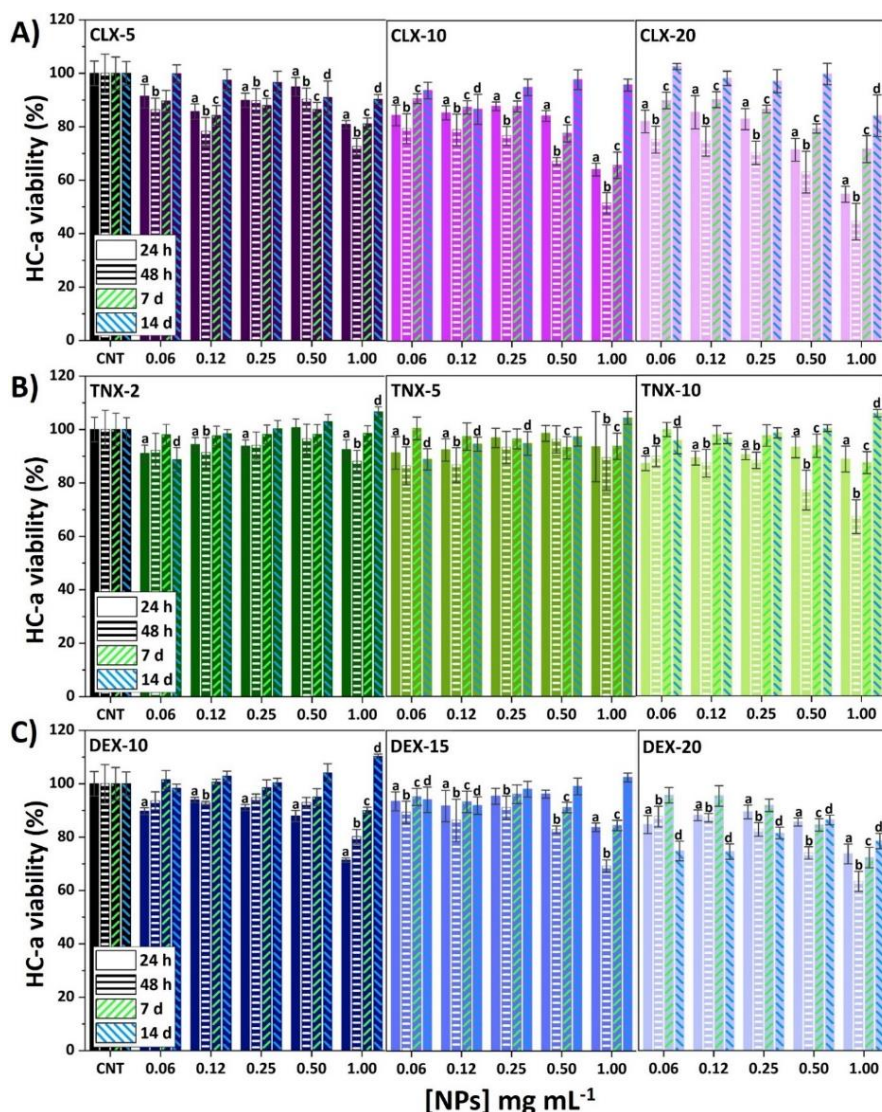


Figure 2. Effect of (A) CLX, (B) TNX and (C) DEX NPs on HC-a viability after 24 and 48 h, 7 and 14 days. Mean  $\pm$  SD values are relative to control cells without NP treatment (CNT) for each time, in which cell viability was taken as 100%. ANOVA of the results was performed with respect to their corresponding CNT at a significance level of  $p < 0.05$  (a, b, c and d correspond to statistical significance for 24 h, 48 h, 7 and 14 days samples, respectively).

Cytotoxicity of CLX NPs was dependent on time, CLX concentration and NP concentration (figure 2A). The lowest HC-a viability was observed after 48 h of NP treatment for all CLX formulations and, after this time, cell viability was recovered reaching values over 80% for all the formulations after 14 days. CLX-5 NPs did not affect cell viability at any NP concentration, while for CLX-10 and CLX-20, viabilities below 70% were observed for the two most concentrated suspensions (0.50 and 1.00 mg mL<sup>-1</sup>). Figure S3 shows HC-a viabilities after 24 h in contact with free or nanoencapsulated drugs against drug concentration. For CLX (figure S3A), the three systems CLX-5, CLX-10 and CLX-20 achieved a remarkable reduction of free CLX cytotoxicity. Hence, going back to figure 2A, a wide range of CLX and NP concentrations were demonstrated to be noncytotoxic at any time, reaching only cytotoxic effects for CLX encapsulated concentrations of 0.025 and 0.050 mg mL<sup>-1</sup> (CLX-10 at 0.50 and 1.00 mg mL<sup>-1</sup> of NPs) and 0.039 and 0.078 mg mL<sup>-1</sup> (CLX-20 at 0.50 and 1.00 mg mL<sup>-1</sup> of NPs). In any case, the three formulations presented lower toxicity than free CLX at the same concentration as the encapsulated drug.

Regarding TNX NPs (figure 2B), the only NP suspension reducing HC-a viability below 70% was TNX-10 at 1.00 mg mL<sup>-1</sup> after 48 h. However, an interesting increase in cell viability after 14 days was observed for TNX-2, 5 and 10 NPs at 1.00 mg mL<sup>-1</sup> that was statistically significant ( $p < 0.05$ ) for TNX-2 and TNX-10. Comparing the results at 24 h with the results of free TNX (figure S3B) no statistically significant changes were observed between nanoencapsulated or free TNX, as the concentrations of nanoencapsulated TNX were not cytotoxic in its free form.

For DEX NPs (figure 2C), the lowest viabilities were found after 24 or 48 h, having viabilities below 70% for DEX-10, 15 and 20 at 1.00 mg mL<sup>-1</sup>. Moreover, the same effect as for TNX was observed for DEX-10 at 1.00 mg mL<sup>-1</sup> after 14 days, in which a significant increase on cell viability was observed. In any case, after 14 days of NP treatment, HC-a presented viabilities over 80% for all NPs. As observed in figure S3C, the nanoencapsulation of DEX led to a significant reduction of its free form cytotoxicity, confirming the suitability of this polymeric system to reduce the cytotoxicity of both, CLX and DEX.

In conclusion, a reduction of CLX and DEX toxicity in HC-a was observed after their nanoencapsulation. Additionally, a wide range of CLX, TNX and DEX formulations did not cause cytotoxic effects on HC-a, making them suitable for the treatment of OA or other cartilage-related conditions.

### **3.3. Effect on RAW264.7 viability and NO release**

Macrophages are key regulators of OA-related inflammation, secreting inflammatory mediators such as cytokines and chemokines, controlling the activity of the adaptive immune system, and also conditioning other cells such as chondrocytes [58-60]. To elucidate the effect of the NPs on the viability of RAW264.7 macrophages, an AlamarBlue® assay was performed after 24 h of exposure to NPs using the same protocol as for HC-a. Results are shown in figure 3A.

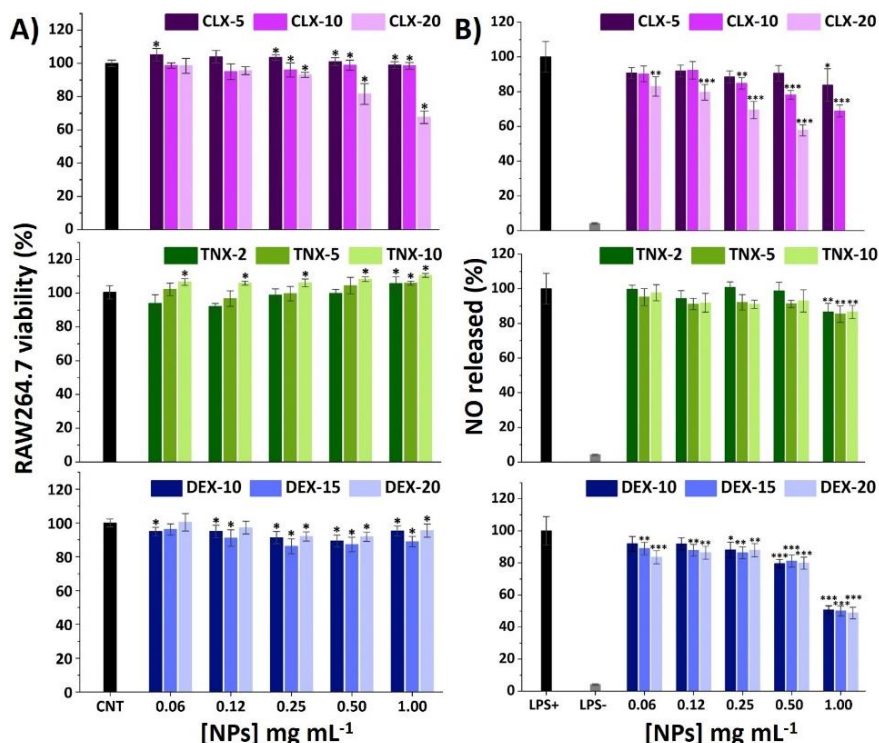


**Figure 3. (A) Effect of CLX, TNX and DEX NPs on RAW264.7 viability after 24 h.** Mean  $\pm$  SD values are relative to control cells without NP treatment (CNT), in which cell viability was taken as 100%. ANOVA of the results was performed with respect to CNT at a significance level of  $*p < 0.05$ . **(B) Effect of CLX, TNX and DEX NPs on NO production in LPS-stimulated cells.** Mean  $\pm$  SD values are relative to control LPS+, in which NO production was taken as 100%. CLX-20 NPs at a concentration of 1.00 mg mL<sup>-1</sup> were not tested since they showed cytotoxic effects on the AlamarBlue® viability test. ANOVA of the results was performed with respect to LPS+ at significance levels of  $*p < 0.05$ ,  $**p < 0.005$  and  $***p < 0.001$ .

For CLX NPs, the only formulation causing a decrease on viability below 70% was CLX-20 at 1.00 mg mL<sup>-1</sup>. This formulation presents the highest drug content as can be seen in table 2 (0.078 in 1.00 mg mL<sup>-1</sup> NP suspension). For the rest of NPs, cell viabilities were maintained between 80 and 110%. Comparing these results with the ones of free CLX (figure S4A) a reduction on

the cytotoxicity of CLX when encapsulated into this polymeric vehicle was observed.

When treated with TNX NPs, RAW264.7 viability increased with TNX load and NP concentration, reaching 111% of viability for TNX-10 at 1.00 mg mL<sup>-1</sup>, as happened to HC-a (figure 2B). Moreover, non-encapsulated TNX (free form) did not cause any cytotoxic effect at the TNX nanoencapsulated concentrations, as occurred with HC-a, so the comparison of free and nanoencapsulated TNX cytotoxicity could not be performed.

Finally, the treatment with DEX NPs resulted in cell viabilities around 100% in the whole range of the studied concentrations (0.06–1.00 mg mL<sup>-1</sup>). Comparing these results with the RAW264.7 viability results of free DEX (figure S4C), a reduction of the drug cytotoxicity was achieved for similar concentrations of the free and nanoencapsulated drug, similar to CLX NPs. Therefore, the reduction in cytotoxicity obtained for CLX and DEX NPs in RAW264.7 further encourages the use of this polymeric nanocarrier as a delivery system to reduce the cytotoxic effects of these drugs.

It is well recognized that bacterial lipopolysaccharide (LPS) stimulation induces RAW264.7 M<sub>0</sub> polarization into an M<sub>1</sub> pro-inflammatory phenotype through the binding of LPS to cellular Toll-like receptors (TLR), particularly TLR4 [61,62]. This leads to the activation of the NF- $\kappa$ B signaling pathway activating the release of different pro-inflammatory mediators, such as NO, ROS and different cytokines and chemokines. Among these factors, NO overproduction plays a major regulatory role in tissue damage associated with chronic inflammation presented in OA. Different polymeric NPs have demonstrated a reduction of NO in LPS-stimulated RAW264.7 encapsulating CLX [28] and DEX [23,63,64]. Unloaded NPs were deeply studied in a previous work and the reduction in NO production was not observed in LPS-stimulated RAW264.7 macrophages [40]. Hence, the immunomodulatory effects that are noticed here are expected to be due to the loaded anti-inflammatory drugs. Results of NO production for the studied NPs are shown in figure 3B. Basal levels of NO in unstimulated cells treated with PBS (LPS-) were around 5% with respect to the LPS+ control (LPS-stimulated cells treated with PBS).

For CLX NPs, there was a drug content and NP concentration-dependent effect, reducing NO release to 60% for CLX-20 at 0.50 mg mL<sup>-1</sup> and to 70% for CLX-10 at 1.00 mg mL<sup>-1</sup>. In the case of TNX NPs, only the most concentrated NP suspensions (1.00 mg mL<sup>-1</sup>) significantly reduced NO levels to 85%, independently of TNX content. Ultimately, DEX NPs showed a NO reduction of 50% at 1.00 mg mL<sup>-1</sup> for all drug contents without differences between them, which is in accordance with the very closed encapsulated DEX concentration values of these three systems (table 2), suggesting that the anti-inflammatory effect of the NPs correlates with the amount of encapsulated drug. These results suggest that the incorporation of the drugs inside the polymeric nanovehicle does not compromise their anti-inflammatory properties in terms of NO reduction. According to these results, CLX-10, TNX-5 and DEX-15 at 0.50 mg mL<sup>-1</sup> were chosen for the following inflammatory studies.

### **3.4. Effect on RAW264.7 release of inflammatory factors**

Apart from NO, M<sub>1</sub> macrophages are in charge of the release of multiple other inflammatory mediators such as cytokines and chemokines that lead to leukocyte recruitment. To have a general view of the anti-inflammatory potential of the selected CLX-10, TNX-5 and DEX-15 NPs, a semi-quantitative inflammation antibody array was used. All the inflammatory mediators studied in the inflammation antibody array are listed in table S1. Inflammatory factors that were released by RAW264.7 when stimulated with LPS were IL-1 $\alpha$ , IL-4, IL-6, MCP-1, MIP-1 $\alpha$ , MIP-1 $\gamma$ , TIMP-2, TNF- $\alpha$ , sTNF-RI, sTNFRII, RANTES and MCSF. In figure 4, the relative fold of those factors that were significantly repressed in LPS-stimulated cells by the action of CLX-10 and DEX-15 NPs are represented. TNX-5 NPs did not significantly reduce any of the overexpressed inflammatory factors in the inflammation antibody array.

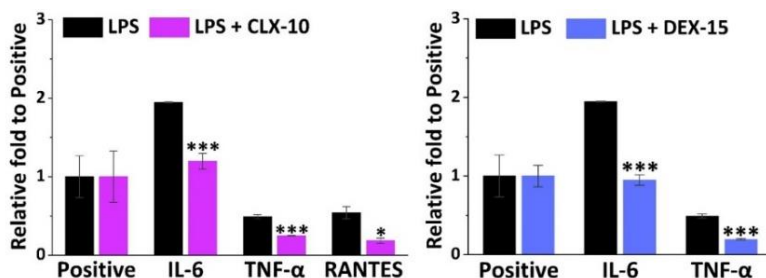


**Figure 4.** Effect of CLX-10 and DEX-15 NPs ( $0.50 \text{ mg mL}^{-1}$ ) on the production of inflammatory mediators that were upregulated in LPS-stimulated RAW264.7 (LPS) using a mouse inflammation antibody array. Mean  $\pm$  SD values are relative to the positive control of each membrane, which was given an arbitrary value of 1. ANOVA between inflammatory (LPS) and treatment membranes (LPS + CLX-10 and DEX-15) was performed at significance levels of \*  $p < 0.05$  and \*\*\*  $p < 0.001$ .

IL-6 was the cytokine more notably overexpressed in LPS-stimulated RAW264.7, 1.9-fold to the positive control, and was significantly reduced in CLX-10 and DEX-15 NPs. TNF- $\alpha$  was the second most overproduced cytokine (0.5-fold to positive) and then reduced upon CLX-10 and DEX-15 NP treatment. For CLX-10, an additional chemokine, RANTES (regulated on activation, normal T cell expressed and secreted) was also reduced by the action of the NPs. The rest of the overproduced inflammatory factors were not significantly inhibited upon treatment with NPs.

In order to deepen the effect of the NPs in RAW264.7 secretion of osteoarthritic inflammatory factors, specific ELISAs were performed for TNF- $\alpha$  and IL-6 cytokines, but additionally for IL-1 $\beta$ , PGE $_2$  and IL-10. Pro-inflammatory cytokines TNF- $\alpha$ , IL-1 $\beta$  and IL-6, and the inflammatory mediator PGE $_2$ , have a key role in the development and progression of OA, which makes their inhibition an appealing potential target in the treatment of OA [8,65]. Anti-inflammatory cytokines such as IL-10 also play a major role in the pathophysiology of OA, counteracting the action of pro-inflammatory mediators.

In LPS-stimulated (LPS+) RAW264.7 TNF- $\alpha$ , IL-6 and PGE $_2$  were produced to a greater extent (11,000, 6,000 and 5,500  $\text{pg mL}^{-1}$ , respectively)



compared to IL-1 $\beta$  and IL-10 (58 and 6 pg mL<sup>-1</sup>, respectively), as seen in figure 5.

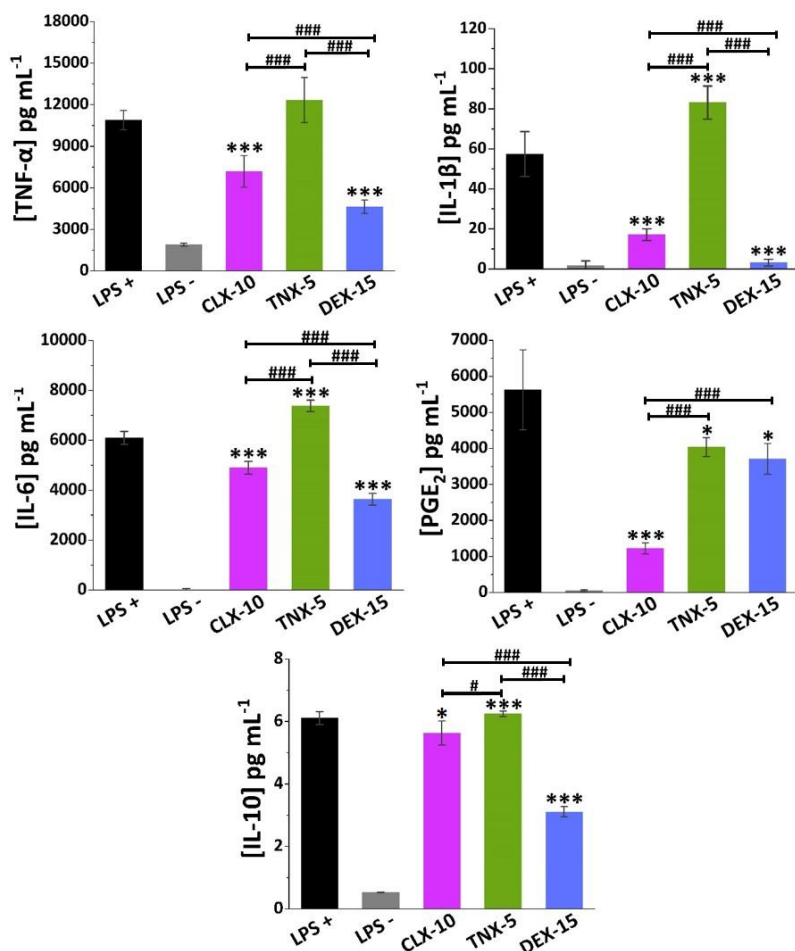


Figure 5. Effect of CLX-10, TNX-5 and DEX-15 (0.50 mg mL<sup>-1</sup>) on the release of the inflammatory mediators TNF- $\alpha$ , IL-1 $\beta$ , IL-6, PGE<sub>2</sub> and IL-10 in LPS+ RAW264.7 using ELISA kits. Data is represented as mean  $\pm$  SD values. ANOVA between each NP formulation and LPS+ (\* $p$  < 0.05 and \*\*\* $p$  < 0.001) and between NPs (# $p$  < 0.05 and ### $p$  < 0.001) were performed.

NSAIDs exert their anti-inflammatory action mainly through the unspecific inhibition of both COX-1 and COX-2 enzymes, in the case of traditional NSAIDs, and selectively COX-2, in the case of coxibs. These COX enzymes are in charge of prostanoids synthesis from arachidonic acid, including PGE<sub>2</sub>, one of the major catabolic mediators involved in cartilage inflammation and degradation during OA [66]. However, while COX-1 regulates many cellular processes related, for instance, to the gastrointestinal and renal tracts, COX-2 is an inducible enzyme that increases during inflammatory processes. Nevertheless, other anti-inflammatory COX-independent pathways have been reported for NSAIDs, including their interaction with transcription factors like NF- $\kappa$ B or AP-1, or with cellular kinases that regulate gene expression of inflammatory molecules like NO, COX-2, TNF- $\alpha$ , IL-1 $\beta$  or IL-6, among others [67,68].

TNX is a traditional NSAID of the oxicam family, acting as an inhibitor of both COX enzymes, but primarily COX-1. Here, TNX-5 NPs reduced PGE<sub>2</sub> RAW264.7 release while increasing IL-10 levels. However, an increase in the pro-inflammatory cytokine IL-1 $\beta$  and IL-6 levels were observed. As far as we are aware, few studies have been made on the effect of TNX in cell cultures. Nonetheless, piroxicam, a TNX analogue, has been encapsulated into liposomes showing, for instance, a reduction of TNF- $\alpha$ , IL-1 $\beta$  and PGE<sub>2</sub> while increasing IL-10 in LPS-stimulated RAW264.7 [69].

CLX demonstrated to reduce not only COX-2 and PGE<sub>2</sub> levels in different *in vitro* and *in vivo* models and in synovial fluid collected from OA patients, but also levels of several pro-inflammatory cytokines such as TNF- $\alpha$ , IL-1 $\beta$  and IL-6 [70,71]. Beside this anti-inflammatory action, recent *in vitro* and *in vivo* investigations suggest that CLX has additional disease-modifying effects such as chondroprotective effects, prevention of synovial hyperplasia or inhibition of bone destruction, that could slow OA disease progression [72]. The CLX-10 loaded NPs described here showed a reduction of all the pro-inflammatory factors TNF- $\alpha$ , IL-1 $\beta$ , IL-6 and PGE<sub>2</sub>, but also of IL-10.

Finally, DEX is a glucocorticoid whose anti-inflammatory potential is mainly mediated by its binding to the glucocorticoid receptor, which is

activated and translocated to the nucleus of immune cells, inducing or repressing the transcription of multiple inflammation related genes [73]. Moreover, it can exert its anti-inflammatory effect by interfering with key inflammatory transcriptional regulators like NF- $\kappa$ B and AP-1, or by suppressing the enzyme phospholipase A<sub>2</sub> (PLA<sub>2</sub>) and, therefore, the conversion of phospholipids into arachidonic acid [15]. Here, DEX-15 NPs achieved the highest inhibition of RAW264.7 release of all inflammatory factors with the exception of PGE<sub>2</sub>. As for CLX-10 NPs, IL-10 was also reduced, which may be due to the overall reduction of the inflammatory cascade.

Altogether, these loaded NPs are potential candidates for the treatment of OA since they were demonstrated to be *in vitro* modulators of the cellular release of different osteoarthritic inflammatory markers.

### **3.5. Histological evaluation: *In vivo* biocompatibility**

Biocompatibility is a prerequisite for the successful use of drug delivery systems *in vivo*. Here, NP *in vivo* biocompatibility was assessed by a subcutaneous injection of the loaded NPs (CLX-10, TNX-5 and DEX-15) in the dorsal of Wistar rats. The biocompatibility of unloaded NPs was demonstrated in a previous study [40]. Unloaded NPs evidenced no dermo-epidermal alterations and no inflammatory infiltrates. A control group containing PBS was evaluated for comparative purposes. The histological response of each group was evaluated after one and two weeks of the injection (figures 6 and 7).

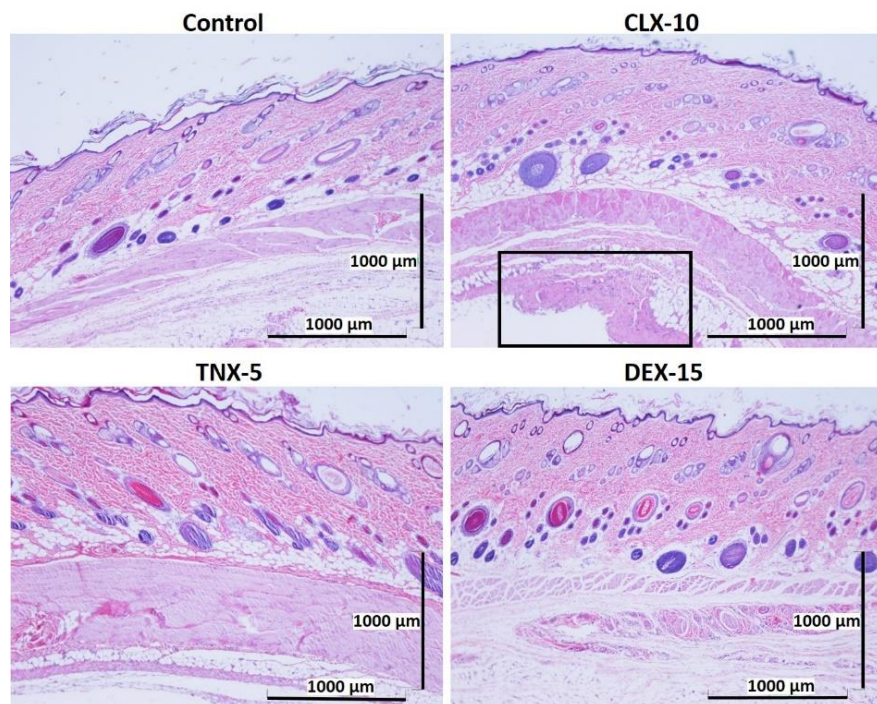


**Figure 6. Representative histological photomicrographs of skin cross-sections of rats subcutaneously injected with CLX-10, TNX-5 and DEX-15 NPs compared to the control group after one week. In the image corresponding to CLX-10 treated rats, some tissue reaction (squared and amplified in figure S5) was observed, mainly based on macrophage infiltration (H-E).**

After one (figure 6) and two (figure 7) weeks of implantation the control group did not show infiltration of inflammatory cells in the epidermis, dermis or deep muscle layers. Harvested tissues from these samples were evaluated as histologically normal. In the same way, rats treated with CLX-10, TNX-5 and DEX-15 NPs did not show tissue alterations. Visual observation of skin modification was not appreciated, and the epidermis, dermis and subcutaneous tissue appeared mostly intact. These tissues were histologically normal as in the control group after one and two weeks, except for CLX-10 NPs after the first week (squared at figure 6). In this case, one of the rats treated with CLX-10 NPs showed a small connective tissue below the muscle layers (figure S5). A reduced localized area of macrophage infiltration in the

subcutaneous tissue was observed with small-congested vessels. This minimal inflammation was not maintained in time, since, after two weeks of the treatment, inflammation was completely resolved. The recruitment of inflammatory cells, mainly macrophages, normally involves phagocytic processes. Scattered capillaries and small vessels were observed in one of the rats treated with CLX-10 NPs after one week. The presence of erythrocytes in the vessel lumina (figure S5) suggested functional blood vessels. Moreover, the development of connective tissue, considered as a normal reaction, implies collagen synthesis and plays a crucial role in tissue repair [74]. Thereby, this occasional tissue reaction, which did not occur in the rest of the CLX-10 NP treated animals, could be attributed to the normal healing process of the injection.

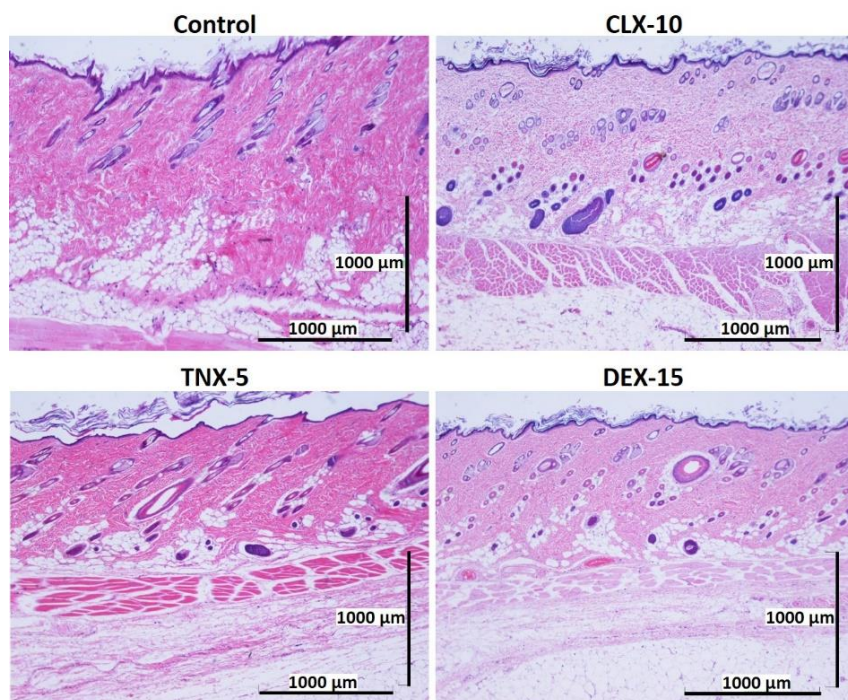


**Figure 7. Representative histological photomicrographs of skin cross-sections of rats subcutaneously injected with CLX-10, TNX-5 and DEX-15-loaded NPs compared to the control group after two weeks. (H-E).**

The demonstrated *in vitro* and *in vivo* biocompatibility of the described NPs was confirmed firstly *in vitro*, both in HC-a and RAW264.7 cytotoxicity assays, and then in an *in vivo* subcutaneous injection model in rats, demonstrating the suitability of these systems for further *in vivo* models.

## 4. Conclusions

In this study, CLX, TNX and DEX-loaded NPs were successfully developed using an amphiphilic terpolymer nanovehicle. In all cases, NPs showed spherical morphologies, unimodal size distributions with sizes between 110 and 130 nm, and moderately negative charges between  $-1$  and  $-5$  mV. Encapsulation efficiencies were highly dependent of the drug water solubility, obtaining the highest values for CLX followed by TNX and DEX. *In vitro* cellular results demonstrated a wide range of non-cytotoxic drug and NP concentrations and a reduction of the cytotoxicity of free CLX and DEX when nanoencapsulated. Loaded NPs showed an immunoregulatory effect on different osteoarthritic inflammatory markers in an LPS-stimulated RAW264.7 model by reducing the cellular release of NO, TNF- $\alpha$ , IL-1 $\beta$ , IL-6, PGE $_2$  and IL-10 in the case of CLX and DEX NPs, having the strongest inhibition with DEX NPs for all the factors but PGE $_2$ . On the other hand, TNX NPs showed an inhibition of the release of NO and PGE $_2$ , although a significant stimulation of inflammatory markers IL-1 $\beta$ , IL-6 and IL-10 was evidenced. Lastly, the *in vivo* biocompatibility of the three loaded NPs in a NP subcutaneous injection rat model showed no histological differences between NP treated and control rats after two weeks of injection. In conclusion, the suitable physicochemical characteristics, the *in vitro* anti-inflammatory activity and the *in vivo* biocompatibility properties of these NPs allow us to propose them as potential therapeutic agents of OA, as regulators of the cellular release of inflammatory factors. Taking the physicochemical and biological results overall, we consider that CLX NPs are the most optimal systems, in particular CLX-10 NPs at  $0.50 \text{ mg mL}^{-1}$ , followed by DEX-15 NPs at  $0.50 \text{ mg mL}^{-1}$ . It is worth saying that currently, further *in vitro* and *in vivo* animal models are being performed to fully elucidate the potential of these anti-inflammatory-loaded NPs as local intra-articular treatments of OA.

## Acknowledgment

The authors appreciate the considerate help of David Gómez (ICTP-CSIC) in the SEM studies, Rosa Ana Ramirez in the cell culture experiments and the Histology Area of the Department of Human Anatomy and Histology of Faculty of Medicine (University of Salamanca) for the assistance in the histological processing.

## Bibliography

- [1] Berenbaum, F. Osteoarthritis as an inflammatory disease (osteoarthritis is not osteoarthrosis!). *Osteoarthr. Cartil.* 2013, 21, 16-21.
- [2] Goldring, M.B.; Otero, M. Inflammation in osteoarthritis. *Curr. Opin. Rheumatol.* 2011, 23, 471-478.
- [3] Minguzzi, M.; Cetrullo, S.; D'Adamo, S.; Silvestri, Y.; Flamigni, F.; Borzi, R.M. Emerging Players at the Intersection of Chondrocyte Loss of Maturational Arrest, Oxidative Stress, Senescence and Low-Grade Inflammation in Osteoarthritis. *Oxid. Med. Cell Longev.* 2018, 2018, 3075293.
- [4] Zhang, H.; Cai, D.; Bai, X. Macrophages regulate the progression of osteoarthritis. *Osteoarthr. Cartil.* 2020, 28, 555-561.
- [5] Kontinen, Y.T.; Sillat, T.; Barreto, G.; Ainola, M.; Nordstrom, D.C. Osteoarthritis as an autoinflammatory disease caused by chondrocyte-mediated inflammatory responses. *Arthritis Rheum.* 2012, 64, 613-616.
- [6] Wu, C.L.; Harasymowicz, N.S.; Klimak, M.A.; Collins, K.H.; Guilak, F. The role of macrophages in osteoarthritis and cartilage repair. *Osteoarthr. Cartil.* 2020, 28, 544-554.
- [7] Yang, C.Y.; Chanalaris, A.; Troeberg, L. ADAMTS and ADAM metalloproteinases in osteoarthritis—Looking beyond the 'usual suspects'. *Osteoarthr. Cartil.* 2017, 25, 1000-1009.
- [8] Mabey, T.; Honsawek, S. Cytokines as biochemical markers for knee osteoarthritis. *World J. Orthop.* 2015, 6, 95-105.
- [9] Pontes-Quero, G.M.; García-Fernández, L.; Aguilar, M.R.; Román, J.S.; Cano, J.P.; Vázquez-Lasa, B. Active viscosupplements for osteoarthritis treatment. *Semin. Arthritis Rheum.* 2019, 49, 171-183.
- [10] Tomić, M.; Micov, A.; Pecikoza, U.; Stepanović-Petrović, R. Clinical Uses of Nonsteroidal Anti-Inflammatory Drugs (NSAIDs) and Potential Benefits of NSAIDs Modified-Release Preparations. In *Microsized and Nanosized Carriers for Nonsteroidal Anti-Inflammatory Drugs*; Academic Press: New York, NY, USA, 2017; pp. 1-29.
- [11] Niederberger, E.; Tegeder, I. NSAIDs, COX-Independent Actions. In *Encyclopedia of Pain*; Schmidt, R.F., Willis, W.D., Eds; Springer Berlin Heidelberg: Berlin/Heidelberg, Germany, 2007; pp. 1470-1473.
- [12] Grzanka, A.; Misiólek, M.; Golusiński, W.; Jarzab, J. Molecular Mechanisms of Glucocorticoids Action: Implications for

Treatment of Rhinosinusitis and Nasal Polyposis. *Eur. Arch. Oto-Rhino-Laryngol.* 2011, 268, 247-253.

[13] Deeks, J.J.; Smith, L.A.; Bradley, M.D. Efficacy, tolerability, and upper gastrointestinal safety of celecoxib for treatment of osteoarthritis and rheumatoid arthritis: Systematic review of randomised controlled trials. *BMJ* 2002, 325, 619-619.

[14] Todd, P.A.; Clissold, S.P. Tenoxicam. An update of its pharmacology and therapeutic efficacy in rheumatic diseases. *Drugs* 1991, 41, 625-646.

[15] Coutinho, A.E.; Chapman, K.E. The anti-inflammatory and immunosuppressive effects of glucocorticoids, recent developments and mechanistic insights. *Mol. Cell. Endocrinol.* 2011, 335, 2-13.

[16] Yang, X.; Du, H.; Zhai, G. Progress in intra-articular drug delivery systems for osteoarthritis. *Curr. Drug Targets* 2014, 15, 888-900.

[17] García-Couce, J.; Almirall, A.; Fuentes, G.; Kaijzel, E.; Chan, A.; Cruz, L.J. Targeting Polymeric Nanobiomaterials as a Platform for Cartilage Tissue Engineering. *Curr. Pharm. Des.* 2019, 25, 1915-1932.

[18] Kumari, A.; Yadav, S.K.; Yadav, S.C. Biodegradable polymeric nanoparticles based drug delivery systems. *Colloids Surf. B Biointerfaces* 2010, 75, 1-18.

[19] Joseph, R.M.; Hunter, A.L.; Ray, D.W.; Dixon, W.G. Systemic glucocorticoid therapy and adrenal insufficiency in adults: A systematic review. *Semin. Arthritis Rheum.* 2016, 46, 133-141.

[20] Ni, R.; Song, G.; Fu, X.; Song, R.; Li, L.; Pu, W.; Gao, J.; Hu, J.; Liu, Q.; He, F.; et al. Reactive oxygen species-responsive dexamethasone-loaded nanoparticles for

targeted treatment of rheumatoid arthritis via suppressing the iRhom2/TNF- $\alpha$ /BAFF signaling pathway. *Biomaterials* 2020, 232, 119730.

[21] Yu, C.; Li, X.; Hou, Y.; Meng, X.; Wang, D.; Liu, J.; Sun, F.; Li, Y. Hyaluronic Acid Coated Acid-Sensitive Nanoparticles for Targeted Therapy of Adjuvant-Induced Arthritis in Rats. *Molecules* 2019, 24, 146.

[22] Lorscheider, M.; Tsapis, N.; Ur-Rehman, M.; Gaudin, F.; Stolfa, I.; Abreu, S.; Mura, S.; Chaminade, P.; Espeli, M.; Fattal, E. Dexamethasone palmitate nanoparticles: An efficient treatment for rheumatoid arthritis. *J. Control. Release* 2019, 296, 179-189.

[23] Espinosa-Cano, E.; Aguilar, M.R.; Portilla, Y.; Barber, D.F.; Roman, J.S. Anti-Inflammatory Polymeric Nanoparticles Based on Ketoprofen and Dexamethasone. *Pharmaceutics* 2020, 12, 723.

[24] Li, X.; Yu, C.; Meng, X.; Hou, Y.; Cui, Y.; Zhu, T.; Li, Y.; Teng, L.; Sun, F.; Li, Y. Study of double-targeting nanoparticles loaded with MCL-1 siRNA and dexamethasone for adjuvant-induced arthritis therapy. *Eur. J. Pharm. Biopharm.* 2020, 154, 136-143.

[25] Bajpayee, A.G.; Quadir, M.A.; Hammond, P.T.; Grodzinsky, A.J. Charge based intra-cartilage delivery of single dose dexamethasone using Avidin nano-carriers suppresses cytokine-induced catabolism long term. *Osteoarthr. Cartil.* 2016, 24, 71-81.

[26] Ha, E.S.; Choo, G.H.; Baek, I.H.; Kim, M.S. Formulation, characterization, and in vivo evaluation of celecoxib-PVP solid dispersion nanoparticles using supercritical antisolvent process. *Molecules* 2014, 19, 20325-20339.

[27] El-Gogary, R.I.; Khattab, M.A.; Abd-Allah, H. Intra-articular multifunctional celecoxib loaded hyaluronan nanocapsules for the suppression of inflammation in an



osteoarthritic rat model. *Int. J. Pharm.* 2020, 583, 119378.

[28] Crivelli, B.; Bari, E.; Perteghella, S.; Catenacci, L.; Sorrenti, M.; Mocchi, M.; Farago, S.; Tripodo, G.; Prina-Mello, A.; Torre, M.L. Silk fibroin nanoparticles for celecoxib and curcumin delivery: ROS-scavenging and anti-inflammatory activities in an in vitro model of osteoarthritis. *Eur. J. Pharm. Biopharm.* 2019, 137, 37-45.

[29] Khattab, A.; Abouhusein, D.M.N.; Mohammad, F.E. Development of injectable tenoxicam in situ forming microparticles based on sesame oil and poly-DL-lactide: Characterization, efficacy and acute toxicity. *J. Drug Deliv. Sci. Technol.* 2019, 51, 682-694.

[30] Goindi, S.; Narula, M.; Kalra, A. Microemulsion-Based Topical Hydrogels of Tenoxicam for Treatment of Arthritis. *AAPS PharmSciTech* 2016, 17, 597-606.

[31] Ammar, H.O.; Ghorab, M.; El-Nahhas, S.A.; Higazy, I.M. Proniosomes as a carrier system for transdermal delivery of tenoxicam. *Int. J. Pharm.* 2011, 405, 142-152.

[32] Negi, L.M.; Chauhan, M.; Garg, A.K. Nano-appended transdermal gel of Tenoxicam via ultradeformable drug carrier system. *J. Exp. Nanosci.* 2013, 8, 657-669.

[33] Sánchez-Rodríguez, C.; Palao-Suay, R.; Rodríguez, L.; Aguilar, M.R.; Martín-Saldaña, S.; Román, J.S.; Sanz-Fernández, R.  $\alpha$ -Tocopheryl Succinate-Based Polymeric Nanoparticles for the Treatment of Head and Neck Squamous Cell Carcinoma. *Biomolecules* 2018, 8, 97.

[34] Palao-Suay, R.; Aguilar, M.R.; Parra-Ruiz, F.J.; Maji, S.; Hoogenboom, R.; Rohner, N.A.; Thomas, S.N.; Román, J.S.  $\alpha$ -TOS-based RAFT block copolymers and their NPs for the treatment of cancer. *Polym. Chem.* 2016, 7, 838-850.

[35] Palao-Suay, R.; Martín-Saavedra, F.M.; Aguilar, M.R.; Escudero-Duch, C.; Martín-Saldaña, S.; Parra-Ruiz, F.J.; Rohner, N.A.; Thomas, S.N.; Vilaboa, N.; Román, J.S. Photothermal and photodynamic activity of polymeric nanoparticles based on  $\alpha$ -tocopheryl succinate-RAFT block copolymers conjugated to IR-780. *Acta Biomater.* 2017, 57, 70-84.

[36] Palao-Suay, R.; Aguilar, M.R.; Parra-Ruiz, F.J.; Martín-Saldaña, S.; Rohner, N.A.; Thomas, S.N.; Román, J.S. Multifunctional decoration of alpha-tocopheryl succinate-based NP for cancer treatment: Effect of TPP and LTVSPWY peptide. *J. Mater. Sci. Mater. Med.* 2017, 28, 152.

[37] Martín-Saldana, S.; Palao-Suay, R.; Trinidad, A.; Aguilar, M.R.; Ramirez-Camacho, R.; Roman, J.S. Otoprotective properties of Galpha-methylprednisolone-loaded nanoparticles against cisplatin: In vitro and in vivo correlation. *Nanomedicine* 2016, 12, 965-976.

[38] Martín-Saldana, S.; Palao-Suay, R.; Aguilar, M.R.; García-Fernández, L.; Arevalo, H.; Trinidad, A.; Ramirez-Camacho, R.; Roman, J.S. pH-sensitive polymeric nanoparticles with antioxidant and anti-inflammatory properties against cisplatin-induced hearing loss. *J. Control. Release* 2018, 270, 53-64.

[39] Martín-Saldaña, S.; Palao-Suay, R.; Aguilar, M.R.; Ramírez-Camacho, R.; Román, J.S. Polymeric nanoparticles loaded with

dexamethasone or  $\alpha$ -tocopheryl succinate to prevent cisplatin-induced ototoxicity. *Acta Biomater.* 2017, 53, 199-210.

[40] Pontes-Quero, G.; Benito-Garzón, L.; Cano, J.P.; Aguilar, M.; Vázquez-Lasa, B. Amphiphilic polymeric nanoparticles encapsulating curcumin: Antioxidant, anti-inflammatory and biocompatibility studies. *Mater. Sci. Eng. C* 2021, 121, 111793.

- [41] National Center for Biotechnology Information. "PubChem Compound Summary for CID 2662, Celecoxib" PubChem. Available online <https://pubchem.ncbi.nlm.nih.gov/compound/Celecoxib> (accessed on 22 February 2021).
- [42] National Center for Biotechnology Information. "PubChem Compound Summary for CID 54677971, Tenoxicam" PubChem. Available online: <https://pubchem.ncbi.nlm.nih.gov/compound/Tenoxicam> (accessed on 22 February 2021).
- [43] National Center for Biotechnology Information. "PubChem Compound Summary for CID 5743, Dexamethasone" PubChem, <https://pubchem.ncbi.nlm.nih.gov/compound/Dexamethasone> (accessed on 22 February 2021).
- [44] Liu, Y.; Yang, G.; Baby, T.; Tengjisi, Chen, D.; Weitz, D.A.; Zhao, C.X. Stable Polymer Nanoparticles with Exceptionally High Drug Loading by Sequential Nanoprecipitation. *Angew. Chem.-Int. Ed.* 2020, 59, 4720-4728.
- [45] Liu, Y.; Yang, G.; Zou, D.; Hui, Y.; Nigam, K.; Middelberg, A.P.J.; Zhao, C.-X. Formulation of Nanoparticles Using Mixing- Induced Nanoprecipitation for Drug Delivery. *Ind. Eng. Chem. Res.* 2020, 59, 4134-4149.
- [46] Macedo, A.; Carvalho, E.O.; Cardoso, V.; Correia, D.M.; Tubio, C.; Fidalgo-Marijuan, A.; Botelho, G.; Lanceros-Méndez, S. Tailoring electroactive poly(vinylidene fluoride-co-trifluoroethylene) microspheres by a nanoprecipitation method. *Mater. Lett.* 2019, 261, 127018.
- [47] Danhier, F.; Feron, O.; Pr  at, V. To exploit the tumor microenvironment: Passive and active tumor targeting of nanocarriers for anti-cancer drug delivery. *J. Control. Release* 2010, 148, 135-146.
- [48] Murugan, K.; Choonara, Y.E.; Kumar, P.; Bijukumar, D.; du Toit, L.C.; Pillay, V. Parameters and characteristics governing cellular internalization and trans-barrier trafficking of nanostructures. *Int. J. Nanomed.* 2015, 10, 2191-2206.
- [49] Foroozandeh, P.; Aziz, A.A. Insight into Cellular Uptake and Intracellular Trafficking of Nanoparticles. *Nanoscale Res. Lett.* 2018, 13, 339.
- [50] Li, Y.; Kr  ger, M.; Liu, W.K. Shape effect in cellular uptake of PEGylated nanoparticles: Comparison between sphere, rod, cube and disk. *Nanoscale* 2015, 7, 16631-16646.
- [51] Gustafson, H.H.; Holt-Casper, D.; Grainger, D.W.; Ghandehari, H. Nanoparticle Uptake: The Phagocyte Problem. *Nano Today* 2015, 10, 487-510.
- [52] Jiang, Z.; Liu, H.; He, H.; Ribbe, A.E.; Thayumanavan, S. Blended Assemblies of Amphiphilic Random and Block Copolymers for Tunable Encapsulation and Release of Hydrophobic Guest Molecules. *Macromolecules* 2020, 53, 2713-2723.
- [53] Imai, S.; Hirai, Y.; Nagao, C.; Sawamoto, M.; Terashima, T. Programmed Self-Assembly Systems of Amphiphilic Random Copolymers into Size-Controlled and Thermoresponsive Micelles in Water. *Macromolecules* 2018, 51, 398-409.
- [54] National Center for Biotechnology Information. "PubChem Compound Summary for CID 969516, Curcumin" PubChem. Available online: <https://pubchem.ncbi.nlm.nih.gov/compound/Curcumin> (accessed on 4 December 2020).
- [55] Zhang, T.; Liu, H.; Li, Y.; Li, C.; Wan, G.; Chen, B.; Li, C.; Wang, Y. A pH-sensitive nanotherapeutic system based on a marine sulfated polysaccharide for the treatment of metastatic breast cancer through combining chemotherapy and COX-2 inhibition. *Acta Biomater.* 2019, 99, 412-425.

- [56] Albisa, A.; Piacentini, E.; Sebastian, V.; Arruebo, M.; Santamaria, J.; Giorno, L. Preparation of Drug-Loaded PLGA-PEG Nanoparticles by Membrane-Assisted Nanoprecipitation. *Pharm. Res.* 2017, *34*, 1296-1308.
- [57] Chiesa, E.; Pisani, S.; Colzani, B.; Dorati, R.; Conti, B.; Modena, T.; Braekmans, K.; Genta, I. Intra-Articular Formulation of GE11-PLGA Conjugate-Based NPs for Dexamethasone Selective Targeting-In Vitro Evaluation. *Int. J. Mol. Sci.* 2018, *19*, 2304.
- [58] Umbarino, A.; Gambaro, F.M.; Kon, E.; Andon, F.T. Therapeutic Manipulation of Macrophages Using Nanotechnological Approaches for the Treatment of Osteoarthritis. *Nanomaterials* 2020, *10*, 1562.
- [59] Pavillon, N.; Hobro, A.J.; Akira, S.; Smith, N.I. Noninvasive detection of macrophage activation with single-cell resolution through machine learning. *Proc. Natl. Acad. Sci. USA* 2018, *115*, E2676-E2685.
- [60] Canton, J.; Khezri, R.; Glogauer, M.; Grinstein, S. Contrasting phagosome pH regulation and maturation in human M1 and M2 macrophages. *Mol. Biol. Cell* 2014, *25*, 3330-3341.
- [61] Jones, E.; Adcock, I.M.; Ahmed, B.Y.; Punchard, N.A. Modulation of LPS stimulated NF-kappaB mediated Nitric Oxide production by PKCepsilon and JAK2 in RAW macrophages. *J. Inflamm.* 2007, *4*, 23.
- [62] Hwang, S.J.; Kim, Y.W.; Park, Y.; Lee, H.J.; Kim, K.W. Anti-inflammatory effects of chlorogenic acid in lipopolysaccharide stimulated RAW264.7 cells. *Inflamm. Res.* 2014, *63*, 81-90.
- [63] Yu, X.; Zhang, R.; Lei, L.; Song, Q.; Li, X. High drug payload nanoparticles formed from dexamethasone-peptide conjugates for the treatment of endotoxin-induced uveitis in rabbit. *Int. J. Nanomed.* 2019, *14*, 591-603.
- [64] Cao, J.; Naeem, M.; Noh, J.-K.; Lee, E.H.; Yoo, J.-W. Dexamethasone phosphate-loaded folate-conjugated polymeric nanoparticles for selective delivery to activated macrophages and suppression of inflammatory responses. *Macromol. Res.* 2015, *23*, 485-492.
- [65] Wojdasiewicz, P.; Poniatowski, Ł.A.; Szukiewicz, D. The role of inflammatory and anti-inflammatory cytokines in the pathogenesis of osteoarthritis. *Mediat. Inflamm.* 2014, *2014*, 561459.
- [66] Gosset, M.; Berenbaum, F.; Levy, A.; Pigenet, A.; Thirion, S.; Cavadias, S.; Jacques, C. Mechanical stress and prostaglandin E2 synthesis in cartilage. *Biorheology* 2008, *45*, 301-320.
- [67] Takada, Y.; Bhardwaj, A.; Potdar, P.; Aggarwal, B.B. Nonsteroidal anti-inflammatory agents differ in their ability to suppress NF-κB activation, inhibition of expression of cyclooxygenase-2 and cyclin D1, and abrogation of tumor cell proliferation. *Oncogene* 2004, *23*, 9247-9258.
- [68] Liu, T.; Zhang, L.; Joo, D.; Sun, S.-C. NF-κB signaling in inflammation. *Signal. Transduct. Target. Ther.* 2017, *2*, 17023.
- [69] Chiong, H.S.; Yong, Y.K.; Ahmad, Z.; Sulaiman, M.R.; Zakaria, Z.A.; Yuen, K.H.; Hakim, M.N. Cytoprotective and enhanced anti-inflammatory activities of liposomal piroxicam formulation in lipopolysaccharide-stimulated RAW264.7 macrophages. *Int. J. Nanomed.* 2013, *8*, 1245-1255.
- [70] Nakata, K.; Hanai, T.; Take, Y.; Osada, T.; Tsuchiya, T.; Shima, D.; Fujimoto, Y. Disease-modifying effects of COX-2 selective inhibitors and non-selective NSAIDs in osteoarthritis: A systematic review. *Osteoarthr. Cartil.* 2018, *26*, 1263-1273.
- [71] Gallelli, L.; Galasso, O.; Falcone, D.; Southworth, S.; Greco, M.; Ventura, V.;

Romualdi, P.; Corigliano, A.; Terracciano, R.; Savino, R.; et al. The effects of nonsteroidal anti-inflammatory drugs on clinical outcomes, synovial fluid cytokine concentration and signal transduction pathways in knee osteoarthritis. A randomized open label trial. *Osteoarthr. Cartil.* 2013, 21, 1400-1408.

[72] Zweers, M.C.; de Boer, T.N.; van Roon, J.; Bijlsma, J.W.J.; Lafeber, F.P.J.G.; Mastbergen, S.C. Celecoxib: Considerations regarding its potential disease-modifying properties in

osteoarthritis. *Arthritis Res. Ther.* 2011, 13, 239.

[73] Rhen, T.; Cidlowski, J.A. Anti-inflammatory action of glucocorticoids—New mechanisms for old drugs. *N. Engl. J. Med.* 2005, 353, 1711-1723.

[74] Anderson, J.M. Biological Responses to Materials. *Annu. Rev. Mater. Res.* 2001, 31, 81-110.

# Supplementary material

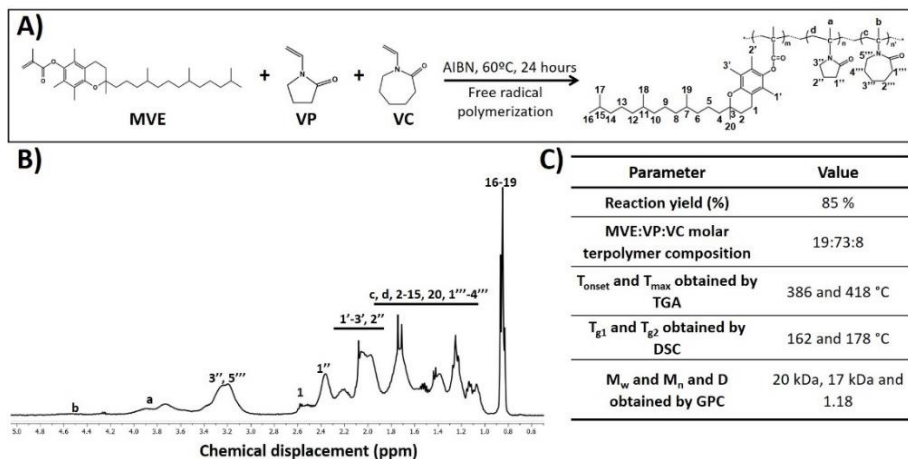
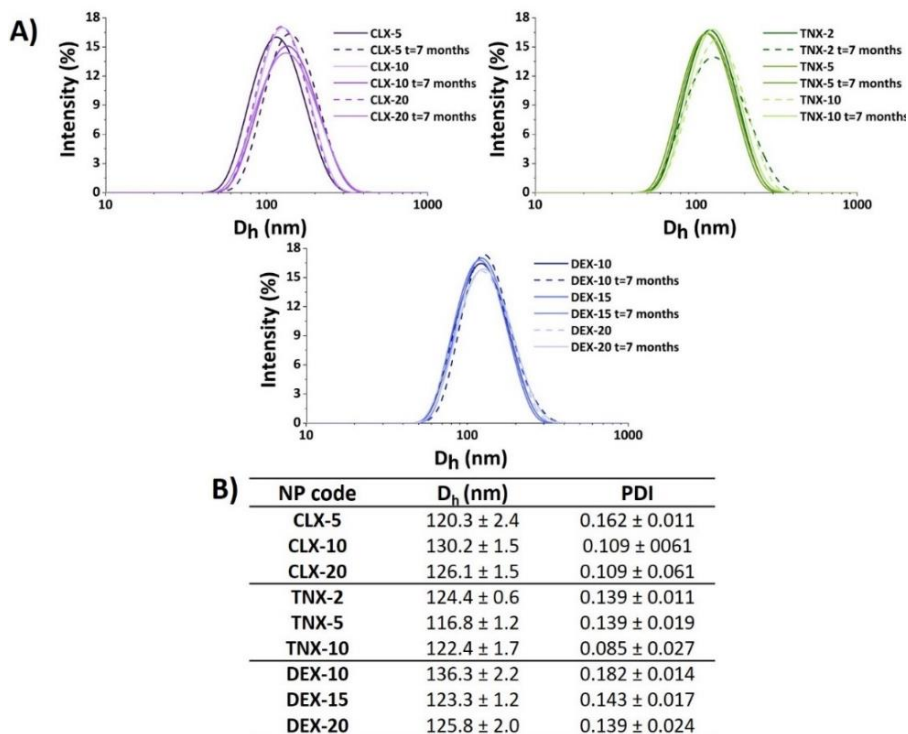


Figure S1. (A) Scheme of terpolymer poly(MVE-co-VP-co-VC) synthesis. (B) Terpolymer  $^1\text{H}$ -NMR spectrum (400 MHz) in  $\text{CDCl}_3$ . (C)  $^1\text{H}$ -NMR, TGA, DSC and GPC characterization of the terpolymer.  $T_{\text{onset}}$ , temperature at the onset of the major decay;  $T_{\text{max}}$ , maximum thermal degradation rate temperature;  $T_g$ , glass transition temperature;  $M_w$ , weight average molecular weight;  $M_n$ , number average molecular weight;  $D$ , polydispersity index.



**Figure S2. NP stability in terms of aggregation. (A) NP size distribution assessment by DLS immediately after synthesis and after 7 months of static storage at 4 °C. (B) Hydrodynamic diameter ( $D_h$ ) and polydispersity index (PDI) of loaded NPs after 7 months of static storage at 4 °C.**

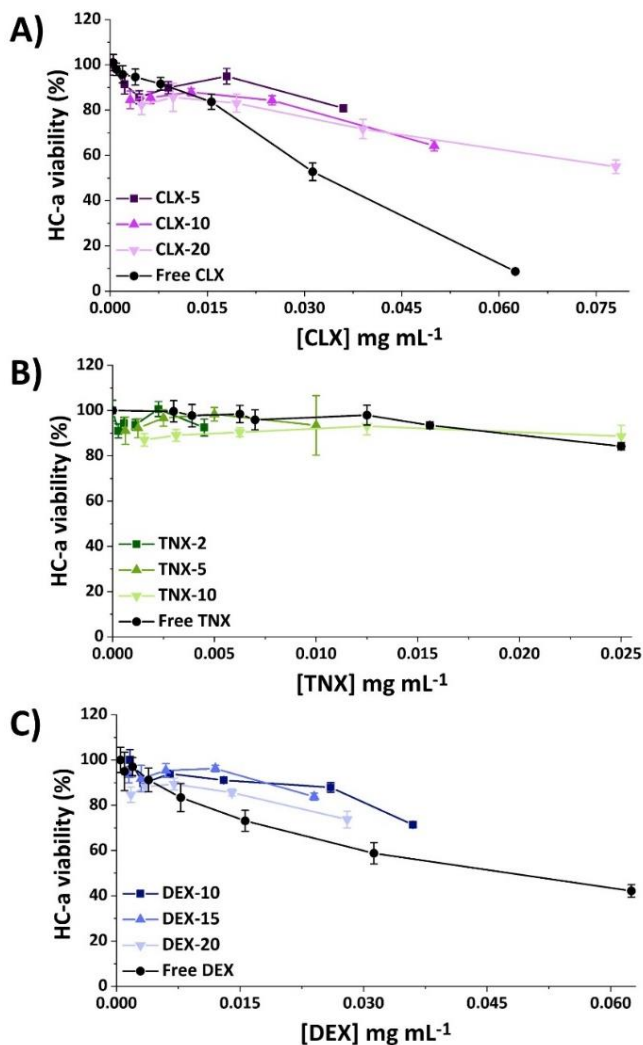


Figure S3. Representation of HC-a viabilities after 24 h of exposure to the NPs or to the corresponding free drug against the encapsulated concentrations of (A) CLX, (B) TNX and (C) DEX.

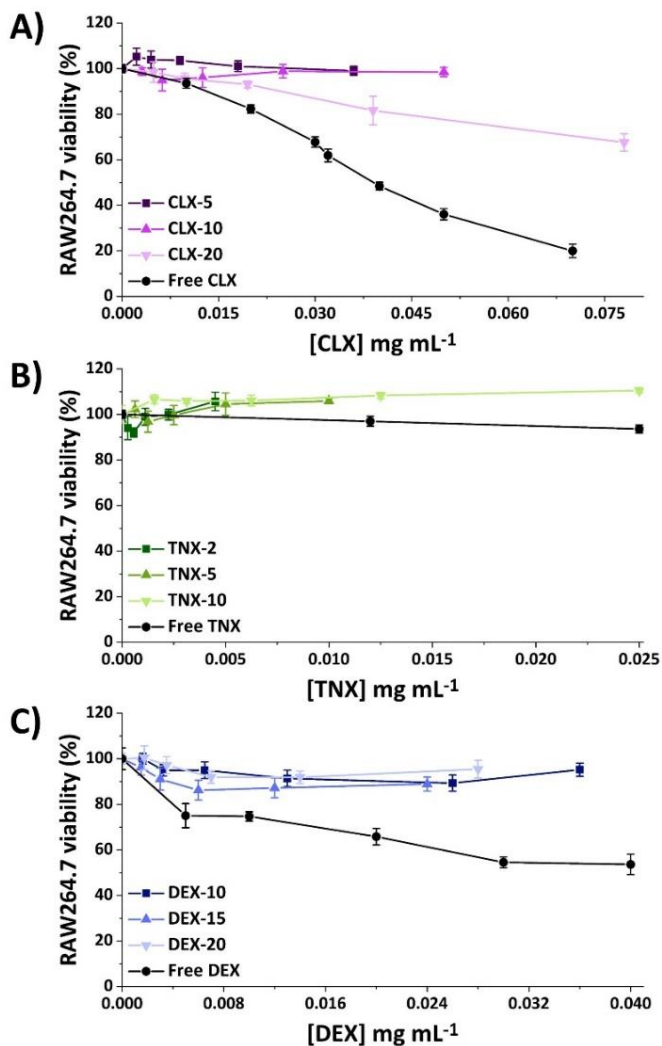
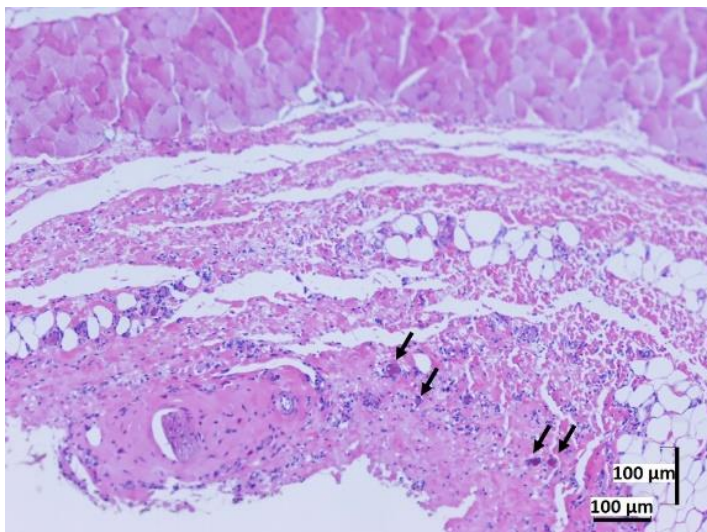


Figure S4. Representation of RAW264.7 viabilities after 24 h of exposure to the NPs or to the corresponding free drug against the encapsulated concentrations of A) CLX, B) TNX and C) DEX.





**Figure S5.** Representative image of tissue section of rats treated with CLX-10 NPs 1 week after injection. A small inflammatory reaction was appreciated mainly based on macrophage infiltration at the subcutaneous tissue. Small vessels are highlighted with arrows. (H-E, scale bar: 100  $\mu\text{m}$ ).

**Table S1.** Inflammatory factors studied in the mouse inflammation antibody array.

Inflammatory factors under study
BLC, CD30L, Eotaxin, Eotaxin-2, Fas Ligand, Fractalkine, GCSF, GM-CSF, IFN- $\gamma$ , IL-1 $\alpha$ , IL-1 $\beta$ , IL-2, IL-3, IL-4, IL-6, IL-9, IL-10, IL-12 p40/p70, IL-12 p70, IL-13, IL-17, I-TAC, KC/CXCL1, Leptin/OB, LIX, Lymphotactin, MCP-1, MCSF, MIG, MIP-1 $\alpha$ , MIP-1 $\gamma$ , RANTES, SDF-1, TCA-3, TECK, TIMP-1, TIMP-2, TNF- $\alpha$ , sTNF RI, sTNF-RII



**Chapter V. Advanced  
viscosupplements based  
on hyaluronic acid  
hydrogels loaded with  
anti-inflammatory NPs**

***CONFIDENTIAL***



# **Chapter VI. Studies on mesenchymal stem cells derived secretomes for the treatment of OA**

***CONFIDENCIAL***



# **Chapter VII. Conclusions and future perspectives**





## Chapter VII. Conclusions and future perspectives

---

In this thesis, **polymeric formulations based on anti-inflammatory-loaded polymeric nanoparticles and hyaluronic acid hydrogels** were successfully prepared for the intra-articular treatment of osteoarthritis. Furthermore, regenerative intra-articular therapies based on stem cell derivatives have been explored.

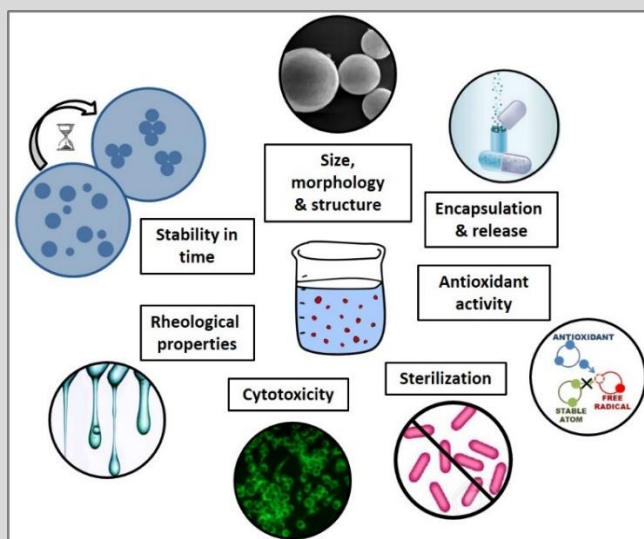
- A **terpolymer** system based on  $\alpha$ -tocopheryl methacrylate, 1-vinyl-2-pyrrolidone and *N*-vinylcaprolactam was successfully synthesized by free radical polymerization. The **amphiphilic nature** of the developed terpolymer allowed its **self-assembly in aqueous media**, forming core-shell nanoparticles able to encapsulate hydrophobic drugs in the core. The terpolymer demonstrated, firstly, to be **non-cytotoxic** to articular chondrocytes and RAW264.7 macrophages and, secondly, to have an **intrinsic antioxidant activity** by free radical scavenging in a DPPH test and in a ROS quantification *in vitro* model of H<sub>2</sub>O<sub>2</sub>-stimulated RAW264.7 macrophages.
- Four different **anti-inflammatory drugs** with poor water solubility, low bioavailability and potential toxicity were effectively loaded into the polymeric NPs: **curcumin**, a natural polyphenol; **tenoxicam**, a traditional nonsteroidal anti-inflammatory drug; **celecoxib**, a selective COX-2 inhibitor; and **dexamethasone**, a glucocorticoid.
- NPs loading CUR demonstrated **suitable hydrodynamic properties** including narrow and unimodal particle size distributions with hydrodynamic diameters in the range of 114 and 135 nm, surface charges near neutral, spherical morphologies and encapsulation efficiencies over 70%. The **prolonged release of CUR** from the polymeric nanovehicle was also demonstrated for the formulation CUR-5 NPs. A wide range of

concentrations of CUR-loaded NPs showed to be **non-cytotoxic** in both articular chondrocytes and RAW264.7 macrophages. Furthermore, a significant **reduction of free CUR toxicity** was achieved for all formulations. The intrinsic radical scavenging activity of nude NPs was increased when CUR was loaded, demonstrating that NPs had a **double antioxidant effect** and maintained the loaded drug properties. CUR-loaded NPs also demonstrated **anti-inflammatory activity** by the reduction of the *in vitro* release of several inflammatory mediators in both RAW264.7 macrophages (including NO, IL-6, MCP-1 and TNF- $\alpha$ ) and articular chondrocytes (IL-8, MIP-1 $\alpha$  and MCP-2). Finally, non-loaded NPs and CUR bearing NPs demonstrated to be **biocompatible *in vivo*** by their subcutaneous injection in rats.

- Drug delivery systems based on **CLX, TNX and DEX-loaded NPs** were successfully prepared by the nanoprecipitation method. All the systems presented **suitable hydrodynamic properties** for their use in biological applications: hydrodynamic sizes below 150 nm, surface charges nearly neutral and spherical morphology. The **encapsulation efficiency was dependent on the drug hydrophobicity**, achieving the highest values for CLX followed by TNX and DEX.
- Biological studies on the developed CLX and DEX-loaded NPs showed a **reduction of the free drug cytotoxicity** in both chondrocytes and macrophages and a wide range of non-cytotoxic loaded NP concentrations. The anti-inflammatory activity of the nanoencapsulated drugs was demonstrated using LPS-stimulated RAW264.7 macrophages and quantifying the release of several inflammatory mediators. On the one hand, TNX-loaded NPs were capable of reducing the *in vitro* release of NO and PGE<sub>2</sub> while CLX and DEX-loaded NPs reduced NO, TNF- $\alpha$ , IL-1 $\beta$ , IL-6 PGE<sub>2</sub> and IL-10. Ultimately, all loaded NPs demonstrated excellent ***in vivo* biocompatibility** when subcutaneously injected in rats.
- **Advanced viscosupplements** were developed based on HA hydrogels and drug delivery systems. Moreover, MSC derived secretomes have been obtained as an alternative OA therapy.

# Annex I. Characterization Techniques for Emulsion-Based Antioxidant Carriers with Biomedical Applications

Gloria María Pontes-Quero\*, Eva Espinosa-Cano, Daniel Fernández-Villa, Miguel Huerta-Madroñal, María Rosa Aguilar, and Blanca Vázquez-Lasa



**Aboudzadeh M.A. (eds) Emulsion-based Encapsulation of Antioxidants. Food Bioactive Ingredients. Springer**



# Chapter 12

## Characterization Techniques for Emulsion-Based Antioxidant Carriers with Biomedical Applications



**Gloria María Pontes-Quero, Eva Espinosa-Cano, Daniel Fernández-Villa, Miguel Huerta-Madroñal, María Rosa Aguilar, and Blanca Vázquez-Lasa**

### 12.1 Introduction

Depending on the application, emulsions can be developed to have different physical or chemical properties. Their benefit as vehicles of bioactive components such as antioxidants is becoming popular in order to improve, for instance, the stability or bioavailability of the encapsulated compound. An emulsion is a mixture of two immiscible liquids where one of them (i.e. internal or discontinuous phase) is dispersed as droplets into the other liquid (i.e. continuous phase) (Gurpreet and Singh 2018). In the food industry or in biological applications, it is normally interesting to have an aqueous continuous phase while in the cosmetic industry an oil continuous phase is preferred. In order to achieve an efficient encapsulation of antioxidant

---

Gloria María Pontes-Quero, Eva Espinosa-Cano, Daniel Fernández-Villa, Miguel Huerta-Madroñal, contributed equally to the work.

---

G. M. Pontes-Quero (✉)

Group of Biomaterials, Department of Polymeric Nanomaterials and Biomaterials, Institute of Polymer Science and Technology, ICTP-CSIC, Madrid, Spain

Alodia Farmacéutica SL, Madrid, Spain

Networking Biomedical Research Centre in Bioengineering, Biomaterials and Nanomedicine, CIBER-BBN, Madrid, Spain

E. Espinosa-Cano · M. R. Aguilar · B. Vázquez-Lasa

Group of Biomaterials, Department of Polymeric Nanomaterials and Biomaterials, Institute of Polymer Science and Technology, ICTP-CSIC, Madrid, Spain

Networking Biomedical Research Centre in Bioengineering, Biomaterials and Nanomedicine, CIBER-BBN, Madrid, Spain

D. Fernández-Villa · M. Huerta-Madroñal

Group of Biomaterials, Department of Polymeric Nanomaterials and Biomaterials, Institute of Polymer Science and Technology, ICTP-CSIC, Madrid, Spain

molecules, it is important to assess their polarity and stability in either water or oil internal phases. Hydrophobic antioxidants are currently encapsulated into oil/water (O/W) type emulsions whereas hydrophilic ones in water/oil (W/O) or water/oil/water (W/O/W) emulsions depending on the optimal external phase for the application.

Antioxidants are widely used as dietary supplements and have also industrial applications such as food and cosmetic preservatives, or the prevention of metal corrosion. The medical use of antioxidants dates back to the ancient Egyptians although the term *antioxidant* appears in the medical literature in the early nineteenth century; and were first thought to prevent oxidation of unsaturated fats. However, it was in the 1990s when oxidative stress was discovered to play a key role in cell death and, as a consequence, antioxidants became important in medicine (Lobo et al. 2010). The application of antioxidant delivery systems based on emulsions is primarily found in the biomedical and food industries. The antioxidant carrier can be the emulsion itself, having the antioxidant as the dispersed phase, or solid particles fabricated by an emulsification process. In any case, to ensure the successful performance of these antioxidant carriers, knowledge of analytical methods and instruments to characterize them is needed. In this chapter, different characterization techniques have been discussed. The chapter has been organized attending to the physicochemical property of the antioxidant carrier under study. Although there are numerous emulsion-based systems that could be described, this chapter makes emphasis on emulsion-based carriers used in the biomedical field (Fig. 12.1).

Regarding the fact that emulsions are thermodynamically unstable in nature, it is necessary to study their long-term stability as one of the most important properties governing their shelf-life. Here, emphasis has also been placed on droplet size, morphology and structure as they are crucial parameters that can dramatically affect factors such as stability of antioxidant emulsion systems. The study of the antioxidant activity of the system is also essential to ensure the antioxidant performance of the system. Moreover, the rheological properties of the antioxidant emulsion depend on both the dispersed and continuous phases, and can affect the emulsion stability, making necessary its study and understanding. Finally, both sterility and cytotoxicity issues are of pivotal relevance when the carriers have been designed to be used on humans, in order to ensure the safety of the antioxidant system.

## 12.2 Size and Zeta Potential

One of the key parameters of any antioxidant carrier is the assessment of the particle size. Most emulsion droplets have a mean diameter of  $>1\ \mu\text{m}$  but mini- and nano-emulsions can be also formed with droplet sizes in the 100–500 nm range. The most commonly used technique for size analysis of antioxidant emulsion droplets is light scattering (static or dynamic light scattering). This method measures droplet sizes by detecting the percentage and angle of back-scattered light when a

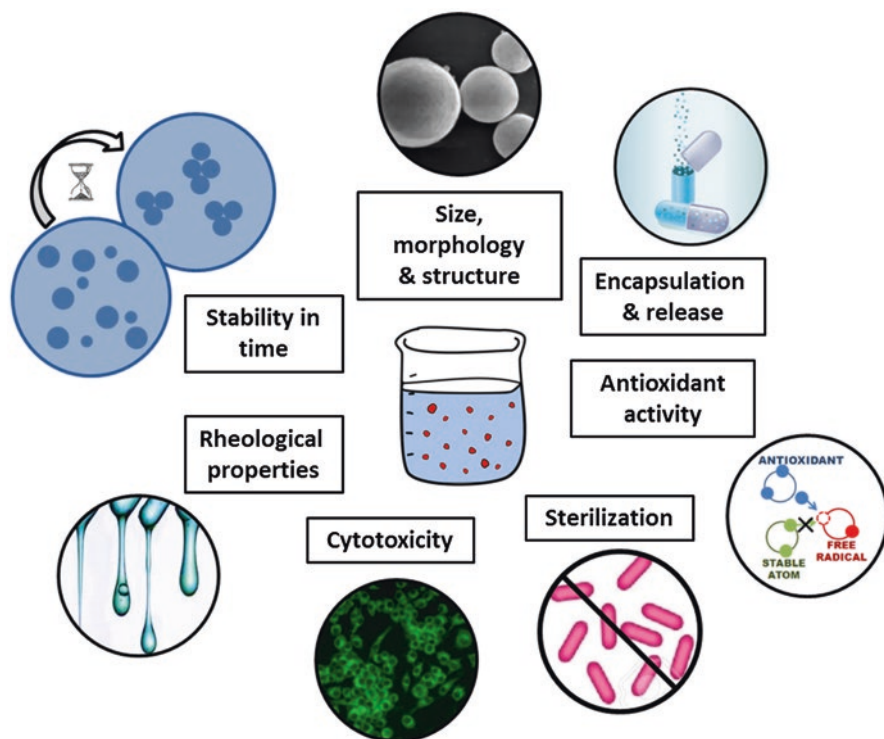


**Fig. 12.1** Scheme of the main properties of emulsion-based antioxidant carriers

monochromatic beam of near infrared light is directed through the sample (Hu et al. 2017). In particular, static light scattering (SLS) measures the intensity of the scattered light as a function of the scattering angle or concentration. On the contrary, dynamic light scattering (DLS) measures the time-dependent fluctuations in the scattered light intensity, which allows the determination of the translational diffusion coefficients (i.e. Brownian motion). Hence, by assuming that smaller particles show faster Brownian motion than larger ones and create a larger rate of intensity fluctuations, it is possible to determine particle/molecular size (Stetefeld et al. 2016). SLS allows determining the particle size within the range of 100 nm to 1000  $\mu\text{m}$ , whereas DLS is used to detect particles of 1 nm to 5  $\mu\text{m}$  in size (McClements 2007). As a clear example of the usefulness of light scattering methods to characterize emulsions and optimize formulations, Acevedo-Fani et al. measured the size distribution as a function of the surfactant concentration by DLS. They formulated single layer and multilayer emulsions based on lactoferrin and alginate containing the antioxidant resveratrol. They used DLS to optimize the size distribution of emulsion droplets to avoid aggregation phenomena by modifying lactoferrin concentration (Acevedo-Fani et al. 2017). The main disadvantage of traditional light scattering methods is that they do not provide accurate measurements for concentrated emulsions (Hu et al. 2017), and some authors draw on diluting the

emulsions before measuring (Acevedo-Fani et al. 2017; Tian et al. 2019). In order to avoid artifacts because of multiple scattering, 3D cross-correlation light scattering can be used. This technique performs two light scattering experiments at the same time, with the same scattering vector and sample volume in order to obtain common information to both (Block and Scheffold 2010).

Other less common techniques for droplets size analysis include electrical pulse counting, nanoparticle tracking analysis (NTA), single particle optical sizing (SPOS) and ultrasonic spectrophotometry. They present some advantages when compared to light scattering techniques. On the one hand, electrical pulse counting, NTA and SPOS allow measuring size of individual droplets, one at a time, leading to a more precise size distribution analysis but requiring significant dilution of samples. On the other hand, ultrasonic spectrophotometry does not require sample dilution, providing an interesting alternative when highly concentrated samples are under investigation (Hu et al. 2017). Microscopic techniques such as scanning electron microscopy (SEM) and transmission electron microscopy (TEM) are also used to measure size of antioxidant carriers. These techniques will be discussed in detail in Sect. 12.3.3.

The surface charge (zeta potential) of the carrier is also an important parameter to be studied. The microelectrophoretic technique is the most commonly used method to measure surface charge of emulsion droplets encapsulating antioxidants. In this technique, a certain voltage is applied across two oppositely charged electrodes at either end of a cell containing the emulsion. Then, charged droplets start moving towards oppositely charged electrode at a certain velocity ( $v$ ). The charge sign is determined by the direction of the motion and the charge magnitude by the velocity. Light scattering measurements allow determining both, direction and velocity of particles displacement by observing the Doppler shift, which is defined as the change in the frequency of light scattered by moving particles; the faster the motion, the higher the shift in frequency in the scattered light (Fig. 12.2) (Uskoković 2012).

At low Reynolds numbers, electrophoretic mobility,  $U_e$ , is defined as the ratio between measured particle velocity ( $v$ ) and the applied electric field ( $E$ ) (Eq. 12.1):

$$U_e = \frac{v}{E} \quad (12.1)$$

From that, the zeta potential is computed using Smoluchowski's mobility equation (Eq. 12.2):

$$U_e = \frac{\varepsilon_r \varepsilon_0 \xi}{\eta} \quad (12.2)$$

where  $\varepsilon_r$  is the dielectric constant of the dispersion medium,  $\varepsilon_0$  is the relative permittivity of free space and  $\eta$  is the dynamic viscosity of the dispersion medium (Ja'afar et al. 2015). The main disadvantage of this technique is the same as for other light



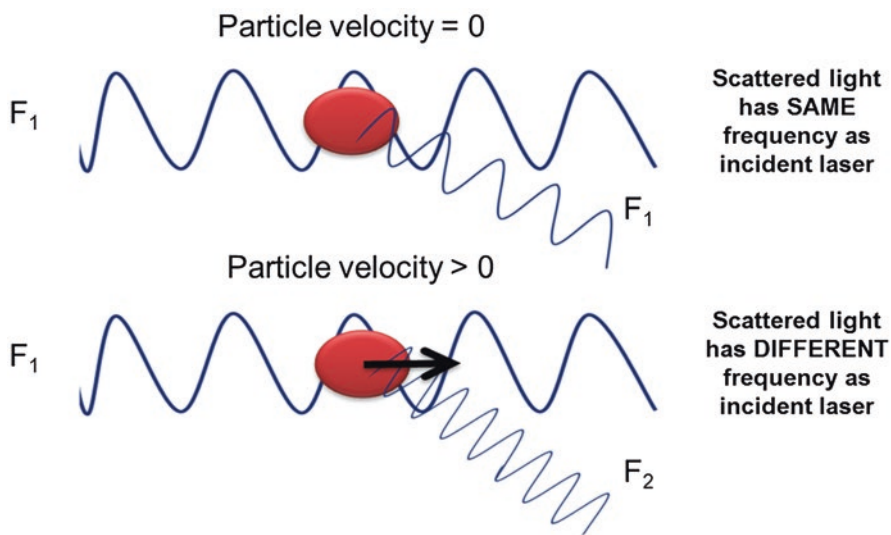


**Fig. 12.2** Scheme showing that the frequency of scattered light ( $F_1$ ) will be the same as the incident laser ( $F_1$ ) for stationary particles, but different ( $F_2$ ) if the particles are moving

scattering techniques; diluted samples are required to avoid multiple scattering effects (Hu et al. 2017).

## 12.3 Morphology and Structure

### 12.3.1 Optical Microscopy

The study of the morphology and the structure of the particles is one of the key parameters when characterizing emulsion-based antioxidant carriers. Optical microscopy is the traditional form of microscopy which employs lens and visible light to closely observe a sample. Optical microscopes, also known as light microscopes, use one or a series of lenses that are placed between the eye of the observer and the specimen to magnify the image of the probe. It is the most used technique to analyze morphology and structure of emulsions because of its simplicity, reduced cost and availability in most research facilities. However, it presents several limitations, most of them related to its relatively limited resolution when compared to other microscopy techniques and poor image contrast (Table 12.1) (Di Gianfrancesco 2017). For instance, using optical microscopy, it could be sometimes difficult to distinguish the nature of emulsion systems (whether they are made of proteins, polysaccharides...). Moreover, due to the similar refractive indexes of different components, contrast among them may be often too low. To solve these issues,

**Table 12.1** Main characteristics of optical microscopy, SEM and TEM

	Optical microscope	SEM	TEM
Source	Light beam	Electron beam	Electron beam
Resolution limit	$\sim 2\ \mu\text{m}$	$\sim 2\ \text{nm}$	$\sim 0.2\ \text{nm}$
Thickness of specimen	Thin	Small enough to fit in the chamber of the scope and coated in metal atoms	Ultra-thin and coated in metals atoms
Image	2D, including intracellular visualization	3D and surface image	2D, including intracellular visualization
Sample	Alive or dead	Dead	Dead
Other requirements	Do not need vacuum and reduced cost	Need vacuum, expensive	Need vacuum, expensive

stains or dyes, as well as optical microscopes with specialized features, can be used to improve image contrast. Dyes or chemical stains are often added to emulsions or dissolved in one of the phases before imaging, allowing to highlight a certain component of an emulsion and to facilitate its observation. Nevertheless, interactions between a compositional material and the coloring agent may occur affecting the emulsion so, chemical stains are not always suitable. Moreover, phase contrast or differential interference contrast microscopy can solve this problem converting small differences in the refractive index into meaningful differences in light intensity (Murphy 2001).

### 12.3.2 *Confocal Laser Scanning Microscopy*

This microscopy technique was developed to improve the optical resolution and contrast of traditional wide-field fluorescence microscope. Employing a point-illumination operation mode at the confocal plane, confocal laser scanning microscopy can eliminate out-of-focus light overcoming the limitation of conventional fluorescence microscopy (Pawley 2006). In addition, it allows obtaining three-dimensional images and surface profiles of samples using its scanning feature. However, this microscopy requires longer exposure time for enough signal intensity, being therefore not desirable, for instance, for samples that are sensitive to light (Hu et al. 2017). Samples that do not naturally fluoresce require the incorporation of a fluorescent agent in order to clearly differentiate continuous and disperse phases in this type of microscopy (Fig. 12.3).

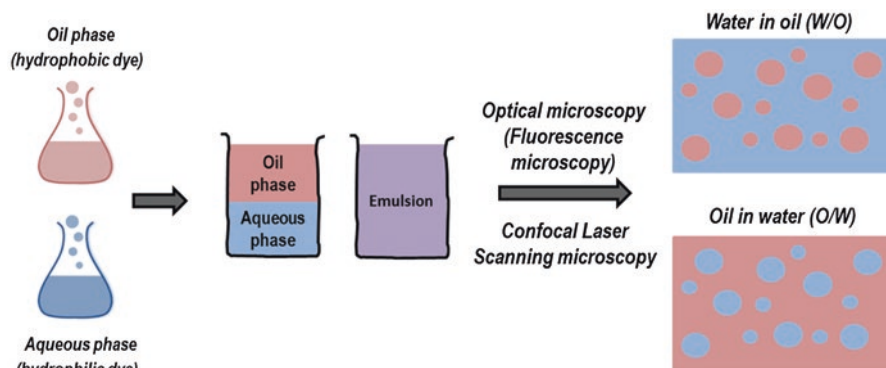


**Fig. 12.3** Emulsion microstructure characterization by confocal or fluorescent microscopy using a fluorescent dye

### 12.3.3 Electron Microscopy

Electron microscopy is one of the most powerful imaging techniques used to investigate the morphology and microstructure of particles formed by emulsification. There are two types of electron microscopy: SEM and TEM. Both of them use a beam of electrons to obtain high-resolution images of the specimen even if the working principle is different (see Fig. 12.4). SEM is used to scan the sample with an electron beam that interacts with the atoms of the specimen, giving rise to information about its surface topography and composition. On the other hand, TEM relies on the transmission of electrons through the sample, which allows microstructure fine details and crystalline state study. Because of this, samples studied by TEM should be thin enough not to hinder electron transmission (Meroni and Raikos 2018).

In the next subsection, a more detail information about the working principle and pros/cons of SEM and TEM are given.

#### 12.3.3.1 Scanning Electron Microscopy (SEM)

SEM is one of the most used techniques for the analysis of antioxidant delivery or carrier systems as it can produce high-resolution images (limited to ~0.5 nm) of the surface of a sample. SEM images are formed by back-scattered electrons and secondary electrons generated during the interaction of primary electrons with the sample. Back-scattered electrons are incident high-energy electrons that are scattered after interaction with the sample, while secondary electrons are produced because of excitation of specimen atoms during sample irradiation. Back-scattered electrons provide both, compositional and topographic information of the sample. On the other hand, secondary electrons are used for topographic analysis, being able to resolve surface structures down to the order of 10 nm or better (Zhou et al. 2007). Since the basis of SEM relies on surface processes rather than electron

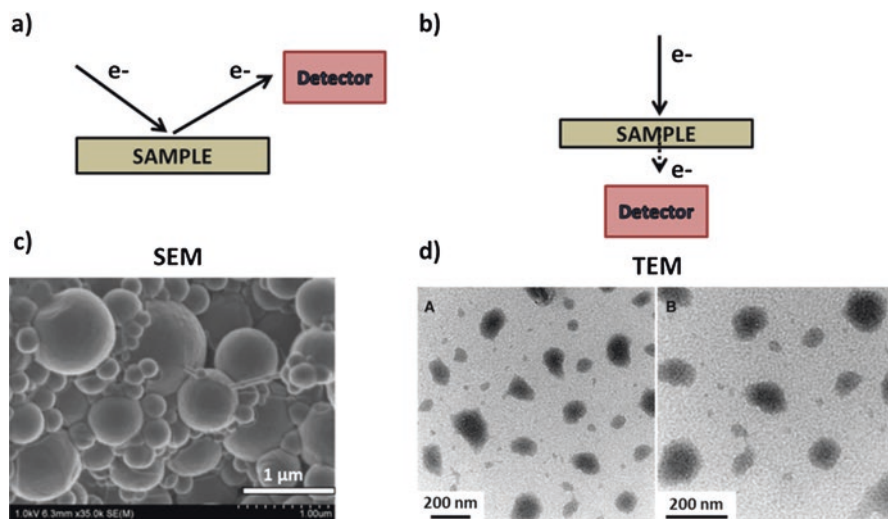


**Fig. 12.4** Schematics of (a) SEM and (b) TEM electron-based image formation and (c) SEM micrograph of curcumin-loaded PLGA (poly(D,L-lactide-co-glycolide) nanoparticles prepared by single emulsion solvent evaporation (d) TEM micrograph of an O/W nanoemulsion containing curcumin. (Reprinted from the references (Umerska et al. 2018) and (Joung et al. 2016) with permission)

transmission, it offers the possibility to obtain three-dimensional images, useful feature for topographic sample analysis. Another advantage is the large field of analysis that can be examined at a glance by SEM. Nevertheless, it is an expensive technique that requires high vacuum and sample conductivity (see Table 12.1).

Xiuhua et al. used SEM to observe and compare raw silymarin and silymarin nanoparticles. While the first one displayed irregular form and different particle size, silymarin nanoparticles were nearly spherical and smaller in size (Xiuhua et al. 2016). Hee et al. studied the influence of different preparation conditions on the shape and morphology of virgin coconut oil microcapsules. They concluded that morphology was independent of the amount of antioxidant loaded since microcapsules with the highest and lowest encapsulation efficiencies were almost identical. In addition, they showed that virgin coconut oil was dispersed in the wall matrix as small droplets and had a homogeneous core distribution (Hee et al. 2017).

### 12.3.3.2 Transmission Electron Microscopy (TEM)

TEM is the other electron microscopy normally used to characterize delivery or carrier systems. In this case, the electron beam is achieved by focusing electrons with metal apertures and electromagnetic lens, which allow only electrons within a small range of energy to pass through. Then, the electron beam is applied to the specimen and transmitted electrons are collected on a screen to form the image (Tang and

Yang 2017). The main advantage of electrons is their small wavelength that guarantees a good resolution (0.2 nm) and, consequently, TEM is a preferable option for detailed characterization of nanoscale samples (see Table 12.1). However, TEM has several disadvantages. The specimen may be damaged by the electron beam and as small sample thickness is required to allow electron transmission, which in some cases could be expensive and time-consuming. Additionally, the atmosphere in a TEM column should maintain a high vacuum to enhance the electron transmission (Hu et al. 2017). There are several examples in literature in which TEM is used to examine and characterize the size and shape of the dispersed phase of antioxidant emulsions. Xiuhua et al., Zhang et al. and Hatanaka et al. used TEM to corroborate nanoparticle size profiles determined by DLS, as well as their spherical shape (Hatanaka et al. 2010; Xiuhua et al. 2016; Zhang et al. 2017b).

Cryo-TEM, which is a type of TEM where samples are frozen to cryogenic temperatures, can also be used to study antioxidant carriers. For example, Cheng et al. studied the structural details in the interaction of molecules and emulsions using this technique (Cheng et al. 2014). In this case, they used cryo-TEM to confirm the adsorption of antioxidant peptides at the interface of soybean O/W emulsions.

### 12.3.4 Atomic Force Microscopy (AFM)

AFM is a microscopy technique that allows high-resolution images of flat sample surfaces. It is based on the raster scanning of a sample previously immobilized with a force-sensing cantilever ended in a sharp tip. AFM uses the force that acts between the tip and sample as the imaging signal (Silva et al. 2012). There are two operating modes of AFM: static and dynamic. In static AFM, the force is translated into a deflection of the cantilever, while in the dynamic mode, the cantilever is deliberately vibrating. Since experimental realization of static AFM is difficult, the dynamic operating mode allows the topographic study of samples without direct contact. Dynamic AFM can be based on amplitude (AM-AFM or tapping mode) or frequency modulation (FM-AFM) in which variations on the amplitude or frequency of the oscillation tip respectively, are used as the feedback signal to image sample topography (Etzler and Drelich 2012; Giessibl 2003). The most common AFM imaging mode is the tapping mode that gives two types of images, a height or topographic image and a phase image, which identifies surface features that cannot be identified with the topographic image (Etzler and Drelich 2012).

AFM offers some advantages compared to SEM and TEM. Sample preparation is not needed, for example, in terms of sample metallization or sample thickness requirements; and the same probe can be manipulated and used several times. In addition, the dynamic mode based on amplitude modulation of AFM allows imaging under physiological conditions, since micrographs of liquid samples in air can be obtained. However, sample damage can appear when operating in the static mode with soft or sticky samples, as the tip is in direct contact with the surface of the probe (Hu et al. 2017).

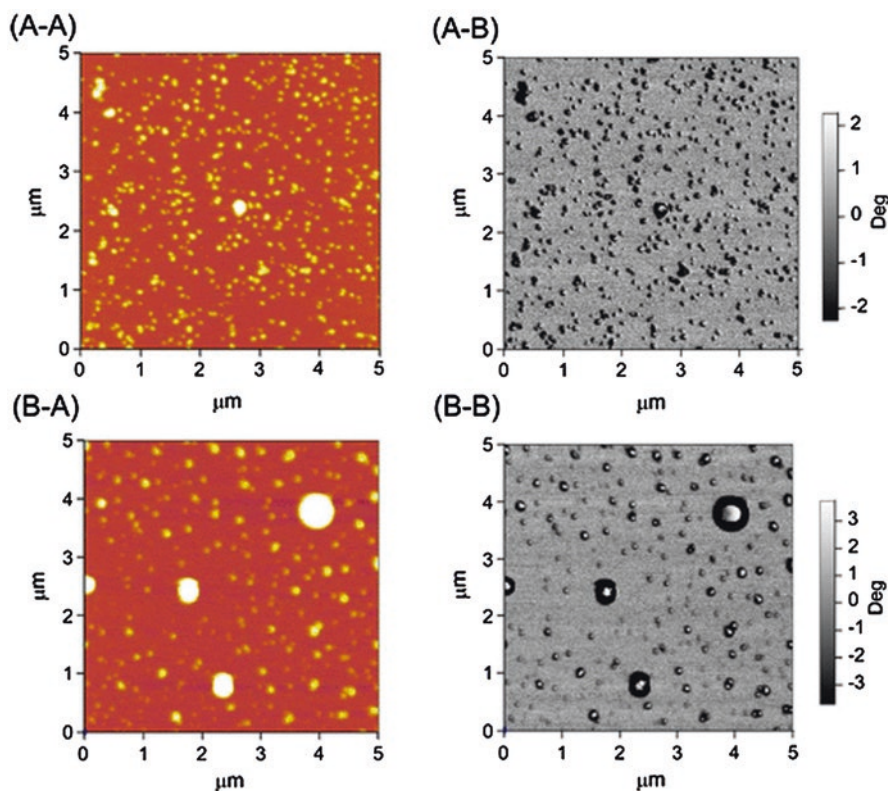


**Fig. 12.5** AFM images of fresh soybean O/W emulsions (10% w/w oil) prepared with 11.1 mg/mL Tween 20 + 20 mg/mL PPH using height retrace mode (A-A) and phase retrace mode (A-B) or with Tween 20 only using height retrace mode (B-A) and phase retrace mode (B-B). (Reprinted with permission from (Cheng et al. 2014). Copyright 2014 American Chemical Society)

For instance, Cheng et al. showed the influence on size and distribution of oil droplets when using Tween 20 or combining it with potato protein hydrolysate (PPH), demonstrating that their cooperativity enabled better oil droplets distribution in aqueous phase (Fig. 12.5) (Cheng et al. 2014). Nikolic et al. used AFM to determine morphological properties, perform microstructural studies and confirm mean droplet size of curcumin-loaded nanoemulsions (Nikolic et al. 2018). Also, spherical shape and sizes of 200 nm were observed by Del Prado et al. using AFM on nanoparticles encapsulating curcumin (Del Prado et al. 2019).

### 12.3.5 *Fourier Transform Infrared (FTIR) Spectroscopy*

In order to study the chemical structure and composition of antioxidant carriers, the FTIR technique could be used. FTIR is based on an infrared radiation (IR) passing through a sample, where most of it is absorbed, while some of it is transmitted. The



infrared region goes from 12800 to 10  $\text{cm}^{-1}$  and is divided into near-IR (14000–400  $\text{cm}^{-1}$ ), mid-IR (4000–400  $\text{cm}^{-1}$ ) and far-IR (400–10  $\text{cm}^{-1}$ ). Molecules absorb these specific frequencies of light since they correspond to the frequency of vibration of the bonds in the molecules. Each sample presents characteristic absorption peaks that correspond to the frequencies of vibration between the bonds of the atoms of the material. As a result of IR absorption, changes in the dipole moment of molecule's bonds occurs, leading to vibrational transitions which give rise to characteristic absorption peaks. The intensity of IR absorption bonds give information about molecular components and structure (Pallua et al. 2011).

The size of the absorption peaks depends on the quantity of a specific bond in a sample, and since materials are composed by a unique combination of atoms, there are not two exact absorption spectrums. For this reason, this technique can be used not only to identify the chemical composition of a compound, but also to detect the amount of different species in a mixture, as well as the interaction between components through particular functional groups. In the same manner, changes in chemical structures, bond formation or cleavage, can be also monitored by FTIR, as they will give rise to different absorption peaks. Therefore, the major advantages of FTIR are the possibility to identify and distinguish compounds in a mixture and evaluate their structure, the small time required for the analysis and its high sensitivity and reproducibility (Jin et al. 2016).

There are several modes in IR spectroscopy. Traditionally, the transmission mode, in which the signal intensity is often expressed as absorbance, was used to obtain surface information, although it requires sample preparation. Solid materials normally have to be diluted with the IR-inactive KBr and pressed to form the KBr pellets, while liquid samples need to be filled into a liquid cell with a suitable path length. Nowadays, IR-measurements are mainly performed in the ATR (Attenuated Total Reflection) mode since this technique is simpler and faster to use. All types of samples are placed undiluted on the ATR crystal, avoiding spectra variations due to sample preparation. Another method is specular reflectance IR, a non-contact and non-destructive mode that works on the principle that every sample has a refractive index that varies with the frequency of light to which it is exposed (Ammar et al. 2015; Beasley et al. 2014). Consequently, by examining the change in the refractive index at different frequency bands, users can make assumptions regarding the absorptivity of the sample.

Because of this, FTIR has been widely used in the last years, for instance, to characterize antioxidant particles formed by emulsification processes. Su et al. showed that the primary interactions between  $\beta$ -lactoglobulin nanoparticles and (-)-Epigallocatechin-3-gallate occurred via hydrogen bonding and hydrophobic effects by FTIR (Su et al. 2020). Also, Shaddel et al. took advantage of FTIR to confirm the chemical cross-linking reaction in the encapsulation of anthocyanins with gelatin and gum Arabic (Shaddel et al. 2018). Finally, conformational changes of phosvitin-resveratrol complexes in microemulsions were observed by Duan et al. employing this infrared spectroscopy (Duan et al. 2016).

### 12.3.6 X-Ray Diffraction (XRD)

Other technique used to investigate the structural characteristics of antioxidant carriers is X-Ray Diffraction (XRD). XRD is a non-destructive analytical technique used to obtain information about the crystallographic structure, chemical composition and physical properties of materials. XRD is based on the observation of the scattered intensity of an X-ray beam hitting a sample as a function of incident and scattered angles, polarization and wavelength (Jin et al. 2016). X-rays are a form of light with wavelengths in the range of 0.01–10 nm. When X-rays scatter from a substance with structure at the nanoscale, interference can take place, giving rise to a pattern of higher and lower intensities. Thus, the result is a diffraction pattern that does not superficially resemble the underlying structure but provides information about the internal structure on length scales from 0.1 to 100 nm.

XRD is mostly used for the identification of crystalline compounds by their diffraction pattern, but in the context of antioxidant carriers formed by emulsification processes, it is a powerful technique that can be used to report the encapsulation of a molecule comparing the diffraction pattern of loaded and unloaded systems, perform stability studies or analyze crystallographic structures of different formulations. Several examples can be found in the literature. Behbahani et al. confirmed curcumin encapsulation in solid lipid nanoparticles produced by micro-emulsion and ultrasonication (Behbahani et al. 2017); Xiuhua et al. evaluated the occurrence of structural changes of silymarin nanoparticles upon modification of several parameters of the nanoemulsion experiment (Xiuhua et al. 2016); and Shaddel et al. analyzed the stability of microencapsulated anthocyanins performing crystallinity studies by XRD (Shaddel et al. 2018). In this last study, gelatin-gum arabic microcapsules showed a semi-crystalline structure in contrast to the core material, which was amorphous as it did not show any peak between  $2\theta$  of  $10^\circ$  and  $80^\circ$ . In fact, microcapsules exhibited a reduced peak in the same range as gelatin and gum arabic confirming its semi-crystalline structure and higher stability than non-encapsulated anthocyanins.

## 12.4 Emulsion Stability

As previously mentioned, emulsions are conformed by two immiscible liquids (continuous and dispersed phases). The polarity difference of internal and external phase liquids makes emulsions thermodynamically unstable, meaning that if the two phases are allowed to stand for long enough time, they will eventually separate (Weiss 2002). Depending on the application, instability of emulsions may lead to different undesirable effects. For instance, unstable emulsions used as drug delivery systems may lead to severe adverse side effects (Ujhelyi et al. 2018) whereas in the food industry instability can decrease the product quality and shorten shelf life (Akbari 2018). Therefore, it is crucial to understand the mechanism that causes



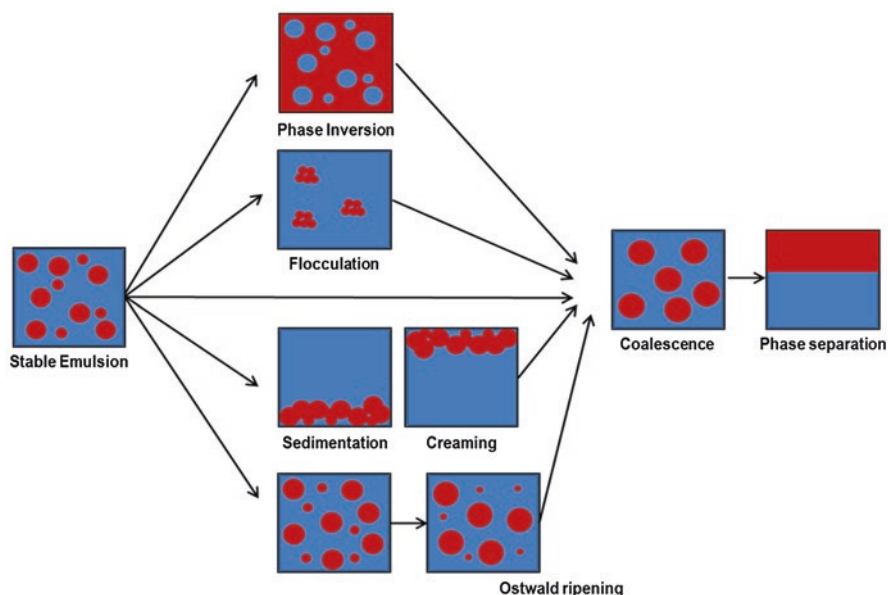


**Fig. 12.6** Schematic representation of instability mechanisms in the emulsion system

emulsion instability and carefully evaluate the stability of such systems. The main mechanisms that cause emulsion instability are gravitational separation (creaming/sedimentation), flocculation and coalescence (aggregation phenomena), Ostwald ripening (change of an inhomogeneous structure over time), and phase inversion and they are summarized in Fig. 12.6 (Hu et al. 2017).

Emulsions stability is influenced by droplet concentration, size, morphology, surface charge, phase-phase interactions, and rheological behavior (Hu et al. 2017). In addition, emulsion stability can be affected by a number of external factors like temperature, pressure or pH (Weiss 2002). This section focuses on the most common used methods to assess emulsion stability.

### 12.4.1 Visual Observation

Visual observation of the emulsion is the simplest, quickest and cheapest method to assess gravitational separation (i.e. sedimentation or creaming). Sedimentation occurs if the internal phase presents higher density than the continuous phase causing droplets to accumulate at the bottom, whereas creaming occurs when droplets move upwards because they present lower density than the continuous phase. For example, Carpenter et al. clearly observed creaming effects after 21 days storage of curcumin-loaded emulsions (Carpenter et al. 2019). However, visual observation does not allow studying other instability phenomena as well as droplets smaller than

100  $\mu\text{m}$ . Thus, the study of emulsion stability usually requires more expensive analytical instruments.

### ***12.4.2 Microscopy***

Droplets and instability phenomena that cannot be observed at naked eye (i.e. diameter below 100  $\mu\text{m}$ ) are observed by microscopic techniques. For example, flocculation can be easily identified when droplets start to get close to each other without merging into unique larger ones. By contrast, Ostwald ripening and coalescence are observed as droplets start fusing together leading to larger droplets or droplets with heterogeneous size distributions. Normally, to test the antioxidant emulsion stability, microscopy is combined with other techniques. The study of the evolution of particle size and size distribution in time using microscopy in combination with particle-sizing techniques like DLS will give more precise information about instability mechanisms. For instance, optical microscope images at 0 and 21 days were taken to confirm stability of rosemary extract-loaded emulsions regarding Ostwald ripening and coalescence that was already observed by DLS size analysis (Erdmann et al. 2015).

### ***12.4.3 Particle Size, Polydispersity and Concentration Analysis in Time***

Gravitational separation (i.e. sedimentation and creaming) can be studied by determining time evolution of the size and concentration of droplets at different regions of the sample under specific external conditions (temperature, time, pH) (Hu et al. 2017). Flocculation or coalescence is characterized by an increase in mean size and polydispersity of sample size distribution with time. Several examples of stability evaluation by measuring size at different time points are found in the antioxidant emulsion literature. For example, Chen et al. described curcumin-loaded O/W emulsion with improved stability in time when compared to the free drug. Significant changes in size occurred at longer time points when curcumin was loaded on emulsion droplets as compared to free curcumin (Chen et al. 2016).

### ***12.4.4 Surface Charge or Zeta Potential Analysis***

Surface charge is another key factor affecting stability of emulsions. Emulsion droplets with surface charge or zeta potential of equal sign experience electrostatic repulsive forces (Hu et al. 2017). A higher surface charge leads to stronger

electrostatic repulsion and, hence, reduces the probability of aggregation. Flocculation is more likely to happen in the presence of weak attractive forces whereas strong attractive forces can lead to fusion of droplets or coalescence. A zeta potential greater than |30 mV| is considered sufficient for stabilization (Gurpreet and Singh 2018).

pH and ionic strength of the emulsion are key variables affecting ionization and surface charge of droplets, especially if ionizable groups are exposed on their surface (Emerenciano et al. 2019). Consequently, the influence of these variables in stability is commonly reported (Uskoković 2012). In some cases, electrostatic stabilization is not sufficient for droplet stabilization and they need to be stabilized via steric or electrosteric mechanisms, usually by means of surfactants. For instance, Peng et al. demonstrated that pH had a significant effect on mean particle size of capsaicin-loaded O/W emulsions (Peng et al. 2018). Moreover, they demonstrated that the effect on size was dependent on the ionic nature of the employed surfactant. Using non-ionic surfactants, they observed an increase in size at lower pH while a decrease in size was observed when using lecithin, a surfactant containing ionizable anionic phospholipid groups at acidic pH. As previously said, antioxidant emulsions are primarily used in the food industry or biomedical applications and, therefore, surface charge and stability are studied at pH values close to physiological pH (Chen et al. 2016; Emerenciano et al. 2019).

Normally, authors determine antioxidant emulsion stability by combining visual observation, size analysis techniques and/or zeta potential determination at different time points and at specific conditions depending on the application. For instance, Acevedo-Fani et al. monitored the mean droplet size and zeta-potential of a resveratrol-containing emulsion at room temperature and applied light to simulate common food storage conditions (Acevedo-Fani et al. 2017). Similarly, when antioxidant emulsions are used for medical applications size and zeta-potential changes are evaluated in time at physiological conditions (Rinaldi et al. 2017).

#### **12.4.5 Emulsion Stability Index – Volumetric Method and BS (Back-Scattering) Method**

Emulsion stability index (ESI) can reflect the ability to resist instabilities of O/W or W/O/W emulsions (Choi et al. 2014; Tian et al. 2019). It gives an estimation of emulsion stability after a determined period of time (Tian et al. 2019). It can be either determined by the firstly described volumetric method (Eq. 12.3) which is based on visual observation or by, the formerly described, back-scattering (BS) method (Eq. 12.4) which is based on the absorbance and back-scattering of light, as it passes through the colloidal suspension. Good correlation has been reported between both methods (Choi et al. 2014):

$$ESI(\%) = \left( 1 - \frac{V_w}{V_e} \right) \times 100 \quad (12.3)$$

where  $V_e$  is the volume of the o/w emulsion and  $V_w$  is the volume of the separated bottom layer after the desired storage period.

$$ESI(\text{min}) = \frac{A_0}{\Delta A} t \quad (12.4)$$

where  $A_0$  is the absorbance of the emulsion right after homogenization,  $\Delta A$  is the change in absorbance after time  $t$  (i.e.  $(A_t - A_0)$ ) and  $t$  is the time interval.

The main advantage of determining ESI by the BS method is that it is an optical non-destructive method and, therefore, no sample dilution is needed; and it provides useful information about aggregation phenomena (flocculation and coalescence) during destabilization methods (Choi et al. 2014). Tian et al. recently used BS method to determine ESI of a tea polyphenol-containing O/W emulsion on a 60 minutes time interval (Tian et al. 2019). They demonstrated that emulsion stability was highly dependent on droplet concentration.

### 12.4.6 Thermal Stability

Temperature has also an influence on antioxidant emulsion stability and antioxidant encapsulation efficiency, degradation or loss of function. That is why stability upon temperature change is also studied by the already described visual, microscopic or hydrodynamic properties monitoring methods. As an example, Sunee et al. visually demonstrated stability of xanthone-loaded microemulsion at room temperature, 45 °C and after 2 months of temperature cycles of 4 °C (48 hours) to 45 °C (48 hours). However, they observed precipitation when storing the emulsion at 4 °C attributed to the lower solubility of xanthone at low temperatures (Sunee et al. 2017).

A common technique also used to study antioxidant emulsion thermal stability is Differential Scanning Calorimetry (DSC) (Silva et al. 2012). DSC is a thermoanalytical technique that allows measuring the thermodynamic parameters associated with thermally induced phase transitions of a sample when compared to a reference material, which does not undergo a phase transition within the temperature range under investigation. Initially, an equal amount of heat is linearly applied to the sample cell and the reference cell, maintaining at zero their differential temperature. Whenever the sample undergoes a temperature induced phase transition, a portion of the heat applied is absorbed or released, leading to a temperature differential between sample and reference material. This difference is detected by the instrumental control system that supplies higher or lower amount of heat to the sample cell to maintain the temperature equal to that of the reference cell (McElhaney 1986). Several examples of the use of DSC to study the thermal stability of emulsion-based antioxidant carriers can be found in the literature. Shaddel et al. proved high thermostability and long residual action of anthocyanins after emulsion-based

encapsulation (Shaddel et al. 2018), while a decrease in thermostability of resveratrol-phosvitin microparticles was assessed by Duan et al. comparing DSC profiles of different formulations (Duan et al. 2016).

### ***12.4.7 Accelerated Stability Tests***

Sometimes, stability of emulsions is tested in accelerated conditions in order to shorten the long term storage studies. The most commonly used methods in the field of antioxidant emulsions are centrifugation and dilution stability tests. Centrifugation stability tests, also called phase separation methods to assess stability, consist of centrifugation of the emulsion at a specific frequency of rotation for a specific time (e.g. 10,000 rpm for 10 minutes) and, then, the investigation of the phase (Rashid et al. 2018). Dilution stability tests are usually needed to ensure that the stability of the emulsion is not compromised by a phase inversion when dilution of the system occurs, for instance, when in contact with blood in case of drug delivery systems (Emerenciano et al. 2019).

## **12.5 Rheological Properties**

Rheological analysis, which is the science of material deformation and flow of antioxidant carrier emulsions, is essential for the design of these systems, as it plays a major role in product stability and performance (Derkach 2009). This characterization is performed with different types of rheometers such as shear rheometers, which control the applied shear stress or strain; or extensional rheometers, that control extensional stress or strain. They provide information about flow behavior, viscosity, yield stress or elastic and loss moduli. The composition and characteristics of both dispersed and continuous phases of an emulsion, play a key role in the rheological behavior of the emulsion (Fig. 12.7) (Kim and Mason 2017). Viscosity and other flow parameters of emulsions can relate to other properties such as the dispersed phase volume fraction, the nature of the continuous phase, the droplet size and morphology, the presence of emulsifiers/surfactant or the colloidal interactions (Tatar et al. 2017).

The volume fraction of the antioxidant droplets in the emulsion is one of the most critical aspects determining the emulsion viscosity. As the antioxidant volume fraction increases, the viscosity increases too, since the packaging of more molecules makes flow more difficult (Tatar et al. 2017). This effect has been observed in multiple antioxidant-containing emulsions (Gomes et al. 2016; Gouda et al. 2017; Lonni et al. 2016; Sellimi et al. 2015). Particle size should not have any effect on the viscosity if there are not attractive or repulsive forces between the particles

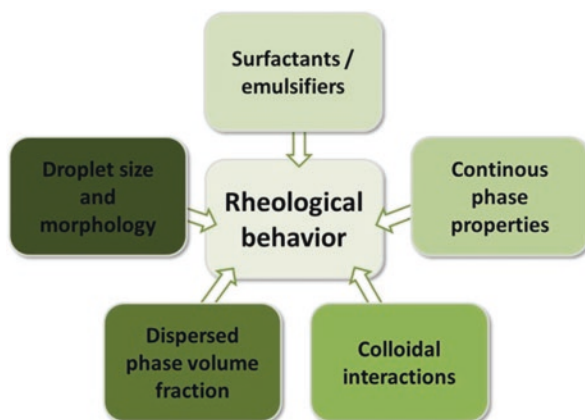


**Fig. 12.7** Possible factors influencing the rheological behavior of antioxidant emulsions

(Tatar et al. 2017). Nonetheless, when particle-particle interactions occur, viscosity may be affected. For instance, various authors explain a reduction or increase in the viscosity of an antioxidant emulsion because of the increased or reduction of droplet sizes, respectively (Chang et al. 2017; Gonzalez et al. 2015).

Loading of an antioxidant into the dispersed phase of an emulsion may also affect the rheological behavior of the system. For example, Gonzalez et al. observed that the incorporation of the lipophilic antioxidant molecule kojic dipalmitate in a multiple emulsion altered the flow behavior from shear-thinning to low-viscosity Newtonian, due to the droplet size reduction occurring with the antioxidant loading, which thinned the flow (Gonzalez et al. 2015). However, other studies have shown that the antioxidant did not exert any change in the flow behavior (Cefali et al. 2015). The amount and nature of surfactants that can be added to stabilize the emulsion system can also alter the emulsion rheology as shown by Peng et al. (2018), who observed that an increase in the water content of the aqueous phase produced a decreased of the emulsion viscosity.

## 12.6 Antioxidant Emulsion Encapsulation and Release

After performing the physicochemical characterization of the emulsion system in terms of size, morphology, structure, rheology and surface charge, it is of crucial importance to confirm the successful antioxidant encapsulation and release of the antioxidant. To evaluate the efficiency of an encapsulating emulsion system, parameters like encapsulation efficiency, release profile and storage stability need to be determined. According to Sunee et al., the antioxidant should be loaded before complete formulation is reached, in order to ensure the highest encapsulation efficacy (Sunee et al. 2017). The amount of antioxidant incorporated within the system is

quantified relative to the original input mass or volume (Eqs. 12.5 and 12.6) (Hu et al. 2017).

$$\text{Encapsulation Efficiency (\%)} = \frac{\text{antioxidant incorporated}}{\text{initial amount of antioxidant}} \times 100 \quad (12.5)$$

$$\text{Loading capacity (\%)} = \frac{\text{mass of antioxidant in the emulsion}}{\text{total mass of emulsion}} \times 100 \quad (12.6)$$

UV/visible spectrophotometry and chromatography are the most common techniques used to determine the antioxidant content in the system and the release kinetics of this compound (i.e. amount of antioxidant within the system at different time points).

### 12.6.1 UV/Visible Spectrophotometry

Antioxidant compounds are normally polyphenols that absorb ultraviolet/visible (UV/VIS) light and can be easily detected by spectroscopic techniques in the range of 200–800 nm. Therefore, UV/VIS spectrophotometry is a non-destructive and rapid technique that can be used for qualitative analysis of compounds that can absorb energy from electromagnetic waves of 200–800 nm, and excite electrons on their surroundings from ground state to excited state. Thereafter, these electrons release the energy to return to their ground state. Depending on their chemical structure, antioxidants would absorb and emit at different specific light wavelengths and, thus, could be differentiated according to their characteristic absorption spectrum. When using this technique, it is important to take caution when choosing the solvent because the absorption spectrum may change depending on it. The UV-VIS absorption is directly related to concentration by the Beer-Lambert law (Eq. 12.7) (Mantele and Deniz 2017).

$$A = \varepsilon \times l \times c \quad (12.7)$$

where  $\varepsilon$  is the molar absorbance coefficient of the antioxidant (L/mol cm),  $l$  is the path length (cm), and  $c$  is the concentration of the antioxidant compound (molarity). Therefore, an increase in absorbance implies an increase in the concentration (Fig. 12.8).

Tang et al. evaluated the release kinetics of resveratrol ( $\lambda_{\text{abs}} = 305$  nm) from an O/W emulsion system at different pH values (Tang et al. 2019). They observed non-significant differences on the amount of released drug at different pH values but a significant improvement was detected when comparing with resveratrol on its free form. In another work, the successful encapsulation of lutein on O/W emulsion systems was assessed by UV spectrophotometry ( $\lambda_{\text{abs}} = 450$  nm), obtaining an encapsulation efficacy ~99.75% and a loading capacity ~48.78%.

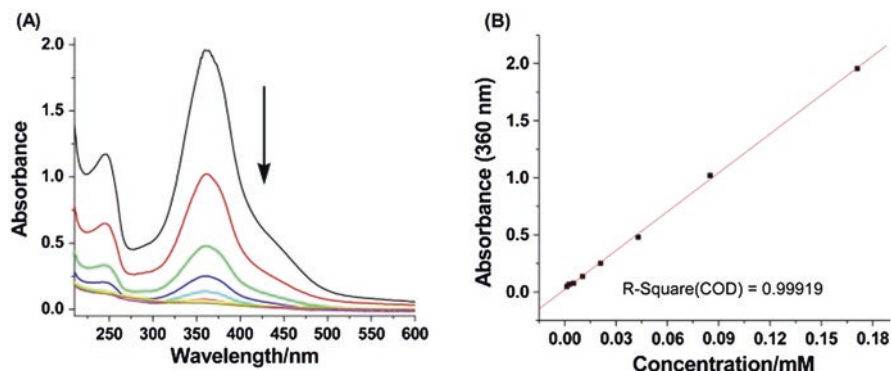


**Fig. 12.8** (a) UV-VIS absorbance of CDAS (a derivative of  $\beta$ -cyclodextrin) in  $H_2O$  at 298 K under different concentrations, and (b) plot of the UV-vis absorbance against the concentration. The absorbance of CDAS was measured at  $\lambda_{\max} = 360$  nm. (Reproduced with permission from the reference (Zhu et al. 2012) (Attribution license: <https://creativecommons.org/licenses/by/4.0/>))

## 12.6.2 Chromatography

Chromatography is the most commonly used technique to determine the concentration of an antioxidant in an emulsion and its release over time. Basically, chromatographic techniques separate compounds in a mixture (mobile phase) by differential retention times on a stationary phase. Compounds can be separated attending to different forces: partition, absorption, ion exchange, size exclusion, or affinity. The mobile phase could be a liquid (liquid chromatography, LC), a gas (gas chromatography, GC) or a supercritical fluid (Coskun 2016).

Among all the available chromatographic instruments, high performance LC (HPLC) is the most commonly used for the quantitative and qualitative analysis of encapsulated compounds. The mobile phase is a liquid, the stationary phase, a solid, and the compounds are separated according to their polarity reaching the detector at different elution times (Hu et al. 2017). Detectors could be (a) universal, which measure any global change in the emerging liquid mobile phase (e.g. infrared, IR, detector), or (b) selective that measure a specific property of the eluting compound (e.g. UV-VIS or fluorescence detector) (Swartz 2010). In UV-VIS detectors, which are the most commonly used, detection of compounds as they come out of the stationary phase is usually done at a specific wavelength (Fig. 12.9). However, several antioxidant compounds can absorb at the same wavelength and separation should be performed in order to quantify different compounds. Therefore, the selection of the stationary/mobile phase is essential for the accuracy of this method. Flow rate is also a crucial variable to achieve proper peak separation (Coskun 2016). At lower flow rates, better peak separation and higher accuracy is achieved. HPLC quantification of antioxidant release or encapsulation efficacy is widely used in literature (Meroni and Raikos 2018). For instance, Sunee et al. introduced xanthone into a microemulsion and successfully evaluated its *in vitro* release by HPLC



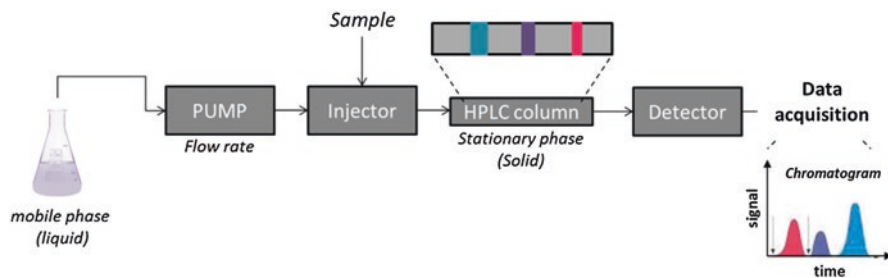


**Fig. 12.9** Scheme of the HPLC technique

measurements with a mobile phase of 100% acetonitrile, flow rate of 1 mL/min at room temperature. The retention time was monitored at  $\lambda = 320$  nm (Sunee et al. 2017).

### 12.6.3 DSC

DSC can also be used to test the encapsulation efficiency. For instance, Rutz et al. used this technique to confirm the high encapsulation efficiency of palm oil and  $\beta$ -carotene into chitosan-based microparticles. Moreover, with thermographs, they suggested a core material protection because of the absence of endothermic events of the encapsulated compounds and predominance of the thermal profiles of the wall materials (Rutz et al. 2016). Evaluation of structural changes at the crystal level of an emulsion is another possible application of DSC. Behbahani et al. demonstrated curcumin solubilization in stearic acid and tripalmitin nanoparticles as the endothermic peak showed by crystalline curcumin disappeared in the nanoparticulated system (Behbahani et al. 2017). Similarly, Xiuhua et al. used DSC to confirm the decrease of crystallinity in silymarin nanoparticles compared to raw silymarin (Xiuhua et al. 2016).

## 12.7 Antioxidant Properties

Oxidative stress can be defined as an imbalance between the production of reactive oxygen and nitrogen species (ROS/RNS) and their elimination by the antioxidant defenses of a biological system. This imbalance can lead to irreversible molecular and cellular damage by the attack of free radicals to the cells (Tan et al. 2018). In humans, oxidative stress is linked to many different diseases such as cancer, obesity, cardiovascular, and degenerative diseases (de Araújo et al. 2016; Matschke et al. 2019). In order to counteract this imbalance, the organism has several endogenous and exogenous antioxidant molecules of enzymatic (superoxide dismutase, catalase

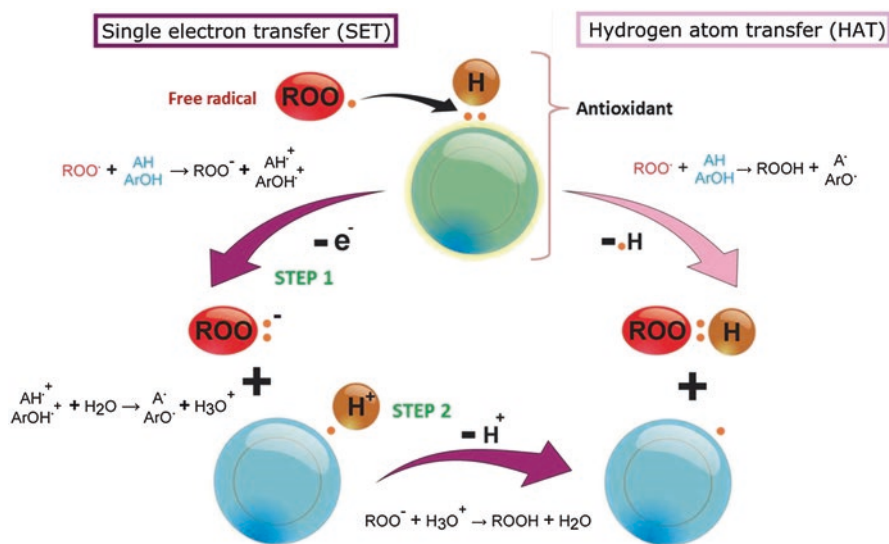


**Fig. 12.10** Schematic representation of single electron or hydrogen transfer methods

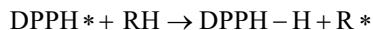
or glutathione peroxide) or non-enzymatic (vitamin A, vitamin C, vitamin E or  $\beta$ -carotene) nature (Liguori et al. 2018).

Various methods can be used to study and compare the antioxidant activity of emulsion-based antioxidant carriers, having each one a specific target. These methods can be classified into two main groups: methods based on a single electron transfer (SET) reaction, where the oxidant is reduced (ABTS and FRAP assays); and hydrogen atom transfer (HAT) methods, where the antioxidant molecule and the substrate compete for free radicals (DPPH, ORAC) (see Fig. 12.10) (Alam et al. 2013; Shivakumar and Yogendra Kumar 2018). Furthermore, in order to get a closer and more realistic insight into the performance of emulsion systems, cellular assays can also be used. For instance, the cellular production of ROS/RNS can be measured using different fluorescent dye-based assays and indirect methods can be used to study damage to DNA, lipids and proteins (Zhang et al. 2017a). In this context, the principal assays used for measuring of the antioxidant capacity of emulsions are described below.

### 12.7.1 DPPH

The DPPH test was first introduced by Blois (1958) and developed by Brand-Williams et al. (1995) and is one of the simplest and quickest methods for the analysis of the radical scavenging activity of a system. The assay measures the ability of an antioxidant system (RH) to reduce the stable free radical

1,1-diphenyl-2-picrylhydrazyl (DPPH\*) through a hydrogen transfer, as represented in the following reaction:



DPPH\*, normally dissolved in methanol, ethanol or isopropyl alcohol, is deep purple in color and turns into pale yellow when radical scavenging occurs. This color change is measured by spectrophotometry at 515–517 nm ( $\lambda_{\text{max}}$  of DPPH\*) where a lower absorbance reading of the sample shows stronger radical scavenging activity (RSA). Finally, the RSA is calculated as stated in Eq. 12.8,

$$\text{RSA}(\%) = \frac{(A_{\text{DPPH}} - A_{\text{SAMPLE}})}{A_{\text{DPPH}}} \cdot 100 \quad (12.8)$$

where  $A_{\text{DPPH}}$  and  $A_{\text{SAMPLE}}$  correspond to the absorbance of DPPH with and without the antioxidant sample, respectively.

### 12.7.2 ABTS

In the ABTS (2,2'-azinobis-(3-ethylbenzothiazoline-6-sulfonate)) or trolox equivalent antioxidant capacity (TEAC) decolorization assay, the relative scavenging ability of an antioxidant system is measured and compared with trolox (an analogue of vitamin E) (Re et al. 1999). In the assay, the radical cation ABTS\* is formed by reacting the ABTS salt with a strong oxidizing compound (e.g. sodium persulfate, potassium permanganate, potassium persulfate). This radical, which is blue-green in color (with absorption maxima at 415, 645, 734 and 815 nm) is converted back to its colorless form when is reduced by a hydrogen-donating antioxidant. The ABTS method is a simple and rapid test, applicable for both hydrophilic and lipophilic antioxidant systems and has good repeatability. As a consequence, it is widely reported for emulsion-based antioxidant systems.

### 12.7.3 FRAP

FRAP (Ferric Reducing Antioxidant Power) is another method to determine the antioxidant capacity of emulsion systems; and was first used to evaluate the antioxidant properties of plasma (Benzie and Strain 1996). The method is based on the reduction at low pH of  $\text{Fe}^{+3}$  tripyridyltriazine to  $\text{Fe}^{+2}$  tripyridyltriazine, a blue complex that gives an absorbance peak at 593 nm, which is proportional to the total antioxidant activity of the system. FRAP has very similar principles to the ABTS assay except that the former is developed under acidic conditions and the latter at neutral pH.

### 12.7.4 ORAC

The Oxygen Radical Absorbance Capacity (ORAC) method is also a spectrophotometric test to quantify the ability of various compounds to quench free radicals. The assay measures the oxidative degradation of a fluorescence probe such as fluorescein in the presence of free radicals generated by azo-initiators like AAPH (2,2'-azobis(2-amidino-propane)dihydrochloride) (Re et al. 1999). The higher the degree of inhibition of fluorescence loss, the higher is the antioxidant activity. The degree of antioxidant-mediated protection is quantified using trolox as a standard.

In Table 12.2, a comparison between the characteristics of the different methods is presented. Usually, characterizing the antioxidant activity of emulsions is not limited to only one method, but is a combination of them, since each one acts by different mechanisms. The DPPH is the most used assay to have a first approach of the antioxidant potential of emulsion-based systems, as it is the simplest and fastest, followed by ABTS and ORAC, and finally FRAP. The value obtained in each assay is different. For example, in the research of Gallego et al. the order, from higher to lower, of antioxidant activity of O/W emulsions containing ethanolic extracts of *Caesalpinia decapetala* was ORAC > TEAC > DPPH > FRAP, values compared to Trolox, since each test measures the antioxidant activity in a different way (Gallego et al. 2017).

Many recent studies have assessed the antioxidant capacity of emulsion-based carriers. For example, Hee et al. concluded by DPPH and ABTS that the antioxidant capacity of virgin coconut oil was not affected by its microencapsulation with supercritical carbon dioxide spray-drying. (Hee et al. 2017). Similar results were obtained in the research of Tirado et al. where the antioxidant activity of astaxanthin was not affected when it was encapsulated in ethyl cellulose by supercritical extraction (Tirado et al. 2019). On the other hand, Giménez-Rota et al. obtained different antioxidant properties of  $\beta$ -carotene when it was encapsulated into *poly-lactic-co-glycolic acid* (PLGA) or poly-lactic acid (PLA) microcarriers, where higher values of antioxidant activity by DPPH in the second type of encapsulation was achieved (Gimenez-Rota et al. 2019).

**Table 12.2** Comparison of different spectrophotometric antioxidant assays for the characterization of emulsion-based antioxidant carriers

Assay	Reaction mechanism	Type of assay	Chromophores	$\lambda$ (nm)	pH
DPPH	HAT	Absorbance	DPPH* radical	515	7–7.4
ABTS/TEAC	SET	Absorbance	ABTS* radical	415, 645, 734, 815	7.4 (in PBS)
FRAP	SET	Absorbance	Ferrous tripyridyltriazine	593	3.6
ORAC	HAT	Fluorescence	Fluorescein	484–520	7.4

### 12.7.5 EPR or ESR

Another less used analytical technique to test the antioxidant activity of emulsion systems is Electron Paramagnetic Resonance (EPR) or Electron Spin Resonance (ESR), which is especially suitable since free radicals are species having unpaired electrons. It is a form of magnetic resonance spectroscopy such as nuclear magnetic resonance but, while in the former atomic nuclei interact with electromagnetic resonance under an external magnetic field, in the case of EPR unpaired electrons are the ones that interact with the radiation. Briefly, electrons have a *spin* which gives them a magnetic moment. Under an external magnetic field, electrons can orient parallel or antiparallel to the direction of the field, creating two energy levels for unpaired electrons. This technique detects and measures the transition between these energy levels. The antioxidant status of an emulsion system can be monitored by this technique as the elimination of stable free radicals such as DPPH or 4-Hydroxy-2,2,6,6-tetramethylpiperidine 1-oxyl (TEMPOL), which have a well-defined EPR spectrum. For example, Aboudzadeh et al. proved that the radical scavenging activity of O/W microemulsions encapsulating  $\alpha$ -tocopherol increased in time, demonstrating at the same time a slow release of  $\alpha$ -tocopherol from the droplets (Aboudzadeh et al. 2018). In a similar O/W microemulsion of carotenoids, Chaari et al. demonstrated that the antiradical properties of carotenoids were not affected by their micro- and nano-encapsulation (Chaari et al. 2018).

### 12.7.6 Cellular Assays

Cellular antioxidant assays are used for biomedical applications where emulsion systems are designed to be in contact with cells and tissues and are normally complemented with other physicochemical techniques. Cellular cultures are increasingly being used since the previously described methods do not reflect the cellular environment. Cells are continuously exposed to different oxidizing agents and stimuli, making possible to study the antioxidant capacity of a system using different oxidative markers (Marrocco et al. 2017; Zhang et al. 2017a). Antioxidant carriers can be either added to the cell culture simultaneously with the stressor or incubated with the antioxidant system to be incorporated into the cells. The direct measurement of cellular ROS/RNS production via binding to a fluorescent dye is one of the most used cellular antioxidant assays. One of the most common dyes is 2', 7'-dichlorodihydrofluorescein diacetate (DCFH-DA), a fluorescent dye which is intracellularly deacetylated by esterases to non-fluorescent 2', 7'-Dichlorodihydrofluorescein (DCFH) and oxidized by free radicals to fluorescent 2', 7'-dichlorodihydrofluorescein (DCF). This dye was used, for example, in the research of Gu et al. to test the effect of encapsulating  $\beta$ -carotene with catechin-egg white protein conjugates on the antioxidant activity of the system (Gu et al. 2018). Indirect methods can also be used such as evaluating DNA/RNA damage, lipid oxidation, or protein oxidation/

nitration caused by oxidative stress (Choudhry et al. 2016; Duan et al. 2016). Measurement of specific analytes or endogenous antioxidant molecules such as glutathione can also test the antioxidant properties of emulsions (Murphy and Lampe 2018).

## 12.8 Sterilization

Sterilization requirements are of pivotal importance when manufacturing products that are designed to be in contact with the human body. There is not an always-functioning sterilization method so, it is necessary to select the most suitable one in a case-by-case manner, taking into consideration both cargo and emulsion compositions.

At the manufacturing stage, there are two well-differentiated operating modes. The first one consists of working on aseptic conditions and it is usually employed with injectable emulsions. This is especially useful when some characteristics of the final product are altered when sterilizing by conventional methods. To solve this, emulsion-based antioxidant carriers are prepared in clean rooms (Class-100 environments), the equipment is previously autoclaved, and the initial substrates are sterilized by different techniques such as filtration or heat sterilization (Toh and Chiu 2013). However, this is a highly regulated process that must meet the good manufacturing practices (GMP) imposed by the U.S. Food and Drug Administration (FDA) or the European Medicines Agency (EMA) (Food and Drug Administration. Guidance for Industry: Sterile Drug Products Produced by Aseptic Processing - Current Good Manufacturing Practice 2004), and therefore, it is usually one of the last options to be considered (Hippalgaonkar et al. 2010). On the contrary, instead of working in aseptic conditions, there are diverse techniques that can be used when the production stage has been completed, named *terminal sterilization techniques*, which are going to be reviewed hereafter.

### 12.8.1 Filtration

Filtration is one of the simplest methods for sterilizing aqueous products. When the emulsion is filtered, it goes through a membrane with pores of 0.22  $\mu\text{m}$  in diameter that blocks particles over that size, including bacteria, yeasts and even spores ("World Health Organization. Methods of sterilization," 2019). However, this diameter is not small enough to avoid virus penetration into the sterile filtrate. At the laboratory scale, filtration is a very useful method because of its quickness and the availability of different commercial sterile filters. Depending on the hydrophilicity of the emulsion system, different filters can be employed such as polyvinylidene fluoride (hydrophilic), polycarbonate (hydrophilic) or cellulose acetate (hydrophobic). Nevertheless, at the industrial scale, filtration has several limitations including

the necessity of aseptic filters and the high pressures to work under, which results in huge costs (Toh and Chiu 2013). Regarding emulsion-based antioxidant carriers, the narrow pores of the membranes limit the applicability of this technique to sterilize emulsions with droplets over 200 nm. However, for nanoemulsions that can be filtered, it is a great option when the carrier or the encapsulated antioxidant is thermolabile (Lidgate et al. 1992).

## ***12.8.2 Terminal Heat Sterilization***

Terminal heat sterilization is one of the most commonly employed techniques for sterilizing samples both at the preclinical and manufacturing stages due to its effectiveness and convenience. In fact, the World Health Organization (WHO) recommends its use whenever possible because of its reliability (“World Health Organization. Methods of sterilization,” 2019). There are two different heat-based sterilizations depending on how the heat transference is carried out.

### **12.8.2.1 Saturated Steam Sterilization (Also Known as Autoclaving)**

In this method, the samples are exposed to saturated steam under pressure in order to denature irreversibly microbial proteins. The process requires the control of temperature, pressure and time, being recommended processes of 15 minutes at 121–124 °C and 200 kPa. Depending on the products, alternative conditions can be proposed. For instance, when sterilizing products containing thermolabile molecules, temperatures can be below 121 °C, although the combination of time, pressure and temperature must be previously validated (“World Health Organization. Methods of sterilization,” 2019).

### **12.8.2.2 Dry Heat Sterilization**

Contrary to steam sterilization, dry heat sterilization is based on the oxidation of cell constituents. Thus, it has been used more for sterilizing non-aqueous, thermo-resistant samples rather than antioxidant ones. Compared to the previous method, applied temperatures are higher and times range are between 30 and 180 minutes (Toh and Chiu 2013; “World Health Organization. Methods of sterilization,” 2019). However, taking into account the sterilization mechanisms underlying these two techniques, both of them might have detrimental effects on the preparations because material hydrolysis directly correlates with temperature and agglomeration, and breakdown and deformation of polymers have been described when applied temperatures were higher than the glass transition temperatures of the polymers (Dubey 2014; Toh and Chiu 2013).

### 12.8.3 *High-Pressure Processes*

High-pressure processes were developed in order to overcome the problems involved in thermolability method. Although this parameter has not been as largely studied as heat sterilization, high pressure techniques can strongly influence different kinds of biomolecules such as proteins or polysaccharides via modifying both their electrostatic and hydrophobic interactions, thus constituting an excellent tool for denaturing microbial proteins (Gharibzahedi et al. 2019). For this reason, high-pressure methods have been used for both, pasteurization and sterilization processes. Pasteurization conditions are milder when compared to sterilization ones, being not intense enough to completely eliminate bacterial spores (e.g. 600 MPa, 5 minutes, 20 °C), and, therefore, it is more used in the food industry. On the other hand, high-pressure sterilization is required for biomedical purposes and these more severe conditions involve increasing the temperature (e.g. 800 MPa, 5 minutes, 80 °C) (van de Ven et al. 2007). However, the high cost of these techniques makes them to be only used in laboratories or pilot plants in small volumes.

Regarding emulsion-based antioxidant carriers, it has been demonstrated that high-pressure processes do not have a detrimental effect on the encapsulated compounds, for example, not being degraded or losing their stability (Young et al. 2018). Moreover, it has been reported that these processes have achieved an increase on the bioactivity of encapsulated antioxidants due to the denaturation of proteins that acted as emulsifiers by increasing the thickness of the interfacial layer between phases and the packing density of proteins (Wan Mohamad et al. 2018).

### 12.8.4 *Irradiation Techniques*

Irradiation techniques include gamma ( $\gamma$ ) and UV-irradiation. The former is sometimes applied on certain drugs and surgical equipment while UV-irradiation is restricted to surfaces sterilization because of its lower penetrance. However, economic and technical limitations are common for both, including the necessity of well-trained staff, specially designed installations and expensive equipment (“World Health Organization. Methods of sterilization,” 2019).

They are not the most suitable methods for sterilizing emulsion-based antioxidant carriers because the degradation of bacterial DNA and membranes occurs via a free radical formation mechanism. While a complete sterilization of the sample would be achieved, the antioxidant cargo might lose its biological activity because of the oxidant nature of the newly-formed free radicals (Toh and Chiu 2013). In fact, it has been reported that adding antioxidants into the emulsions can reduce the effect of these free radicals, being  $\gamma$ -irradiation commonly used for encapsulating cargos with other applications. Another way to reduce the generation of these free radicals consists of freeze-drying the emulsions, avoiding the formation of hydroxyl radicals by eliminating the water phase. However, depending on the carrier, some



coordinated water might remain within the vehicle, and therefore oxidize the cargo (Mohammed et al. 2006; Toh and Chiu 2013).

### 12.8.5 Ethylene Oxide Sterilization

Ethylene oxide ( $C_2H_4O$ ) is a gaseous compound used as a sterilizing product due to its high solubility in water and electrophile behavior. Specifically, one of the carbons of the molecule is attacked by the nitrogen atom of the amino groups of both bacterial nucleic acids and proteins, leading to the alkylation of these molecules and, consequently, to microorganisms death (including virus) (Lonni et al. 2016). However, as other sterilizing techniques, its action mechanism might not be the most adequate for emulsion-based antioxidant carrier sterilization. According to Forman et al., “antioxidants are nucleophilic reductants that directly react with oxidants”, and, therefore, ethylene oxide would reduce their antioxidant activity (Forman et al. 2014). If considered for other applications, ethylene oxide may be a good option to take into account when there are thermolabile carriers involved. In addition, it has been demonstrated not to increment lipid vesicles size and not to aggregate polymeric microspheres when the initial crystallinity of the polymers is high enough (Ah et al. 2001; Choi et al. 2001).

### 12.8.6 Comparison of Different Sterilization Methods

All the aforementioned techniques have been schematized in Table 12.3. To conclude this section, some works comparing the three more appropriate sterilizing techniques for emulsion-based antioxidant carriers are going to be reviewed.

**Table 12.3** Main advantages and limitations of different methods for sterilizing emulsion-based antioxidant carriers

Method	Advantages	Disadvantages	Cost	Utility
Filtration	Admits thermolabile products	Droplets under 0.22 $\mu m$ and economic limitations	High	Med.
Saturated steam	Cost and utility	Thermolability, degradation, agglomeration, etc.	Low	High
Dry heat	Cost and utility	Free radical formation, thermolability, degradation...	High	Low
High-pressure process	Admits thermolabile products and various operating conditions	Still in development, costs and maintenance	High	High
$\gamma$ -irradiation	High penetration	Free radical formation, degradation, agglomeration...	High	Low
UV-irradiation	Low cost and availability	Low penetration and free radical formation	Low	Low
Ethylene oxide	Admits thermolabile products	Free radical formation	Med.	Low

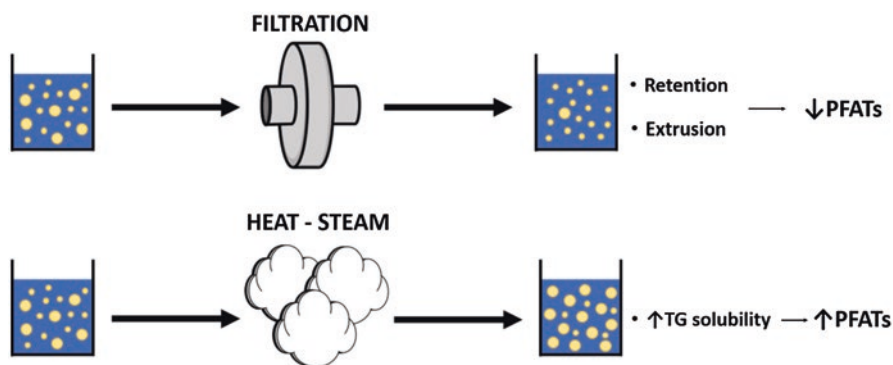


**Fig. 12.11** Effect of the chosen sterilization method on particle size, evaluated as PFATs values. PFATs stands for percentage of fat droplets greater than a determined particle size, and TG, for triglycerides

To conclude this section, some works comparing the three more appropriate sterilizing techniques for emulsion-based antioxidant carriers are reviewing. Recently, Cappellani et al. carried out a study where they compared the properties of a dye-loaded injectable nanoemulsion sterilized by filtration or steam heat sterilization (Rosi Cappellani et al. 2018). Attending to the *in vitro* physicochemical characterization, the most interesting feature of this study is the complementary use of two different techniques for analyzing the size dispersion of the droplets: DLS and SPOS (see Sect. 12.2). In this study, the mean hydrodynamic diameter of filtered emulsions did not significantly vary while it slightly increased when the emulsions were autoclaved. However, these changes were relatively small when compared with the changes on the percentage of the volume of oil droplets with a diameter larger than 1.79 ( $\text{PFAT}_{1.79}$ ) and 5  $\mu\text{m}$  ( $\text{PFAT}_5$ ). Therefore, while filtration strongly reduced both PFATs, by retention of larger droplets or by rupture during extrusion, heat sterilization had the opposite effect, which may be due to the increase in triglycerides (TG) water solubility, leading to a higher rate of Ostwald ripening (see Sect. 12.4) (Fig. 12.11). These PFATs values are of particular importance when the emulsions are intended for parenteral administration. According to United States Pharmacopoeia,  $\text{PFAT}_5$  cannot be over 0.05% in volume because it could lead to pulmonary capillaries obstruction inducing fat embolism syndrome.

In addition, regarding antioxidant carriers, it is important to check also the cargo of the vehicles after the sterilization process. Specifically,  $\beta$ -carotene has been shown to undergo oxidation or isomerization when exposed to heat. As shown by Borba et al., their  $\beta$ -carotene-loaded nanoemulsion was highly stable after the thermal treatment but storing conditions (among other factors) led to its degradation (Borba et al. 2019).

## 12.9 Cytotoxicity

It is also essential to test if these emulsion systems can cause any damage due to their composition or their biological fate inside the body. Nowadays, there is not a specific guideline for testing toxicity of emulsions, but analogous analyses of bio-materials toxicity can be performed.

### 12.9.1 *Emulsions Droplet Fate*

Depending on the application, form of administration and physicochemical characteristics of the tested emulsion, the fate of the emulsion droplets may have different relevance. For example, there has been concern about the use of nanoemulsions because its reduced dimensions may alter the absorption, distribution, metabolism, and excretion processes, thus promoting toxicity (McClements and Rao 2011). However, proper *in vitro* and *in vivo* preclinical studies can support the safety of the systems. For instance, when intended for oral administration, emulsions are usually digested along the gastrointestinal tract and absorbed in the intestine. These emulsions are generally made of biodegradable materials that do not present further complications. However, they can also be made of indigestible oils, such as hydrocarbons or mineral oils, or even having their droplets coated with indigestible shells of dietary fibers, which would avoid its digestion. Therefore, the droplets could be directly absorbed and accumulated in some tissues (McClements and Rao 2011).

Regarding its composition, some of the compounds used during the preparation of the emulsion might be toxic if they have not been previously removed (e.g. organic solvents), or if they are in high concentrations (e.g. surfactants as emulsifiers) (Kralova and Sjöblom 2009). In addition, an increase in the bioavailability of a determined compound does not necessarily correlate with a beneficial effect, especially those that may cause adverse effects at high doses (McClements and Rao 2011). All these factors are highly dependent on the composition and characteristics of the tested emulsion, and for this reason it is so important to fully know the concrete physicochemical characteristics of the system before performing these assays.

### 12.9.2 *Cytotoxicity Testing*

In order to test biocompatibility, cytotoxic tests are carried out for emulsions as for any other kind of delivery systems or biomaterials. These tests analyze the *in vitro* cellular response of different cell types in order to identify vulnerable or altered cells or toxic concentrations, and include: morphology assessment, cell viability, mutagenicity, and oxidative damage tests.

Examining cell morphology is one of the simplest ways to identify cytotoxicity. Every cell type has a characteristic shape and appearance and any modification could mean a toxic insult. Apoptotic and necrotic cells have characteristic signals which indicate cell death such as cytoplasmic vacuolation, granularity and even detachment from the substrate. These features can be observed with an optical microscope but more details can be obtained with further biochemical, immunohistochemical and microscopic evaluation.

Regarding cell viability and cell proliferation, there are many tests that allow us to check the metabolic state of the cell cultures treated with emulsions. The principal ones are commented below.

### 12.9.2.1 Dyes Exclusion

Membrane integrity is a differential feature between living and dead cells. While the first ones have well-regulated systems to avoid some dyes entrance, dead cells have pores or disruptions that allow these dyes to penetrate inside. One example is trypan blue, which is routinely used in cell culture labs to test the viability of cell suspensions. Trypan blue is not able to cross intact membranes and for this reason, it only stains the background and the dead cells, thus showing living cells as refracting dots (Strober 2001).

Other methods are more eye-catching such as the simultaneous staining with fluorescein diacetate and propidium iodide (PI), where viable cells fluorescence in bright-green and dead cells, in bright-red. In this assay, fluorescein passes through living membranes and accumulates inside after being hydrolyzed by intracellular esterases, while PI only enters dead cells, thus causing this color divergence (Jones and Senft 1985).

### 12.9.2.2 Spectrophotometric/Colorimetric Assays

Other assays take advantage of color or absorbance emission at characteristic wavelengths in order to check cell viability status. The lactate dehydrogenase (LDH) assay is a commonly used assay in drug testing that allows to measure necrotic effects (Montenegro et al. 2011; Tzankova et al. 2016). In this sense, necrotic cells release LDH to the culture medium. When the reaction cocktail is added to the supernatants, a reduction reaction takes place with varying intensity, depending on the LDH concentration (Yoon et al. 2018). However, when testing emulsion-based antioxidant carriers, it is important to check if it can bias the colorimetric measurement. Other tests analyze the mitochondrial activity of the culture such as MTT or Alamar Blue (Dhakar et al. 2019; Shenoy et al. 2017; Tzankova et al. 2016). In the first one, a yellow tetrazolium salt (3-(4,5-dimethylthiazol-2-yl)-2,5-diphenyltetrazolium bromide) is reduced by living cells to blue formazan crystals which must be solubilize in another solvent for quantification. In contrast, the Alamar Blue assay has a non-fluorescent dye which is reduced by living cells to a

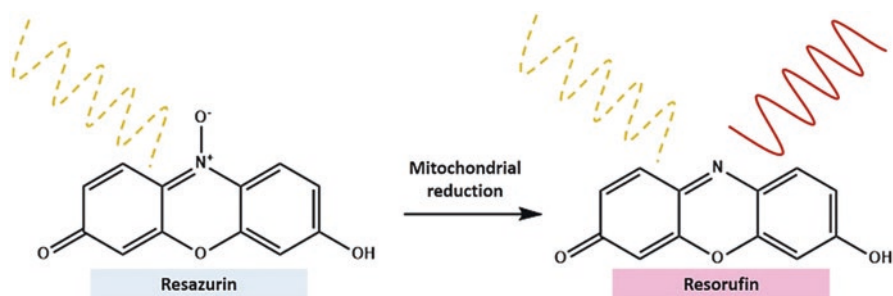


**Fig. 12.12** The non-fluorescent Alamar Blue substrate (resazurin) is reduced by viable cells to a pink-colored, bright red-fluorescent product (resorufin)

pink fluorescent molecule (Fig. 12.12). Both MTT and Alamar Blue assays give an idea of cytotoxic or proliferative effects of a determined compound but some differences can be found. For example, MTT is more cumbersome and can produce false positives when antioxidants are tested (Bruggisser et al. 2002). On the other hand, Alamar Blue is simpler as it can be performed over time, because of its non-cytotoxicity (Bopp and Lettieri 2008). It is important to note that some drugs with high antioxidant properties can indeed cause false-negative results by interfering with the reducing property of viable cells. In these cases, washing with phosphate buffered saline before adding the incubating solution is recommended (Shenoy et al. 2017).

### 12.9.2.3 Flow Cytometry Analyses

Flow cytometry is a perfect technique for assessing cell viability status in a cell-by-cell manner. A cell suspension is passed through the cytometer and cells are aligned and separated so that the cytometer laser can individually analyze them, giving information about size and complexity of each cell. DNA content in each cell can be measured if the suspension is previously permeabilized and PI is added. In this sense, the emitted fluorescence of PI would be directly proportional to DNA content and, therefore, graphics of the cell cycle of the culture could be obtained. Apoptotic cells appeared below G<sub>1</sub> phase (the lapse of the cycle between two mitotic divisions), where there is less DNA due to its degradation (Darzynkiewicz et al. 2010). Different methods can be applied using other markers such as annexin V or clusters of differentiation tagged with fluorescent molecules for more complex analyses.

Tests related to mutagenicity and carcinogenicity issues are not as commonly used as the previous ones. In fact, they are more used in *in vivo* models which are beyond the scope of this chapter. These tests study the possible genotoxic and carcinogenic effects that the samples can have on the living systems, including gene mutations, DNA aberrations and chromosomal alterations. Among these assays, Comet and Ames tests are the most frequently used due to their fastness and simplicity (Omidi et al. 2017). Finally, the oxidative damage of the emulsions should

also be tested, although for antioxidant carriers, it would give idea of the potency of the developed product (see Sect. 12.7).

## 12.10 Conclusions

The performance of an emulsion-based antioxidant carrier will be intimately related to its properties. Therefore, an appropriate characterization of the system is required to ensure its suitability for the desired final application. In this regard, this chapter highlights the main characteristics affecting antioxidant carrier quality and effectiveness; and summarizes the most commonly used techniques for their characterization. The examples referenced in this chapter allow the reader to understand the difference between the analytical methods used to characterize these systems. Choosing the most appropriate techniques for each situation depends on three main factors: the actual characteristics of the analyzed system, the cargo and its future application. It is important to assess the size, morphology and structure of the vehicles because they influence the rheological properties and stability of the antioxidant emulsion. Regarding the cargo, it has to be demonstrated that its loading within the emulsion-based carriers does not affect its structure, functions and antioxidant properties. Finally, when intended to be in contact with humans, cytotoxic and sterility issues need to be addressed. Thus, by knowing the principles underlying these characterization methods and techniques, the reader will be able to choose among the different options attending to their advantages and limitations, and to obtain as much information as possible from ongoing experiments.

## References

- Aboudzadeh MA, Mehravar E, Fernandez M, Lezama L, Tomovska R (2018) Low-energy encapsulation of alpha-tocopherol using fully food grade oil-in-water microemulsions. *ACS Omega* 3(9):10999–11008. <https://doi.org/10.1021/acsomega.8b01272>
- Acevedo-Fani A, Silva HD, Soliva-Fortuny R, Martín-Belloso O, Vicente AA (2017) Formation, stability and antioxidant activity of food-grade multilayer emulsions containing resveratrol. *Food Hydrocoll* 71:207–215. <https://doi.org/10.1016/j.foodhyd.2017.05.007>
- Ah YC, Choi Y, Kim SY, Kim SH, Lee KS, Byun Y (2001) Effects of ethylene oxide gas sterilization on physical properties of poly(L-lactide)-poly(ethylene glycol)-poly(L-lactide) microspheres. *J Biomater Sci Polym Ed* 12(7):783–799. <https://doi.org/10.1163/156856201750411666>
- Akbari S (2018) Emulsion types, stability mechanisms and rheology: a review. *Int J Innov Res Sci Stud* 1(1):14–21
- Alam MN, Bristi NJ, Rafiquzzaman M (2013) Review on in vivo and in vitro methods evaluation of antioxidant activity. *Saudi Pharm J* 21(2):143–152. <https://doi.org/10.1016/j.jsps.2012.05.002>
- Amma S-i, Luo J, Pantano CG, Kim SH (2015) Specular reflectance (SR) and attenuated total reflectance (ATR) infrared (IR) spectroscopy of transparent flat glass surfaces: a case study for soda lime float glass. *J Non-Cryst Solids* 428:189–196. <https://doi.org/10.1016/j.jnoncrsol.2015.08.015>

- Beasley MM, Bartelink EJ, Taylor L, Miller RM (2014) Comparison of transmission FTIR, ATR, and DRIFT spectra: implications for assessment of bone bioapatite diagenesis. *J Archaeol Sci* 46:16–22. <https://doi.org/10.1016/j.jas.2014.03.008>
- Behbahani ES, Ghaedi M, Abbaspour M, Rostamizadeh K (2017) Optimization and characterization of ultrasound assisted preparation of curcumin-loaded solid lipid nanoparticles: application of central composite design, thermal analysis and X-ray diffraction techniques. *Ultrason Sonochem* 38:271–280. <https://doi.org/10.1016/j.ultsonch.2017.03.013>
- Benzie I, Strain J (1996) The ferric reducing ability of plasma (FRAP) as a measure of “antioxidant power” the FRAP assay. *Anal Biochem* 239:70–76
- Block ID, Scheffold F (2010) Modulated 3D cross-correlation light scattering: improving turbid sample characterization. *Rev Sci Instrum* 81(12):123107. <https://doi.org/10.1063/1.3518961>
- Blois MS (1958) Antioxidant determinations by the use of a stable free radical. *Nature* 181(4617):1199–1200. <https://doi.org/10.1038/1811199a0>
- Bopp SK, Lettieri T (2008) Comparison of four different colorimetric and fluorometric cytotoxicity assays in a zebrafish liver cell line. *BMC Pharmacol* 8:8. <https://doi.org/10.1186/1471-2210-8-8>
- Borba CM, Tavares MN, Macedo LP, Araujo GS, Furlong EB, Dora CL, Burkert JFM (2019) Physical and chemical stability of beta-carotene nanoemulsions during storage and thermal process. *Food Res Int* 121:229–237. <https://doi.org/10.1016/j.foodres.2019.03.045>
- Brand-Williams W, Cuvelier ME, Berset C (1995) Use of a free radical method to evaluate antioxidant activity. *LWT Food Sci Technol* 28(1):25–30. [https://doi.org/10.1016/S0023-6438\(95\)80008-5](https://doi.org/10.1016/S0023-6438(95)80008-5)
- Bruggisser R, von Daeniken K, Jundt G, Schaffner W, Tullberg-Reinert H (2002) Interference of plant extracts, phytoestrogens and antioxidants with the MTT tetrazolium assay. *Planta Med* 68(5):445–448. <https://doi.org/10.1055/s-2002-32073>
- Carpenter J, George S, Saharan VK (2019) Curcumin encapsulation in multilayer oil-in-water emulsion: synthesis using ultrasonication and studies on stability and antioxidant and release activities. *Langmuir* 35(33):10866–10876. <https://doi.org/10.1021/acs.langmuir.9b01523>
- Cefali LC, Souza-Moreira TM, Corrêa MA, Salgado HRN, Isaac VLB (2015) Development and evaluation of an emulsion containing lycopene for combating acceleration of skin aging. *Braz J Pharm Sci* 51(3):579–590. <https://doi.org/10.1590/s1984-82502015000300010>
- Chaari M, Theochari I, Papadimitriou V, Xenakis A, Ammar E (2018) Encapsulation of carotenoids extracted from halophilic Archaea in oil-in-water (O/W) micro- and nano-emulsions. *Colloids Surf B Biointerfaces* 161:219–227. <https://doi.org/10.1016/j.colsurfb.2017.10.042>
- Chang C, Li X, Li J, Niu F, Zhang M, Zhou B et al (2017) Effect of enzymatic hydrolysis on characteristics and synergistic efficiency of pectin on emulsifying properties of egg white protein. *Food Hydrocoll* 65:87–95. <https://doi.org/10.1016/j.foodhyd.2016.11.004>
- Chen LC, Chen YC, Su CY, Wong WP, Sheu MT, Ho HO (2016) Development and characterization of lecithin-based self-assembling mixed polymeric Micellar (saMPMs) drug delivery systems for curcumin. *Sci Rep* 6:37122. <https://doi.org/10.1038/srep37122>
- Cheng Y, Chen J, Xiong YL (2014) Interfacial adsorption of peptides in oil-in-water emulsions costabilized by Tween 20 and antioxidative potato peptides. *J Agric Food Chem* 62(47):11575–11581. <https://doi.org/10.1021/jf5038135>
- Choi Y, Kim SY, Moon MH, Kim SH, Lee KS, Byun Y (2001) Poly(ethylene glycol)-poly(L-lactide) diblock copolymer prevents aggregation of poly(L-lactide) microspheres during ethylene oxide gas sterilization. *Biomaterials* 22(9):995–1004. [https://doi.org/10.1016/s0142-9612\(00\)00265-9](https://doi.org/10.1016/s0142-9612(00)00265-9)
- Choi SJ, Won JW, Park KM, Chang P-S (2014) A new method for determining the emulsion stability index by backscattering light detection. *J Food Process Eng* 37(3):229–236. <https://doi.org/10.1111/jfpe.12078>
- Choudhry QN, Kim MJ, Kim TG, Pan JH, Kim JH, Park SJ et al (2016) Saponin-based nanoemulsification improves the antioxidant properties of vitamin A and E in AML-12 cells. *Int J Mol Sci* 17(9). <https://doi.org/10.3390/ijms17091406>



- Coskun O (2016) Separation techniques: chromatography. *North Clin Istanb* 3(2):156–160. <https://doi.org/10.14744/nci.2016.32757>
- Darzynkiewicz Z, Halicka HD, Zhao H (2010) <nihms-247430.pdf>. *Adv Exp Med Biol* 676:137–147
- Araújo, Rosângela F. F. de, Martins, Danyelly Brunessa G., & Borba, Maria Amélia C. S. M. (2016). Oxidative stress and disease. doi:<https://doi.org/10.5772/65366>
- Del Prado M, Magaña J, Mejía-Contreras BA, Borbolla-Jiménez FV, Giraldo D, Pina-Barba M et al (2019) In vitro cell evaluation of curcumin-loaded PCL/F68 nanoparticles for potential application in neuronal diseases. *J Drug Delivery Sci Technol* 52:905–914. <https://doi.org/10.1016/j.jddst.2019.05.042>
- Derkach SR (2009) Rheology of emulsions. *Adv Colloid Interf Sci* 151(1–2):1–23. <https://doi.org/10.1016/j.cis.2009.07.001>
- Dhakar NK, Caldera F, Bessone F, Cecone C, Pedrazzo AR, Cavalli R et al (2019) Evaluation of solubility enhancement, antioxidant activity, and cytotoxicity studies of kynurenic acid loaded cyclodextrin nanosponge. *Carbohydr Polym* 224:115168. <https://doi.org/10.1016/j.carbpol.2019.115168>
- Di Gianfrancesco A (2017) Technologies for chemical analyses, microstructural and inspection investigations:197–245. <https://doi.org/10.1016/b978-0-08-100552-1.00008-7>
- Duan X, Li M, Ma H, Xu X, Jin Z, Liu X (2016) Physicochemical properties and antioxidant potential of phosvitin-resveratrol complexes in emulsion system. *Food Chem* 206:102–109. <https://doi.org/10.1016/j.foodchem.2016.03.055>
- Dubey R (2014) Controlled-release injectable microemulsions: recent advances and potential opportunities. *Expert Opin Drug Deliv* 11(2):159–173. <https://doi.org/10.1517/17425247.2014.870151>
- Emerenciano DP, Baracho BBD, de Medeiros ML, Rocha HAO, Xavier FH Jr, da Veiga VF Jr, Maciel MAM (2019) Physicochemical characterizations and antioxidant property of copaiba oil loaded into SNEDDS systems. *J Braz Chem Soc* 30:234–246
- Erdmann ME, Zeeb B, Salminen H, Gibis M, Lautenschlaeger R, Weiss J (2015) Influence of drop-let size on the antioxidant activity of rosemary extract loaded oil-in-water emulsions in mixed systems. *Food Funct* 6(3):793–804. <https://doi.org/10.1039/c4fo00878b>
- Etzler, Frank M., & Drelich, Jaroslaw. (2012). Atomic force microscopy for characterization of surfaces, particles, and their interactions. 307–331. <https://doi.org/10.1016/b978-1-4377-7883-0.00006-7>
- Food and Drug Administration. Guidance for industry: sterile drug products produced by Aseptic Processing - Current Good Manufacturing Practice. (2004). Available: <https://www.fda.gov/media/71026/download>
- Forman HJ, Davies KJ, Ursini F (2014) How do nutritional antioxidants really work: nucleophilic tone and para-hormesis versus free radical scavenging in vivo. *Free Radic Biol Med* 66:24–35. <https://doi.org/10.1016/j.freeradbiomed.2013.05.045>
- Gallego MG, Skowrya M, Gordon MH, Azman NA, Almajano MP (2017) Effect of leaves of *Caesalpinia decapetala* on oxidative stability of oil-in-water emulsions. *Antioxidants* (Basel) 6(1). <https://doi.org/10.3390/antiox6010019>
- Gharibzadeh SMT, Hernández-Ortega C, Welte-Chanes J, Putnik P, Barba FJ, Mallikarjunan K et al (2019) High pressure processing of food-grade emulsion systems: antimicrobial activity, and effect on the physicochemical properties. *Food Hydrocoll* 87:307–320. <https://doi.org/10.1016/j.foodhyd.2018.08.012>
- Giessibl FJ (2003) Advances in atomic force microscopy. *Rev Mod Phys* 75(3):949–983. <https://doi.org/10.1103/RevModPhys.75.949>
- Gimenez-Rota C, Palazzo I, Scognamiglio MR, Mainar A, Reverchon E, Della Porta G (2019)  $\beta$ -Carotene,  $\alpha$ -tocopherol and rosmarinic acid encapsulated within PLA/PLGA microcarriers by supercritical emulsion extraction: encapsulation efficiency, drugs shelf-life and antioxidant activity. *J Supercrit Fluids* 146:199–207. <https://doi.org/10.1016/j.supflu.2019.01.019>



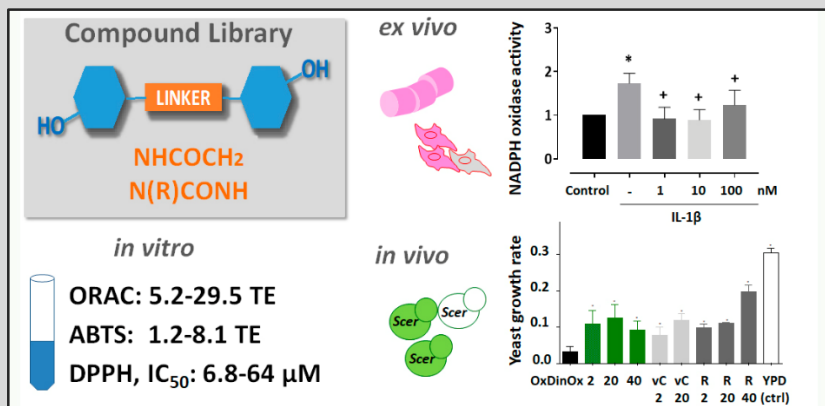
- Gomes A, Costa ALR, de Assis Perrechil F, da Cunha RL (2016) Role of the phases composition on the incorporation of gallic acid in O/W and W/O emulsions. *J Food Eng* 168:205–214. <https://doi.org/10.1016/j.jfoodeng.2015.07.041>
- Gonzalez ML, Marcussi DG, Calixto GM, Correa MA, Chorilli M (2015) Structural characterization and in vitro antioxidant activity of kojic dipalmitate loaded w/o/w multiple emulsions intended for skin disorders. *Biomed Res Int* 2015:304591. <https://doi.org/10.1155/2015/304591>
- Gouda M, Zhang S, Liu Y, Sheng L, Ma M (2017) Effects of four natural antioxidant phenyl terpenes on emulsifying and rheological properties of egg yolk. *LWT Food Sci Technol* 83:59–67. <https://doi.org/10.1016/j.lwt.2017.04.075>
- Gu L, Pan C, Su Y, Zhang R, Xiao H, McClements DJ, Yang Y (2018) In vitro bioavailability, cellular antioxidant activity, and cytotoxicity of beta-carotene-loaded emulsions stabilized by catechin-egg white protein conjugates. *J Agric Food Chem* 66(7):1649–1657. <https://doi.org/10.1021/acs.jafc.7b05909>
- Gurpreet K, Singh SK (2018) Review of nanoemulsion formulation and characterization techniques. *Indian J Pharm Sci* 80(5):781–789
- Hatanaka J, Chikamori H, Sato H, Uchida S, Debari K, Onoue S, Yamada S (2010) Physicochemical and pharmacological characterization of alpha-tocopherol-loaded nano-emulsion system. *Int J Pharm* 396(1–2):188–193. <https://doi.org/10.1016/j.ijpharm.2010.06.017>
- Hee YY, Tan CP, Rahman RA, Noranizan M, Smith RL, Chong GH (2017) Production of virgin coconut oil microcapsules from oil-in-water emulsion with supercritical carbon dioxide spray drying. *J Supercrit Fluids* 130:118–124. <https://doi.org/10.1016/j.supflu.2017.07.037>
- Hippalgaonkar K, Majumdar S, Kansara V (2010) Injectable lipid emulsions-advancements, opportunities and challenges. *AAPS PharmSciTech* 11(4):1526–1540. <https://doi.org/10.1208/s12249-010-9526-5>
- Hu Y-T, Ting Y, Hu J-Y, Hsieh S-C (2017) Techniques and methods to study functional characteristics of emulsion systems. *J Food Drug Anal* 25(1):16–26. <https://doi.org/10.1016/j.jfda.2016.10.021>
- Ja'afar F, Leow CH, Garbin V, Sennoga CA, Tang MX, Seddon JM (2015) Surface charge measurement of SonoVue, definity and optison: a comparison of laser Doppler electrophoresis and micro-electrophoresis. *Ultrasound Med Biol* 41(11):2990–3000. <https://doi.org/10.1016/j.ultrasmedbio.2015.07.001>
- Jin W, Xu W, Liang H, Li Y, Liu S, Li B (2016) Nanoemulsions for food: properties, production, characterization, and applications. In: Grumezescu AM (ed) *Emulsions*. Academic, London, pp 1–36
- Jones KH, Senft JA (1985) An improved method to determine cell viability by simultaneous staining with fluorescein diacetate-propidium iodide. *J Histochem Cytochem* 33(1):77–79. <https://doi.org/10.1177/33.1.2578146>
- Joung HJ, Choi MJ, Kim JT, Park SH, Park HJ, Shin GH (2016) Development of food-grade curcumin nanoemulsion and its potential application to food beverage system: antioxidant property and in vitro digestion. *J Food Sci* 81(3):N745–N753. <https://doi.org/10.1111/1750-3841.13224>
- Kim HS, Mason TG (2017) Advances and challenges in the rheology of concentrated emulsions and nanoemulsions. *Adv Colloid Interf Sci* 247:397–412. <https://doi.org/10.1016/j.cis.2017.07.002>
- Kralova I, Sjöblom J (2009) Surfactants used in food industry: a review. *J Dispers Sci Technol* 30(9):1363–1383. <https://doi.org/10.1080/01932690902735561>
- Lidgate DM, Trattner T, Shultz RM, Maskiewicz R (1992) Sterile filtration of a parenteral emulsion. *Pharm Res* 9(7):860–863. <https://doi.org/10.1023/a:1015836512890>
- Liguori I, Russo G, Curcio F, Bulli G, Aran L, Della-Morte D et al (2018) Oxidative stress, aging, and diseases. *Clin Interv Aging* 13:757–772. <https://doi.org/10.2147/CIA.S158513>
- Lobo V, Patil A, Phatak A, Chandra N (2010) Free radicals, antioxidants and functional foods: impact on human health. *Pharmacogn Rev* 4(8):118–126. <https://doi.org/10.4103/0973-7847.70902>
- Lonni AA, Munhoz VM, Lopes GC, Longhini R, Borghi-Pangoni FB, Dos Santos RS et al (2016) Development and characterization of multiple emulsions for controlled release of *Trichilia cat-*

- igua (Catuaba) extract. *Pharm Dev Technol* 21(8):933–942. <https://doi.org/10.3109/10837450.2015.1081611>
- Mantele W, Deniz E (2017) UV-VIS absorption spectroscopy: Lambert-Beer reloaded. *Spectrochim Acta A Mol Biomol Spectrosc* 173:965–968. <https://doi.org/10.1016/j.saa.2016.09.037>
- Marrocco I, Altieri F, Peluso I (2017) Measurement and clinical significance of biomarkers of oxidative stress in humans. *Oxidative Med Cell Longev* 2017:6501046. <https://doi.org/10.1155/2017/6501046>
- Matschke V, Theiss C, Matschke J (2019) Oxidative stress: the lowest common denominator of multiple diseases. *Neural Regen Res* 14(2):238–241. <https://doi.org/10.4103/1673-5374.244780>
- McClements DJ (2007) Critical review of techniques and methodologies for characterization of emulsion stability. *Crit Rev Food Sci Nutr* 47(7):611–649. <https://doi.org/10.1080/10408390701289292>
- McClements DJ, Rao J (2011) Food-grade nanoemulsions: formulation, fabrication, properties, performance, biological fate, and potential toxicity. *Crit Rev Food Sci Nutr* 51(4):285–330. <https://doi.org/10.1080/10408398.2011.559558>
- McElhaney RN (1986) Differential scanning calorimetric studies of lipid-protein interactions in model membrane systems. *Biochim Biophys Acta Rev Biomembr* 864(3):361–421. [https://doi.org/10.1016/0304-4157\(86\)90004-3](https://doi.org/10.1016/0304-4157(86)90004-3)
- Meroni E, Raikov V (2018) Physicochemical stability, antioxidant properties and bioaccessibility of beta-carotene in orange oil-in-water beverage emulsions: influence of carrier oil types. *Food Funct* 9(1):320–330. <https://doi.org/10.1039/c7fo01170a>
- Mohammed AR, Bramwell VW, Coombes AG, Perrie Y (2006) Lyophilisation and sterilisation of liposomal vaccines to produce stable and sterile products. *Methods* 40(1):30–38. <https://doi.org/10.1016/j.ymeth.2006.05.025>
- Montenegro L, Campisi A, Sarpietro MG, Carbone C, Acquaviva R, Raciti G, Puglisi G (2011) In vitro evaluation of idebenone-loaded solid lipid nanoparticles for drug delivery to the brain. *Drug Dev Ind Pharm* 37(6):737–746. <https://doi.org/10.3109/03639045.2010.539231>
- Murphy DB (2001) Fundamentals of light microscopy and electronic imaging. Wiley-Liss, Inc, New York
- Murphy NP, Lampe KJ (2018) Fabricating PLGA microparticles with high loads of the small molecule antioxidant N-acetylcysteine that rescue oligodendrocyte progenitor cells from oxidative stress. *Biotechnol Bioeng* 115(1):246–256. <https://doi.org/10.1002/bit.26443>
- Nikolic I, Jasmin Lunter D, Randjelovic D, Zugic A, Tadic V, Markovic B et al (2018) Curcumin-loaded low-energy nanoemulsions as a prototype of multifunctional vehicles for different administration routes: physicochemical and in vitro peculiarities important for dermal application. *Int J Pharm* 550(1–2):333–346. <https://doi.org/10.1016/j.ijpharm.2018.08.060>
- Omidi, Meisam, Fatehinya, Atena, Farahani, Masomeh, Akbari, Zahra, Shahmoradi, Saleheh, Yazdian, Fatemeh, et al. (2017). Characterization of biomaterials. 97–115. doi:<https://doi.org/10.1016/b978-0-08-100961-1.00007-4>
- Pallua JD, Pezzei C, Huck-Pezzei V, Schonbichler SA, Bittner LK, Bonn GK et al (2011) Advances of infrared spectroscopic imaging and mapping technologies of plant material. *Curr Bioact Compd* 7(2):106–117. <https://doi.org/10.2174/157340711796011179>
- Pawley JB (2006) Fundamental limits in confocal microscopy. In: Pawley JB (ed) *Handbook of biological confocal microscopy*. Springer US, Boston, pp 20–42
- Peng C, Svirskis D, Lee SJ, Oey I, Kwak HS, Chen G et al (2018) Design of microemulsion system suitable for the oral delivery of poorly aqueous soluble beta-carotene. *Pharm Dev Technol* 23(7):682–688. <https://doi.org/10.1080/10837450.2017.1287729>
- Rashid M, Wani T, Mishra N, Sofi H, Sheikh F (2018) Development and characterization of drug-loaded self-solidnano-emulsified drug delivery system for treatment of diabetes. *Mater Sci Res India* 15:01–11. <https://doi.org/10.13005/msri/150101>
- Re R, Pellegrini N, Proteggente A, Pannala A, Yang M, Rice-Evans C (1999) Antioxidant activity applying an improved ABTS radical cation decolorization assay. *Free Radic Biol Med* 26(9–10):1231–1237. [https://doi.org/10.1016/s0891-5849\(98\)00315-3](https://doi.org/10.1016/s0891-5849(98)00315-3)

- Rinaldi F, Hanieh PN, Longhi C, Carradori S, Secci D, Zengin G et al (2017) Neem oil nanoemulsions: characterisation and antioxidant activity. *J Enzyme Inhib Med Chem* 32(1):1265–1273. <https://doi.org/10.1080/14756366.2017.1378190>
- Rosi Cappellani M, Perinelli DR, Pescosolido L, Schoubben A, Cespi M, Cossi R, Blasi P (2018) Injectable nanoemulsions prepared by high pressure homogenization: processing, sterilization, and size evolution. *Appl Nanosci* 8(6):1483–1491. <https://doi.org/10.1007/s13204-018-0829-2>
- Rutz JK, Borges CD, Zambiasi RC, da Rosa CG, da Silva MM (2016) Elaboration of microparticles of carotenoids from natural and synthetic sources for applications in food. *Food Chem* 202:324–333. <https://doi.org/10.1016/j.foodchem.2016.01.140>
- Sellimi S, Younes I, Ayed HB, Maalej H, Montero V, Rinaudo M et al (2015) Structural, physico-chemical and antioxidant properties of sodium alginate isolated from a Tunisian brown seaweed. *Int J Biol Macromol* 72:1358–1367. <https://doi.org/10.1016/j.ijbiomac.2014.10.016>
- Shaddel R, Hesari J, Azadmard-Damirchi S, Hamishehkar H, Fathi-Achachlouei B, Huang Q (2018) Double emulsion followed by complex coacervation as a promising method for protection of black raspberry anthocyanins. *Food Hydrocoll* 77:803–816. <https://doi.org/10.1016/j.foodhyd.2017.11.024>
- Shenoy N, Stenson M, Lawson J, Abeykoon J, Patnaik M, Wu X, Witzig T (2017) Drugs with anti-oxidant properties can interfere with cell viability measurements by assays that rely on the reducing property of viable cells. *Lab Invest* 97:494–497. <https://doi.org/10.1038/labinvest.2017.18>
- Shivakumar A, Yogendra Kumar MS (2018) Critical review on the analytical mechanistic steps in the evaluation of antioxidant activity. *Crit Rev Anal Chem* 48(3):214–236. <https://doi.org/10.1080/10408347.2017.1400423>
- Silva HD, Cerqueira MÂ, Vicente AA (2012) Nanoemulsions for food applications: development and characterization. *Food Bioprocess Technol* 5(3):854–867. <https://doi.org/10.1007/s11947-011-0683-7>
- Stetefeld J, McKenna SA, Patel TR (2016) Dynamic light scattering: a practical guide and applications in biomedical sciences. *Biophys Rev* 8(4):409–427. <https://doi.org/10.1007/s12551-016-0218-6>
- Strober W (2001) Trypan blue exclusion test of cell viability. *Curr Protoc Immunol*, Appendix 3, Appendix 3B. <https://doi.org/10.1002/0471142735.ima03bs21>
- Su J, Guo Q, Chen Y, Mao L, Gao Y, Yuan F (2020) Utilization of  $\beta$ -lactoglobulin- (–)-Epigallocatechin- 3-gallate(EGCG) composite colloidal nanoparticles as stabilizers for lutein pickering emulsion. *Food Hydrocoll* 98:105293. <https://doi.org/10.1016/j.foodhyd.2019.105293>
- Sunee C, Panee S-a, Ruttiro K (2017) Preparation, characterization and antioxidant activity of xanthone-loaded making (*Hodgsonia heteroclitia*) microemulsions. *Int J Pharm Pharm Sci* 9(3). <https://doi.org/10.22159/ijpps.2017v9i3.16584>
- Swartz M (2010) Hplc detectors: a brief review. *J Liq Chromatogr Relat Technol* 33(9–12):1130–1150. <https://doi.org/10.1080/10826076.2010.484356>
- Tan BL, Norhaizan ME, Liew WP, Sulaiman Rahman H (2018) Antioxidant and oxidative stress: a mutual interplay in age-related diseases. *Front Pharmacol* 9:1162. <https://doi.org/10.3389/fphar.2018.01162>
- Tang, C. Y., & Yang, Z. (2017). Transmission Electron Microscopy (TEM). 145–159. doi:<https://doi.org/10.1016/b978-0-444-63776-5.00008-5>
- Tang H, Xiang S, Li X, Zhou J, Kuang C (2019) Preparation and in vitro performance evaluation of resveratrol for oral self-microemulsion. *PLoS One* 14(4):e0214544. <https://doi.org/10.1371/journal.pone.0214544>
- Tatar, B. C., Sumnu, G., & Sahin, S. (2017). Rheology of emulsions. 437–457. doi:<https://doi.org/10.1016/b978-0-08-100431-9.00017-6>
- Tian B, Wang Y, Wang T, Mao L, Lu Y, Wang H, Feng Z (2019) Structure and functional properties of antioxidant nanoemulsions prepared with tea polyphenols and soybean protein isolate. *J Oleo Sci* 68:689–697. <https://doi.org/10.5650/jos.ess19067>

- Tirado DF, Palazzo I, Scognamiglio M, Calvo L, Della Porta G, Reverchon E (2019) Astaxanthin encapsulation in ethyl cellulose carriers by continuous supercritical emulsions extraction: a study on particle size, encapsulation efficiency, release profile and antioxidant activity. *J Supercrit Fluids* 150:128–136. <https://doi.org/10.1016/j.supflu.2019.04.017>
- Toh M-R, Chiu GNC (2013) Liposomes as sterile preparations and limitations of sterilisation techniques in liposomal manufacturing. *Asian J Pharm Sci* 8(2):88–95. <https://doi.org/10.1016/j.ajps.2013.07.011>
- Tzankova V, Gorinova C, Kondeva-Burdina M, Simeonova R, Philipov S, Konstantinov S et al (2016) In vitro and in vivo toxicity evaluation of cationic PDMAEMA-PCL-PDMAEMA micelles as a carrier of curcumin. *Food Chem Toxicol* 97:1–10. <https://doi.org/10.1016/j.fct.2016.08.026>
- Ujhelyi Z, Vecsernyés M, Fehér P, Kósa D, Arany P, Nemes D et al (2018) Physico-chemical characterization of self-emulsifying drug delivery systems. *Drug Discov Today Technol* 27:81–86. <https://doi.org/10.1016/j.ddtec.2018.06.005>
- Umerska A, Gaucher C, Oyarzun-Ampuero F, Fries-Raeth I, Colin F, Villamizar-Sarmiento MG et al (2018) Polymeric nanoparticles for increasing oral bioavailability of curcumin. *Antioxidants (Basel)* 7(4). <https://doi.org/10.3390/antiox7040046>
- Uskoković V (2012) Dynamic light scattering based microelectrophoresis: main prospects and limitations. *J Dispers Sci Technol* 33(12):1762–1786. <https://doi.org/10.1080/01932691.2011.625523>
- van de Ven C, Courvoisier C, Matser A (2007) High pressure versus heat treatments for pasteurisation and sterilisation of model emulsions. *Innovative Food Sci Emerg Technol* 8(2):230–236. <https://doi.org/10.1016/j.ifset.2006.12.001>
- Wan Mohamad WAF, McNaughton D, Augustin MA, Buckow R (2018) Characterisation of beta-carotene partitioning in protein emulsions: effects of pre-treatments, solid fat content and emulsifier type. *Food Chem* 257:361–367. <https://doi.org/10.1016/j.foodchem.2018.03.027>
- Weiss J (2002) Emulsion stability determination. *Curr Protocol Food Anal Chem* 3(1):D3.4.1–D3.4.17. <https://doi.org/10.1002/0471142913.fad0304s03>
- World Health Organization (2019) Methods of sterilization. Ninth. Retrieved from <http://apps.who.int/phint/pdf/b/7.5.9.5.8-Methods-of-sterilization.pdf>
- Xiuhua Z, Yiping D, Ying Z, Yuangang Z, Bolin L, Mingfang W et al (2016) Silymarin nanoparticles through emulsion solvent evaporation method for oral delivery with high antioxidant activities, bioavailability, and absorption in the liver. *RSC Adv* 6(95):93137–93146. <https://doi.org/10.1039/C6RA12896C>
- Yoon HJ, Zhang X, Kang MG, Kim GJ, Shin SY, Baek SH et al (2018) Cytotoxicity evaluation of turmeric extract incorporated oil-in-water nanoemulsion. *Int J Mol Sci* 19(1). <https://doi.org/10.3390/ijms19010280>
- Young S, Basiana E, Nitin N (2018) Effects of interfacial composition on the stability of emulsion and encapsulated bioactives after thermal and high pressure processing. *J Food Eng* 231:22–29. <https://doi.org/10.1016/j.jfoodeng.2018.02.022>
- Zhang H, Yin M, Huang L, Wang J, Gong L, Liu J, Sun B (2017a) Evaluation of the cellular and animal models for the study of antioxidant activity: a review. *J Food Sci* 82(2):278–288. <https://doi.org/10.1111/1750-3841.13605>
- Zhang J, Zhang X, Wang X, Huang Y, Yang B, Pan X, Wu C (2017b) The influence of maltodextrin on the physicochemical properties and stabilization of beta-carotene emulsions. *AAPS PharmSciTech* 18(3):821–828. <https://doi.org/10.1208/s12249-016-0572-5>
- Zhou W, Apkarian R, Wang ZL, Joy D (2007) Fundamentals of scanning electron microscopy (SEM). In: Zhou W, Wang ZL (eds) *Scanning microscopy for nanotechnology: techniques and applications*. New York, Springer New York, pp 1–40
- Zhu L, Yan H, Zhao Y (2012) Cyclodextrin-based rotaxanes on gold nanoparticles. *Int J Mol Sci* 13(8):10132–10142. <https://doi.org/10.3390/ijms130810132>

# Annex II. Characterization of Novel Synthetic Polyphenols: Validation of Antioxidant and Vasculoprotective Activities



María Jesús Pérez de Vega, Silvia Moreno-Fernández, Gloria María Pontes-Quero, María González-Amor, Blanca Vázquez-Lasa, Beatriz Sabater-Muñoz, Ana M. Briones, María R. Aguilar, Marta Miguel and Rosario González-Muñiz





## Article

# Characterization of Novel Synthetic Polyphenols: Validation of Antioxidant and Vasculoprotective Activities

María Jesús Pérez de Vega <sup>1</sup>, Silvia Moreno-Fernández <sup>2</sup>, Gloria María Pontes-Quero <sup>3,4</sup>,  
María González-Amor <sup>5,6</sup>, Blanca Vázquez-Lasa <sup>3,7</sup>, Beatriz Sabater-Muñoz <sup>8</sup>,  
Ana M. Briones <sup>5,6</sup>, María R. Aguilar <sup>3,7</sup>, Marta Miguel <sup>2</sup> and Rosario González-Muñiz <sup>1,\*</sup>

<sup>1</sup> Instituto de Química Médica, IQM-CSIC, Juan de la Cierva 3, 28006 Madrid, Spain; pdevega@iqm.csic.es

<sup>2</sup> Instituto de Investigación en Ciencias de la Alimentación (CSIC-UAM, CEI+UAM), C/Nicolás Cabrera 9, 28049 Madrid, Spain; silvia.moreno@csic.es (S.M.-F.); marta.miguel@csic.es (M.M.)

<sup>3</sup> Instituto de Ciencia y Tecnología de Polímeros, IQM-CSIC, Juan de la Cierva 3, 28006 Madrid, Spain; pontesquero@gmail.com (G.M.P.-Q.); bvazquez@ictp.csic.es (B.V.-L.); mraguilar@ictp.csic.es (M.R.A.)

<sup>4</sup> Alodia Farmacéutica SL, Santiago Grisolia 2 D130/L145, 28760 Madrid, Spain

<sup>5</sup> Facultad de Medicina, Departamento de Farmacología, Universidad Autónoma de Madrid, Instituto de Investigaciones Biomédicas Hospital La Paz, Arzobispo Morcillo 4, 28029 Madrid, Spain; maria.gonzalezamor@uam.es (M.G.-A.); ana.briones@uam.es (A.M.B.)

<sup>6</sup> Centro de Investigación Biomédica en Red de Enfermedades Cardiovasculares (CIBERCV), 28029 Madrid Spain

<sup>7</sup> Networking Biomedical Research Centre in Bioengineering, Biomaterials and Nanomedicine, CIBER-BBN, 28029 Madrid, Spain

<sup>8</sup> Instituto de Biología Molecular y Celular de Plantas (IBMCP, CSIC-UPV), Ingeniero Fausto Elio, 46022 Valencia, Spain; b.sabater.munoz@gmail.com

\* Correspondence: iqmg313@iqm.csic.es; Tel.: +3-4912-587-434

Received: 31 July 2020; Accepted: 19 August 2020; Published: 25 August 2020



**Abstract:** Antioxidant compounds, including polyphenols, have therapeutic effects because of their anti-inflammatory, antihypertensive, antithrombotic and antiproliferative properties. They play important roles in protecting the cardiovascular and neurological systems, by having preventive or protective effects against free radicals produced by either normal or pathological metabolism in such systems. For instance, resveratrol, a well-known potent antioxidant, has a counteracting effect on the excess of reactive oxygen species (ROS) and has a number of therapeutic benefits, like anti-inflammatory, anti-cancer and cardioprotective activities. Based on previous work from our group, and on the most frequent OH substitutions of natural polyphenols, we designed two series of synthetically accessible bis-polyhydroxyphenyl derivatives, separated by amide or urea linkers. These compounds exhibit high antioxidant ability (oxygen radical absorbance capacity (ORAC) assay) and interesting radical scavenging activity (RSA) values (2,2'-azinobis-(3-ethylbenzothiazoline-6-sulfonic acid) (ABTS) and  $\alpha,\alpha$ -diphenyl- $\beta$ -picrylhydrazyl (DPPH) tests). Some of the best polyphenols were evaluated in two biological systems, endothelial cells (in vitro) and whole aorta (ex vivo), highly susceptible for the deleterious effects of prooxidants under different inflammatory conditions, showing protection against oxidative stress induced by inflammatory stimuli relevant in cardiovascular diseases, i.e., Angiotensin II and IL-1 $\beta$ . Selected compounds also showed strong in vivo antioxidant properties when evaluated in the model organism *Saccharomyces cerevisiae*.

**Keywords:** antioxidants; ORAC; ABTS; DPPH; polyhydroxyphenyl amides; polyhydroxyphenyl ureas; NADPH oxidase; vasculoprotection; *Saccharomyces cerevisiae*



## 1. Introduction

In recent years, antioxidant compounds have become very popular because of their multiple benefits for health. Nutraceuticals are bioactive ingredients of fruits and vegetables, or products elaborated with natural substances, able to modulate metabolic processes. Among nutraceuticals, there are many antioxidant substances, like polyphenols [1–3]. There is an important number of compounds, biosynthesized by the secondary metabolism of plants, known as phytochemicals, which can be extracted from plants and have interesting therapeutic properties in the treatment of infectious diseases, cancer, hypercholesterolemia and immunological disorders [1,4]. Antioxidant compounds, in particular, polyphenols, have beneficial effects for human health, including, among others, anti-inflammatory, antihypertensive, antithrombotic and antiproliferative properties. They play important roles in protecting the cardiovascular and neurological systems, by having preventive or protective effects against the free radicals produced by normal metabolism in such systems [5–9]. As an example, resveratrol, a well-known potent antioxidant, has a counteracting effect to the excess of radical oxygen species (ROS) that is translated in a number of biological activities of therapeutic relevance, like anti-inflammatory and anti-cancer activities, as well as protection against cardiovascular diseases [10,11]. Antioxidants also have applications as additives in food and cosmetics for maintaining the quality of products and for extending their half-life [12,13].

Previous work from our group led us to the preparation of some polyhydroxy diphenylpropanones, which in addition to their activity as  $\alpha 7$  nicotinic acetyl choline receptor positive allosteric modulation (nAChR, PAM), showed interesting antioxidant properties [14,15]. The two phenyl rings in these compounds are separated by a propanone linker. Since this connector could be susceptible to the action of natural nucleophiles from biomacromolecules, possibly leading to covalent complexes, we explored its change by a triazolyl ring, which excludes the possibility of covalent bonds with the linker. The resulting small collection of triazolyl polyphenols allowed us to study the influence of the number and position of OH groups on the antioxidant properties [16]. Although we obtained excellent antioxidants, the yield in the preparation of methoxythiazolyl intermediates was very low in many cases, limiting their future applications. Our interest on new antioxidant structures moved us to further explore the linker chain joining the two phenolic rings, looking for easy, effective reactions. As a result, a small collection of amide and urea polyhydroxyphenyl derivatives **1–18** was prepared and characterized for their antioxidant properties, using different methods, oxygen radical absorbance capacity (ORAC), 2,2'-azinobis-(3-ethylbenzothiazoline-6-sulfonic acid) assay (ABTS), and the  $\alpha, \alpha$ -diphenyl- $\beta$ -picrylhydrazyl (DPPH) free radical scavenging test. Compounds with high antioxidant ability and acceptable aqueous stability were selected for further studies. The potential biological activity as antioxidants was tested in two biological systems highly susceptible for the deleterious effects of prooxidants in different inflammatory conditions, endothelial cells and whole aorta. Selected compounds showed protection against oxidative stress induced by inflammatory stimuli important in cardiovascular diseases, i.e., Angiotensin II and Interleukin  $1\beta$  (IL- $1\beta$ ). Compounds with different in vitro antioxidant profiles were chosen for studying the in vivo antioxidant properties in a model organism, *Saccharomyces cerevisiae*. All of them showed recovery of stressed yeast growth comparable to model antioxidants resveratrol and vitamin C.

## 2. Materials and Methods

### 2.1. Chemistry

General information, as well as the preparation and characterization of methoxy (OMe)-substituted intermediates (**19** to **36**) is described in the Supplementary Material document.

### 2.2. Preparation of Polyhydroxylated Amides (1 to 10)

General procedure for the deprotection of methoxy groups. To a previously cooled solution (0 °C) of the corresponding methoxy-substituted compound (1 equivalent) in dried  $\text{CH}_2\text{Cl}_2$  (15 mL), a 1M



solution of BBr<sub>3</sub> in DCM (2 equivalents for each heteroatom) was slowly added under Ar atmosphere. After stirring 24–48 h at room temperature under Ar, monitoring the total disappearance of the methoxy groups by HPLC-MS, H<sub>2</sub>O was added to the reaction mixture. The solid precipitate, when formed, was separated by filtration and washed with H<sub>2</sub>O and CH<sub>2</sub>Cl<sub>2</sub>. When no precipitate was observed, the product was extracted with EtOAc. The organic extracts were washed with H<sub>2</sub>O and brine, dried over Na<sub>2</sub>SO<sub>4</sub> and then evaporated to give the polyhydroxylated analogous compounds **1** to **10**. The crude products were purified as indicated in each case.

#### 2.2.1. N-(2,4-Dihydroxyphenyl)-2-(2',5'-dihydroxyphenyl)acetamide (1)

Reddish solid, 41% yield. m.p.: 178–180 °C (Precipitated with Et<sub>2</sub>O). HPLC: *t<sub>R</sub>* = 6.06 min (10 min gradient: 15 to 95% of A in B). <sup>1</sup>H-NMR (300 MHz, DMSO-*d*<sub>6</sub>) δ: 3.51 (s, 2H, CH<sub>2</sub>), 6.15 (dd, 1H, *J* = 8.6, 2.5 Hz, 4'-H), 6.29 (d, 1H, *J* = 2.6 Hz, 6'-H), 6.48 (dd, 1H, *J* = 8.5, 2.9 Hz, 5-H), 6.59 (d, 1H, *J* = 2.9 Hz, 3-H), 6.63 (d, 1H, *J* = 8.5 Hz, 6-H), 7.47 (d, 1H, *J* = 8.6 Hz, 3'-H), 8.67 (s, 1H, NH), 9.01 (s, 1H, OH), 9.03 (s, 1H, OH), 9.08 (s, 1H, OH), 9.64 (s, 1H, OH) ppm. <sup>13</sup>C-NMR (75 MHz, DMSO-*d*<sub>6</sub>) δ: 38.2 (CH<sub>2</sub>), 102.9 (C3), 105.6 (C5), 114.2 (C6'), 115.8 (C4'), 117.2 (C1), 118.3 (C3'), 122.5 (C1'), 122.8 (C6), 147.7 (C), 148.7 (C), 149.8 (C), 154.5 (C), 169.5 (CO) ppm. MS (ESI<sup>+</sup>): *m/z* 276.4 (M+H)<sup>+</sup>.

#### 2.2.2. 2-(2',4'-Dihydroxyphenyl)-N-(2,5-dihydroxyphenyl)acetamide (2)

Reddish solid, 44% yield, m.p.: 77–79 °C, (precipitated with Et<sub>2</sub>O). HPLC: *t<sub>R</sub>* = 2.50 min (10 min gradient: 15 to 95% of A in B). <sup>1</sup>H-NMR (300 MHz, DMSO-*d*<sub>6</sub>) δ: 1.91 (s, 2H, CH<sub>2</sub>), 6.19 (dd, 1H, *J* = 8.2, 2.3 Hz, 4'-H), 6.27 (dd, 1H, *J* = 8.5, 2.9 Hz, 5-H), 6.33 (d, 1H, *J* = 2.3 Hz, 6'-H), 6.58 (d, 1H, *J* = 8.5 Hz, 6-H), 6.93 (d, 1H, *J* = 8.2 Hz, 3'-H), 7.49 (d, 1H, *J* = 2.9 Hz, 3-H), 8.70 (br s, 1H, OH), 8.78 (s, 1H, NH), 9.03 (br s, 1H, OH), 9.19 (br s, 1H, OH), 9.61 (br s, 1H, OH) ppm. <sup>13</sup>C-NMR (75 MHz, DMSO-*d*<sub>6</sub>) δ: 38.3 (CH<sub>2</sub>), 102.9 (C3), 106.4 (C6'), 107.3 (C5), 109.8 (C1), 112.4 (C4'), 115.4 (C3'), 127.1 (C1'), 131.4 (C6), 138.8 (C), 149.8 (C), 156.0 (C), 157.5 (C), 170.0 (CO) ppm. MS (ESI<sup>+</sup>): *m/z* 276.4 (M+H)<sup>+</sup>.

#### 2.2.3. 2-(2',5'-Dihydroxyphenyl)-N-(4-hydroxyphenyl)acetamide (3)

White lyophilized solid, purified by column chromatography, EtOAc-Hex (gradient from 1:2 to 3:1). Yield of 79%, m.p.: 185–187 °C<sup>d</sup>. HPLC: *t<sub>R</sub>* = 2.17 min (5 min gradient: 15 to 95% of A in B). <sup>1</sup>H-NMR (400 MHz, DMSO-*d*<sub>6</sub>) δ: 3.46 (s, 2H, CH<sub>2</sub>), 6.45 (dd, 1H, *J* = 8.3, 2.9 Hz, 4'-H), 6.58 (d, 1H, *J* = 2.8 Hz, 6'-H), 6.59 (d, 1H, *J* = 8.6 Hz, 3'-H), 6.68 (d, 2H, *J* = 8.8 Hz, 3-H, 5-H), 7.37 (d, 1H, *J* = 8.6 Hz, 2-H, 6-H), 8.63 (br s, 1H, OH), 8.84 (br s, 1H, OH), 9.16 (br s, 1H, NH), 9.80 (s, 1H, OH) ppm. <sup>13</sup>C-NMR: (75 MHz, DMSO-*d*<sub>6</sub>) δ: 38.0 (CH<sub>2</sub>), 113.9 (C4'), 115.0 (C3, C5), 115.6 (C3'), 117.1 (C6'), 120.9 (C2, C6), 123.2 (C1'), 130.9 (C1), 147.7 (C), 149.7 (C), 153.24 (C), 169.0 (CO) ppm. MS (ESI<sup>+</sup>): *m/z* 260.33 (M+H)<sup>+</sup>.

#### 2.2.4. N-(2,5-Dihydroxyphenyl)-2-(2',5'-dihydroxyphenyl)acetamide (4)

Reddish lyophilized solid, purified by column chromatography, EtOAc-Hex (gradient from 1:1 to 4:1). Yield of 79%, m.p.: 204–207 °C<sup>d</sup>. HPLC: *t<sub>R</sub>* = 2.24 min (5 min gradient: 15 to 95% of A in B). <sup>1</sup>H-NMR (400 MHz, DMSO-*d*<sub>6</sub>) δ: 3.53 (s, 2H, CH<sub>2</sub>), 6.28 (dd, 1H, *J* = 8.6, 2.9 Hz, 4-H), 6.49 (dd, 1H, *J* = 8.6, 2.9 Hz, 4'-H), 6.60 (m, 2H, 3'-H, 6'-H), 8.65 (d, 1H, *J* = 8.6 Hz, 3-H), 7.48 (d, 1H, *J* = 2.9 Hz, 6-H), 8.71 (s, 1H, OH), 8.73 (s, 1H, OH), 8.95 (s, 1H, NH), 0.03 (s, 1H, OH), 9.07 (br s, 1H, OH) ppm. <sup>13</sup>C-NMR: (75 MHz, DMSO-*d*<sub>6</sub>) δ: 39.8 (CH<sub>2</sub>), 107.6 (C6), 110.0 (C3), 114.4 (C4), 115.5 (C4'), 115.7 (C3'), 117.2 (6'), 122.5 (C1'), 127.0 (C1), 138.3 (C), 147.6 (C), 149.8 (C), 149.8 (C), 169.5 (CO) ppm. MS (ESI<sup>+</sup>): *m/z* 276.27 (M+H)<sup>+</sup>.

#### 2.2.5. N-(2,4-Dihydroxyphenyl)-2-(2',4'-dihydroxyphenyl)acetamide (5)

White lyophilized solid, purified by column chromatography, EtOAc-Hex (gradient from 1:1 to 4:1). Yield of 94%, m.p.: 75–78 °C<sup>d</sup> (MeOH). HPLC: *t<sub>R</sub>* = 2.24 min (5 min gradient: 15 to 95% of A in B). <sup>1</sup>H-NMR (400 MHz, DMSO-*d*<sub>6</sub>) δ: 3.43 (s, 2H, CH<sub>2</sub>), 6.13 (dd, 1H, *J* = 8.7, 2.6, 4'-H), 6.16 (dd, 1H,

$J = 8.1, 2.4, 4\text{-H}$ ), 6.25 (d, 1H,  $J = 2.6$  Hz, 6'-H), 6.29 (d, 1H,  $J = 2.4$  Hz, 6-H), 6.90 (d, 1H,  $J = 8.2$  Hz, 3'-H), 7.48 (d, 1H,  $J = 8.7$  Hz, 3-H), 8.84 (br s, 1H, NH), 9.12 (br s, 2H, OH), 9.51 (br s, 2H, OH) ppm.  $^{13}\text{C-NMR}$ : (75 MHz, DMSO- $d_6$ )  $\delta$ : 37.8 ( $\text{CH}_2$ ), 102.6 ( $\text{C}3'$ ), 102.9 ( $\text{C}3$ ), 105.7 ( $\text{C}5$ ), 106.4 ( $\text{C}5'$ ), 112.7 ( $\text{C}6$ ), 118.5 ( $\text{C}6'$ ), 122.2 ( $\text{C}1'$ ), 131.3 ( $\text{C}1$ ), 148.4 ( $\text{C}$ ), 154.4 ( $\text{C}$ ), 156.1 ( $\text{C}$ ), 157.4 ( $\text{C}$ ), 170.0 ( $\text{CO}$ ) ppm. MS ( $\text{ESI}^+$ ):  $m/z$  276.34 ( $\text{M}+\text{H}$ ) $^+$ .

#### 2.2.6. 2-(2',5'-Dihydroxyphenyl)-N-(3,4-dihydroxyphenyl)acetamide (6)

Reddish lyophilized solid, purified by column chromatography EtOAc-Hex (gradient from 1:1 to 2:1), 56% yield, m.p.: 180 °C $^d$ . HPLC:  $t_R = 4.02$  min (5 min gradient: 2 to 95% of A in B).  $^1\text{H-NMR}$  (400 MHz, DMSO- $d_6$ )  $\delta$ : 3.34 (s, 2H,  $\text{CH}_2$ ), 6.45 (dd, 1H,  $J = 8.5, 2.9$ , 5'-H), 6.57 (d, 1H,  $J = 2.9$ , 6'-H), 6.59 (d, 1H,  $J = 8.5$  Hz, 5-H), 6.62 (d, 1H,  $J = 8.5$  Hz, 4'-H), 6.79 (dd, 1H,  $J = 8.5, 2.4$  Hz, 6-H), 7.14 (d, 1H,  $J = 2.4$  Hz, 2-H), 8.57 (s, 1H, OH), 8.62 (s, 1H, OH), 8.85 (s, 1H, NH), 8.92 (s, 1H, OH), 9.69 (s, 1H, OH) ppm.  $^{13}\text{C-NMR}$ : (75 MHz, DMSO- $d_6$ )  $\delta$ : 38.2 ( $\text{CH}_2$ ), 107.9 ( $\text{C}2$ ), 110.4 ( $\text{C}6$ ), 113.9 ( $\text{C}4'$ ), 115.2 ( $\text{C}5$ ), 115.6 ( $\text{C}3'$ ), 117.1 ( $\text{C}6'$ ), 123.2 ( $\text{C}1'$ ), 131.3 ( $\text{C}1$ ), 141.2 ( $\text{C}$ ), 144.9 ( $\text{C}$ ), 147.7 ( $\text{C}$ ), 149.7 ( $\text{C}$ ), 169.0 ( $\text{CO}$ ) ppm. MS ( $\text{ESI}^+$ ):  $m/z$  276.27 ( $\text{M}+\text{H}$ ) $^+$ .

#### 2.2.7. 2-(3',4'-Dihydroxyphenyl)-N-(4-hydroxyphenyl)acetamide (7)

White lyophilized solid, purified by column chromatography EtOAc-Hex (gradient from 1:1 to 3:1), 75% yield, m.p.: 192–194 °C. HPLC:  $t_R = 2.09$  min (5 min gradient: 15 to 95% of A in B).  $^1\text{H-NMR}$  (400 MHz, DMSO- $d_6$ )  $\delta$ : 3.36 (s, 2H,  $\text{CH}_2$ ), 6.54 (dd, 1H,  $J = 8.0, 2.1$ , 6'-H), 6.64 (d, 1H,  $J = 8.0$ , 3'-H), 6.66 (d, 2H,  $J = 8.9$  Hz, 3-H, 5-H), 6.72 (d, 1H,  $J = 2.1$  Hz, 2'-H), 7.35 (d, 2H,  $J = 8.9$  Hz, 2-H, 6-H), 8.70 (s, 1H, OH), 8.81 (br s, 1H, OH), 9.14 (s, 1H, NH), 9.76 (br s, 1H, OH) ppm.  $^{13}\text{C-NMR}$ : (75 MHz, DMSO- $d_6$ )  $\delta$ : 43.0 ( $\text{CH}_2$ ), 115.3 ( $\text{C}3, \text{C}5$ ), 115.6 ( $\text{C}2'$ ), 116.6 ( $\text{C}5'$ ), 120.0 ( $\text{C}6'$ ), 121.1 ( $\text{C}2, \text{C}6$ ), 127.3 ( $\text{C}1'$ ), 131.3 ( $\text{C}1$ ), 144.2 ( $\text{C}$ ), 145.3 ( $\text{C}$ ), 153.5 ( $\text{C}$ ), 169.2 ( $\text{CO}$ ) ppm. MS ( $\text{ESI}^+$ ):  $m/z$  260.33 ( $\text{M}+\text{H}$ ) $^+$ .

#### 2.2.8. 2-(2',4'-Dihydroxyphenyl)-N-(4-hydroxyphenyl)acetamide (8)

White lyophilized solid, purified by column chromatography EtOAc-Hex (gradient from 1:3 to 2:1), 80% yield, precipitated with Et $_2$ O (m.p.: 186–189 °C). HPLC:  $t_R = 2.43$  min (5 min gradient: 15 to 95% of A in B).  $^1\text{H-NMR}$  (400 MHz, DMSO- $d_6$ )  $\delta$ : 3.45 (s, 2H,  $\text{CH}_2$ ), 6.17 (dd, 1H,  $J = 8.2, 2.4$ , 5'-H), 6.27 (d, 1H,  $J = 2.4$ , 3'-H), 6.67 (d, 2H,  $J = 8.8$  Hz, 3-H, 5-H), 6.88 (d, 1H,  $J = 8.2$  Hz, 6'-H), 7.36 (d, 2H,  $J = 8.8$  Hz, 2-H, 6-H), 9.07 (s, 1H, NH), 9.14 (s, 1H, OH), 9.39 (br s, 1H, OH), 9.69 (br s, 1H, OH) ppm.  $^{13}\text{C-NMR}$ : (75 MHz, DMSO- $d_6$ )  $\delta$ : 37.4 ( $\text{CH}_2$ ), 102.5 ( $\text{C}3$ ), 106.1 ( $\text{C}5'$ ), 113.1 ( $\text{C}1'$ ), 115.0 ( $\text{C}3, \text{C}5$ ), 120.9 ( $\text{C}2, \text{C}6$ ), 131.0 ( $\text{C}1$ ), 131.1 ( $\text{C}6'$ ), 153.2 ( $\text{C}$ ), 156.1 ( $\text{C}$ ), 157.1 ( $\text{C}$ ), 169.6 ( $\text{CO}$ ) ppm. MS ( $\text{ESI}^+$ ):  $m/z$  260.33 ( $\text{M}+\text{H}$ ) $^+$ .

#### 2.2.9. 2-(2',5'-Dihydroxyphenyl)-N,N-bis(4-hydroxyphenyl)acetamide (9)

White lyophilized solid, purified by column chromatography EtOAc-Hex (gradient from 1:2 to 2:1), 72% yield, precipitated with Et $_2$ O, m.p.: 124–126 °C. HPLC:  $t_R = 4.57$  min (5 min gradient: 2 to 95% of A in B).  $^1\text{H-NMR}$  (400 MHz, DMSO- $d_6$ )  $\delta$ : 3.26 (s, 2H,  $\text{CH}_2$ ), 6.34 (dd, 1H,  $J = 8.5, 2.9$ , 4'-H), 6.27 (d, 1H,  $J = 2.9$ , 6'-H), 6.43 (d, 1H,  $J = 8.5$  Hz, 3'-H), 6.62 (d, 2H,  $J = 8.1$  Hz, 3-H, 5-H), 6.68 (d, 2H,  $J = 8.2$  Hz, 3''-H, 5''-H), 6.98 (d, 2H,  $J = 8.2$  Hz, 2''-H, 6''-H), 7.10 (d, 2H,  $J = 8.1$  Hz, 2-H, 6-H), 8.51 (s, 1H, OH), 8.57 (s, 1H, OH), 9.33 (br s, 1H, OH), 9.57 (br s, 1H, OH) ppm.  $^{13}\text{C-NMR}$ : (75 MHz, DMSO- $d_6$ )  $\delta$ : 35.7 ( $\text{CH}_2$ ), 113.6 ( $\text{C}3'', \text{C}5''$ ), 115.2 ( $\text{C}4'$ ), 115.3 ( $\text{C}3, \text{C}5$ ), 115.9 ( $\text{C}3', \text{C}6'$ ), 117.2 ( $\text{C}2'', \text{C}6''$ ), 123.4 ( $\text{C}2, \text{C}6$ ), 127.8 ( $\text{C}1'$ ), 129.4 ( $\text{C}1''$ ), 134.9 ( $\text{C}1$ ), 147.6 ( $\text{C}$ ), 149.5 ( $\text{C}$ ), 155.4 ( $\text{C}$ ), 156.6 ( $\text{C}$ ), 170.9 ( $\text{CO}$ ) ppm. MS ( $\text{ESI}^+$ ):  $m/z$  352.29 ( $\text{M}+\text{H}$ ) $^+$ .

#### 2.2.10. N-(2',5'-Dihydroxybenzyl)-2-(2'',5''-dihydroxyphenyl)-N-(4-hydroxyphenyl) acetamide (10)

White lyophilized solid, purified by column chromatography EtOAc-Hex (gradient from 1:2 to 2:1), 81% yield, precipitated with Et $_2$ O, m.p.: 114–116 °C. HPLC:  $t_R = 4.64$  min (5 min gradient: 2 to

95% of A in B).  $^1\text{H-NMR}$  (400 MHz,  $\text{DMSO-d}_6$ )  $\delta$ : 3.25 (s, 2H,  $\text{CH}_2$ ), 4.66 (s, 2H,  $\text{NCH}_2$ ), 6.41–6.46 (m, 3H, 4'H, 4''H, 6''H), 6.49 (d, 1H,  $J = 2.9$ , 6'-H), 6.52 (d, 1H,  $J = 8.2$  Hz, 3'H), 6.54 (d, 1H,  $J = 8.5$  Hz, 3''H), 6.74 (d, 2H,  $J = 8.7$  Hz, 3H, 5H), 7.01 (d, 2H,  $J = 8.7$  Hz, (d, 2H,  $J = 8.1$  Hz, 2H, 6H), 8.56 (s, 1H, OH), 8.60 (s, 1H, OH), 8.68 (s, 1H, OH), 8.73 (br s, 1H, OH), 9.63 (br s, 1H, OH) ppm.  $^{13}\text{C-NMR}$ : (75 MHz,  $\text{DMSO-d}_6$ )  $\delta$ : 35.0 ( $\text{CH}_2$ ), 48.2 ( $\text{N-CH}_2$ ), 113.8 ( $\text{C4''}$ ), 114.6 ( $\text{C6''}$ ), 115.4 ( $\text{C3''}$ ), 115.8 ( $\text{C3}$ ,  $\text{C5}$ ), 115.9 ( $\text{C4'}$ ), 117.4 ( $\text{C3'}$ ,  $\text{C6'}$ ), 123.1 ( $\text{C1'}$ ), 123.7 ( $\text{C1''}$ ), 129.1 ( $\text{C2}$ ,  $\text{C6}$ ), 133.7 ( $\text{C1}$ ), 147.4 ( $\text{C}$ ), 147.7 ( $\text{C}$ ), 149.5 ( $\text{C}$ ), 149.6 ( $\text{C}$ ), 156.7 ( $\text{C}$ ), 171.7 ( $\text{CO}$ ) ppm. MS ( $\text{ESI}^+$ ):  $m/z$  382.29 ( $\text{M}+\text{H}$ ) $^+$ .

### 2.3. Synthesis of Polyhydroxylated Ureas (11 to 18)

Treatment with  $\text{BBr}_3$  of the corresponding methoxylated ureas, following the same procedure above described for the synthesis of amide derivatives **1** to **10**, led to the polyhydroxylated ureas **11** to **18**.

#### 2.3.1. N-(2,4-Dihydroxyphenyl)-N'-(2',5'-dihydroxyphenyl)urea (11)

Whitish lyophilized solid, 95% yield, precipitated with  $\text{Et}_2\text{O}$ , m.p.:  $>155$  °C $^d$ . HPLC:  $t_R = 5.97$  min (15 min gradient: 2 to 40% of A in B).  $^1\text{H-NMR}$  (500 MHz,  $\text{DMSO-d}_6$ )  $\delta$ : 6.16 (dd, 1H,  $J = 8.6$ , 3.0 Hz, 4'-H), 6.18 (dd, 1H,  $J = 8.5$ , 2.9 Hz, 5-H), 6.31 (d, 1H,  $J = 2.7$  Hz, 3-H), 6.58 (d, 1H,  $J = 8.5$  Hz, 3'-H), 7.43 (d, 1H,  $J = 8.7$  Hz, 6-H), 7.46 (d, 1H,  $J = 2.9$  Hz, 6'-H), 8.45 (s, 1H, NH), 8.47 (s, 1H, NH), 8.59 (br s, 1H, OH), 8.93 (br s, 1H, OH), 9.00 (s, 1H, OH), 9.58 (s, 1H, OH) ppm.  $^{13}\text{C-NMR}$  (125 MHz,  $\text{DMSO-d}_6$ )  $\delta$ : 102.7 ( $\text{C-3}$ ), 105.6 ( $\text{C6'}$ ), 106.7 ( $\text{C4'}$ ), 107.6 ( $\text{C5}$ ), 115.0 ( $\text{C3'}$ ), 119.0 ( $\text{C1}$ ), 122.3 ( $\text{C6}$ ), 128.6 ( $\text{C1'}$ ), 138.4 ( $\text{C}$ ), 148.5 ( $\text{C}$ ), 149.9 ( $\text{CO}$ ), 153.4 ( $\text{C}$ ), 153.6 ( $\text{C}$ ) ppm. MS ( $\text{ESI}^+$ ):  $m/z$  277.3 ( $\text{M}+\text{H}$ ) $^+$ .

#### 2.3.2. N-(2,5-Dihydroxyphenyl)-N'-(4'-hydroxyphenyl)urea (12)

White prisms, 56% yield, m.p.: 180–182 °C ( $\text{MeOH}$ ). HPLC:  $t_R = 2.49$  min (10 min gradient: 15 to 95% of A in B).  $^1\text{H-NMR}$  (400 MHz,  $\text{DMSO-d}_6$ )  $\delta$ : 6.15 (dd, 1H,  $J = 8.4$ , 2.8 Hz, 4-H), 6.59 (d, 1H,  $J = 8.5$  Hz, 3-H), 6.67 (d, 2H,  $J = 8.8$  Hz, 3'-H, 5'-H), 7.20 (d, 2H,  $J = 8.8$  Hz, 2'-H, 6'-H), 7.58 (d, 1H,  $J = 2.8$  Hz, 6-H), 7.94 (d, 1H, NH), 8.60 (s, 1H, NH), 8.97 (s, H, OH), 9.03 (s, 1H, OH), 9.1 (s, 1H, OH) ppm.  $^{13}\text{C-NMR}$ : (75 MHz,  $\text{DMSO-d}_6$ )  $\delta$ : 106.2 ( $\text{C6}$ ), 107.3 ( $\text{C4}$ ), 114.8 ( $\text{C3}$ ), 115.3 ( $\text{C3'}$ ,  $\text{C5'}$ ), 120.1 ( $\text{C2'}$ ,  $\text{C6'}$ ), 128.7 ( $\text{C1}$ ), 131.5 ( $\text{C1'}$ ), 137.9 ( $\text{C}$ ), 150.0 ( $\text{C}$ ), 152.4 ( $\text{CO}$ ), 152.7 ( $\text{C}$ ), ppm. MS ( $\text{ESI}^+$ ):  $m/z$  261.28 ( $\text{M}+\text{H}$ ) $^+$ .

#### 2.3.3. N-(2,5-Dihydroxyphenyl)-N'-(3',4'-dihydroxyphenyl)urea (13)

White prisms, 68% yield, m.p.: 141–143 °C ( $\text{Cl}_2\text{CH}_2/\text{MeOH}$ ). HPLC:  $t_R = 1.73$  min (10 min gradient: 15 to 95% of A in B).  $^1\text{H-NMR}$  (400 MHz,  $\text{DMSO-d}_6$ )  $\delta$ : 6.1–6.2 (m, 2H, 4,6'-H), 6.31 (d, 1H,  $J = 2.6$ , 2'-H), 6.58 (d, 1H,  $J = 8.5$  Hz, 3-H), 7.43 (d, 1H,  $J = 8.7$  Hz, 5'-H), 7.46 (d, 1H,  $J = 2.9$  Hz, 6-H), 8.44 (s, 1H, NH), 8.47 (s, 1H, OH), 8.59 (s, 1H, OH), 8.94 (s, 1H, OH), 9.01 (s, 1H, OH), 9.59 (s, 1H, NH) ppm.  $^{13}\text{C-NMR}$ : (75 MHz,  $\text{DMSO-d}_6$ )  $\delta$ : 102.8 ( $\text{C6}$ ), 105.6 ( $\text{C2'}$ ), 106.8 ( $\text{C4}$ ), 107.7 ( $\text{C5'}$ ), 115.1 ( $\text{C3}$ ), 119.0 ( $\text{C6'}$ ), 122.4 ( $\text{C1}$ ), 128.6 ( $\text{C1'}$ ), 138.4 ( $\text{C}$ ), 148.6 ( $\text{C}$ ), 149.9 ( $\text{C}$ ), 153.4 ( $\text{C}$ ), 153.6 ( $\text{CO}$ ) ppm. MS ( $\text{ESI}^+$ ):  $m/z$  277.29 ( $\text{M}+\text{H}$ ) $^+$ .

#### 2.3.4. N-(3,4-Dihydroxyphenyl)-N'-(4'-hydroxyphenyl)urea (14)

White prisms, 60% yield, m.p.: 184–187 °C ( $\text{MeOH}/\text{Cl}_2\text{CH}_2$ ). HPLC:  $t_R = 2.12$  min (10 min gradient: 15 to 95% of A in B).  $^1\text{H-NMR}$  (400 MHz,  $\text{DMSO-d}_6$ )  $\delta$ : 6.14 (dd, 1H,  $J = 8.7$ , 2.6 Hz, 6-H), 6.32 (d, 1H,  $J = 2.6$  Hz, 2-H), 6.66 (d, 1H,  $J = 8.8$  Hz, 3'-H, 5'-H), 7.18 (d, 1H,  $J = 8.8$  Hz, 2'-H, 6'-H), 7.59 (d, 1H,  $J = 8.7$  Hz, 5-H), 7.68 (d, 1H, OH), 8.72 (s, 1H, OH), 8.87 (s, 1H, NH), 8.99 (s, 1H, NH), 9.69 (s, 1H, OH) ppm.  $^{13}\text{C-NMR}$ : (75 MHz,  $\text{DMSO-d}_6$ )  $\delta$ : 102.5 ( $\text{C2}$ ), 105.5 ( $\text{C5}$ ), 115.2 ( $\text{C3'}$ , 5'), 119.61 ( $\text{C6}$ ), 120.0 ( $\text{C2'}$ ,  $\text{C6'}$ ), 120.6 ( $\text{C1}$ ), 131.7 ( $\text{C1'}$ ), 147.2 ( $\text{C}$ ), 152.2 ( $\text{C}$ ), 152.7 ( $\text{CO}$ ), 153.2 ( $\text{C}$ ) ppm. MS ( $\text{ESI}^+$ ):  $m/z$  261.31 ( $\text{M}+\text{H}$ ) $^+$ .

### 2.3.5. N,N'-bis(4-Hydroxyphenyl)urea (15)

White prisms, 84% yield, m.p.: 245 °C<sup>d</sup> (MeOH; m.p. Lit [17] = 240 °C<sup>d</sup>). HPLC:  $t_R$  = 2.59 min (10 min gradient: 15 to 95% of A in B). <sup>1</sup>H-NMR (400 MHz, DMSO-d<sub>6</sub>) δ: 6.66 (d, 4H,  $J$  = 8.8, 3-H, 5-H), 7.18 (d, 4H,  $J$  = 8.8 Hz, 2-H, 6-H), 8.16 (s, 2H, NH), 8.99 (s, 2H, OH), ppm. <sup>13</sup>C-NMR: (75 MHz, DMSO-d<sub>6</sub>) δ: 115.2 (C3, C5), 120.3 (C2, C6), 131.5 (C1), 152.3 (C4), 153.1 (CO), ppm. MS (ESI<sup>+</sup>):  $m/z$  245.30 (M+H)<sup>+</sup>.

### 2.3.6. N,N'-bis(2,5-Dihydroxyphenyl)urea (16)

Lyophilized solid, purified by column chromatography EtOAc-Hex (gradient from 1:3 to 4:1), 20% yield, m.p.: 109 °C<sup>d</sup>. HPLC:  $t_R$  = 1.76 min (10 min gradient: 15 to 95% of A in B). <sup>1</sup>H-NMR (500 MHz, DMSO-d<sub>6</sub>) δ: 6.19 (dd, 2H,  $J$  = 8.5, 2.9 Hz, 4-H), 6.59 (d, 2H,  $J$  = 8.5 Hz, 3-H), 7.47 (d, 2H,  $J$  = 2.9 Hz, 6-H), 8.6 (s, 1H, NH), 8.74 (s, 2H, OH), 8.99 (s, 2H, OH) ppm. <sup>13</sup>C-NMR: (125 MHz, DMSO-d<sub>6</sub>) δ: 107.2 (C6), 108.0 (C4), 115.1 (C3), 128.4 (C1), 138.7 (C2), 149.9 (C5), 153.0 (CO) ppm. MS (ESI<sup>+</sup>):  $m/z$  277.39 (M+H)<sup>+</sup>.

### 2.3.7. N,N-bis(4-Hydroxyphenyl)-N'-(4'-hydroxyphenyl)urea (17)

Lyophilized solid, purified by column chromatography EtOAc-Hex (gradient from 1:2 to 3:1), 68% yield, m.p.: 186–187 °C<sup>d</sup>. HPLC:  $t_R$  = 7.15 min (10 min gradient: 2 to 95% of A in B). <sup>1</sup>H-NMR (400 MHz, DMSO-d<sub>6</sub>) δ: 6.60 (d, 2H,  $J$  = 8.9, 3'-H, 5'-H), 6.72 (d, 4H,  $J$  = 8.8, 3-H, 5-H), 7.05 (d, 4H,  $J$  = 8.7 Hz, 2-H, 6-H), 7.12 (d, 2H,  $J$  = 8.9 Hz, 2'-H, 6'-H), 7.41 (s, 1H, NH), 9.02 (s, 1H, OH), 9.43 (s, 2H, OH) ppm. <sup>13</sup>C-NMR: (75 MHz, CDCl<sub>3</sub>) δ: 114.7 (C3', C5'), 115.7 (C3, C5), 122.3 (C2', C6'), 128.7 (C2, C6), 131.2 (C), 134.9 (C), 152.8 (C), 154.6 (CO), 155.4 (C) ppm. MS (ESI<sup>+</sup>):  $m/z$  337.32 (M+H)<sup>+</sup>.

### 2.3.8. N-(2',5'-Dihydroxybenzyl)-N'-(2'',5''-dihydroxyphenyl)-N-(4-hydroxyphenyl)urea (18)

White lyophilized solid, purified by column chromatography EtOAc-Hex (gradient from 1:3 to 4:1), 10% yield, m.p.: 114–115 °C (MeOH). HPLC:  $t_R$  = 5.40 min (10 min gradient: 15 to 95% of A in B). <sup>1</sup>H-NMR (400 MHz, DMSO-d<sub>6</sub>) δ: 4.67 (s, 2H, N-CH<sub>2</sub>), 6.14 (dd, 1H,  $J$  = 8.5, 2.8, 4''-H), 6.43–6.48 (m, 2H, 4'-H, 3'-H), 6.56 (d, 1H,  $J$  = 8.6 Hz, 3''-H), 6.59 (d, 1H,  $J$  = 2.8 Hz, 6'-H), 6.80 (d, 1H,  $J$  = 8.7 Hz, 3-H, 5-H), 7.05 (s, 1H, NH), 7.10 (d, 1H,  $J$  = 8.7 Hz, 2-H, 6-H), 7.57 (d, 1H,  $J$  = 2.8 Hz, 6''-H), 8.62 (br s, 1H, OH), 8.65 (br s, 1H, OH), 8.78 (br s, 1H, OH), 8.88 (br s, 1H, OH), 9.72 (br s, 1H, OH) ppm. <sup>13</sup>C-NMR: (100 MHz, DMSO-d<sub>6</sub>) δ: 47.9 (N-CH<sub>2</sub>), 105.6 (C6''), 107.6 (C6'), 114.4 (C4''), 114.5 (C4'), 115.3 (C3''), 115.9 (C3'), 116.5 (C3, C5), 124.7 (C), 128.2 (C), 129.5 (C2, C6), 132.0 (C), 137.5 (C), 147.2 (C), 149.7 (C), 150.0 (C), 154.4 (CO), 156.9 (C) ppm. MS (ESI<sup>+</sup>):  $m/z$  383.25 (M+H)<sup>+</sup>.

## 2.4. Antioxidant Activity

### 2.4.1. Oxygen Radical Absorbance Capacity (ORAC) Experiment

The ORAC assay was performed following Ou et al. [18], as modified by Garcés-Rimón et al. [19]. All samples and reagents were dissolved in phosphate buffer (75 mM; pH 7.4). The reaction was performed in a final volume of 200 µL: 20 µL test samples or 20 µL 6-hydroxy-2,5,7,8-tetramethylchroman-2-carboxylic acid (Trolox) solutions (0.2–2 nM), 120 µL fluorescein solution (1.17 mM) and 60 µL 2,2'-azo-bis-(2-methylpropionamidine) dihydrochloride (AAPH) 1.3% solution (all from Sigma Aldrich, Alcobendas, Spain) were added to the wells of a black 96-well plate. The fluorescence was recorded at 40 °C every 55 s for 95 min using a fluorimeter (SpectraMax M2; Molecular Devices, California, USA), with excitation and emission wavelengths of 480 and 520 nm, respectively. All samples were tested in triplicate. ORAC values were expressed as µmol of Trolox equivalents (TE)/µmol of pure compound.

#### 2.4.2. ABTS Experiment

The 2,2'-azino-bis (3-ethylbenzothiazoline-6-sulfonic acid) diammonium salt (ABTS) assay was performed according to Re et al. [20] and modified by Oki et al. [21] for its use in microplates. Samples were diluted in methanol. An ABTS<sup>•+</sup> stock solution was prepared by adding 44 µL of potassium persulfate (140 mmol/L) to a 2.5 mL ABTS<sup>•+</sup> aqueous solution (7 mmol/L). The working solution of the radical ABTS<sup>•+</sup> was prepared by diluting the stock solution 1:75 (*v/v*) in a sodium phosphate buffer (5 mmol/L, pH 7.4) to obtain an absorbance value of 0.7±0.02 at 734 nm. Samples (30 µL) were added to 270 µL of the working solution of ABTS<sup>•+</sup> in a microplate. Absorbance was measured at 734 nm and 30 °C for 20 min, every 5 min in a Synergy HT plate spectrophotometer (Biotek Instruments, Winoosky, VT, USA). A calibration curve was made with Trolox (20–250 µM). All samples were analyzed in triplicate. Results were expressed in µmol TE/µmol of pure compound, as for the ORAC assays.

#### 2.4.3. DPPH Experiment

For the 2,2'-diphenylpicrylhydrazyl (DPPH) assay, antioxidant compounds were dissolved in ethanol with a stock concentration of 4 mM and stirred for 24 h. DPPH (Alfa Aesar) was also dissolved in ethanol at 0.127 mM. Different compound solutions were prepared by serial dilutions of each stock solution (4, 2, 1, 0.5, 0.25, 0.125, 0.063, 0.031, 0.015, and 0.007 M). Resveratrol was prepared using the same protocol and used as antioxidant control. Amounts of 80 µL of each solution and 80 µL of DPPH were added in a 96-well plate. The absorbance was measured at different times (10, 20 and 30 min and 1 and 2 h) by a Multi-Detection Microplate Reader Synergy HT ( $\lambda_{MAX} = 515$  nm). Radical scavenging activity (RSA, %) was calculated using Equation (1)

$$RSA(\%) = \frac{A_{DPPH} - A_{EXTRACT}}{A_{DPPH}} \cdot 100 \quad (1)$$

where  $A_{EXTRACT}$  and  $A_{DPPH}$  correspond to the absorbance of DPPH with and without the extracts, respectively. Eight replicates were used for each compound and results were expressed as mean value ± standard deviation. The RSA half-maximal inhibitory concentration ( $IC_{50}$ ) values were calculated from the relationship curve of RSA versus concentrations by a non-linear fit using the software GraphPad Prism 7.

### 2.5. *In Vitro* Cellular Assays

#### Cell Viability

Cytotoxicity of selected antioxidant compounds was assessed using human dermal fibroblasts (HDF, Innoprot, P10856) and an AlamarBlue assay. Human fibroblasts were grown and maintained using Dulbecco's Modified Eagle Medium high glucose (DMEM, Sigma Aldrich, D6171), supplemented with 10% Fetal Bovine Serum (FBS), 2% L-glutamine and 1% penicillin/streptomycin. Cells were incubated at 37 °C, 95% relative humidity and 5% CO<sub>2</sub>. Additionally, DMEM-high glucose, HEPES, no phenol red (Gibco, 2106329) was used to prepare the AlamarBlue solution. Stock solutions of the antioxidant compounds **3**, **8**, **15** and **17** were prepared in dimethyl sulfoxide (DMSO). Compound **7** was not soluble enough in DMSO to obtain a cell viability  $IC_{50}$  value. Serial dilutions of the antioxidant compounds were prepared using the previously mentioned stock solutions and DMEM. Final DMSO concentration was maintained lower than 1% *v/v* in the cell culture experiments. HDF were seeded at  $9 \times 10^4$  cells/well in a 96-well plate and incubated for 24 h. The medium was replaced by the corresponding antioxidant solutions and incubated for an additional 24 h. Then, compounds were removed, cells were washed with Dulbecco's Phosphate Buffered Saline (PBS, Sigma Aldrich) and treated with a 10% *v/v* AlamarBlue (Invitrogen) solution prepared in DMEM without phenol red. After 3 h of incubation, absorbance was monitored at 570 nm by a Multi-Detection Microplate Reader Synergy HT. Cells treated with DMEM without any antioxidant compound were used as the 100%

viability control. Eight replicates were used for each antioxidant solution. IC<sub>50</sub> values were obtained by a non-linear fit using the software GraphPad Prism 7.

## 2.6. Reduced Nicotinamide Adenine Dinucleotide Phosphate (NADPH) Oxidase Activity Assay in Vascular Systems

The human microvascular endothelial cells line (HMEC-1) (ATCC<sup>®</sup>, Middlesex, UK; CRL-3243<sup>™</sup>) was used. Cells were cultured according to the manufacturer instructions with MCDB131 medium (Corning, NY, USA, Cat. No. 702564) supplemented with 10 ng/mL epidermal growth factor (Sigma-Aldrich, Alcobendas, Spain), 1 µg/mL hydrocortisone (Sigma-Aldrich), 10 mmol/L glutamine (Sigma-Aldrich), 10% fetal bovine serum (FBS, Sigma-Aldrich), 100 U/mL of penicillin and 100 µg/mL of streptomycin. At 80% confluence, cells were serum-deprived for 24 h before stimulation. HMEC were treated with AngII (1 nmol/L for 6 h; Sigma-Aldrich) in the absence or in the presence of the different compounds that were added 30 min before stimulation.

Aortic segments from three-month-old C57BL/6J mice were incubated with IL-1β (10 ng/mL, 6 h, Sigma Aldrich) in the presence and in the absence of the different compounds that were added 30 min before stimulation.

The O<sub>2</sub> production generated by NADPH oxidase was determined by a chemiluminescence assay. Briefly, endothelial cells or aortic segments were homogenized in phosphate buffer (50 mmol/L KH<sub>2</sub>PO<sub>4</sub>, 1 mmol/L EGTA, 150 mmol/L sucrose, pH 7.4). The reaction was started by the addition of a lucigenin (5 µmol/L) and NADPH (100 µmol/L; Sigma-Aldrich) mixture to the protein sample in a final volume of 250 µL. Chemiluminescence was determined every 2.4 s for 3 min in a microtiter plate luminometer (Enspire Perkin Elmer). Basal activity in the absence of NADPH was subtracted from each reading and normalized to protein concentration. Data were normalized vs. control situation.

All data are expressed as mean values ± standard mean error and n represents the number of animals or different cell cultures. Statistical analysis was performed using GraphPad Prism Software (v7.04). Data distribution (by Shapiro–Wilk normality test) was used to choose the appropriate statistics test. Results were analyzed by the Mann–Whitney non-parametric or Student's t-tests when appropriate (two-tailed) or one-way Anova or Kruskal–Wallis test when appropriate followed by Bonferroni's post hoc test or uncorrected Dunn's test, respectively.

## 2.7. In Vivo Antioxidant Capacity in Stressed Yeasts

### 2.7.1. Yeast Strain and Induction of Oxidative Stress

*Saccharomyces cerevisiae* haploid strain BY4741 was used as described previously [16,22]. Briefly, 20 µL of glycerol stock culture was revived in 5 mL of YPD medium (1% yeast extract, 2% bacteriological peptone and 2% dextrose) at 28 °C, with shaking (210 rpm). Fifty microliters of 20-h-old culture was used to inoculate fresh 5 mL YPD (control medium) or 5 mL of oxidative stress medium (YPOxD: YPOxD; 1% yeast extract, 2% bacteriological peptone, 1% dextrose and 3% H<sub>2</sub>O<sub>2</sub>). Stress (and control) was conducted during 16 h at 28 °C, with shaking (220 rpm).

### 2.7.2. Measurement of Antioxidant Capacity

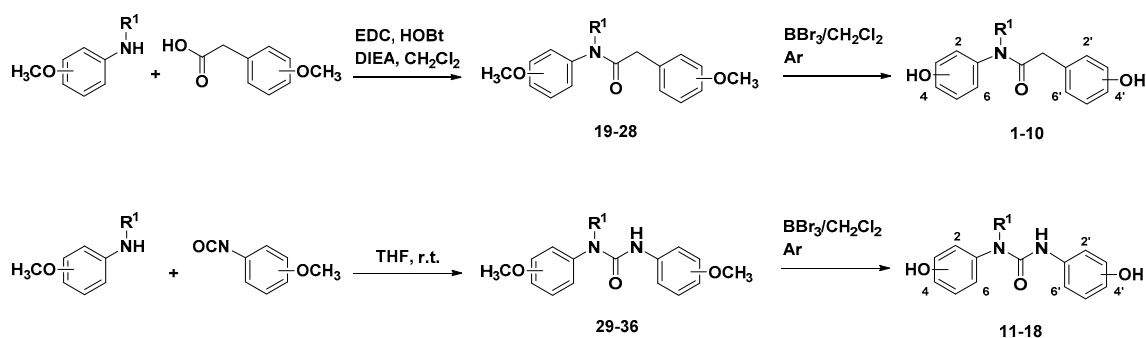
In vivo antioxidant capacity was determined as recovery of growth rate in stressed yeasts (yeast grown in YPOxD for 16 h) challenged by compounds **8**, **15** and **17** (dissolved in methanol at 2 mg/mL), and compared to Resveratrol and vitamin C (dissolved in methanol at 2 mg/mL) as positive controls at four different doses (2, 10, 20 and 40 µg of each pure compound) or compared to stressed cells directly, as previously described [16,23]. Growth rate was determined from growth kinetics using the BioScreen C plate-reader system (OY Growth Curves Ab Ltd., Helsinki, Finland). Stressed yeast cultures (16 h old) were used to inoculate 200 µL of fresh media to an initial OD<sub>595</sub> of 0.05–0.07, being distributed in 100-well honeycomb plates (Oy Growth Curves) in triplicate per each condition (each different dose of each compound). Plates were then incubated at 28 °C for 72 h, with shaking

(High force), taking OD measurement each 15 min in the Bioscreen C. Maximum growth rate ( $\mu_{\max}$ ) and biomass production (carrying capacity) were determined in R using ‘Growthcurver’ package version 0.3 [24]. Growth curves were constructed in EXCEL, represented as mean  $\pm$  SEM (standard error of mean). One-way ANOVA followed by Tukey’s multiple comparisons test was performed with PRISMA v 6.0 software to compare among maximum growth rate or carrying capacity between tested compounds, Resveratrol, Vitamin C or control yeasts (grown in YPD or in YPOxD). In addition, to measure survival after oxidative stress and antioxidant effectiveness of each compound, yeast cells from each challenge were serially diluted in 96-well plates, and each dilution was spotted (with a 8  $\times$  6 stainless steel replica platter from SIGMA) in triplicate to determine viable colonies after 24–48 h at 28 °C. Survivors (mean  $\pm$  SEM) were compared between treatments with one-way ANOVA, Fisher’s LSD test, with alpha at 0.05 for significance.

### 3. Results and Discussion

#### 3.1. Preparation of Designed Polyphenols

As indicated, two series of compounds were designed, both containing two polyphenol rings separated by a three-atoms linker, either containing an amide or a urea moiety. Combinations of 4-, 2,4-, 3,4-(catechol) and 2,5-OH were selected based on our previous results on the triazole series [16], and by their incidence in many polyphenols from natural sources. The synthesis of the amide and urea polyhydroxyphenyl derivatives **1** to **18** was performed following conventional methods, as depicted in Scheme 1.



**Scheme 1.** Synthetic route to polyhydroxy amides **1** to **10**, and polyhydroxy ureas **11** to **18**.

The methoxyphenyl amide derivatives **19** to **28** were prepared by reaction of the conveniently substituted aniline and the corresponding phenylacetic acid, in  $\text{CH}_2\text{Cl}_2$ , using 1-ethyl-3-(3-dimethylaminopropyl) carbodiimide (EDC·HCl) and 1-hydroxybenzotriazole (HOBt) as coupling agents, in the presence of *N,N*-diisopropylethylamine (DIEA) as a base. Further treatment of methoxy-substituted intermediates **19** to **28** with  $\text{BBr}_3$  led to the desired hydroxylated amides, compounds **1** to **10** (Scheme 1). On the other hand, the preparation of the ureido compounds **29–36** was carried out from the corresponding methoxyanilines and the methoxy-substituted isocyanates, by reaction at room temperature in tetrahydrofuran (THF) (Scheme 1). The final hydroxyl derivatives (**11** to **18**) were prepared from **29** to **36** also by demethylation reaction with  $\text{BBr}_3$ . The synthesis proceeded very smoothly and most compounds were obtained in moderate-to-good yields with elevated grade of purity (Tables 1 and 2). The acylation reaction was especially difficult in the case of the secondary bis-4-methoxyphenylamine to obtain methoxy amide **27**, and during the urea formation of intermediate **36**. Low yields in some demethylation reactions seem to be related to low stability of the final polyhydroxylated compounds (as explained later).



**Table 1.** Structures and yield of synthetic polyhydroxy amides (**1** to **10**), and ureas (**11** to **18**) prepared.

$R^1 = \text{H}, (4\text{-OH})\text{Ph}, (2,5\text{-OH})\text{Bn}$   
 $R^2\text{-}R^5, R^{2'}\text{-}R^{5'} = \text{H}, \text{OH}$   
 $X = \text{CH}_2, \text{NH}$

**1-18**

Compound	R1	R2	R3	R4	R5	R2'	R3'	R4'	R5'	X	Yield (%)
1	H	OH	H	OH	H	OH	H	H	OH	CH <sub>2</sub>	41
2	H	OH	H	H	OH	OH	H	OH	H	CH <sub>2</sub>	44
3	H	H	H	OH	H	OH	H	H	OH	CH <sub>2</sub>	79
4	H	OH	H	H	OH	OH	H	H	OH	CH <sub>2</sub>	79
5	H	OH	H	OH	H	OH	H	OH	H	CH <sub>2</sub>	94
6	H	H	OH	OH	H	OH	H	H	OH	CH <sub>2</sub>	56
7	H	H	H	OH	H	H	OH	OH	H	CH <sub>2</sub>	75
8	H	H	H	OH	H	OH	H	OH	H	CH <sub>2</sub>	80
9	(4-OH)Ph	H	H	OH	H	OH	H	H	OH	CH <sub>2</sub>	72
10	(2,5-OH)Bn	H	H	OH	H	OH	H	H	OH	CH <sub>2</sub>	81
11	H	OH	H	OH	H	OH	H	H	OH	NH	95
12	H	OH	H	H	OH	H	H	OH	H	NH	56
13	H	OH	H	H	OH	H	OH	OH	H	NH	68
14	H	H	OH	OH	H	H	H	OH	H	NH	60
15	H	H	H	OH	H	H	H	OH	H	NH	84
16	H	OH	H	H	OH	OH	H	H	OH	NH	20
17	(4-OH)Ph	H	H	OH	H	H	H	OH	H	NH	68
18	(2,5-OH)Bn	H	H	OH	H	OH	H	H	OH	NH	10

**Table 2.** Structures and yield of OMe precursors prepared, amides **19** to **28** and ureas **29** to **36**.

$R^1 = \text{H}, (4\text{-OMe})\text{Ph}, (2,5\text{-OMe})\text{Bn}$   
 $R^2\text{-}R^5, R^{2'}\text{-}R^{5'} = \text{H}, \text{OMe}$   
 $X = \text{CH}_2, \text{NH}$

**19-36**

Compound	R <sup>1</sup>	R <sup>2</sup>	R <sup>3</sup>	R <sup>4</sup>	R <sup>5</sup>	R <sup>2'</sup>	R <sup>3'</sup>	R <sup>4'</sup>	R <sup>5'</sup>	X	Yield (%)
19	H	OMe	H	OMe	H	OMe	H	H	OMe	CH <sub>2</sub>	81
20	H	OMe	H	H	OMe	OMe	H	OMe	H	CH <sub>2</sub>	77
21	H	H	H	OMe	H	OMe	H	H	OMe	CH <sub>2</sub>	50
22	H	OMe	H	H	OMe	OMe	H	H	OMe	CH <sub>2</sub>	65
23	H	OMe	H	OMe	H	OMe	H	OMe	H	CH <sub>2</sub>	74
24	H	H	OMe	OMe	H	OMe	H	H	OMe	CH <sub>2</sub>	73
25	H	H	H	OMe	H	H	OMe	OMe	H	CH <sub>2</sub>	81
26	H	H	H	OMe	H	OMe	H	OMe	H	CH <sub>2</sub>	76
27	(4-OMe)Ph	H	H	OMe	H	OMe	H	H	OMe	CH <sub>2</sub>	28
28	(2,5-OMe)Bn	H	H	OMe	H	OMe	H	H	OMe	CH <sub>2</sub>	74
29	H	OMe	H	OMe	H	OMe	H	H	OMe	NH	55



Table 2. Cont.

Compound	R <sup>1</sup>	R <sup>2</sup>	R <sup>3</sup>	R <sup>4</sup>	R <sup>5</sup>	R <sup>2'</sup>	R <sup>3'</sup>	R <sup>4'</sup>	R <sup>5'</sup>	X	Yield (%)
30	H	OMe	H	H	OMe	H	H	OMe	H	NH	85
31	H	OMe	H	H	OMe	H	OMe	OMe	H	NH	69
32	H	H	OMe	OMe	H	H	H	OMe	H	NH	42
33	H	H	H	OMe	H	H	H	OMe	H	NH	80
34	H	OMe	H	H	OMe	OMe	H	H	OMe	NH	84
35	(4-OMe)Ph	H	H	OMe	H	H	H	OMe	H	NH	63
36	(2,5-OMe)Bn	H	H	OMe	H	OMe	H	H	OMe	NH	17

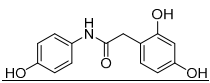
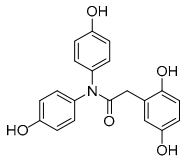
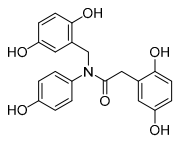
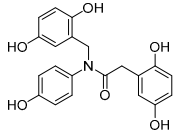
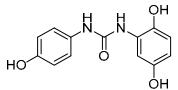
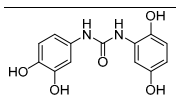
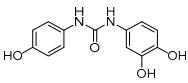
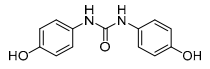
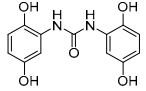
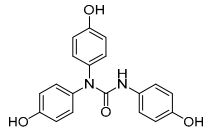
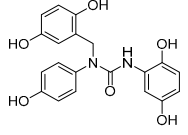
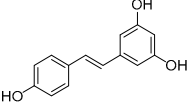
### 3.2. Antioxidant Characterization of the New Polyphenols Collection

The antioxidant capacity of the small collection of new polyphenols (Table 1) was firstly evaluated in an Oxygen Radical Absorbance Capacity (ORAC) assay (Table 3). All compounds exhibited strong radical scavenging activities; 14 out of the 18 compounds tested, showed values even higher than those found for resveratrol (own data), a well-known natural antioxidant used as control. Compared to resveratrol (TE 8  $\mu\text{mol trolox}/\mu\text{mol}$ , TE: Trolox Equivalents), six of the compounds show 2–3-fold higher antioxidant capacity. Thus, some of the results found were quite outstanding, as in the case of compounds **9** and **10** that showed values above 25 TE per sample, and **3**, **7**, **8** and **17** with >19 TE. Compounds **1**, **4**, **12**, **16**, and **18** still display higher antioxidant activity than resveratrol, while derivatives **2**, **6**, **13** and **15** are comparable to the control, and only polyphenols **5** and **11** have lower antioxidant ability compared to resveratrol (Table 3).

**Table 3.** Antioxidant activity (oxygen radical absorbance capacity (ORAC)) and chemical stability of compounds **1** to **18**.

Compound	Chemical Structure	ORAC <sup>a</sup>	Aqueous Stability <sup>b</sup> (%)
1		11.0 ± 0.4	2
2		8.1 ± 0.1	-
3		19.2 ± 0.2	77
4		14.4 ± 0.2	0
5		5.2 ± 0.4	-
6		9.4 ± 0.4	0
7		19.2 ± 0.4	90

Table 3. Cont.

Compound	Chemical Structure	ORAC <sup>a</sup>	Aqueous Stability <sup>b</sup> (%)
8		19.3 ± 0.5	98
9		29.5 ± 0.5	0
10		27.6 ± 0.5	0
11		6.6 ± 0.1	-
12		12.5 ± 0.7	0
13		7.8 ± 0.3	-
14		9.6 ± 0.1	0
15		8.9 ± 0.4	90
16		11.9 ± 0.4	0
17		19.4 ± 0.7	93
18		15.3 ± 0.7	0
Resveratrol		8.1 ± 1.17	-

<sup>a</sup> μmol of trolox/μmol of pure compound. <sup>b</sup> Percentage of remaining pure compound (measured by HPLC) after two months at room temperature in aqueous solution (+20% acetonitrile).

Going into more detail through the data from the ORAC assay, and taking into consideration the chemical structure, we firstly focused on the compounds having only two phenyl rings in their structure. In general, it can be said that amide derivatives showed higher TE values than ureas. Comparing compounds with the same pattern of hydroxyl substituents, TE values showed by amides **1**, **3**, **7** and **8**, are higher than those of their corresponding urea derivatives **11**, **12**, **13** and **14**. In the case of **8** and **14**, the value was the double for the former. Besides, for the three best amides, **3**, **7** and **8**, it is remarkable that all of them have a *p*-monohydroxyphenyl ring at the N-amide atom, while the benzyl ring has two hydroxyl groups in 2,5-, 2,4- or 3,4- positions, respectively (Table 3).

On the other hand, both in the case of amide and urea derivatives, the antioxidant capacity was increased by incorporation of a third phenolic ring at N position, like in **9**, **10**, **17** and **18** compounds. A 4-hydroxyphenyl substitution (**9** and **17**) led to slightly better TE values than a 2,5-dihydroxybenzyl moiety (compounds **10** and **18**).

ORAC values for most of the prepared compounds were also higher than those found for other natural antioxidants, like quercetin, hydrotyrosol, D-catechin and (-)-epicatechin (Table S1).

Considering the high tendency to oxidation of polyphenols, and before further characterization of this series of compounds, we decided to check the stability in aqueous media of all polyphenol derivatives showing higher antioxidant capacity than resveratrol (Table 3). To facilitate the solubility, compounds were dissolved in a mixture of H<sub>2</sub>O/acetonitrile (80:20%) and maintained at room temperature. The solutions were checked by HPLC-MS at regular intervals of time for 60 days. Only amides **3**, **7**, **8** and ureas **15** and **17** proved to be sufficiently stable after two months. The rest of the compounds suffered progressive degradation, with complete disappearance from the solution after 10 or 20 days. The most unstable polyphenol derivatives were **4** and **10** (Figure S1), having both two *p*-dihydroxy substitutions in the phenyl rings, which points to the rapid and easy oxidation to the *p*-hydroquinone. From the four compounds with three phenyl rings, only one was stable in aqueous solution (**17**).

After checking the chemical stability, only the five more stable compounds (**3**, **7**, **8**, **15** and **17**) were selected to complete their characterization as antioxidants. For this purpose, we used ABTS and DPPH assays, two spectrophotometric methods normally applied to show the radical scavenging ability of antioxidant compounds (Table 4). First, the compounds were evaluated in the ABTS (2,2'-azinobis-(3-ethylbenzothiazoline-6-sulfonic acid) assay [20]. In the presence of oxidant agents, ABTS form a stable radical cation (ABTS<sup>•+</sup>) chromophore, with an absorbance band at 734 nm. The presence of this radical cation is reduced by hydrogen-donating compounds, like polyphenols, producing a discoloration of the solution proportional to the amount of antioxidant. In this assay, four out of five compounds showed TE values higher than resveratrol (Table 4), with amide derivative **7** as the best radical scavenger (nearly fourfold higher than control). However, urea **15**, which has already the lowest ORAC value among the selected compounds, was worse than resveratrol in this assay. The radical scavenging ability of compounds **7** and **8** is higher and comparable, respectively, to those of quercetin and (-)-epicatechin natural products in this ABTS assay (Table S1).

**Table 4.** Antioxidant profile of selected stable compounds.

Comp	Chemical Structure	ORAC <sup>a</sup>	ABTS <sup>a</sup>	DPPH PSA IC <sub>50</sub> (μM) <sup>b</sup>	
				10 min	2 h
3		19.2 ± 0.2	3.27 ± 0.1	8.30	6.77
7		19.2 ± 0.	8.12 ± 0.09	24.10	23.30
8		19.3 ± 0.5	5.00 ± 0.09	150.90	64.20
15		8.9 ± 0.4	1.17 ± 0.01	ND <sup>c</sup>	ND <sup>c</sup>
17		19.4 ± 0.7	3.57 ± 0.00	17.92	9.60
Resveratrol		8.08 ± 1.2	2.13 ± 0.02	66.22	19.48

<sup>a</sup> μmol of trolox/μmol of pure compound. <sup>b</sup> The half-maximal inhibitory concentration (IC<sub>50</sub>) values for the α,α-diphenyl-β-picrylhydrazyl (DPPH) assay correspond to the amount of compound needed to reach 50% of radical scavenging activity (RSA) after 10 min and 2 h of addition. <sup>c</sup> ND: not determined.

Another frequently used method for antioxidant determination is the DPPH assay, based on the capacity of the 2,2-diphenyl-1-picryl-hydrazyl, DPPH free radical to be reduced in the presence of an antioxidant [25]. According to the previous results, only four compounds, three amides, **3**, **7** and **8**, and the urea derivative **17** were evaluated in this assay, always using resveratrol as control. The antioxidant capacity was measured at different concentrations in a progressive descending order, going from 2 to 0.003 mM, and additionally, at an interval of time for each concentration (five measures from 10 min to 2 h). For all of them, a concentration dependent behavior was observed (Figure 1). Comparing the maximum antioxidant capacities observed at the highest concentration (2 mM), at the beginning of the experiment (10 min time) the four compounds showed RSA percentage values comparable to the control, resveratrol (77%). Compounds **3** and **17**, reached about the same values as control, 78% and 72%, respectively, **8** showed a slightly lower percentage of 67%, and amide **7** proved to have a slightly higher capacity than resveratrol, 82% (Figure 1). As for the potency, the IC<sub>50</sub> values shown in Table 4 indicate that the best compound in this assay is amide **3**, followed by urea **17** and amide **7**. Compared to resveratrol, the RSA capacity after 10 min was 8-, 2.8- and 3.7-fold higher for **3**, **7** and **17**, respectively.

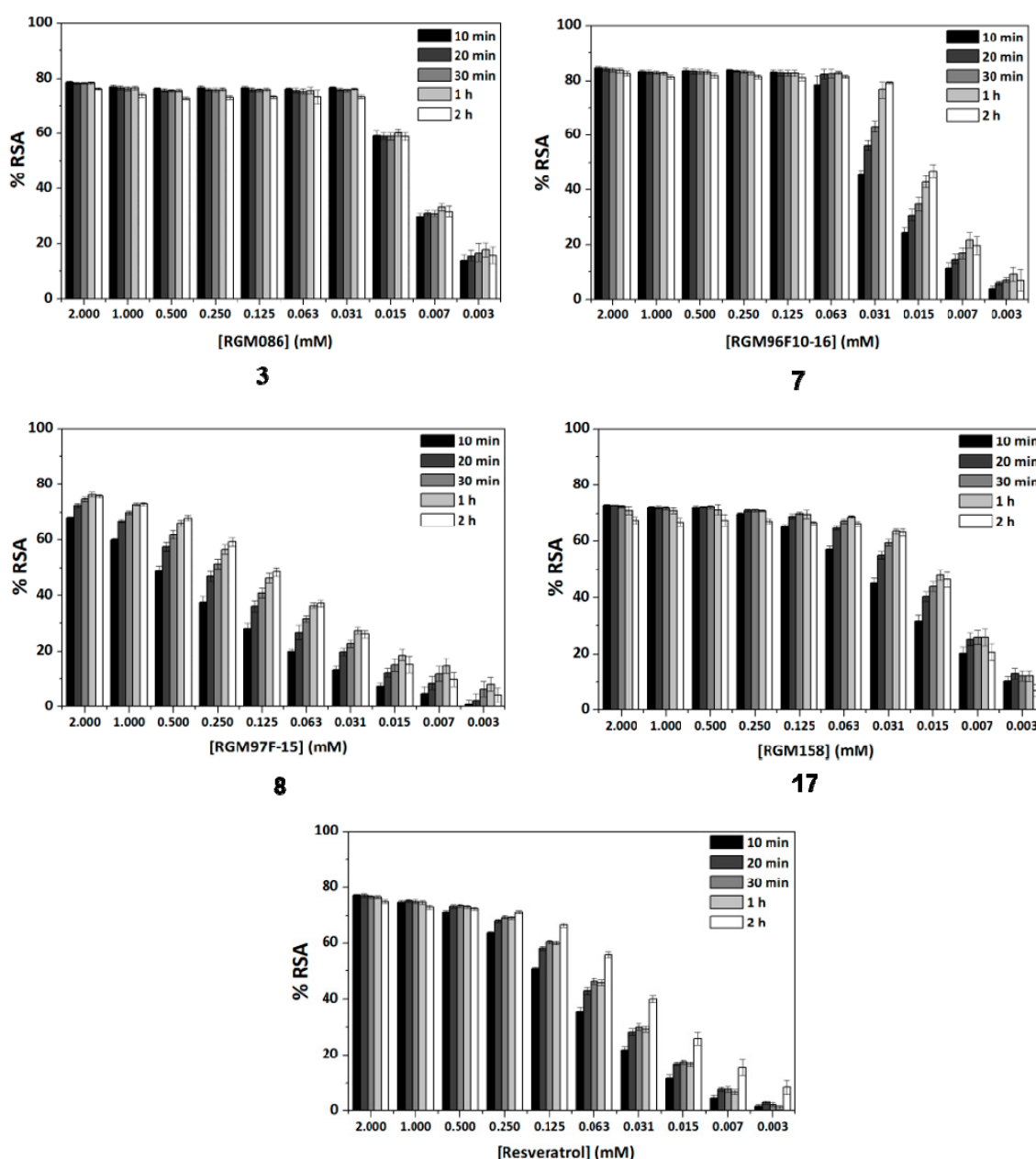


**Figure 1.** Study of the radical scavenging activity (RSA) capacity showed by compounds **3**, **7**, **8** and **17** and control (resveratrol) low in the DPPH assay. Variations with sample concentration and time.

Looking at how the RSA capacity of compounds is modified with time (Figure 1), resveratrol (right graph) maintained the RSA capacity at concentrations above 0.5 mM. However, at lower concentrations the RSA percentages clearly diminished as a function of concentration, but increased with time (RSA 2h > RSA 10 min). In our case, compound **8**, shows this time-dependent behavior already from high concentrations (Figure S2). However, compounds **3**, **7** and **17** maintained the RSA ability nearly at the same percentage levels, independently on time, until quite low concentrations, 0.031, 0.063 and 0.25 mM, respectively, which is a remarkable difference with resveratrol (Figure 1). This behavior of **3**, **7** and **17**, will allow the use of low concentrations of sample for achieving a high effect. On the other hand, like for resveratrol, and with the exception of compound **3**, at the low concentration of 0.031 mM for **7** and **17**, the RSA ability increased with time (Figure 1).

Compound **3**, at a concentration of 0.031 mM, still shows a remarkably high RSA (78%), which is maintained with time, from 10 min to 2 h. This time-independent behavior is observed even at lower

concentrations (0.015–0.003 M), which can be an advantage for those applications that require an immediate antioxidant effect.

### 3.3. Biological Evaluation of Synthetic Polyphenols

#### 3.3.1. Cell Viability

To evaluate the potential cytotoxicity of the selected compounds, an AlamarBlue assay was performed and the cell viability  $IC_{50}$  values were extrapolated using a non-linear fit. Compound **15** crystallized when in contact with DMEM and did not allow a correct absorbance measurement in the microplate reader. For compounds **3**, **8**, and **17**,  $IC_{50}$  values were 0.246, 1.411 and 1.789 mM, respectively (Table S3, Figure S2). Compounds **17** and **8** showed a similar  $IC_{50}$ , both of them over 1.4 mM, while **3** was slightly more cytotoxic, having an  $IC_{50}$  value about 5–7-fold lower (0.24 mM). Nonetheless, considering the high antioxidant capacity shown by compounds **3**, **8** and **17** with RSA  $IC_{50}$  values in the 10 min DPPH assay of 8.30, 150.90 and 17.92  $\mu$ M, respectively, the concentrations needed to produce 50% of cytotoxicity are at least one order of magnitude higher than those required to reduce 50% RSA for amides **3** and **8**, and two orders greater in the case of urea **17**. Compound **7** did not show any significant cytotoxic effects at the range of concentrations where the compound was soluble in DMSO (up to 6 mM). In general, a non-cytotoxic behavior can be assured in a range of concentrations where the antioxidant compounds exhibit RSA potential. Therefore, the compounds were progressed to further, parallel biological characterization in different systems.

#### 3.3.2. Antioxidant Activity in Vascular Systems

First, we tested the ability of two of the best antioxidant compounds, **3** and **7**, on NADPH oxidase activity in human endothelial cells stimulated with Angiotensin II, one of the most important mediators of oxidative stress and vascular damage [26]. NADPH oxidase enzymes are the major producers of ROS at the vascular level and one of the protective effect of polyphenols versus the oxidative stress is mediated by the inhibition of the expression and activity of the NADPH oxidase complex [5]. Compared to the control antioxidant resveratrol, compound **3** and **7** showed high ORAC (>19 vs. 8 TE) and ABTS (3.2 and 8.1 vs. 2.1 TE, respectively) figures, and better and comparable DPPH values, respectively (Table 4).

As shown in Figure 2, compounds **3** and **7** were able to protect the cells against the oxidative stress promoted by Angiotensin II, decreasing NADPH oxidase activity levels in the same order as resveratrol (used as control). No remarkable differences were observed between the activities of both compounds.

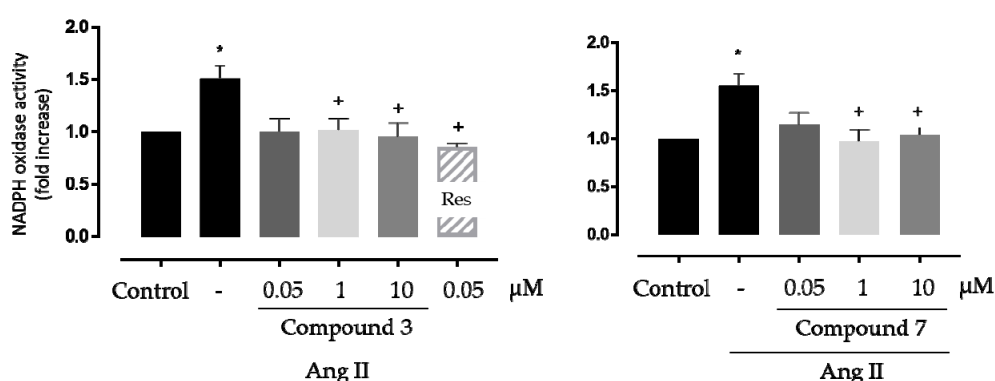


**Figure 2.** Effect of compounds **3** and **7** on Nicotinamide Adenine Dinucleotide Phosphate (NADPH) oxidase activity induced by Angiotensin II (Ang II) in cultured human microvascular endothelial cells.

\*  $p < 0.05$  vs. control, +  $p < 0.05$  vs. Ang II. Res: resveratrol (dashed bars) was used as positive control. N = 8 for compound **3** and n = 7 for compound **7**.

To further confirm the beneficial effects of these compounds in oxidative stress models at the vascular level, their antioxidant capacity was evaluated in an ex vivo whole organ system. Thus, we tested the effects of compounds **3** and **7** on NADPH oxidase activity in mice aorta stimulated ex vivo with IL-1 $\beta$ , another inducer of vascular NADPH oxidase expression and activity in vascular cells [27]. Additionally, considering the good results obtained for **17** in the ORAC, ABTS and DPPH antioxidant assays, and its low toxicity, we decided to extend the study to this compound in the aorta experiment. As shown in Figure 3, IL-1 $\beta$  increased NADPH oxidase activity under ex vivo conditions, whereas all the three tested compounds showed significant inhibition of the IL-1 $\beta$  effects.

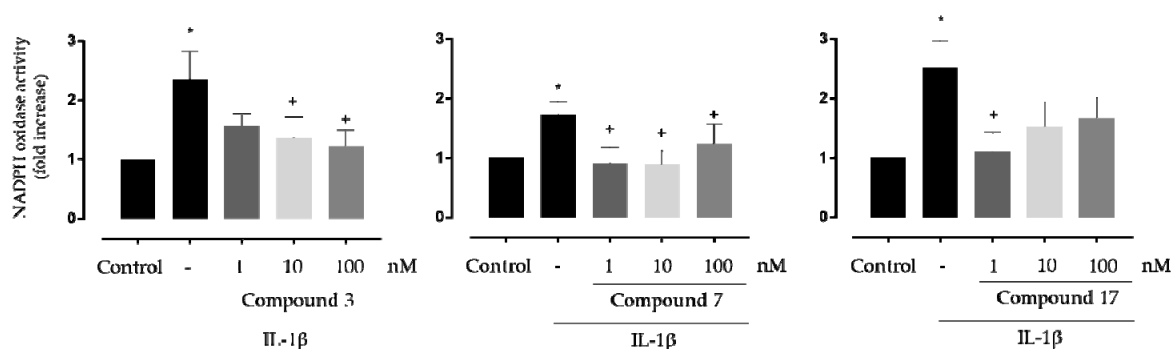


**Figure 3.** Effect of compounds **3**, **7** and **17** on NADPH oxidase activity induced by IL-1 $\beta$  in segments of aorta from C57BL/6J mice. \*  $p < 0.05$  vs. control, +  $p < 0.05$  vs. IL-1 $\beta$ .  $n = 9$  for compound **3**,  $n = 8$  for compound **7** and  $n = 7$  for compound **17**.

Altogether, our results demonstrate in vitro and ex vivo antioxidant capacity of the selected compounds and suggest that they are versatile antioxidants in response to a variety of stimuli (i.e., Ang II and IL-1 $\beta$ ) important in cardiovascular disease at the clinical level. Eventually, these compounds might be used in the treatment of vascular alterations such as endothelial dysfunction, vascular smooth muscle cells proliferation and migration, extracellular matrix remodeling, or inflammation which depend on oxidative stress milieu and that are characteristic of a number of vascular diseases including hypertension, obesity, atherosclerosis or abdominal aortic aneurysms.

### 3.3.3. In Vivo Antioxidant Activity of Selected Compounds in Yeasts

Bioavailability, in vivo reactivity and stability, and tissue differential storage are compound properties not associated with in vitro antioxidant assays, increasing the difficulties of correlating between in vitro and in vivo transfer of activities. Therefore, we required in vivo evidence supporting the in vitro-based antioxidant activity of our compounds. In this respect, *Saccharomyces cerevisiae* is a model organism used to investigate oxidative stress and the effect of nutraceuticals in resistance to oxidative stress [16,28–30], among many other biological processes linked to human health. Actually, the yeast *S. cerevisiae* had become a model for the study of effects of nutraceuticals and its transfer to humans due to the new EU regulation (EC 1924/2006), because it is easy to handle, millions of cells can be studied in a single-small culture, and its genetics, biochemistry and physiology are transferrable. Indeed, yeast and humans share one in four genes as orthologues, both in sequence and in function (as reviewed in [31–33]). Moreover, several studies have characterized the interaction of L-ascorbic acid (vitamin C) or resveratrol, two compounds with a variety of antioxidant properties, with endogenous cellular antioxidative defense systems in *S. cerevisiae* yeast strains, which will aid in the comparison of results [32,34].

In this study, we have performed experiments with *S. cerevisiae* strain BY4741 to assess the putative in vivo antioxidant effects of compounds **8**, **15** and **17**, by assessing the growth recovery ability of yeast cells subjected to oxidative stress for at least 16h, as described previously [16]. These three compounds were selected by their differential behavior in the three in vitro antioxidant experiments. Compounds **8** and **17** show higher ORAC activity than resveratrol (used as control), while **15** is comparable to the

natural product (Table 4). In the ABTS assay, urea **15** shows a lowest value than resveratrol, while the other two polyphenolic derivatives have higher radical scavenging capacities. Finally, among all selected compounds, **8** displays the shorter DPPH value.

DMSO affects oxidative stress-induced cytotoxicity, inhibits methionine sulfoxide reductase A, and reduces cell viability and survival, depending on the concentration used (as reviewed in [35], and references herein). However, methanol only affects yeast growth, by reducing its growth rate, due to the inhibition of nutrients uptake, when used at more than 10% concentration [36]. Therefore, we select methanol (up to 0.1%) as solvent for compounds in our study of determination of in vivo antioxidant and oxidant-resistance properties of the selected polyphenols. This study was performed as previously described; BY4741 yeast cells were exposed to H<sub>2</sub>O<sub>2</sub> as oxidative agent for 16h, and then cultures were challenged by different doses to ascertain changes in growth curve parameters and in yeast cell survivorship [16,30]. Growth ability was assessed with Bioscreen c, on which H<sub>2</sub>O<sub>2</sub>-stressed cells were challenged by each compound **8**, **15** and **17**, along with Resveratrol and vitamin C as control antioxidants, at three different doses (2, 20 and 40 µg). Plates also contained several types of controls (un-inoculated media, un-inoculated media with methanol, completely stressed cells in YPOxD and un-stressed cells cultured in YPD medium), all at least in triplicate. From the visual analysis of growth curve shape, tested compounds were enhancing growth recovery as compared with completely stressed cells (OxDinOxD), similarly as resveratrol or vitamin C, the two control antioxidants used (see an example in Figure S3). However, nearly none of the tested doses achieved a complete recovery similar to non-oxidative stressed cells (YPD (CTRL)).

To ascertain if this observed recovery of growth curve shape is statistically significant, two growth parameters were assessed: growth rate (r) and carrying capacity (k). Optical values (OD) were analyzed with Growthcurver R package, and obtained parameters r and k were compared with yeast cells under complete oxidative stress (OxDinOxD) or with completely unstressed cells (YPD (CTRL)). Growth rate (r) was significantly higher than the values obtained for completely stressed cells, indicating a recovery of biological functions in the yeast, but not the complete return to normality. As the unstressed yeasts, all tested compounds-treated yeast cells showed a highly significant higher growth rate ( $r = 0.3056 \pm 0.0063 \text{ h}^{-1}$ ;  $F_{(22,46)} = 31.43$ ;  $p < 0.0001$ ). The comparison of growth rate (r) between treatments (Figure 4A) indicates that apparently the best performing antioxidant is compound **17** at each single dose tested, whereas compounds **15** and **8**, showed a dose-related antioxidant effect, with the best growth rate values at a 2-µg dose. None of the tested compounds nor control antioxidants, vitamin C or resveratrol, recover completely growth rate, as mean values were significantly different from unstressed yeast (YPD(CTRL)). This recovery of growth rate is similar to that obtained with other synthetic [16] or food-derived phenolic compounds like onion skin extracts or cocoa polyphenols [30,37] or elements like selenium [38]. When comparing the carrying capacity (k) (Figure 4B), all three compounds at each single dose tested were able to recover the carrying capacity of yeast cells similarly as control antioxidants, and even to the same levels of unstressed yeast cells. In this case, compound **15**, at a low 2 µg dose, seems slightly better than the other two polyphenols and resveratrol, and comparable to vitamin C. In general, measured growth rate and carrying capacity are quite similar for the three new polyphenols. Therefore, we validate the *S. cerevisiae* as a good model for measuring antioxidant activity in vivo.



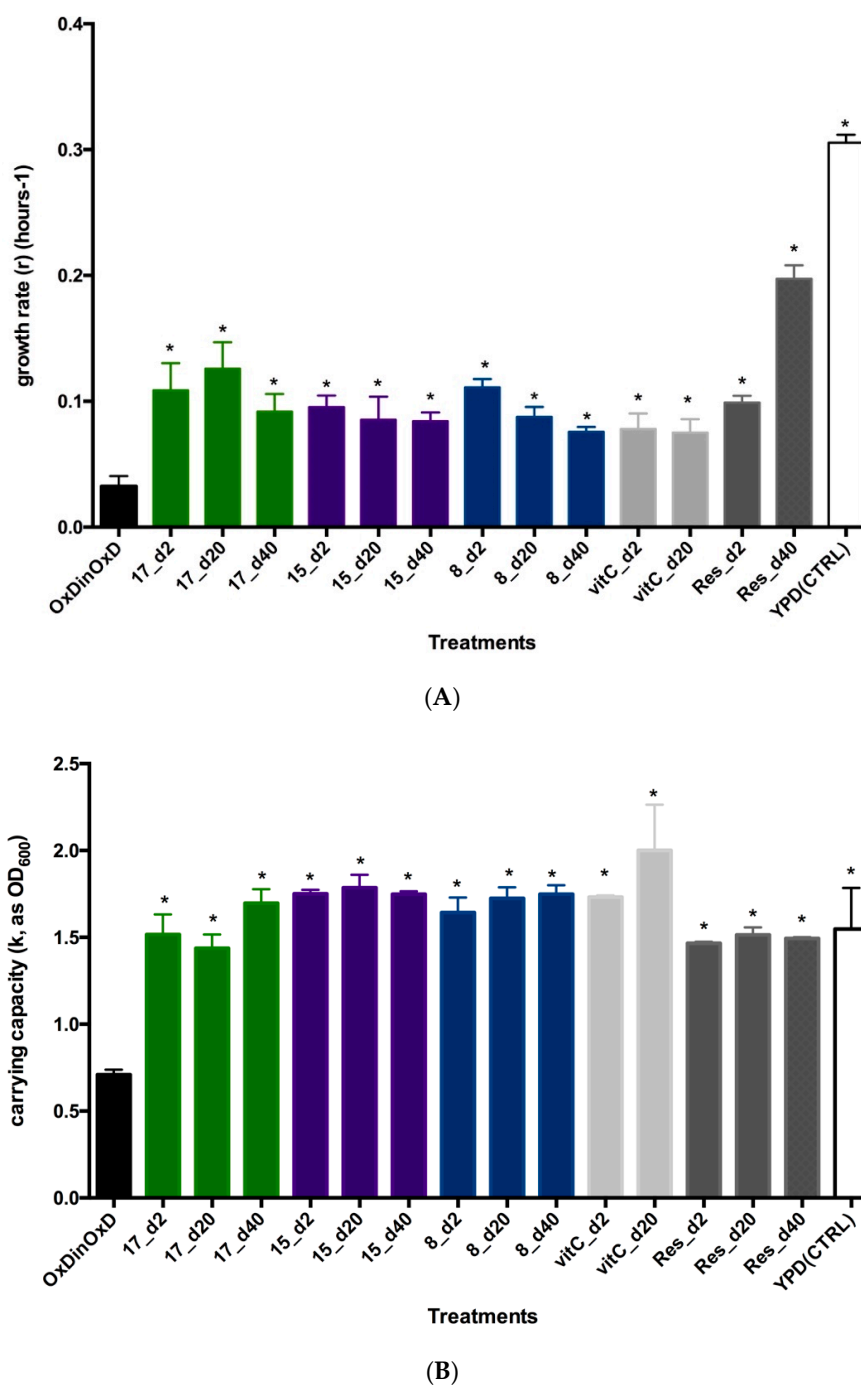


**Figure 4.** *Saccharomyces cerevisiae* growth parameters comparisons. **(A)** Comparison of growth rate ( $r$ ) as mean  $\pm$  SEM ( $\text{h}^{-1}$ ) of *S. cerevisiae* subjected to oxidative damage (grown in YPOxD medium) and challenged by different doses of compounds **17**, **15** and **8**, or by the antioxidants vitamin C (vitC) or resveratrol (Res). Comparisons have been made against completely stressed cells (OxDinOxD). To account for the oxidative damage, control lines (YPD(CTRL)) were also included, and consisted in *S. cerevisiae* cells grown in YPD (normal) medium, on which yeast cells can grow at maximum speed. Notice that oxidative stress reduces highly the growth rate, which is significantly recovered (\*) after being challenged by compounds **17**, **15** or **8**, in a similar way as the control antioxidant resveratrol. **(B)** Comparison of carrying capacity ( $k$ ) as mean  $\pm$  SEM, after oxidative stress in *S. cerevisiae*. As above, yeast cultures responded positively recovering carrying capacity after being challenged by different doses of compounds **17**, **15** and **8**. In this case, carrying capacity was similarly recovered to unstressed yeast cells (YPD(CTRL)). Asterisks denote statistical significance with alpha 0.05.

This carrying capacity also reflects the ability of yeast cells to respond to oxidative damage by producing viable offspring or survivors, which sometimes is called stress tolerance assays. These studies represent the capacity of the cells to counteract and resist the oxidative damage, representing cell survival [30,31,36,38–42]. Even showing statistical differences between applied doses, and being significantly different from completely stressed yeasts (OxDinOxD) and unstressed ones (YPD), our results indicate that tested compounds enhance biological functions enabling the complete recovery of cell biochemistry and metabolism. Indeed, tested compounds counteract the oxidative damage induced by the used  $H_2O_2$  medium and increase significantly the oxidative protection rate when compared to resveratrol (Figure 5). Considering how this effect is possible, we do not yet know about the exact molecular mechanisms behind this antioxidant activity.

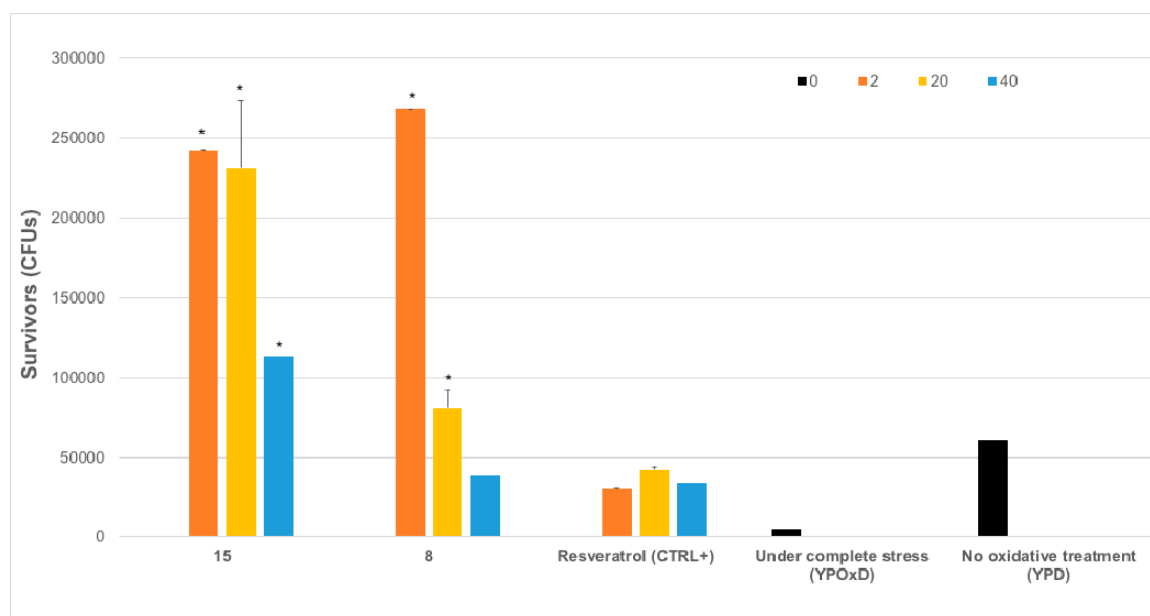


**Figure 5.** *Saccharomyces cerevisiae* survivors (mean CFUs (colony forming units)  $\pm$  SEM) to oxidative stress after treatment with compounds 15 and 8. Yeast cells were subjected to oxidative stress by growing in YPOxD medium, after 16h, cells were subjected to treatment with different doses (2, 10, 20 or 40  $\mu$ g, check color code in legend) in triplicate, and after 60 h of growth monitorization by OD600 measurement in Bioscreen c, cells were serially diluted in 10% glycerol and plated in YPD medium plates, to determine number of CFUs per ml. Stressed yeasts without antioxidant treatment (under complete stress (YPOxD)), non-stressed yeasts (no oxidative treatment (YPD)) and stressed yeasts treated with resveratrol (resveratrol (CTRL+)) were also included. Statistical significance (F-test with  $p$ -value lower than 0.05) was assessed first between YPOxD and YPD yeast survivors; and then between YPOxD stressed and antioxidant-treated, followed by comparison between control antioxidant (Resveratrol) and tested compounds at each dose. Asterisk indicates statistically significant comparisons ( $\alpha = 0.05$ ).

The obtained data supported the recovery of growth rate, whole metabolic capability and reproductive physiology by the selected synthetic polyphenols. However, the data also indicate that *S. cerevisiae* endogenous cellular antioxidative defense systems are enhanced at a similar or even better rate than those measured for well-known antioxidants resveratrol and vitamin C (Figure 5) [34,38].

#### 4. Final Remarks and Conclusions

Polyphenols are widely distributed in nature (tea, coffee, chocolate, fruits, legumes, etc.), they function as antioxidants and protect us from free radical damage in several chronic diseases (cancer, diabetes, cardiovascular and neurodegenerative diseases). Among different applications, such as oil, food and cosmetic preservatives, synthetic polyphenols could also be of interest in the

search for new bioactive agents. Following our previous work on antioxidant triazolyl polyphenols, and inspired by the OH substitutions in natural products, we designed a small collection of amide and urea polyhydroxyphenyl analogues. Synthetically more accessible than the triazolyl derivatives, compounds 1–18 were first analyzed by their antioxidant capacity in ORAC assays, with most compounds comparing favorably to resveratrol (6.6–27.6 TE versus 8.1 TE). Measurement of the aqueous stability allowed the identification of polyphenol derivatives prone to oxidization to the corresponding quinones, which were removed from further characterization to avoid misinterpretations. The most stable polyphenols (3, 7, 8, 15 and 17) were selected for further characterization, using ABTS and DPPH experiments, where most derivatives showed comparable and even higher radical scavenging abilities than the natural product resveratrol, except for 15. Selected compounds were further evaluated in different biological systems, namely endothelial cells, whole aorta and/or yeast. Compounds 3 and 7 were able to protect cultured human microvascular endothelial cells against oxidative stress promoted by Angiotensin II, decreasing the levels of NADPH activity. In addition, these polyphenols and urea 17 inhibited the effects of IL-1 $\beta$ -induced NADPH oxidase activity ex vivo, at 1nM concentration or higher, confirming their beneficial effects in oxidative stress models at the vascular level. To have in vivo evidence supporting the in vitro-based antioxidant activity of our compounds, a *Saccharomyces cerevisiae* model organism was used to investigate the effect of selected synthetic polyphenols with different in vitro profiles (8, 15 and 17). All investigated amide and urea derivatives displayed similar in vivo antioxidant properties in this model, with recovery of growth rate and of whole metabolic capability similar or even better than model antioxidants (resveratrol and vitamin C). Polyphenol 17 is the most balanced compound in the series, because of the good in vitro, ex vivo and in vivo antioxidant properties, and its low toxicity. The synthetic polyphenols described here could have future applications in the treatment of aging and many clinical conditions characterized by high oxidative-stress levels, such as cancer, cardiovascular diseases, chronic obstructive pulmonary disease, chronic kidney illness, and different neurodegenerative processes. Confirmation of other therapeutic uses will require additional experiments on different models.

**Supplementary Materials:** The following are available online at <http://www.mdpi.com/2076-3921/9/9/787/s1>, Chemical description of MeO analogues, Figure S1: HPLC-MS study of aqueous stability of compounds in aqueous solution, Table S1: Antioxidant evaluation of several natural products, Table S2: Theoretical Log P values and aqueous thermodynamic solubility measured for selected compounds, Table S3: Variations with sample concentration and time, Figure S2: Cytotoxicity, IC<sub>50</sub> values for selected compounds and non-linear fits, Figure S3: In vivo growth ability of selected compounds in yeast.

**Author Contributions:** Conceptualization, R.G.-M.; synthesis, M.J.P.d.V and R.G.-M.; ORAC and ABTS assays, S.M.-F.; DPPH, G.M.P.-Q., and B.V.-L.; vascular assays, M.G.-A.; in vivo yeast assay, B.S.-M.; supervision, A.M.B., M.R.A., M.M., R.G.-M.; writing, original draft preparation, contributions by all authors. All authors have read and agreed to the published version of the manuscript.

**Funding:** This research was funded by grants from the Spanish Ministerio de Ciencia, Innovación y Universidades (MICIU-FEDER) grant number RTI2018-097189-B-C22 to RGM, SAF2016-80305P to AMB, and CSIC grant number 2019E030 to RGM.

**Acknowledgments:** We thank Daniel Toledo and Jessy Medina for technical assistance with purification of compounds and stability studies. We also thank Víctor Gutiérrez for his help with some experiments.

**Conflicts of Interest:** The authors declare no conflict of interest.

## References

1. Nicoletti, M. Nutraceuticals and botanicals: Overview and perspectives. *Int. J. Food Sci. Nutr.* **2012**, *63*, 2–6. [CrossRef]
2. Piccolella, S.; Crescente, G.; Candela, L.; Pacifico, S. Nutraceutical polyphenols: New analytical challenges and opportunities. *J. Pharm. Biomed. Anal.* **2019**, *175*, 112774. [CrossRef]
3. Sharma, R.; Padwad, Y. Perspectives of the potential implications of polyphenols in influencing the interrelationship between oxi-inflammatory stress, cellular senescence and immunosenescence during aging. *Trends Food Sci. Technol.* **2020**, *98*, 41–52. [CrossRef]

4. Thomford, N.E.; Senthebane, D.A.; Rowe, A.; Munro, D.; Seele, P.; Maroyi, A.; Dzobo, K. Natural products for drug discovery in the 21st century: Innovations for novel drug discovery. *Int. J. Mol. Sci.* **2018**, *19*, 1578. [[CrossRef](#)] [[PubMed](#)]
5. Serino, A.; Salazar, G. Protective Role of Polyphenols against Vascular Inflammation, Aging and Cardiovascular Disease. *Nutrients* **2019**, *11*, 53. [[CrossRef](#)]
6. Moss, J.W.E.; Williams, J.O.; Ramji, D.P. Nutraceuticals as therapeutic agents for atherosclerosis. *Biochim. Biophys. Acta Mol. Basis Dis.* **2018**, *1864*, 1562–1572. [[CrossRef](#)] [[PubMed](#)]
7. Rasines-Perea, Z.; Teissedre, P.-L. Grape polyphenols' effects in human cardiovascular diseases and diabetes. *Molecules* **2017**, *22*, 68. [[CrossRef](#)] [[PubMed](#)]
8. Sajadimajd, S.; Bahramsoltani, R.; Iranpanah, A.; Kumar Patra, J.; Das, G.; Gouda, S.; Rahimi, R.; Rezaeihamiri, E.; Cao, H.; Giampieri, F.; et al. Advances on natural polyphenols as anticancer agents for skin cancer. *Pharmacol. Res.* **2020**, *151*, 104584. [[CrossRef](#)]
9. Xing, L.; Zhang, H.; Qi, R.; Tsao, R.; Mine, Y. Recent advances in the understanding of the health benefits and molecular mechanisms associated with green tea polyphenols. *J. Agric. Food Chem.* **2019**, *67*, 1029–1043. [[CrossRef](#)]
10. Galiniak, S.; Aebischer, D.; Bartusik-Aebischer, D. Health benefits of resveratrol administration. *Acta Biochim. Pol.* **2019**, *66*, 13–21. [[CrossRef](#)]
11. Dyck, G.; Raj, P.; Zieroth, S.; Dyck, J.; Ezekowitz, J. The effects of resveratrol in patients with cardiovascular disease and heart failure: A narrative review. *Int. J. Mol. Sci.* **2019**, *20*, 904. [[CrossRef](#)] [[PubMed](#)]
12. Martillanes, S.; Rocha-Pimienta, J.; Cabrera-Bañegil, M.; Martín-Vertedor, D.; Delgado-Adámez, J. Application of phenolic compounds for food preservation: Food additive and active packaging. In *Phenolic Compounds—Biological Activity*; InTech: London, UK, 2017.
13. Michalak, I.; Chojnacka, K.; Saeid, A. Plant growth biostimulants, dietary feed supplements and cosmetics formulated with supercritical CO<sub>2</sub> algal extracts. *Molecules* **2017**, *22*, 66. [[CrossRef](#)] [[PubMed](#)]
14. Criado, M.; Balsera, B.; Mulet, J.; Sala, S.; Sala, F.; de la Torre-Martínez, R.; Fernández-Carvajal, A.; Ferrer-Montiel, A.; Moreno-Fernández, S.; Miguel, M.; et al. 1,3-diphenylpropan-1-ones as allosteric modulators of  $\alpha 7$  nACh receptors with analgesic and antioxidant properties. *Future Med. Chem.* **2016**, *8*, 731–749. [[CrossRef](#)] [[PubMed](#)]
15. Pérez De Vega, M.J.; Fernandez-Mendivil, C.; De La Torre Martínez, R.; González-Rodríguez, S.; Mullet, J.; Sala, F.; Sala, S.; Criado, M.; Moreno-Fernández, S.; Miguel, M.; et al. 1- (2', 5'-Dihydroxyphenyl)-3- (2-fluoro-4-hydroxyphenyl)-1-propanone (RGM079): A positive allosteric modulator of  $\alpha 7$  nicotinic receptors with analgesic and neuroprotective activity. *ACS Chem. Neurosci.* **2019**, *10*, 3900–3909. [[CrossRef](#)] [[PubMed](#)]
16. Bonache, M.A.; Moreno-Fernández, S.; Miguel, M.; Sabater-Muñoz, B.; González-Muñoz, R. Small library of triazolyl polyphenols correlating antioxidant activity and stability with number and position of hydroxyl groups. *ACS Comb. Sci.* **2018**, *20*, 694–699. [[CrossRef](#)] [[PubMed](#)]
17. Franz, R.A.; Applegath, F.; Morriss, F.V.; Baiocchi, F.; Bolze, C. A New synthesis of ureas. III. the reaction of aromatic amines with carbon monoxide and sulfur. *J. Org. Chem.* **1961**, *26*, 3309–3312. [[CrossRef](#)]
18. Ou, B.; Hampsch-Woodill, M.; Prior, R.L. Development and validation of an improved oxygen radical absorbance capacity assay using fluorescein as the fluorescent probe. *J. Agric. Food Chem.* **2001**, *49*, 4619–4626. [[CrossRef](#)]
19. Garcés-Rimón, M.; López-Expósito, I.; López-Fandiño, R.; Miguel, M. Egg white hydrolysates with in vitro biological multiactivities to control complications associated with the metabolic syndrome. *Eur. Food Res. Technol.* **2016**, *242*, 61–69. [[CrossRef](#)]
20. Re, R.; Pellegrini, N.; Proteggente, A.; Pannala, A.; Yang, M.; Rice-Evans, C. Antioxidant activity applying an improved ABTS radical cation decolorization assay. *Free Radic. Biol. Med.* **1999**, *26*, 1231–1237. [[CrossRef](#)]
21. Oki, T.; Nagai, S.; Yoshinaga, M.; Nishiba, Y.; Suda, I. Contribution of BETA.-carotene to radical scavenging capacity varies among orange-fleshed sweet potato cultivars. *Food Sci. Technol. Res.* **2006**, *12*, 156–160. [[CrossRef](#)]
22. Mattenberger, F.; Sabater-Muñoz, B.; Hallsworth, J.E.; Fares, M.A. Glycerol stress in *Saccharomyces cerevisiae*: Cellular responses and evolved adaptations. *Environ. Microbiol.* **2017**, *19*, 990–1007. [[CrossRef](#)] [[PubMed](#)]
23. Mattenberger, F.; Sabater-Muñoz, B.; Toft, C.; Fares, M.A. The phenotypic plasticity of duplicated genes in *Saccharomyces cerevisiae* and the origin of adaptations. *G3 Genes Genomes Genet.* **2017**, *7*, 63–75. [[CrossRef](#)] [[PubMed](#)]

24. Sprouffske, K.; Wagner, A. Growthcurver: An R package for obtaining interpretable metrics from microbial growth curves. *BMC Bioinform.* **2016**, *17*, 172. [[CrossRef](#)] [[PubMed](#)]
25. Brand-Williams, W.; Cuvelier, M.E.; Berset, C. Use of a free radical method to evaluate antioxidant activity. *LWT—Food Sci. Technol.* **1995**, *28*, 25–30. [[CrossRef](#)]
26. Touyz, R.M.; Briones, A.M. Reactive oxygen species and vascular biology: Implications in human hypertension. *Hypertens. Res.* **2011**, *34*, 5–14. [[CrossRef](#)]
27. Aguado, A.; Fischer, T.; Rodríguez, C.; Manea, A.; Martínez-González, J.; Touyz, R.M.; Hernanz, R.; Alonso, M.J.; Dixon, D.A.; Briones, A.M.; et al. Hu antigen R is required for NOX-1 but not NOX-4 regulation by inflammatory stimuli in vascular smooth muscle cells. *Hypertens. Res.* **2016**, *34*, 253–265. [[CrossRef](#)]
28. Herrero, M.; Mendiola, J.A.; Cifuentes, A.; Ibáñez, E. Supercritical fluid extraction: Recent advances and applications. *J. Chromatogr. A* **2010**, *1217*, 2495–2511. [[CrossRef](#)]
29. Korczyński, M.; Witkowska, Z.; Opaliński, S.; Świniarska, M.; Dobrzański, Z. Algae extract as a potential feed additive. In *Marine Algae Extracts*; Wiley-VCH Verlag GmbH & Co. KGaA: Weinheim, Germany, 2015.
30. Martorell, P.; Forment, J.V.; De Llanos, R.; Montón, F.; Llopis, S.; González, N.; Genovés, S.; Cienfuegos, E.; Monzó, H.; Ramón, D. Use of *Saccharomyces cerevisiae* and *Caenorhabditis elegans* as model organisms to study the effect of cocoa polyphenols in the resistance to oxidative stress. *J. Agric. Food Chem.* **2011**, *59*, 2077–2085. [[CrossRef](#)]
31. De La Torre-Ruiz, M.; Pujol, N.; Sundaran, V. Coping with oxidative stress. The yeast model. *Curr. Drug Targets* **2015**, *16*, 2–12. [[CrossRef](#)]
32. Jamieson, D.J. Oxidative stress responses of the yeast *Saccharomyces cerevisiae*. *Yeast* **1998**, *14*, 1511–1527. [[CrossRef](#)]
33. Lushchak, V.I. Budding yeast *Saccharomyces cerevisiae* as a model to study oxidative modification of proteins in eukaryotes. *Acta Biochim. Pol.* **2006**, *53*, 679–684. [[CrossRef](#)] [[PubMed](#)]
34. Saffi, J.; Sonogo, L.; Varela, Q.D.; Salvador, M. Antioxidant activity of L-ascorbic acid in wild-type and superoxide dismutase deficient strains of *Saccharomyces cerevisiae*. *Redox Rep.* **2006**, *11*, 179–184. [[CrossRef](#)] [[PubMed](#)]
35. Sadowska-Bartos, I.; Paczka, A.; Moloń, M.; Bartosz, G. Dimethyl sulfoxide induces oxidative stress in the yeast *Saccharomyces cerevisiae*. *FEMS Yeast Res.* **2013**, *13*, 820–830. [[CrossRef](#)] [[PubMed](#)]
36. Antoce, O.A.; Antoce, V.; Takahashi, K.; Yoshizako, F. Quantitative study of yeast growth in the presence of added ethanol and methanol using a calorimetric approach. *Biosci. Biotechnol. Biochem.* **1997**, *61*, 664–669. [[CrossRef](#)]
37. Piechowiak, T.; Balawejder, M. Onion skin extract as a protective agent against oxidative stress in *Saccharomyces cerevisiae* induced by cadmium. *J. Food Biochem.* **2019**, *43*, e12872. [[CrossRef](#)] [[PubMed](#)]
38. Kieliszek, M.; Błażej, S.; Bzducha-Wróbel, A.; Kot, A.M. Effect of selenium on growth and antioxidative system of yeast cells. *Mol. Biol. Rep.* **2019**, *46*, 1797–1808. [[CrossRef](#)]
39. Poljak, A.; Dawes, I.W.; Ingelse, B.A.; Duncan, M.W.; Smythe, G.A.; Grant, C.M. Oxidative damage to proteins in yeast cells exposed to adaptive levels of H<sub>2</sub>O<sub>2</sub>. *Redox Rep.* **2003**, *8*, 371–377. [[CrossRef](#)]
40. Sha, W.; Martins, A.M.; Laubenbacher, R.; Mendes, P.; Shulaev, V. The genome-wide early temporal response of *Saccharomyces cerevisiae* to oxidative stress induced by cumene hydroperoxide. *PLoS ONE* **2013**, *8*, e74939. [[CrossRef](#)]
41. Cao, L.; Tang, Y.; Quan, Z.; Zhang, Z.; Oliver, S.G.; Zhang, N. Chronological lifespan in yeast is dependent on the accumulation of storage carbohydrates mediated by Yak 1, Mck 1 and Rim 15 kinases. *PLoS Genet.* **2016**, *12*, e1006458. [[CrossRef](#)]
42. Kim, I.-S.; Kim, Y.-S.; Kim, Y.-H.; Park, A.-K.; Kim, H.-W.; Lee, J.-H.; Yoon, H.-S. Potential application of the *Oryza sativa* monodehydroascorbate reductase gene (OsMDHAR) to improve the stress tolerance and fermentative capacity of *Saccharomyces cerevisiae*. *PLoS ONE* **2016**, *11*, e0158841.



# ABBREVIATIONS

<b>AA</b>	Arachidonic acid
<b>ACI</b>	Autologous chondrocyte implantation
<b>ACLT</b>	Anterior cruciate ligament transection
<b>ACR</b>	American College of Rheumatology
<b>ADAMTS</b>	A disintegrin and metalloproteinase with thrombospondin motifs
<b>AIA</b>	Adjuvant-induced arthritis
<b>AIBN</b>	Azobisisobutyronitrile
<b>AMPK</b>	AMP-Activated kinase
<b>ANOVA</b>	One way analysis of variance
<b>AP-1</b>	Activator protein 1
<b>ATR</b>	Attenuated total reflection
<b>BMAC</b>	Bone marrow aspirate concentrate
<b>CFA</b>	Freund's adjuvant
<b>cHA</b>	Cross-linked hyaluronic acid
<b>CIA</b>	Collagen-induced arthritis
<b>CLX</b>	Celecoxib
<b>CNT</b>	Control
<b>COX</b>	Cyclooxygenase
<b>CUR</b>	Curcumin
<b>C6</b>	Coumarin-6
<b>DAMP</b>	Damage-associated molecular patterns
<b>DCFH-DA</b>	2',7' dichlorofluorescein diacetate
<b>DDS</b>	Drug delivery system
<b>DEX</b>	Dexamethasone
<b>D<sub>h</sub></b>	Hydrodynamic diameter
<b>DLS</b>	Dynamic light scattering
<b>DMEM</b>	Dulbecco's Modified Eagles Medium
<b>DMOAD</b>	Disease modifying osteoarthritis drugs
<b>DPPH</b>	2,2-diphenyl-1-picrylhydrazyl
<b>DMSO</b>	Dimethyl sulfoxide
<b>DSC</b>	Differential scanning calorimetry
<b>DVS</b>	Divinyl sulfone
<b>ECM</b>	Extracellular matrix
<b>EDA</b>	Ethylenediamine
<b>EE</b>	Encapsulation efficiency

<b>EGF</b>	Epidermal growth factor
<b>EGR-1</b>	Early growth response 1
<b>ELISA</b>	Enzyme-linked immunoabsorbent assay
<b>ERK</b>	Extracellular-regulated kinase
<b>EMA</b>	European Medicines Agency
<b>EULAR</b>	European League Against Rheumatism
<b>FDA</b>	Food and Drug Administration
<b>FBS</b>	Fetal bovine serum
<b>FGF18</b>	Fibroblast growth factor 18
<b>FLS</b>	Fibroblast-like synoviocyte
<b>FTIR</b>	Fourier Transform infrared Spectroscopy
<b>G'</b>	Elastic modulus
<b>G''</b>	Viscous modulus
<b>GAL-3</b>	Galectin-3
<b>GAG</b>	Glycosaminglycan
<b>GILZ</b>	GC-induced zipper
<b>GM-CSF</b>	Granulocyte macrophage colony-stimulating factor
<b>GR</b>	Glucocorticoid receptor
<b>HA</b>	Hyaluronic acid
<b>HC-a</b>	Human articular chondrocytes
<b>H-E</b>	Hematoxylin and eosin
<b>HFLS</b>	Human fibroblast like synoviocyte
<b>hPL</b>	Human platelet lysate
<b>HPLC</b>	High performance liquid chromatography
<b>Huc-MSC</b>	Human umbilical cord mesenchymal stem cell
<b>ICAM</b>	Intercellular adhesion molecule
<b>IC<sub>50</sub></b>	Half maximal inhibitory concentration
<b>IDO</b>	Indoleamine 2,3-dioxygenase
<b>IFN</b>	Interferon
<b>IGF-1</b>	Insulin like growth factor 1
<b>IHC</b>	Immunohistochemistry
<b>IKK</b>	Inhibitor $\kappa$ B kinase complex
<b>IL</b>	Interleukin
<b>IL6R</b>	Interleukin-6 receptors
<b>iNOS</b>	Inducible nitric oxide synthase
<b>IOA</b>	Ioxaglic acid
<b>IP-10</b>	Interferon gamma-induced protein 10
<b>JAK/STAT</b>	Janus kinase/signal transducers and activators of transcription
<b>KGN</b>	Kartogenin

<b>KLF</b>	Kruppel like transcription factors
<b>LDE</b>	Laser Doppler electrophoresis
<b>LIF</b>	Leukemia inhibitory factor
<b>LPS</b>	Lipopolysaccharide
<b>LVE</b>	Linear viscoelastic region
<b>MACI</b>	Matrix-assisted autologous matrix implantation
<b>MAPK</b>	Mitogen-activated protein kinase
<b>MCL-1</b>	Myeloid cell leukemia-1
<b>MCP</b>	Monocyte chemoattractant protein
<b>MCSF</b>	Macrophage colony stimulating factor
<b>MIA</b>	Monoidioacetic-induced arthritis
<b>MIP</b>	Macrophage inflammatory protein
<b>MKP1</b>	MAPK phosphatase1
<b>MLS</b>	Macrophage-like synoviocyte
<b>MMP</b>	Matrix metalloproteinase
<b>MP</b>	Microparticle
<b>mPGE<sub>2</sub></b>	Microsomal PGE synthase-1
<b>MSC</b>	Mesenchymal stem cell
<b>M<sub>w</sub></b>	Molecular weight
<b>MVE</b>	Methacrylic derivative of $\alpha$ -tocopherol
<b>NC</b>	Nanocapsule
<b>NGF</b>	Nerve growth factor
<b>NF-<math>\kappa</math>B</b>	Nuclear factor-kappa B
<b>NK</b>	Natural killer
<b>NLR</b>	NOD-like receptors
<b>NMR</b>	Nuclear magnetic resonance
<b>NO</b>	Nitric oxide
<b>NOD</b>	Nucleotide oligomerization domain
<b>NOS</b>	Nitric oxide synthases
<b>NP</b>	Nanoparticle
<b>NSAID</b>	Nonsteroidal anti-inflammatory drug
<b>OA</b>	Osteoarthritis
<b>OARSI</b>	Osteoarthritis Research Society International
<b>OD</b>	Optical density
<b>PAMP</b>	Pathogen-associated molecular patterns
<b>PBS</b>	Phosphate buffered saline
<b>PDI</b>	Polydispersity index
<b>PEG</b>	Polyethylene glycol
<b>PES</b>	Polyethersulfone



<b>PG</b>	Prostaglandin
<b>PKB</b>	Protein kinase B
<b>PLA</b>	Poly(lactic acid)
<b>PLA<sub>2</sub></b>	Phospholipase A <sub>2</sub>
<b>PLGA</b>	Poly(lactide- <i>co</i> -glycolide) acid
<b>PRP</b>	Platelet-rich plasma
<b>PRR</b>	Pattern recognition receptors
<b>PVP</b>	Poly(1-vinyl-2-pyrrolidone)
<b>PVC</b>	Poly( <i>N</i> -vinylcaprolactam)
<b>RA</b>	Rheumatoid arthritis
<b>RANTES</b>	Regulated upon activation normal T cell expressed and secreted
<b>RNS</b>	Reactive nitrogen species
<b>ROS</b>	Reactive oxygen species
<b>RSA</b>	Radical scavenging activity
<b>SD</b>	Standard deviation
<b>SEC</b>	Size exclusion chromatography
<b>SEM</b>	Scanning electron microscopy
<b>siRNA</b>	Small interfering RNA
<b>sTNF-R</b>	Soluble tumor necrosis factor receptor
<b>SYSADOA</b>	Slow-acting drugs for osteoarthritis
<b>TA</b>	Triamcinolone acetoneide
<b>TEM</b>	Transmission electron microscopy
<b>T<sub>g</sub></b>	Glass transition temperature
<b>TGA</b>	Thermogravimetric analysis
<b>TGF-β</b>	Transforming growth factor β
<b>TH</b>	Triamcinolone hexacetoneide
<b>TIMP</b>	Tissue inhibitor of metalloproteinases
<b>TLR</b>	Toll-like receptors
<b>TNF-α</b>	Tumor necrosis factor α
<b>TNFR</b>	TNF receptor
<b>TRAF-2</b>	TNF receptor-associated factor 2
<b>TNX</b>	Tenoxicam
<b>Uc-MSC</b>	Umbilical cord mesenchymal stem cell
<b>VC</b>	<i>N</i> -vinylcaprolactam
<b>VEGF</b>	Vascular endothelial growth factor
<b>VP</b>	1-vinyl-2-pyrrolidone



